EFFECT OF INTERMEDIATE DIAPHRAGMS TO PRESTRESSED CONCRETE BRIDGE GIRDERS IN OVER-HEIGHT TRUCK IMPACTS

WA-RD 696.1

Research Report
April 2008

Washington State
Department of Transportation

EFFECT OF INTERMEDIATE DIAPHRAGMS TO PRESTRESSED CONCRETE BRIDGE GIRDERS IN OVER-HEIGHT TRUCK IMPACTS

FINAL REPORT

by

Pizhong Qiao, Ph.D., P.E.[1]
Mijia Yang, Ph.D., P.E.[2]
David I. McLean, Ph.D., P.E.[1]
[1]Department of Civil and Environmental Engineering
Washington State University
Pullman, WA 99164-2910

[2]Department of Civil and Environmental Engineering
The University of Texas at San Antonio
San Antonio, TX 78249-0668

Wood Materials and Engineering Laboratory (WMEL)
Washington State University
Pullman, WA 99164-1806

A final report prepared for

Research Office
Washington State Department of Transportation
Transportation Building, MS: 7372
Olympia, Washington 98504-7372

January 21, 2008
Draft final report was submitted on Dec. 10, 2007

TECHNICAL REPORT STANDARD TITLE PAGE

1. REPORT NO.	2. GOVERNMENT ACCESSION NO.	3. RECIPIENTS CATALOG NO
WA-RD 696.1		

4. TITLE AND SUBTITLE	5. REPORT DATE
Effect of Intermediate Diaphragms to Prestressed Concrete Bridge Girders in Over-Height Truck Impacts	January 2008
	6. PERFORMING ORGANIZATION CODE

7. AUTHOR(S)	8. PERFORMING ORGANIZATION REPORT NO.
Pizhong Qiao, Mijia Yang, and David McLean	

9. PERFORMING ORGANIZATION NAME AND ADDRESS	10. WORK UNIT NO.
Washington State Transportation Center (TRAC) Washington State University, Civil & Environmental Engineering PO Box 642910 Pullman, WA 99164-2910	11. CONTRACT OR GRANT NO.

12. SPONSORING AGENCY NAME AND ADDRESS	13. TYPE OF REPORT AND PERIOD COVERED
Washington State Department of Transportation Research Office Transportation Building, MS 47372 Olympia, WA 98504-7372 Research Manager, Kim Willoughby 360.705.7978	Research Report
	14. SPONSORING AGENCY CODE

15. SUPPLEMENTARY NOTES

This study was conducted in cooperation with the U.S. Department of Transportation, Federal Highway Administration.

16. ABSTRACT

The objectives of this study are three-fold: (1) develop/validate dynamic numerical finite element models to simulate the prestressed concrete bridge girders with intermediate diaphragms, (2) perform numerical parametric study to evaluate the effect of the critical factors on design of intermediate diaphragms, and (3) provide recommendations and guideline to better design of intermediate diaphragms to impact of over-height trucks. The conducted study aims to shed light on improved impact protection of prestressed concrete bridge girders with intermediate diaphragms and aid the WSDOT in design, analysis, and construction of prestressed concrete bridges.

The findings of this study assist in developing the specific standard of practice (such as, amendments to AASHTO standard specifications, WSDOT standard specifications, policy directives, implementation manuals, or operating procedures) for design of prestressed concrete bridge girders with intermediate diaphragms. More importantly, the proposed recommendations and guideline help the bridge engineers to make better design decision for prestressed concrete bridges.

17. KEY WORDS	18. DISTRIBUTION STATEMENT
Intermediate diaphragms, prestressed concrete, bridge girders, over-height trucks	

19. SECURITY CLASSIF. (of this report)	20. SECURITY CLASSIF. (of this page)	21. NO. OF PAGES	22. PRICE
None	None	141	

DISCLAIMER

The contents of this report reflect the views of the authors, who are responsible for the facts and the accuracy of the data presented herein. The contents do not necessarily reflect the official views or policies of the Washington State Transportation Commission, Department of Transportation, or the Federal Highway Administration. This report does not constitute a standard, specification, or regulation.

TABLE OF CONTENTS

LIST OF FIGURES

Appendix A

Appendix B

Appendix C

Appendix D

Appendix E

Appendix F

Appendix G

Appendix H

Appendix I

LIST OF TABLES

1. RESEARCH BACKGROUND

Bridges have been impacted by over-height trucks, which causes damage and service interruption of bridges. The application of intermediate diaphragms in concrete girders may improve impact resistance and thus survivability of bridges. However, there is only a limited study in the literature to address the effect of intermediate diaphragms to impact damage protection of bridge girders, and the role of intermediate diaphragms in improving the impact resistance is not well defined. There is an immediate need to evaluate the effect of intermediate diaphragms in providing impact damage protection to the bridge girders.

A great number of prestressed concrete bridge girders in the U.S. have been damaged by the impacts of over-height trucks (Shanafelt and Horn, 1980). The reinforced concrete intermediate diaphragms are usually provided to help minimize impact damage and improve the impact resistance of prestressed concrete bridge girders. Only a few limited studies are available to discuss the effect of intermediate diaphragms in impact protection of bridge girders. Andrawes (2001) investigated lateral impact response for prestressed concrete girder bridges with intermediate diaphragms. Comparisons of finite element models and experimentally measured data for a large-scale, laboratory, model bridge were made between the strain and displacement results, thus validating and calibrating the finite element models used in the analyses of prestressed concrete bridge girders with intermediate diaphragms. Finite-element models were then used for simulations of non-skewed and skewed PC-girder bridges, and they were analyzed for lateral-impact loads that were applied to the bottom flange of the exterior girders at the diaphragms location and away from the diaphragms location. A comparison was made among the strains and displacements induced in the girders with different types of intermediate-diaphragms. Abendroth and Fanous (2003) studied the lateral impacts of prestressed concrete girders in bridges with intermediate diaphragms. In their study, a comparison of steel vs. concrete intermediate diaphragms was made, and they concluded that the reinforced concrete intermediate diaphragms provide more protection for the girders than that by the structural steel ones, when the lateral impact load is applied at the location of the intermediate diaphragm; whereas there is no apparent difference in impact resistance of two types of the intermediate diaphragms if the impact load is applied away from the diaphragm location. Green, et al. (2004) studied the contribution of intermediate diaphragms in enhancing the precast bridge girder performance, and their results indicated that intermediate diaphragms have a modest positive effect of reducing the maximum deflections for the chosen girder.

Though some preliminary studies on lateral impact of prestressed concrete bridges with intermediate diaphragms were conducted by the researchers at Iowa State University (Andrawes 2001; Abendroth and Fanous 2003), there is no extensive evaluation on role of intermediate diaphragms in enhancing the bridge impact resistance. Also in these previous studies, only the strain and displacement results under the pulse impact were considered. A thorough investigation from impact/contact mechanics and energy absorption points of view should be adapted to study the effect of intermediate diaphragms and develop proper design recommendations and guideline for intermediate diaphragm design.

The effect of intermediate diaphragms to prestressed concrete bridge girders in over-height truck impacts can be addressed by conducting dynamic numerical finite element analysis (FEA) (e.g., using commercial software ABAQUS and/or LS-DYNA3D), and the factors in intermediate diaphragm design can include, but not be limited to: (1) location of intermediate diaphragms within span, (2) size of intermediate diaphragms (e.g., height and width), (3) girder spacing, (4) different girder types (e.g., effect of wide flange and girder height), (5) framing action (e.g., aspect ratio of the bridge, and number of girders in the bridge), and (6) truck speed and impact force and types (e.g., the forces by various types of over-height trucks and effect of bridge initial mass). Better understanding of these influencing factors in design of intermediate diaphragms will greatly reduce impact damage to bridge girders and promote the safety and integrity of the bridge superstructure.

The standard specifications (AASHTO 2002) recommend that the intermediate diaphragms should be used at the point of maximum positive moment for spans in excess of 12 m (40 ft.), and the clear reasons for such requirements were not given. While the LRFD specifications (AASHTO 2004) state that the intermediate diaphragms can improve live load distributions, and this effect is not included in the calculation of load distribution factors. Articles 8.12.1 for reinforced concrete and 9.10.1 for prestressed concrete bridges in AASHTO (2002) allow omitting the intermediate diaphragms where tests or structural analyses show adequate strength. Article 5.13.2.2 in AASHTO (2004) has a similar statement allowing omitting the intermediate diaphragms if tests or structural analyses show that they are unnecessary.

However, the benefits of using intermediate diaphragms are much debated and are still controversial. There are many arguments in favor of using intermediate diaphragms, because (Garcia, 1999): (1) they can transfer lateral loads to and from the deck; and (2) they can distribute lateral impact loads from overheight trucks to all girders, thus reducing the total damage. But, there are also some other reasons in favor of eliminating the intermediate diaphragms, because instead of limiting damage from overheight trucks, the intermediate diaphragms actually spread the damage. But this issue is more due to the complicated behavior of impact of trucks and bridges. One issue is the maximal impact force generated, and the other one is the maximal energy dissipated. For an impact between the overheight truck and the bridge, if the stiffness of the bridge is increased due to the intermediate diaphragms, the maximal impact force will be increased, leading to more damage to the structure. However, this situation can be changed if a soft layer is used over the impact girder flange to reduce the contact stiffness between the overheight truck and the girder. Without considering the contact process and when the bridges are under the same loading, the deflection and strain in the bridge with the intermediate diaphragms must be small comparing with the one of no-intermediate diaphragm cases. In terms of given kinetic energy, the case with intermediate diaphragms will have larger safety margin comparing to the case without intermediate diaphragms. In this study, the role of intermediate diaphragms in enhancing impact protection and minimizing potential impact-associated damage is investigated.

2. OBJECTIVES OF THE STUDY

The objectives of this study are three-fold: (1) develop/validate dynamic numerical finite element models to simulate the prestressed concrete bridge girders with intermediate diaphragms, (2) perform numerical parametric study to evaluate the effect of the critical factors on design of intermediate diaphragms, and (3) provide recommendations and guideline to better design of intermediate diaphragms to impact of over-height trucks. The conducted study aims to shed light on improved impact protection of prestressed concrete bridge girders with intermediate diaphragms and aid the WSDOT in design, analysis, and construction of prestressed concrete bridges.

3. DEVELOPMENT AND VALIDATION OF FINITE ELEMENT MODEL

In this section, the validation of the numerical finite element (FE) model with the existing available testing data (Abendroth, et al. 2004) and the preliminary quasi-static and dynamic analyses of a three-girder PC bridge are presented.

3.1 Validation of FE Model

In order to validate the numerical finite element (FE) model used in this study, a comparison of the proposed numerical FE model with the experiment conducted at Iowa State University (ISU) (Abendroth, et al. 2004) is made.

3.1.1 Bridge in the experiment

The bridge used in the experiment is a one-span, two-lane PC bridge shown in Figures 1 and 2, with the lane width of 6.0 ft., span of 40.4 ft., overhang of 3.0 ft on each side, and supported by three PC I-girders. The size of I-girder is shown in Figure 3, the size of intermediate diaphragm (ID) is extended to the top edge of the bottom flange in the I-girder (Figure 3). The cross-section of the abutment is detailed in Figure 4. The applied load locations in the experiment are shown in Figures 5 and 6.

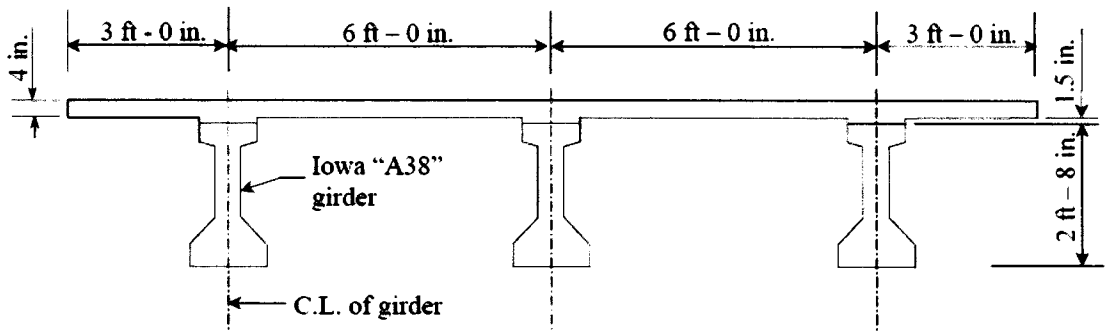

Figure 1. Cross-section view of the bridge in the experiment

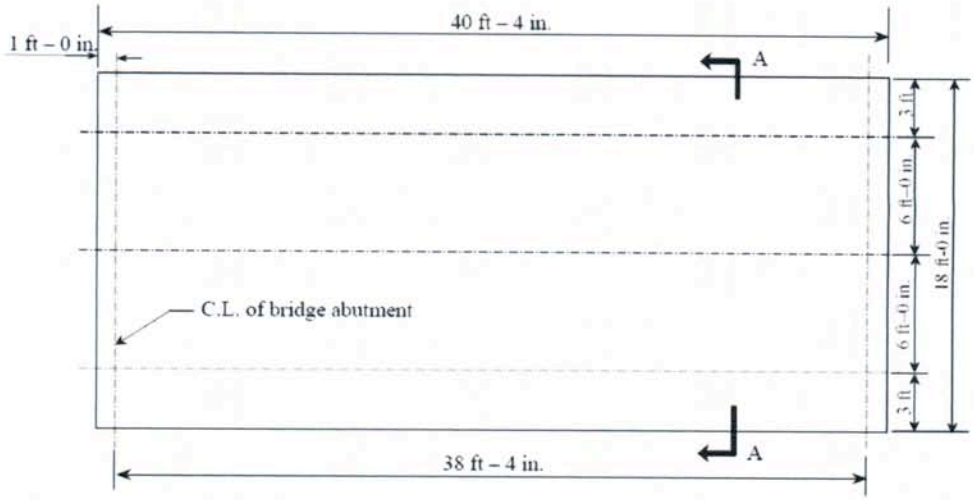

Figure 2. Plan view of the bridge in the experiment

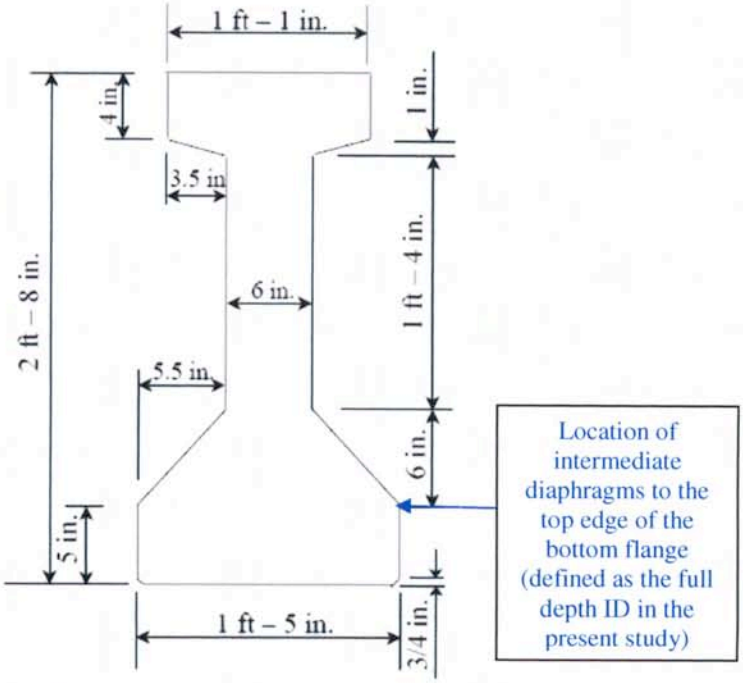

Figure 3. The details of the PC I-girder in the bridge

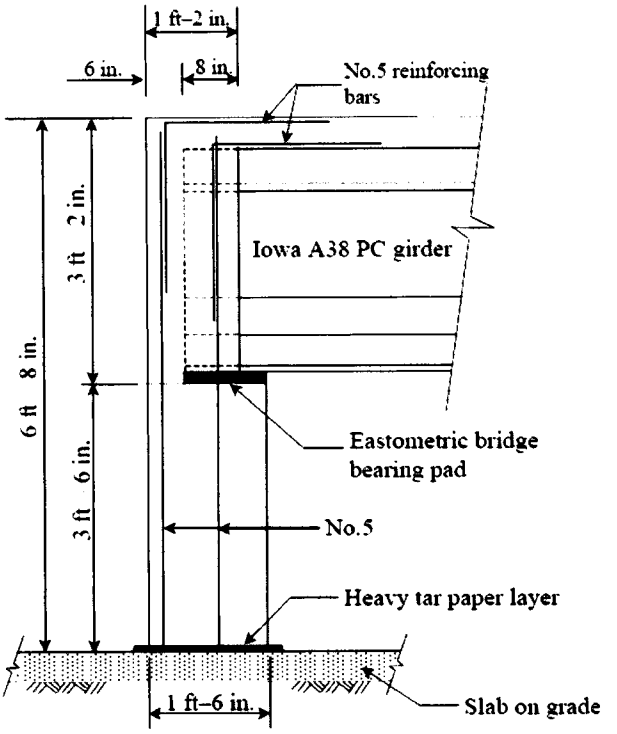

Figure 4. Abutment configuration

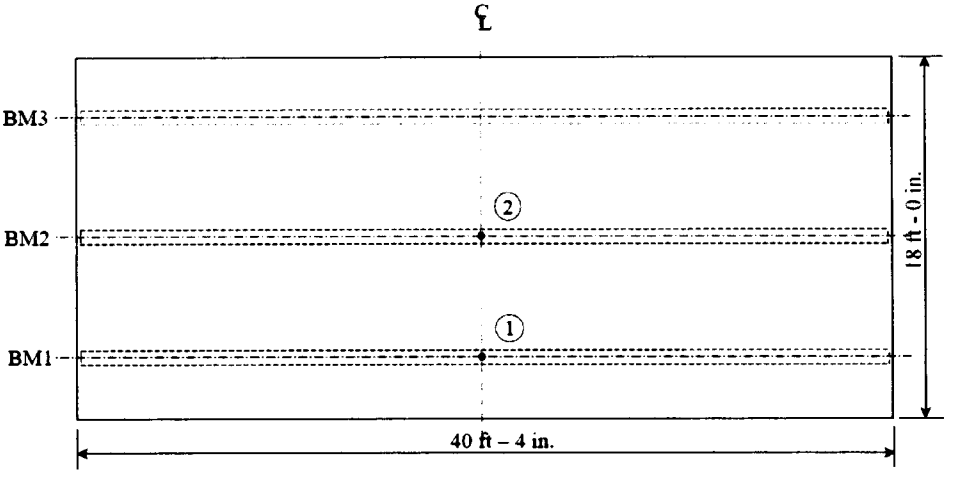

Figure 5. Applied load locations

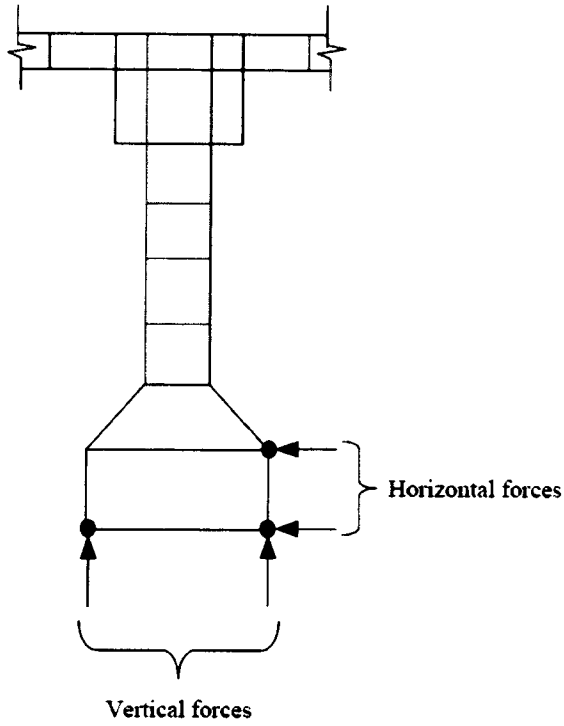

Figure 6. The details of applied loads on the girder

Material model and parameters

In the report of ISU (Abendroth, et al. 2004), an elastic model or an elastic brittle-damage model was used since the linear load-displacement curve was shown. A close comparison of the simulation results with the experimental data was found when the elastic models with the material properties of $E = 4.084 \times 10^6$ psi and $\nu = 0.15$ were used. These material properties are adopted in the present study as well.

Load type and locations

The load simulated in the ABAQUS model is taken as the concentrated loads, applied at two points at the bottom flange of either Girder I or II as shown in Figure 6, one for horizontal forces and the other for vertical forces. For horizontal forces, each load increases linearly from 0 kips to 37.5 kips (the total force at two loading points (see Figure 6) thus increases from 0 kips to 75 kips). For vertical forces, each load increases linearly from 0 kips to 12.5 kips (the total force thus increases at two loading points (see Figure 6) from 0 kips to 25.0 kips).

3.1.2 Numerical finite element modeling

The numerical analysis is conducted using the commercial finite element software ABAQUS, which is an integrated software for preprocessing, solution and post-processing.

Preprocessing in ABAQUS is completed using ABAQUS CAE, which defines material properties, material and geometrical modeling, boundary and loading conditions, and connections between different component parts. Solution solver in ABAQUS is divided into several options, from static general, static risk for post failure analysis, to explicit dynamic analysis and implicit dynamic analysis (including eigenvalue analysis). Post-processing is used to retrieve analysis results in various ways, and the stress or strain contours can be obtained in the post-processing stage.

The same physical model as in the ISU study (Abendroth, et al. 2004) is set up in the proposed numerical model in this study, and the numerical FE results are compared with their experimental ones. The numerical model is shown in Figure 7 with the finite element meshes refined along the contact regions of girders and the deck.

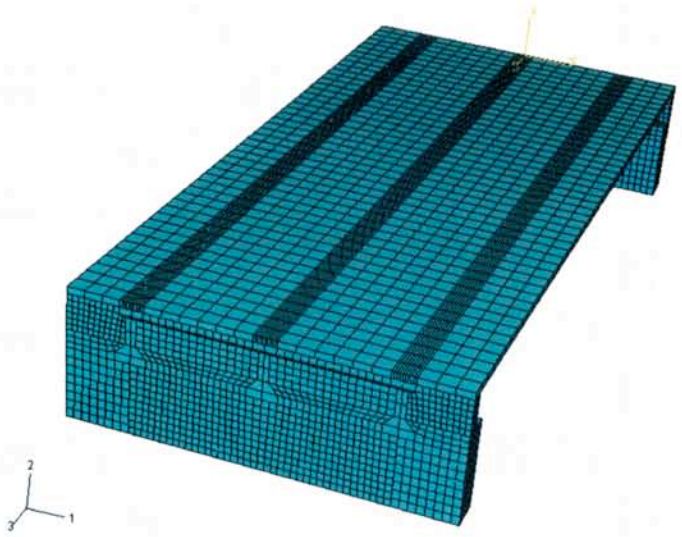

Figure 7. Finite element mesh of the bridge without intermediate diaphragms

Definition of von Mises Stress

The von Mises stress is usually used to compare with the yield strength of the material, and it includes all the principal stresses. It is defined as:

$$\sigma_v = \sqrt{\frac{(\sigma_1 - \sigma_2)^2 + (\sigma_2 - \sigma_3)^2 + (\sigma_1 - \sigma_3)^2}{2}} \quad (1)$$

where σ_1, σ_2 and σ_3 are the principal stresses. In this study, the von Mises stress is considered as the representative stress in comparison and later used to compare with the strength values of the material to indicate the failure state.

3.1.3 Comparisons and validation with experiment

The von-misses stress and displacement distributions under static loading are shown in Figures 8 and 9. As aforementioned, the horizontal and vertical loads are applied separately at location (1) or (2) shown in Figure 5. The horizontal and vertical displacements are measured at the same point as the load is applied (see Figure 6). In all these plots, the load is the total load of the two loading points (either horizontally or vertically) (see Figure 6); while the displacement is taken as the average displacement of the two loading points.

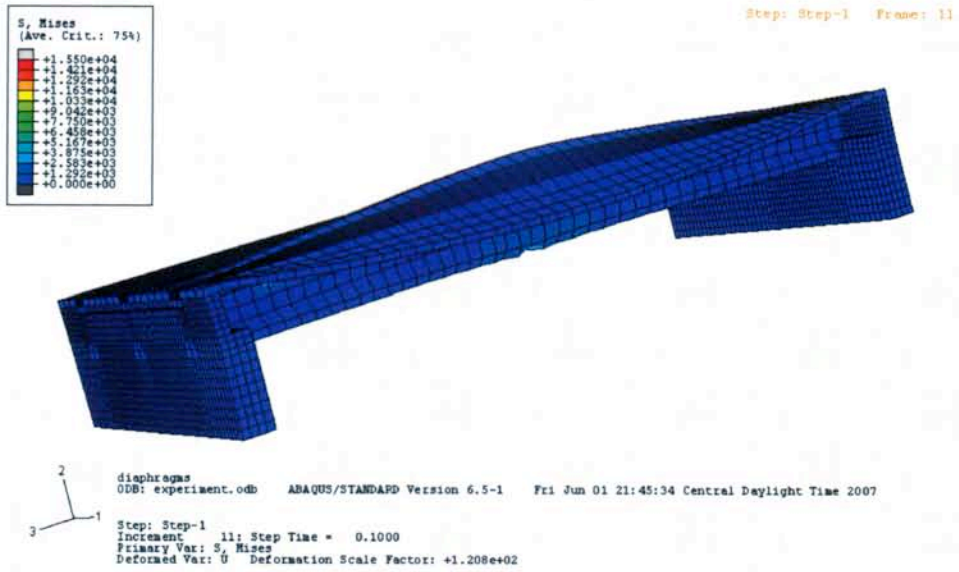

Figure 8. Von Misses stress distribution without intermediate diaphragms

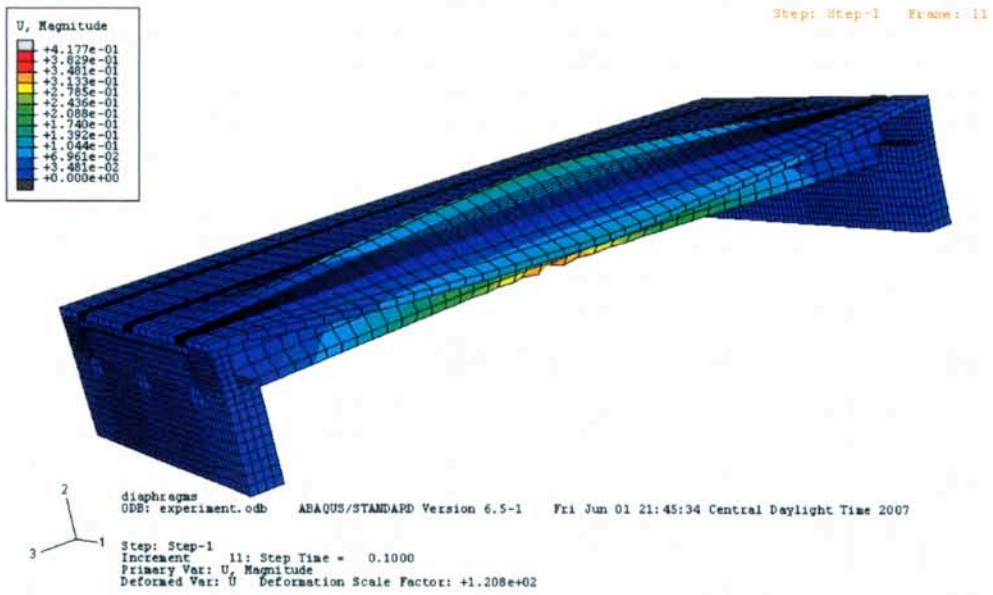

Figure 9. Total displacement distribution without intermediate diaphragms

Vertical displacement

The comparisons of vertical load (applied at location (1) in Figure 5) versus vertical deflection between the experimental and simulated results are shown in Figure 10, for the cases with and without intermediate diaphragms. As indicated by the experimental results, the intermediate diaphragms (IDs) have insignificant effects on the vertical displacement, which is also shown in the finite element modeling. However, the ABAQUS model predicts less displacement compared to the experimental results, and it may be due to the reason that the effects of concrete cracking in ABAQUS modeling is not included. The same pattern for the vertical load applied at location (2) is shown in Figure 11. The maximum differences between the finite element modeling and the experimental results for the case without IDs are 24% and 10% for the load applied at locations 1 and 2, respectively. The maximum difference between the finite element modeling and the experimental results for the case with IDs are 23.5% and 27% for the load applied at locations 1 and 2, respectively. Again, the increased differences for the case with IDs could have been resulted from the existence of cracks in the experimental bridge deck after the case without IDs was tested as indicated in the ISU report. However, compared to the ISU simulation results (in their comparison, the minimum differences are 18% and 29% for the cases without and with IDs, respectively), the current numerical FE results show improved correlations with the experiment. The improved comparison in the current numerical FE simulation may be caused by the solid elements used in the present study, compared to the shell element used in the ISU report (Abendroth, et al. 2004).

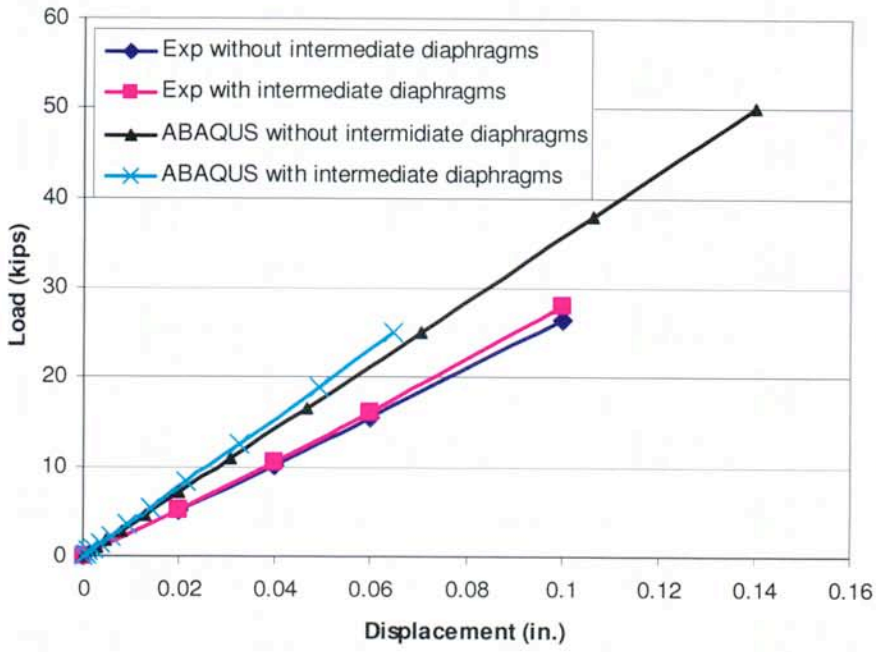

Figure 10. Comparison of ABAQUS results with the experiment for the case of vertical load applied at location 1

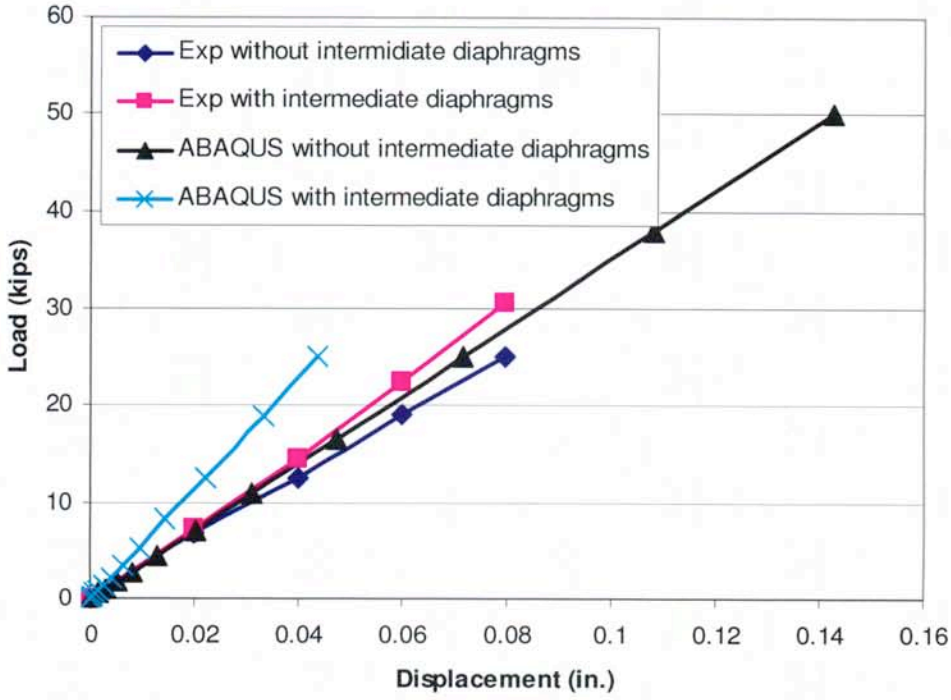

Figure 11. Comparison of ABAQUS results with the experiment for the case of vertical load applied at location 2

Horizontal displacement

Similarly, the comparison of horizontal load versus horizontal deflection of the experimental bridge with the FE simulation results for the cases with the load applied at location 1 is shown in Figure 12. The maximum differences between the modeling and experiment results are 25.0% and 24.4% for the cases without and with intermediate diaphragms (IDs), respectively. The comparison of the horizontal load versus horizontal deflection of the experimental bridge with the simulation results for the cases with the load applied at location 2 is shown in Figure 13, and an excellent agreement between the numerical simulation and experiment is achieved with the maximum differences of 0.5% 0.1% for the cases without and with IDs, respectively.

In all the cases of static load vs. displacement, the FE predictions are higher than the experimental results, excepted for the case of the bridge with IDs under the horizontal loading (see Figure 12). The reason of this discrepancy compared to other cases might be due to that the average displacement over the two loading points is used as the ABAQUS FE prediction; while the experiment only measured one point using the hydraulic jacket which was applied close to the upper surface of the bottom flange of the girder. Thus, the experimental results showed a less displacement, resulting in a larger stiffness.

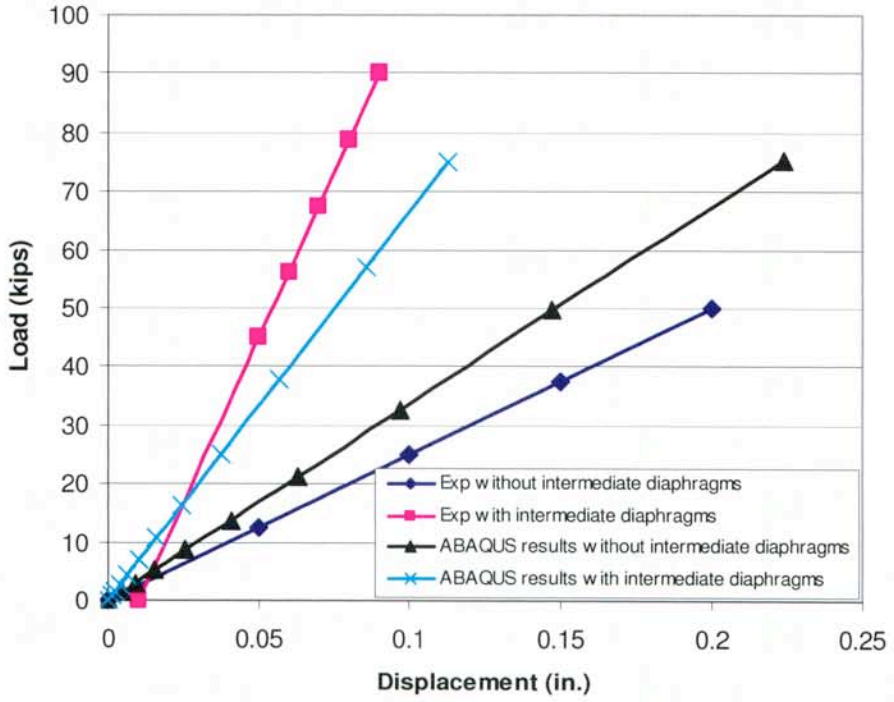

Figure 12. Comparison of ABAQUS results with the experiment for the case of horizontal load applied at location 1

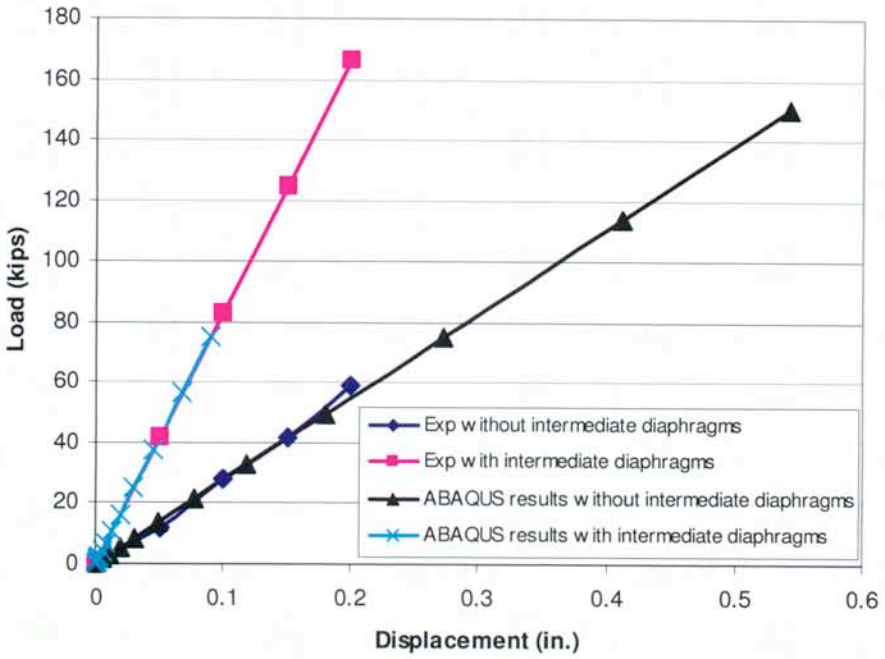

Figure 13. Comparison of ABAQUS results with the experiment for the case of horizontal load applied at location 2

Strain comparison

The strain comparison between the experimental and numerical simulation results for the case with intermediate diaphragms (IDs) and with the load applied at either the location (1) or (2) is reported in Table 1. The comparison with the applied load at location (1) exhibits a close trend. The comparison with the applied load at location (2) shows the similar pattern, except with the strain measured at the middle of diaphragm 1, which may be due to the inappropriate measurement of the strain during the experiment.

Table 1. Strain comparison between the experiment (exp.) and finite element modeling (FEM) (in microstrain)

Location	Exp. with load at Location 1	FEM with load at Location 1	Exp. with load at Location 2	FEM with load at Location 2
1R	-8.9	5.34	3.9	16.8
1L	110.7	98.2	21.8	87.7
2R	-59.0	-50.1	-42.5	-57.7
2L	12.1	20.5	140.2	63.0
3R	-38.9	-68.6	-90.6	-81.7
3L	7.8	-12.3	-7.0	-16.1
ID	-159.9	-153.8	3.9	67.5

Validation summary

As indicated by the above results, the predictions by the finite element modeling (FEM) relatively emulate the experimental measured data (Abendroth, et al. 2004), thus validating the proposed numerical FE model and providing confidence of applying the FE model to the dynamics/impact analysis of the PC bridges.

3.2 Quasi-static Modeling of Bridge Considering Plasticity

3.2.1 Geometrical and material model

The elastic-plastic quasi-static modeling for concrete damage plasticity is considered in the present study. The material properties of concrete considered are $E_s = 4.084 \times 10^6$ psi and $v = 0.15$. To include the effect of plasticity of concrete, the plastic strain under the different yielding stress in compression is given in Table 2; while the tensile behavior of concrete is included with the tensile strength and cracking strain shown in Table 3, and it is adapted in this study to simulate the tensile damage-induced softening, i.e., when the cracking strain increases, its tensile strength reduces considerably.

Table 2. The effect of concrete plasticity in compression

Yielding stress (psi)	Plastic strain
3900.49	0
4495.41	0.001
5823.56	0.0012
6932.8	0.002
6932.8	0.2

Table 3. Tensile behavior of concrete to account for tensile damage-induced softening

Tensile strength (psi)	Cracking strain
481	0
252	0.5

3.2.2 Finite element modeling

The bridge model is shown in Figure 14 with the I-girder type of W42G and a deck of 4 in. thick. The intermediate diaphragm (ID) is 8 in. thick extended to the up-surface of the bottom flange of the bridge girder (it is defined as full-depth ID in this study, see Figure 3), and located in the middle of the span. The abutment detail is not included, and a simply supported boundary condition is considered (see the FE mesh and boundary condition shown in Figures 15 and 16, respectively). The horizontal loads are applied at the two points (each point with a load of 60 kips) along the bottom flange of I-girder, with a total magnitude of 120 kips (Figure 17). The load duration of 0.1 s and magnitude

of 120 kips shown in Figure 17 is defined as for a full design load in this study to emulate the impact load from the overheight truck.

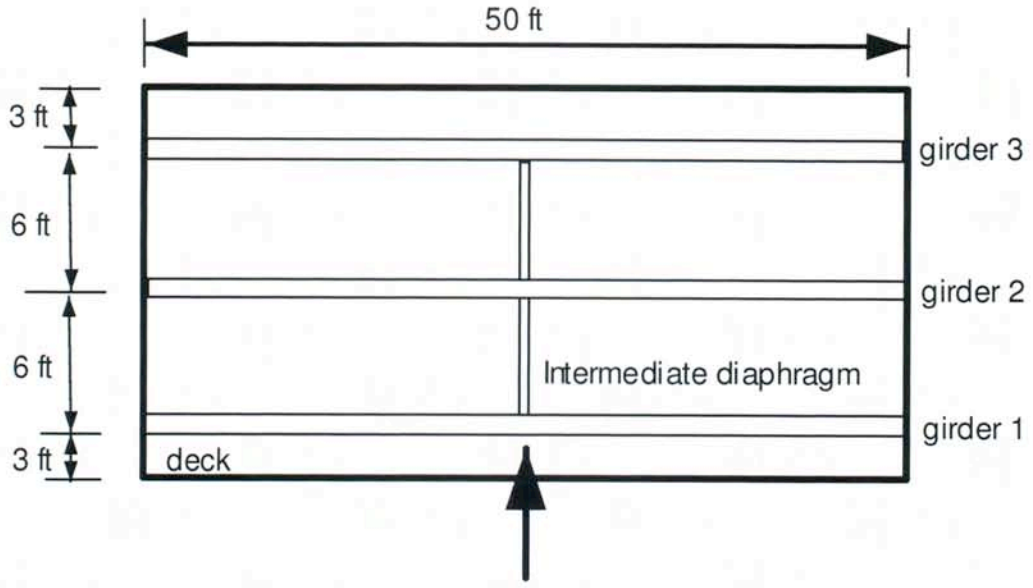

Figure 14. Geometry of FE simulation of the bridge

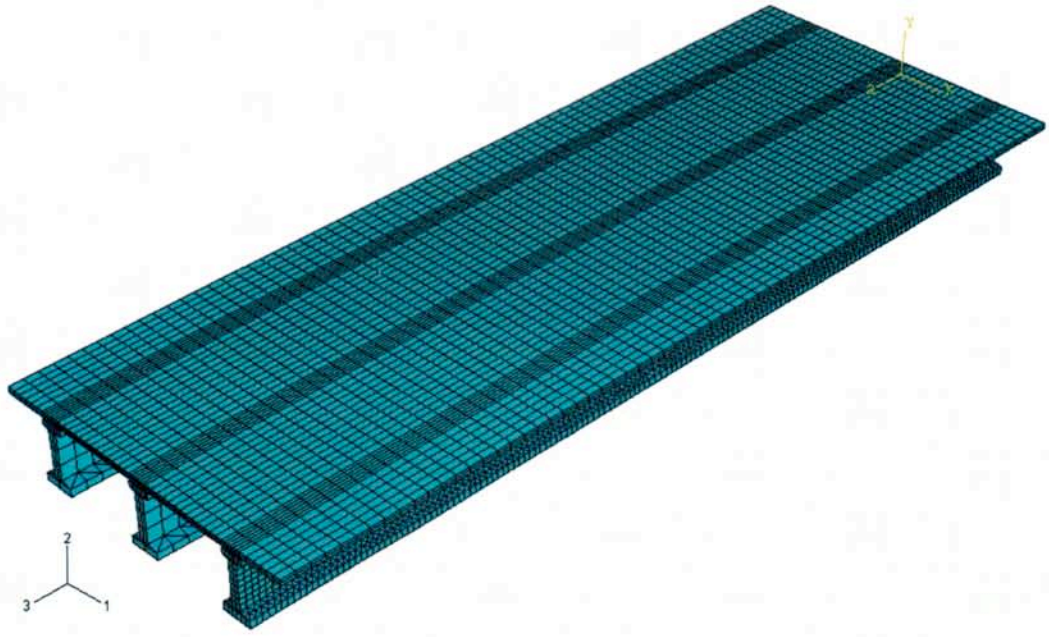

Figure 15. FE mesh of the one-span, three-girder bridge

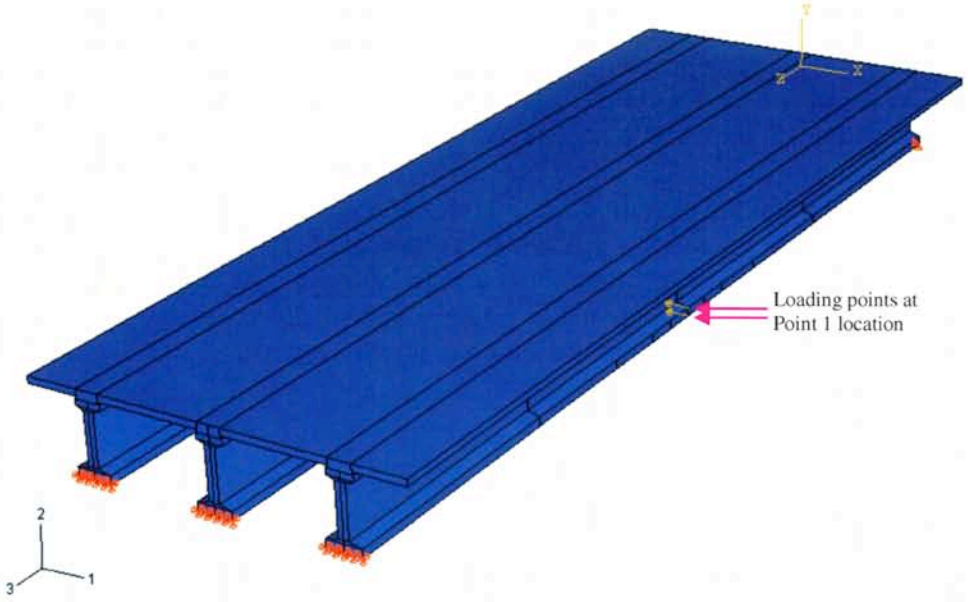

Figure 16. Boundary and loading conditions of the simulated bridge (the horizontal load is applied by two points at the bottom flange)

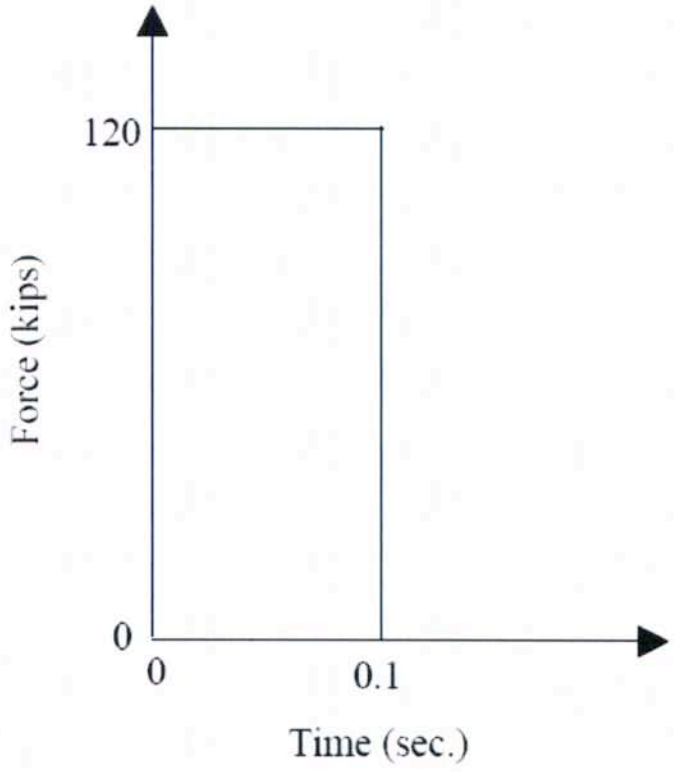

Figure 17. The total load magnitude and type

3.2.3 Numerical results

The load vs. displacement relation at the loading point under the quasi-static loading of Figure 17 is shown in Figure 18. While the displacement and strain histories are shown in Figures 19 and 20, respectively. As shown in Figure 19, the maximal displacement reaches to 0.42 in. with a permanent deformation of 0.15 in. As shown in Figure 20, the maximal tensile strain of 359.0 με is observed at the opposite side of the loading bottom flange of girder I (shown in Figure 21). Thus, the quasi-static model showcases the plastic damage effect in the simulation and better mimics the actual situation during the impact event of the bridge. It also illustrates the capacity of the present proposed model in simulation of concrete plastic damage.

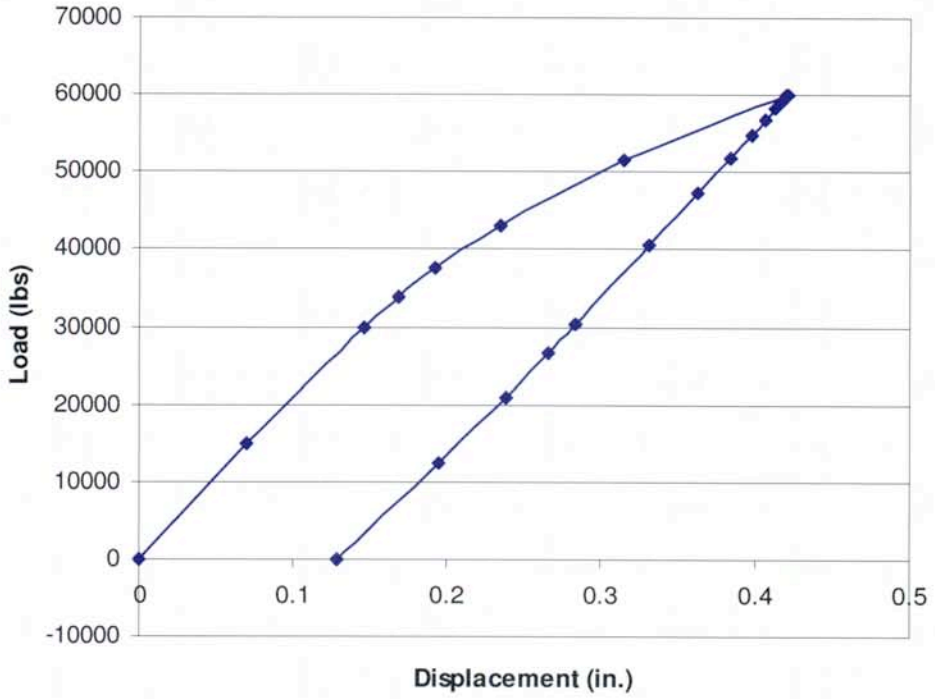

Figure 18. Load vs. displacement curve at point 1 with the load applied at location 1 (the load applied at one point of the bottom flange is 60 kips)

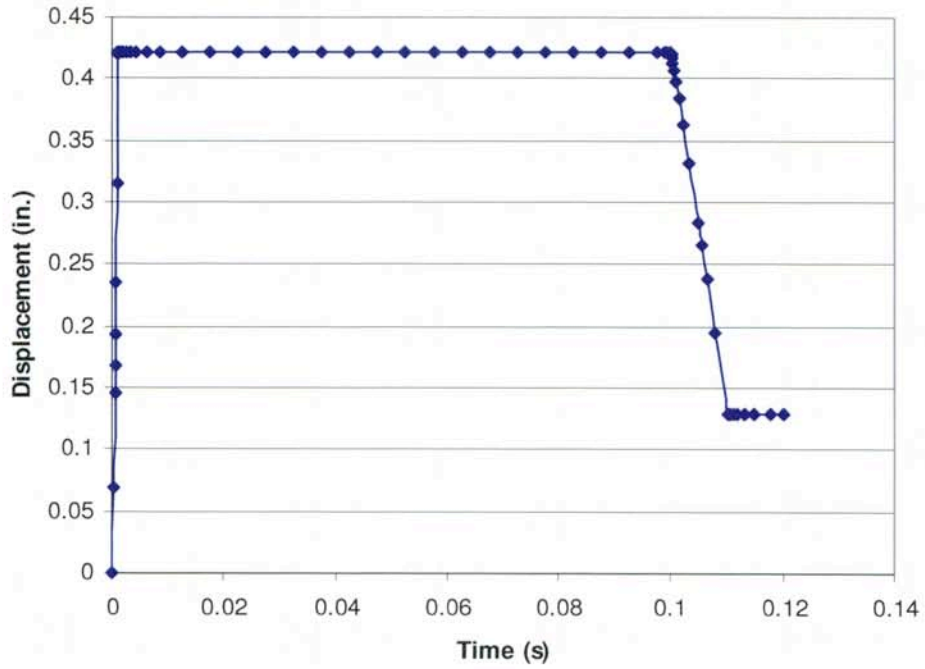

Figure 19. Displacement time history of point 1 with the load applied at location 1

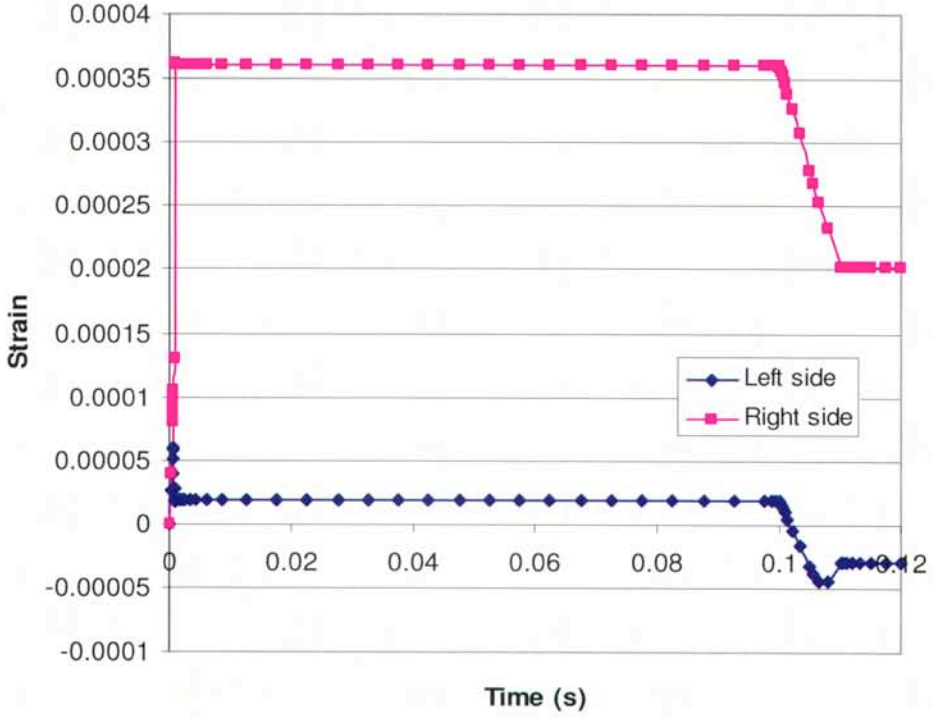

Figure 20. Strain time history on the two sides of the bottom flange for the case of point 1 with the load applied at location 1 (left side is the back; while right side is the front)

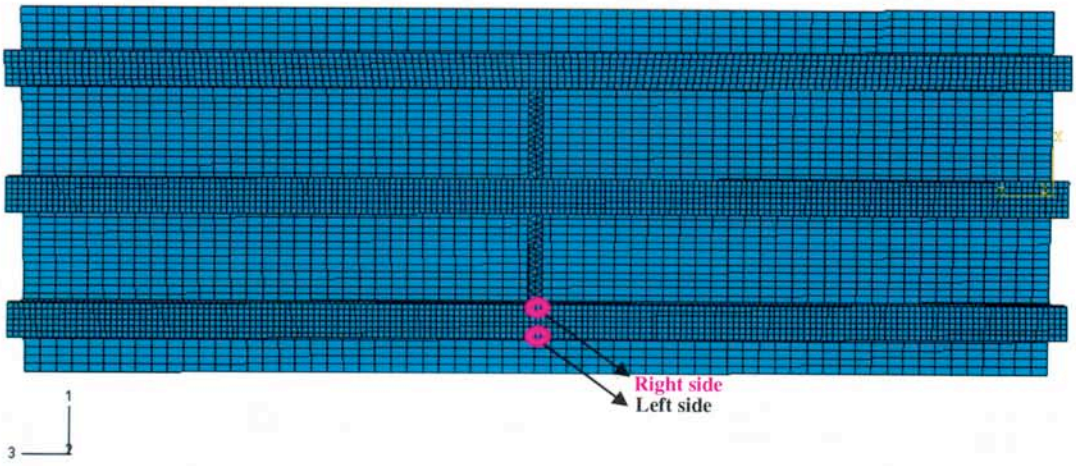

Figure 21. The locations of strain measurement

3.3 Dynamic Simulation of Three-girder Bridge System

The geometrical and material properties as well as the boundary conditions used for the dynamic simulation are the same as the ones in the quasi-static simulation. But, in the preliminary study, only the elastic material with E = 4.084 x 10^6 psi and ν = 0.15 is considered. The load still employs the impact pulse load shown in Figure 17, and the bridge system is solved using ABAQUS/Explicit considering large deformation.

The displacement history at the mid-span of Girder I is shown in Figure 22, and the maximal displacement reaches to 0.19 in. While the strain history at the mid-span of the three girders is shown in Figure 23, and the maximal strain reaches 298.0 με. Also as shown in Figure 23, the strains decay from Girder I (the load-applying point) to Girder III.

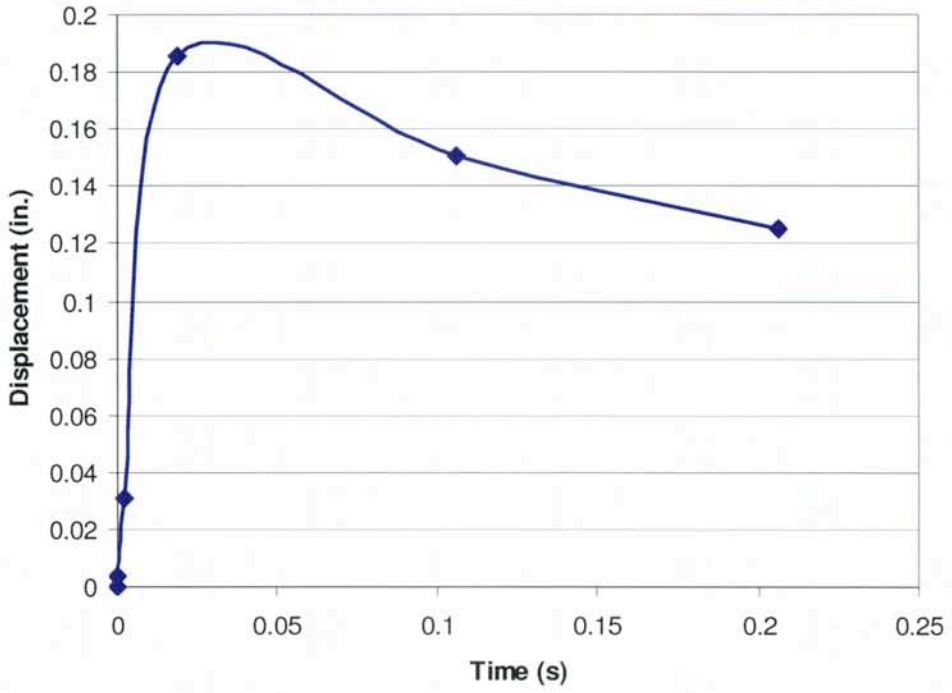

Figure 22. Load displacement curve for the case of point 1 with the load applied at location 1

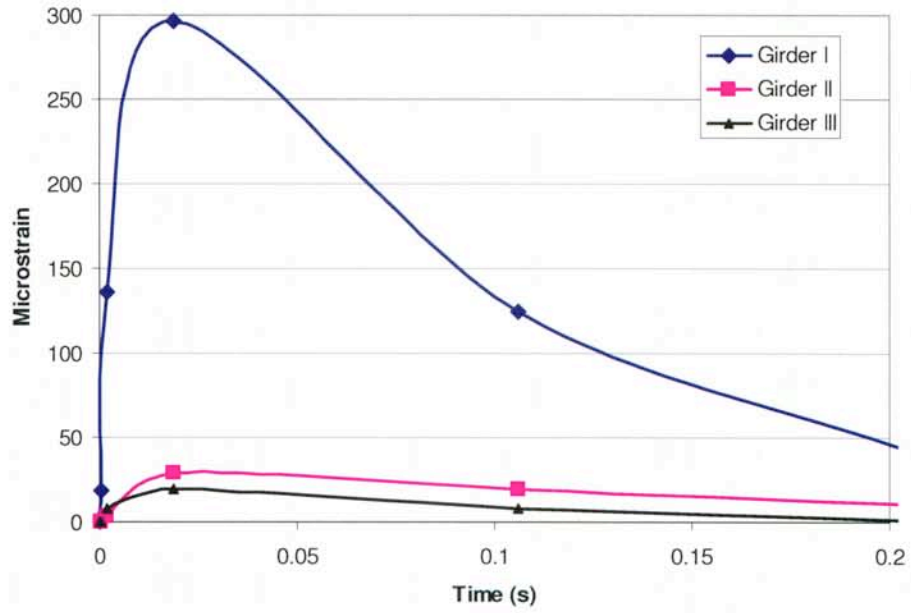

Figure 23. Maximal principal strain time history curve at the mid-span of three girders for the case of point 1 with the load applied at location 1

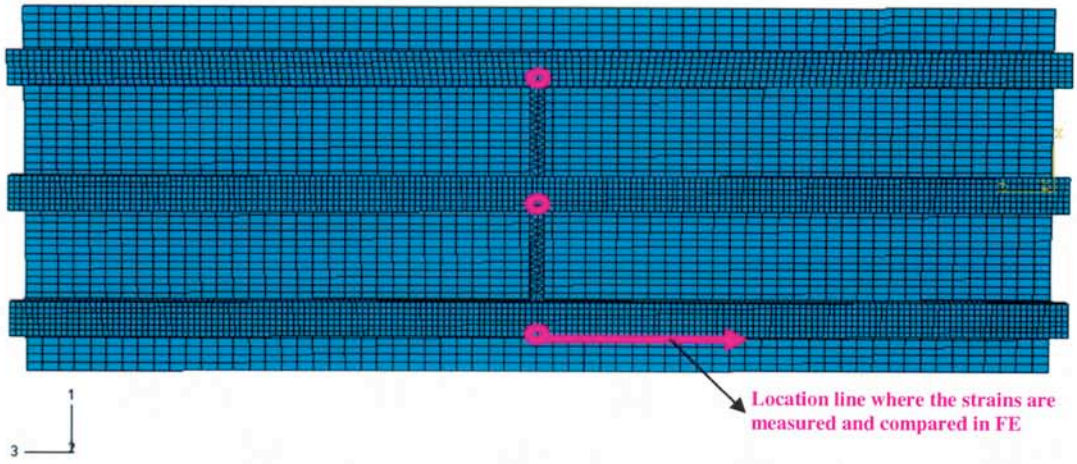

Figure 24. The locations of strain measurement

As shown in Figure 24, the outside line at the bottom flange of Girder I is chosen to show the strain decay away from the mid-span location (impact loading point). As in Figure 25, the strains decay rapidly from the loading point to other locations due to the intermediate diaphragm restraining effect. The tensile bending strain (right side) and the compressive strain (left side) are also shown in Figure 26.

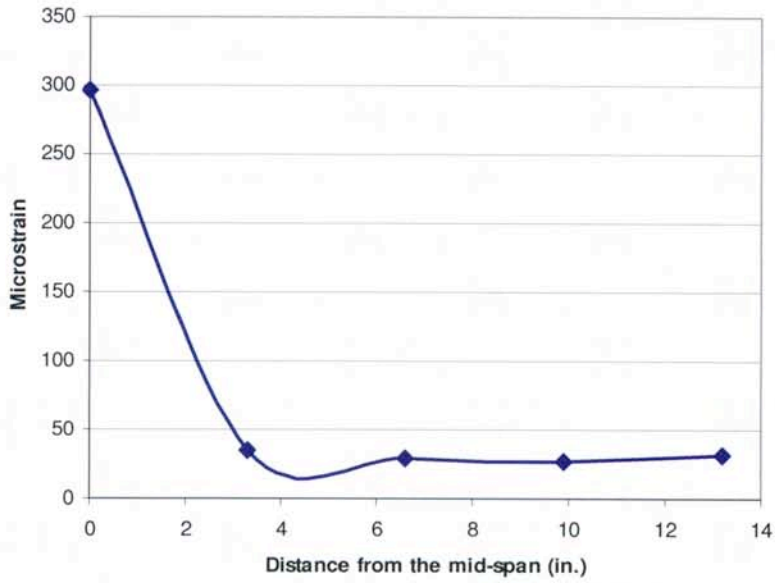

Figure 25. Maximal principal strain curve along a portion of girder I for the case of point 1 with the load applied at location 1

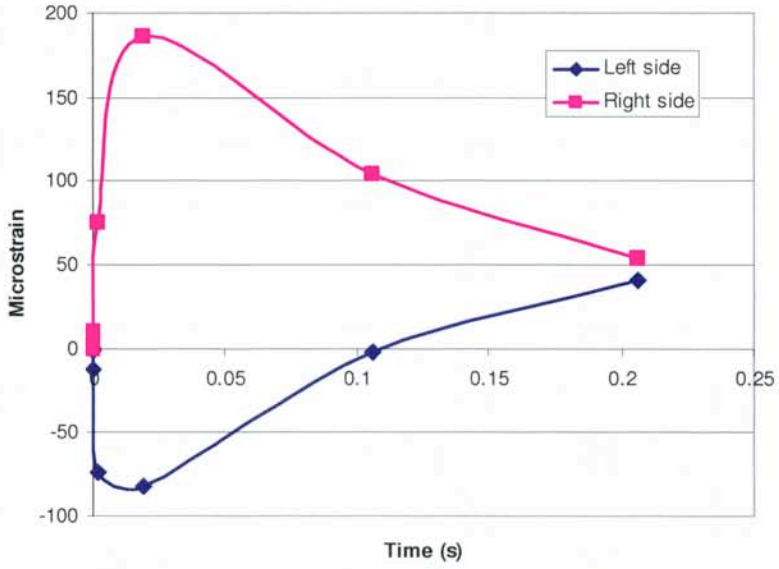

Figure 26. Strain time history of the two sides of the bottom flange for the case of point 1 with the load applied at location 1

The von Mises stress distribution under the dynamic load is shown in Figure 27, which shows the stress concentration near the loading points and the supports. While the total displacement distribution, maximum principal strain, and vertical displacement are shown in Figures 28 to 30, respectively. From the deformed shape, it is observed that due to the impact loading applied at the bottom flange, the deck is bent into a crust shape with the far side deformed upward and the near side sunk down.

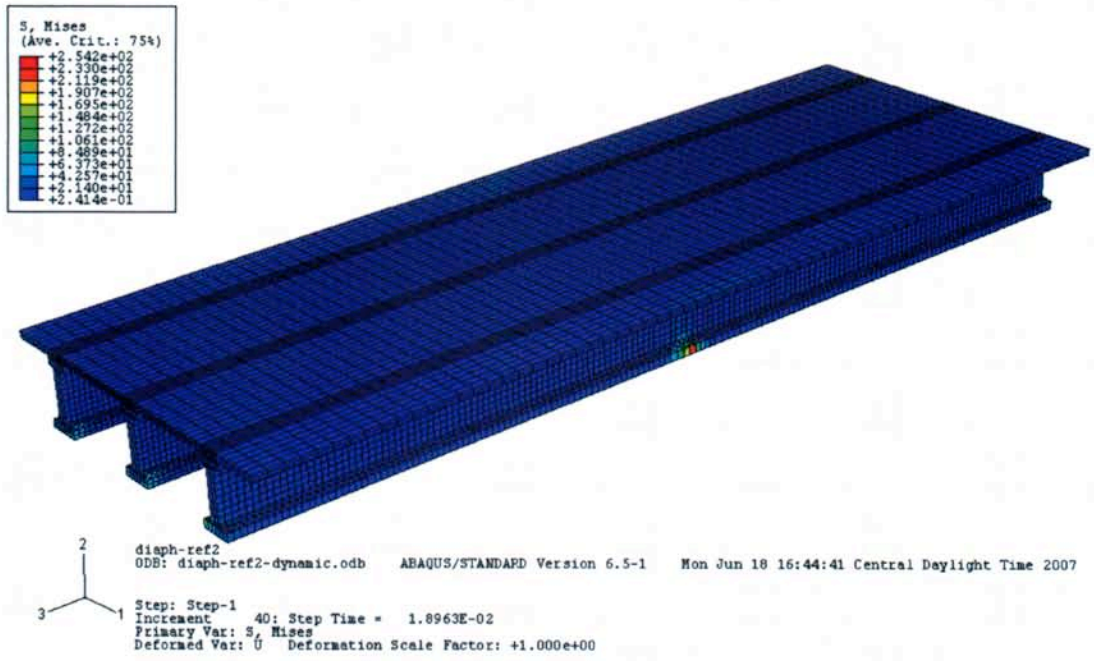

Figure 27. von Mises stress distribution

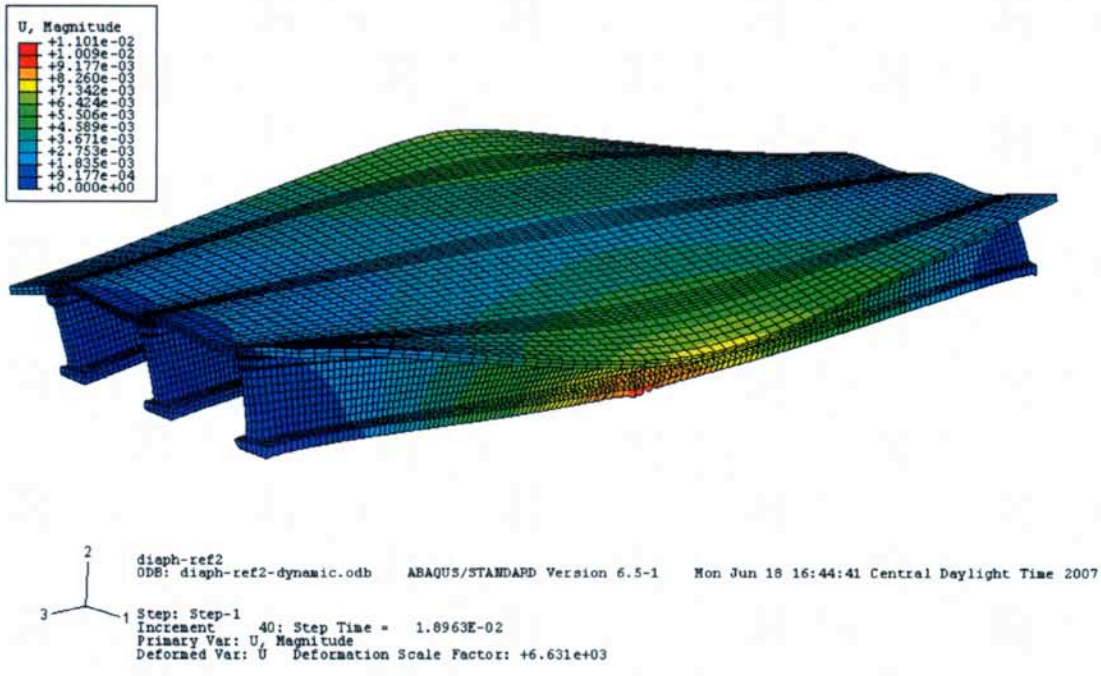

Figure 28. Total displacement distribution

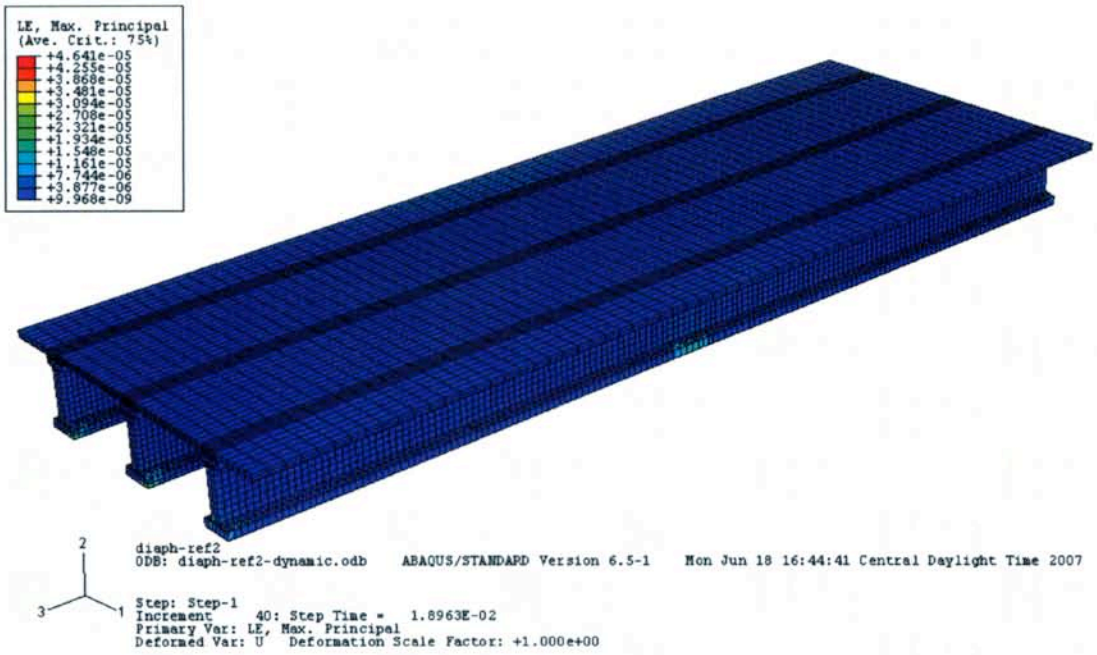

Figure 29. Maximal principal strain distribution

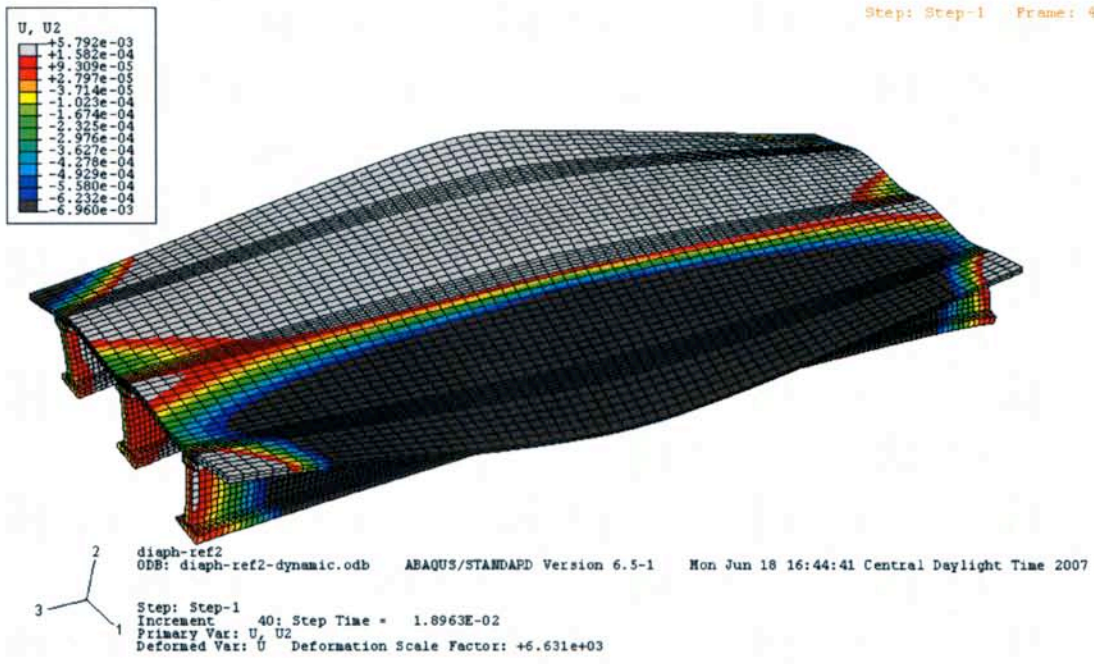

Figure 30. Vertical deflection distribution

The preliminary dynamic analysis illustrates the capabilities and analytical aspects of the FE model. In the next section, the detailed analyses with consideration of influential factors are performed.

4. ROLE OF INTERMEDIATE DIAPHRAGMS IN IMPACT PROTECTION

After the validated numerical FE models are established in the above section, an extensive numerical parametric study to evaluate the effect of the critical factors on design of intermediate diaphragms (IDs) is conducted. The factors considered in the analysis for ID design include: (1) Location of IDs within the span, (2) Size of IDs (e.g., thickness and depth), (3) Girder spacing, (4) Girder types, (5) Framing action, and (6) impact types and contact interface.

The dynamic numerical analysis is performed for each case, and the analytical results and comparisons among different factors/models are provided. The following analytical results and data are considered and compared:

(1) Stress distribution, such as the von Mises stress, longitudinal (along the bridge length direction) stress, and/or transverse stress (along the loading direction).
(2) Strain distribution along the longitudinal and/or transverse direction, including the plastic strain.
(3) Displacement distribution, such as the vertical displacement and horizontal displacement.
(4) Deflection and strain history of girders.
(5) Energy distribution in the bridge system and plastically dissipated energy.

In this study, the 3rd direction is defined as the longitudinal (bridge span) direction; while the 1st direction is considered as the transverse (horizontal) direction, coinciding with the loading direction. A 0.1-s duration and 120-kips quasi-static pulse load (Figure 17) is applied in the analysis, and it is considered as the full design load.

4.1 Locations of Intermediate Diaphragms within Span

The effect of the location of the intermediate diaphragms (IDs) is first evaluated. The loading point is located at the middle location of the span and acted on the bottom flange of the girder (as shown in Figure 6). The bridge in the similar configuration as shown in Figures 1 and 2 is simulated, i.e., a one-span PC bridge supported by three PC I-girders. The type of I-girder is I-girder type of W42G, and the size of intermediate diaphragm (ID) is extended to the top edge of the bottom flange in the I-girder (Figure 3) with ID thickness of 8" and girder spacing of 6 ft. The locations of IDs within span as well as the impact load locations with respect to (e.g., at or away from) the locations of IDs are investigated. In this section, the effect of the number of intermediate diaphragms used in a 100 ft bridge is studied, and two cases are evaluated: (a) IDs at ½ point of span, and (b) IDs at 1/3 points of span.

The bridge with only one intermediate diaphragm (ID) location at ½ span as well as the bridge with two intermediate diaphragms (IDs) location case at 1/3 span and 2/3 span between two adjacent girders are simulated and compared. The impact load is still applied at the mid-span, and the bridge is simply supported. A summary of key performance responses is shown in Table 4. Comparing these two cases, it is noted that the case with two IDs between two adjacent girders (i.e., at 1/3 spans) distribute the load more evenly, and the local bending effects are reduced significantly. In addition, the damage area is greatly reduced. As shown in Figure 31, the bridge with the ID at ½ span shows significantly larger area of damage than the one with the IDs at 1/3 and 2/3 span.

Table 4. Effect of spacing of intermediate diaphragms under full design load

Location and No. of IDs	Totally damaged area (in^2)	Maximal horizontal displacement (in.)	Maximal vertical displacement (in.)	Maximal Principal strain	Maximal tensile stress (psi)	Maximal plastic dissipative energy (lbs-in)
One ID at ½ span	15000.0	4.27	1.42	4.15E-3	497.0	120,663.0
Two IDs at 1/3 and 2/3 span	180.0	4.38	1.45	4.15E-3	494.0	120,663.0

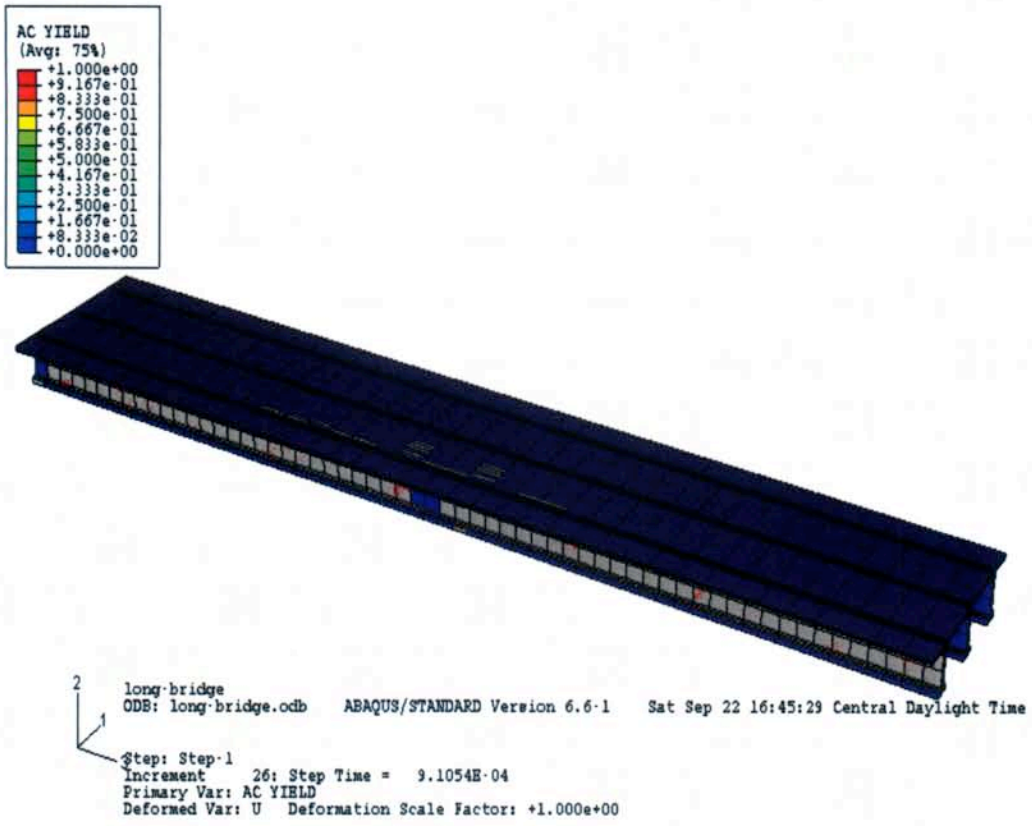

(a) Bridge with intermediate diaphragms at mid-span (1/2 span)

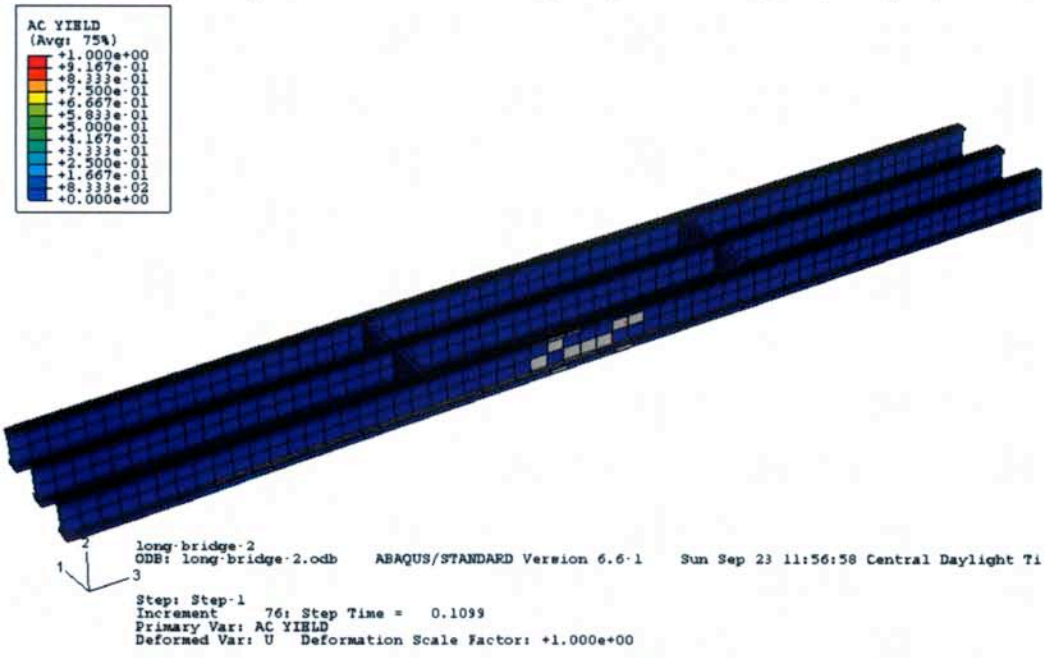

(b) Bridge with intermediate diaphragms at one-third-span (1/3 and 2/3 span)

Figure 31. Failed elements shown in the outside girders at the end of the pulse loading (the elements in gray color indicates the failed elements)

All the numerical analysis results are provided in Appendix A. Both the von Mises and longitudinal stress distributions for the two cases are presented in Figures A1 and A2, respectively, and the stress distributions in two cases are in comparative ranges with the ½ span ID showing a little large stress concentration at the loading point. The transverse displacement distribution along the long span bridge with a large displacement observed at the loading area is shown in Figure A3. According to beam theory, by increasing the span of length 2 times, the deflection will increase 8 times for a simply-supported beam. As shown in Figure A3(a), a 7.07 time increase of deflection along the loading direction is observed for a fully nonlinear analysis, when compared to the maximal deflection 0.56 in. for a 50 ft span bridge (see Table 5). The longitudinal strain distributions of the two cases are shown in Figure A4, with similar maximal strain for the case of the bridge with ½ span ID and the case of the bridge with 1/3 and 2/3 span IDs. The transverse plastic strain distributions (along the loading direction) of the bridge for the two cases are shown in Figure A5, and the case with ½ span ID shows similar induced plastic strain under impact load with the case of IDs at 1/3 and 2/3 spans; while the longitudinal plastic strain distributions are shown in Figure A6. The transverse displacement history at the loading location is shown in Figure A7, and a larger displacement is observed at the loading location for the bridge with IDs at 1/3 and 2/3 spans. It is observed that for a long span bridge of 100 ft., one ID is not enough in preventing impact loading with much larger damaged areas, since a local stiffness is increased for the case of ID at ½ span, leading to small deformation, higher maximal stress, and more damaged areas. Compared with the one-ID case, the intermediate diaphragms (IDs) at the multiple locations are better in transferring loads to decks and the other girders with large horizontal displacement along the loading direction at the back girder (Girder 3) observed (Figure A8), verifying that one of the primary functions of intermediate diaphragms is to transfer loads to deck and other girders. Even though a large energy dissipation (Figure 32) and similar maximal plastic strain (Figure A9) is observed for both the cases, the bridge with two diaphragms has experienced less damage area (see Figure 31).

In summary, the bridge with multiple and distributed IDs is better in resisting impact and transferring large deformations to other girders and decks, thus reducing the damaged areas and absorbing more kinetic energy. Based on the simulation, a suitable distance of ID spacing can be determined for a particular loading, and it is recommended that a spacing of 25 to 40 feet for 100 ft. or longer span of the bridges is better in impact protection.

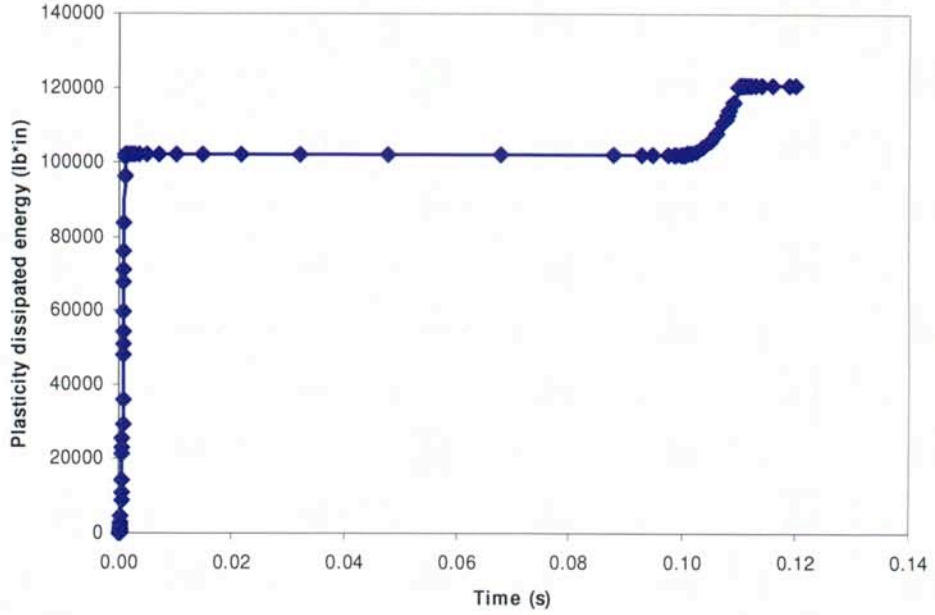

(a) Bridge with intermediate diaphragms at mid-span (1/2 span)

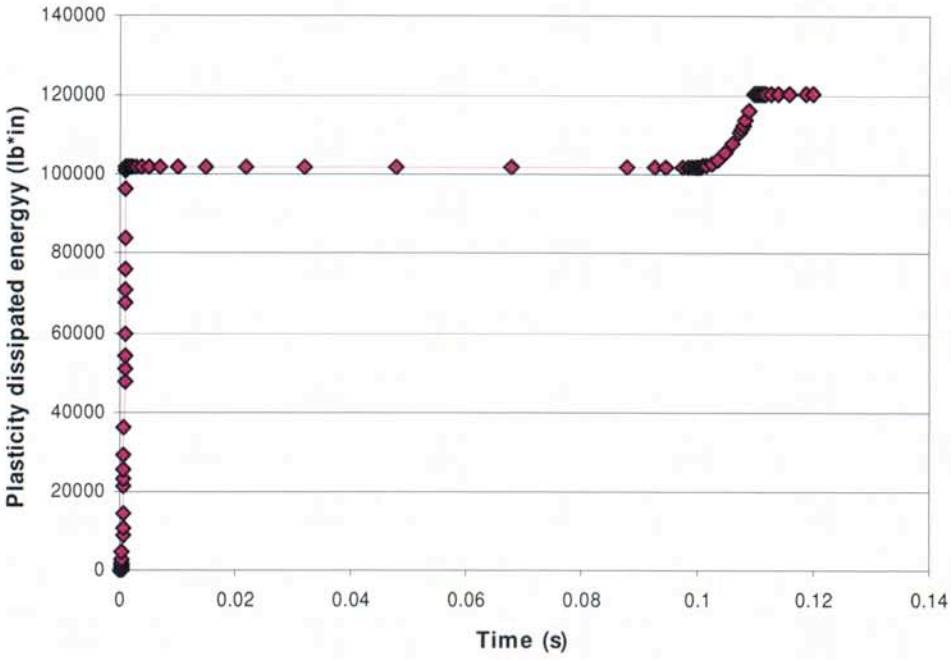

(b) Bridge with intermediate diaphragms at one-third-span (1/3 and 2/3 span)

Figure 32. Plastic energy dissipation of the bridge

4.2 Size of Intermediate Diaphragms

The effect of height and thickness of the intermediate diaphragms (IDs), such as partial height vs. full height of ID and 8 in. vs 12 in. thickness of ID, are studied. The cases of different ID thickness with different ID depth are simulated. The impact load is applied at the middle location of the bridge span of 50 ft. and acted on the bottom flange of the girder, and only the case with the IDs at the mid-span is simulated.

4.2.1 Effect of thickness of intermediate diaphragms

The effect of thickness of intermediate diaphragm (ID) on the impact response of bridges is first addressed, and two different thicknesses of ID (i.e., 8 in. vs. 12 in.) with full depth (i.e., the depth of ID to the top edge of bottom flange, see Figure 3) are considered and compared. The numerical results are summarized in Tables 5 and 6, for the full design (120 kips) and one half design (60 kips) loads, respectively.

Table 5. Effect of thickness of intermediate diaphragms under full design load

Thickness of IDs	Totally damaged area (in^2)	Maximal horizontal displacement (in.)	Maximal vertical displacement (in.)	Maximal Principal strain	Maximal tensile stress (psi)	Maximal plastic dissipative energy (lbs-in)
No IDs	> 700.00	> 8.800	> 6.000	> 0.0530	> 518.1	> 400,000.0
8 in. thick	26.25	0.56612	0.4187	0.03553	524.4	15,955.7
12 in. thick (not convergent)	22.50	0.23773	0.2401	0.01520	534.9	Not-recorded

Note: Element size is approximated about 1.25 in^2 each for the impacted area of the girder. For the 12 in. thick ID case, the analysis is not converged due to large distortion of some elements. So the results in this case cannot be taken into consideration.

Table 6. Effect of thickness of intermediate diaphragms under half design load

Thickness of IDs	Totally damaged area (in^2)	Maximal horizontal displacement (in.)	Maximal vertical displacement (in.)	Maximal Principal strain	Maximal tensile stress (psi)	Maximal plastic dissipative energy (lbs-in)
8 in. thick	2.5	0.16913	0.1326	0.0001844	530.0	507.272
12 in. thick	2.5	0.16397	0.1213	0.0001817	528.9	251.808

Note: The size of elements is about 1.25 in^2.

In the numerical analysis, the 12 in. thick ID case under the full design load of 120 kips is not convergent due to large local distortion of some elements. When the load is reduced by a half, the convergence is reached for both of the cases (i.e., 8 in. and 12 in. IDs, see Table 6), the damage area is reduced considerably (from about over 20 in^2 to 2.5 in^2) from the full to a half design load.

From Table 5, it is observed that even though the 12 in. thick ID case under full design load is not convergent due to large local distortion of some elements, it still shows that the larger thickness of ID increases the stiffness of the bridge system, leading to less maximal horizontal and vertical displacement at reduced strain. The total damage area is also reduced. However, the effect of increasing thickness of ID is not obvious based on the results of bridge system under a half design load (See Table 6).

Based on the results in Table 6, under a half design load, the bridge with 12 in. thickness ID endures a 3% less horizontal displacement and a 9.3% less vertical displacement. Both the damaged elements and plastic dissipated energy are significantly reduced. Please note that the totally-damaged area is different from the damaged elements defined (partially damaged). The damaged elements in this study are associated with the elements with the plastic dissipative energy, and more damaged elements mean more plastic energy dissipated in the system.

The failure patterns of the bridges with 8 in and 12 in thick IDs are shown in Figure 33(a) and 33(b), respectively. The spalling damage near the bottom flange of the girder at the load applied location is observed for both the cases. Similar damage scenario is observed in the actual bridge (see Figure 33(c)). The side view of bridge (along the span length direction) is shown in Figure 34, and both the tensile failure of the girder in the face opposite to the loading applied front and the compression failure of the ID between the 1st and 2nd girders are observed. A field photo (Figure 34(c)) also shows the tensile failure at the bottom flange on the back of the girder, though the impact load was not exactly applied at the location of ID.

For the case of the bridge without the intermediate diaphragms (IDs), the bridge is not capable of sustaining the full design load, and large areas of damage are observed (see Table 5). All the numerical analysis results for the bridges without the intermediate diaphragms (IDs) are presented in Appendix H. As a comparison, the case of the bridge of 6 ft. girder spacing with the IDs at the mid-span is also given in Appendix H. As demonstrated in the figures of Appendix H and comparisons of the two cases (i.e., with and without IDs), a significantly large damage area is induced for the bridge without IDs.

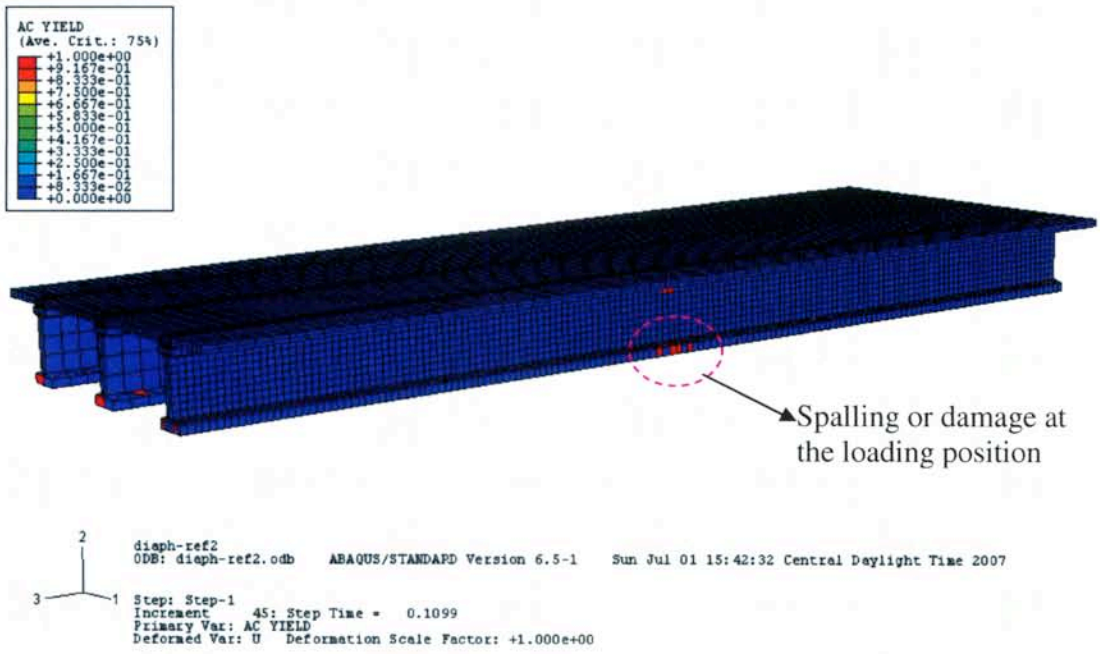

(a) 8 in. thick intermediate diaphragm

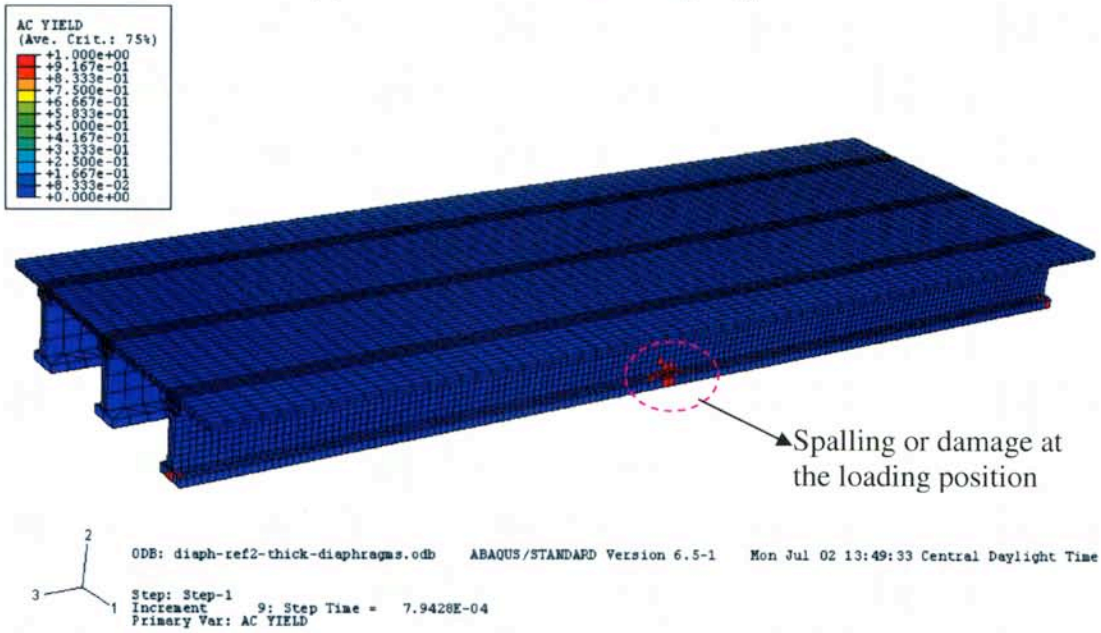

(b) 12 in. thick intermediate diaphragm

(c) Comparison with the observation from the real scenario – spallation of front faces at the bottom of girders

Figure 33. Front view of failure pattern in the girder bridge system

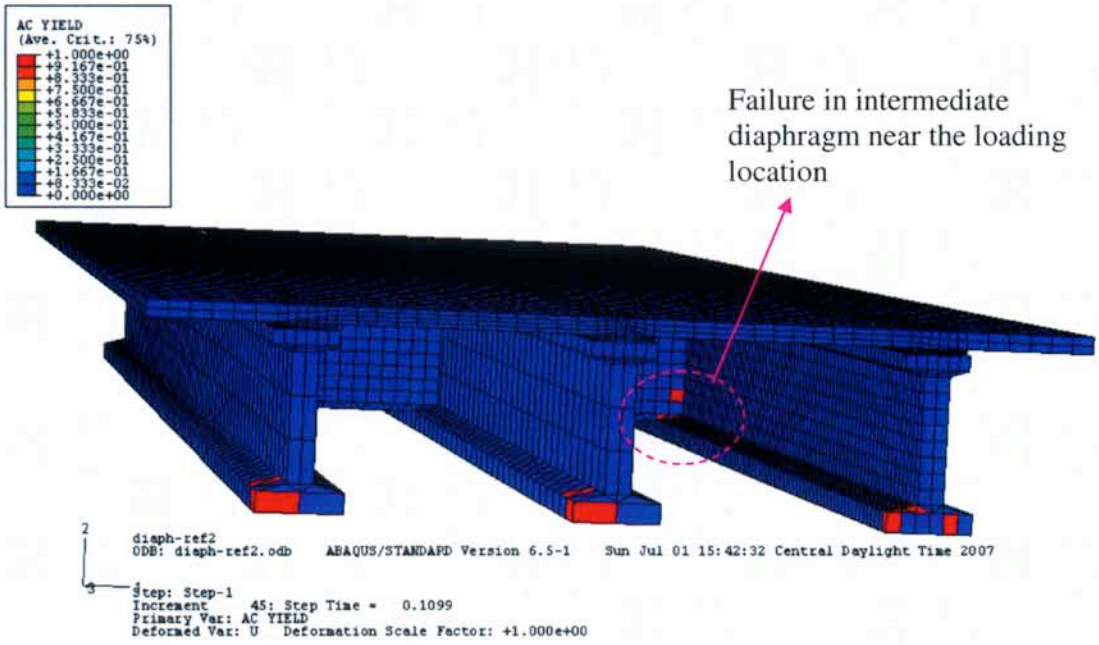

(a) 8 in. thick intermediate diaphragms

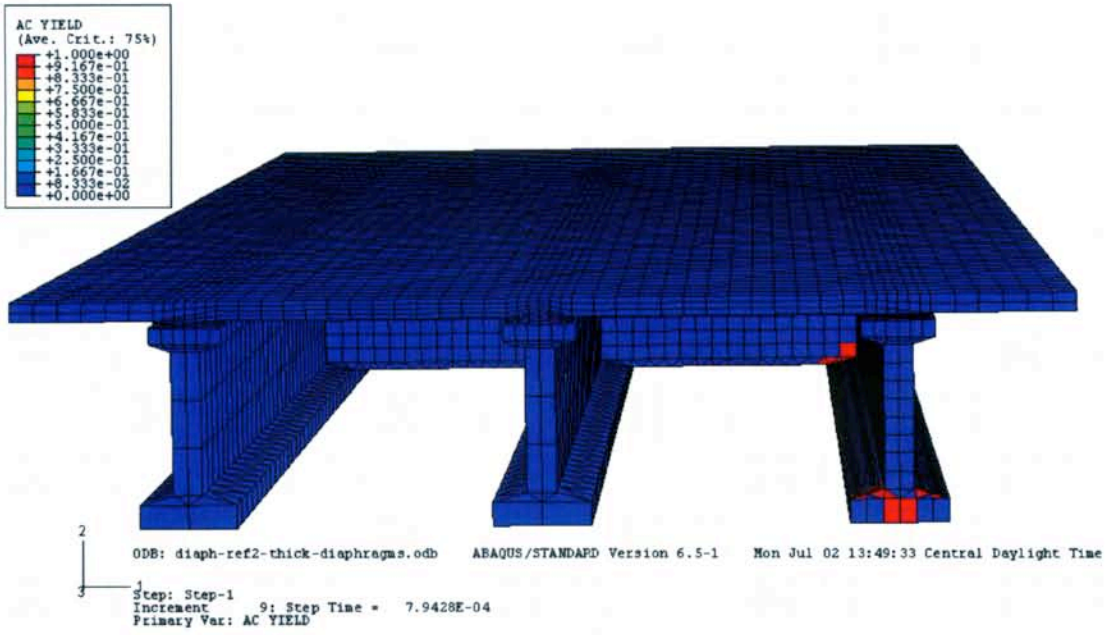

(b) 12 in. thick intermediate diaphragms

(c) Comparison with the real scenario (as shown in the photo, the impact loading position is a little bit away from the intermediate diaphragm, and a small area of the tensile failure developed on the back face of the girder flange, the same as showed in the simulation plots of (a) and (b))

Figure 34. Side view of failure pattern in the girder bridge system with failure developed in the intermediate diaphragm near the loading location

All the numerical analysis results with respect to two different thicknesses of IDs are provided in Appendix B. Both the von Mises and longitudinal stress distributions for the two cases of 8 in. vs. 12 in. thick IDs are presented in Figure B1 and B2, respectively, and the stress distributions in the two cases are in comparative ranges with the 12" thick ID showing a little large stress concentration at the loading point, due to increased local stiffness. The transverse (horizontal) displacement distribution along the long span bridge with a large displacement observed at the loading area is shown in Figure B3, and a larger transverse displacement is induced in the bridge girder with 8 in thick ID. Similarly, a larger vertical displacement in the bridge girder with 8 in thick ID is observed in Figure B4. The displacement history of the bridge girder with two different thicknesses of IDs is shown in Figure B5, and under the same impact load, the bridge with thicker (12 in.) ID exhibits less deformation and higher stiffness. The strain history under impact load is shown in Figure B6, and due to large distortion of some element in the bridge system with 12 in. thick ID, the numerical analysis is not converged.

The failure areas in term of failed elements (red colored) are illustrated in Figure B7, and only small areas of damage around 26 in^2 and 23 in^2 for the respective 8 in. and 12 in. thick IDs are observed. Again, the displacement and strain at the loading point are shown in Figures B8 and B9, respectively. Though no major difference of deformation within two ID thicknesses, the bridge with 8 in. thick ID shows a slight larger displacement and strain. Please note that the strains in Figures B6 and B9 are for the full design and the half load, respectively. The plastically dissipated energy is shown in Figure B10, and the bridge with the 8 in. thick ID dissipates more plastic energy leading to more damage in the system.

As expected, the bridge with a thicker ID lead to high stiffness and reduced deformation in the system. However, the performance differences between two thickness of ID are not apparent (see Tables 5 and 6), particularly for the case of one half design load, which means that the thickness of ID is not a sensitive factor considerably influencing the impact behavior of the bridge.

4.2.2 Effect of depth of intermediate diaphragms

In order to analyze the depth effect of intermediate diaphragms (IDs) on the impact response of the bridge, three different cases with the ID thickness of 8 in. under a full design load of Figure 3 are analyzed, and they correspond to (1) the full depth case (to the top edge of bottom flange, Figure 35(a)), (2) partial depth case (to the bottom of web, Figure 35(b)) and (3) the almost half depth case (to 2/3 web depth, Figure 35(c)). The numerical results of the analysis for the three cases are shown in Table 7.

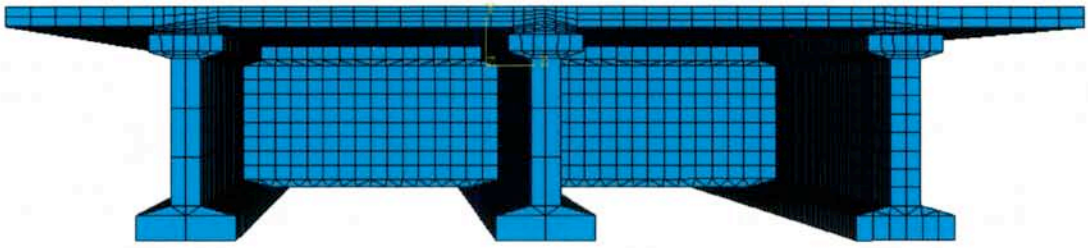

(a) Full depth of IDs (to the top edge of bottom flange)

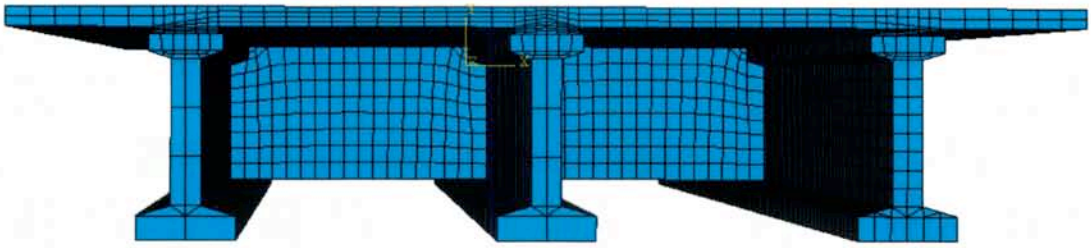

(b) Partial depth of IDs (to the bottom of web)

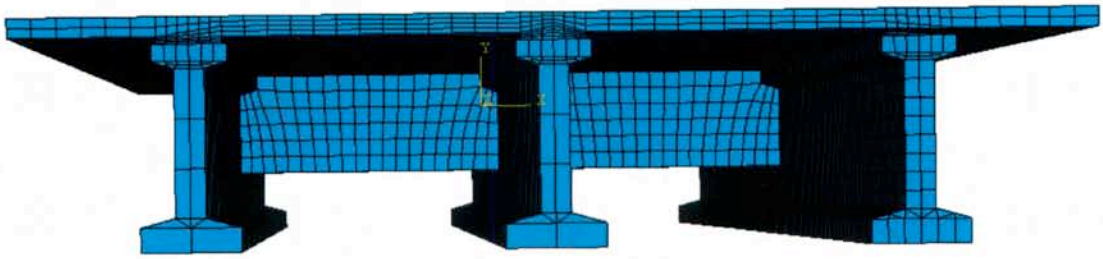

(c) Partial depth of diaphragms (to the 2/3 depth of web)

Figure 35. Side view of the bridge system showing different depths of IDs

Table 7. Effect of depth of intermediate diaphragms

Depth of IDs	Totally damaged area (in^2)	Maximal horizontal displacement (in.)	Maximal vertical displacement (in.)	Maximal Principal strain	Maximal tensile stress (psi)	Maximal plastic dissipative energy (lbs-in)
No IDs	> 700.00	> 8.800	> 6.000	> 0.0530	> 518.1	> 400,000.0
Full	26.25	0.56612	0.4187	0.0071376	524.4	15,955.7
Partial	50.00	0.56928	0.6991	0.0083508	528.5	26,268.5
2/3 web	> 625.00	8.2560 in.	5.4220 in.	0.0483	518.0	400,000.0

The full design load is applied. The plastic dissipative energy is described as the dissipated energy through damage or failure of elements, including partially damaged elements. More plastic dissipative energy means more damage developed in the bridge.

In Table 7, it is observed that the depth of ID has a great influence on the maximal horizontal displacement and the maximal vertical displacement. The large deformation in the bridge with reduced ID depth is primarily caused by the increased rotation of bottom girder flange. Reducing depth of ID increases the plastic dissipative energy significantly, which means more damage to the bridge system in order to generate the dissipated energy.

Different from the effect of the thickness of IDs, the influence of the depth of ID is quite pronounced (see Table 7), and the shallower of the ID depth, the more vulnerable (more induced damage) the system becomes, due to relatively large deformation and rotation of the girder associated with a shallower depth of ID. As demonstrated in Figures 36 to 37, the respective horizontal (transverse) displacement, longitudinal strains, and plastically-dissipated energy are significantly increased for the case of a shallow (partial) depth of ID (i.e., 2/3 web depth). Thus, a full depth of ID is recommended to maximize the impact resistance.

All the additional numerical analysis data related to the effect of ID depth of partial and 2/3 web cases are given in Appendix C; while the data in Appendix B is related to analysis of the ID with full depth. The failure elements are shown in Figures B1, B2, C1 and C2, for the three cases, and the failure area are increased due to the decreased depth of IDs (a decreased depth means that the diaphragm depth decreases from the full depth (to the top of bottom flange), to the bottom of web, eventually to the 2/3 web depth). The von Mises and longitudinal stress distributions are shown in Figures C3 and C4, respectively. The horizontal (transverse) and vertical displacement distributions of the bridge system are shown in Figures C5 and C6, respectively. The comparisons of the maximum horizontal (transverse) displacement and longitudinal strain for the cases of full and partial ID depth are provided in Figures C7 and C8, respectively, showing the enlarged deformation with the partial ID depth case. The plastically dissipated energy in the partial ID depth is also larger than the one of the full depth (Figure C9), indicating more failure-dissipated energy associated with the case of partial ID depth and more vulnerable of the system under impact.

Again for the case of the bridge without the intermediate diaphragms (IDs), similar conclusions are reached for the case of the effect of ID depth (see Table 7). The bridge without IDs is not capable of sustaining the full design load, and large areas of damage are induced (see Table 7). All the numerical analysis results for the bridges without the intermediate diaphragms (IDs) are presented in Appendix H.

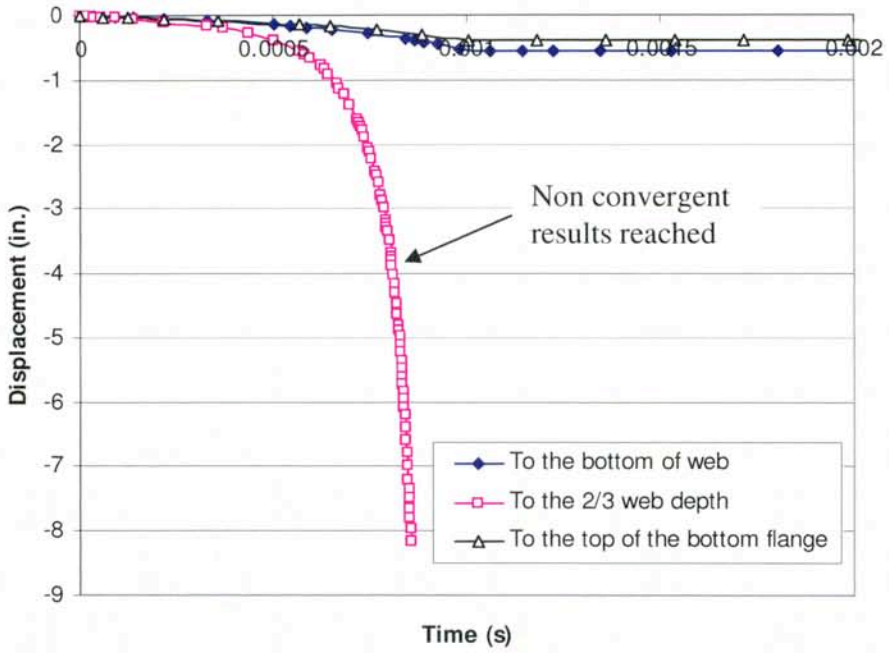

Figure 36. Effect of depth of ID on the horizontal displacement at the loading point

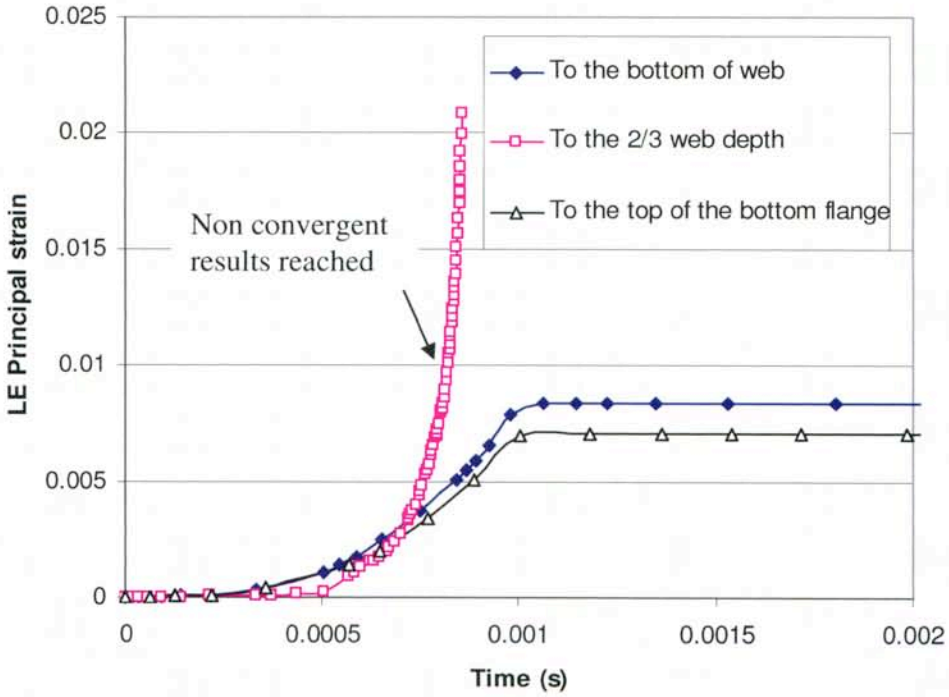

Figure 37. Effect of depth of ID on the maximal principal strain at the loading point

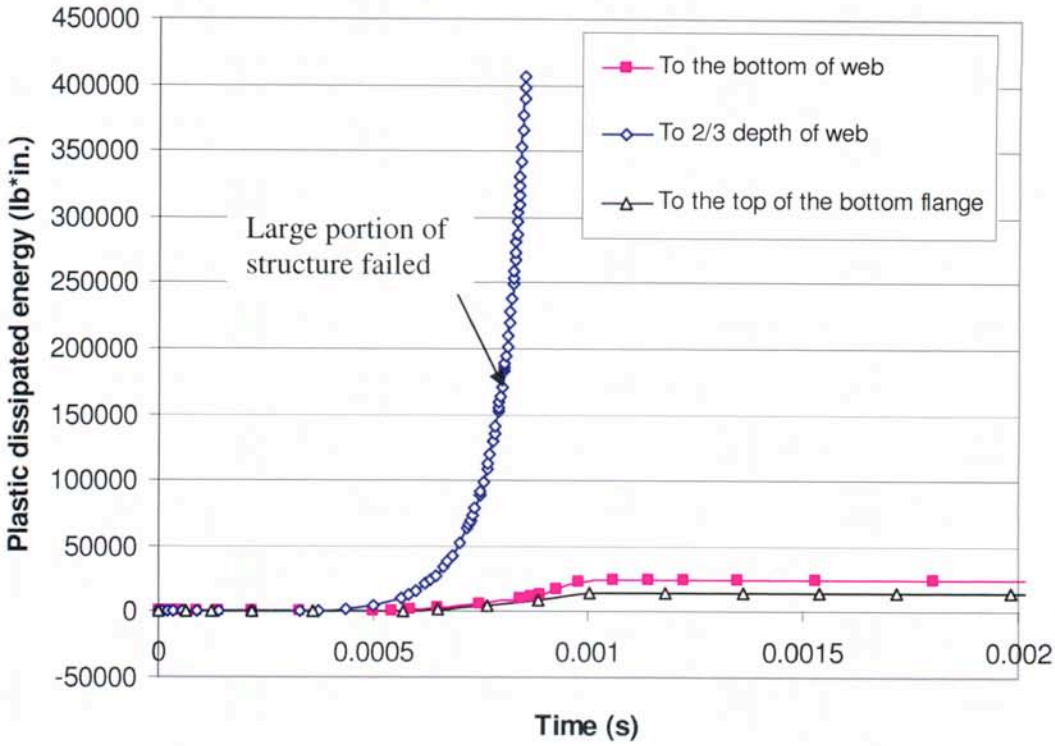

Figure 38. Effect of depth of ID on the plastically dissipated energy (failure-dissipated energy)

4.2.3 Summery on size effect of intermediate diaphragms

In summary, both the thickness and depth of the IDs have some effect on the impact protection of the PC girder bridge from impact. The effect of thickness (e.g., in the cases of 8" vs. 12" thicknesses) to impact protection is not significant, and thus a moderate thick ID (e.g., 8") is adequate. The thickness of ID is primarily associated with the axial stiffness of the ID, and the ID is usually under axial loading during the horizontal impact event to transfer the load to the adjacent girder. The increase of the axial stiffness could also be realized by adding more steel reinforcement. Thus, based on the thickness effect analysis, it may be concluded that the axial stiffness of ID does not much influence the capacity of ID in impact protection. On the other hand, the effect of depth of ID on impact protection is quite detrimental: the deeper the ID, the less rotation of the girder and the better the impact protection to the bridge system. It thus recommends that a full-depth ID should be implemented in the construction to maximize the capacity of ID in the impact protection.

4.3 Girder Spacing

Girder spacing is also a very important parameter when designing and implementing the intermediate diaphragms (IDs) in the bridge construction. In this section, for a bridge of 50 ft. span and considering one diaphragm at 1/2 span, the cases of different girder spacing are evaluated.

The bridge with a girder spacing of 8 ft. and 10 ft. is modeled. A summary of the analysis for the two cases of 8 ft and 10 ft girder spacing is given in Table 8. Comparing the results from the cases of 8 ft and 10 ft girder spacing, the case of 10 ft. girder spacing generates more failed elements and spread the energy dissipation into large areas. As aforementioned, the plastic dissipative energy combines all the energy dissipation from the total damaged elements and partially damaged elements, and the maximal plastically-dissipated energy between two cases is almost identical (see Figure 39). All the numerical analysis data for the study of girder spacing are included in Appendix D. The maximal horizontal (Figure D1) and vertical (Figure D2) displacements are increased more as well for the 10 ft. girder spacing than the ones with the 8 ft. girder case. The longitudinal plastic strain history is presented in Figure D3; while the transverse plastic strain history is given in Figure D4. In the plastic strains, both the cases show similar longitudinal plastic strain, but the front girder with 8 ft. girder spacing shows a significantly larger transverse plastic strain, depicting the strengthened effect of the shorter girder spacing. The von Mises stress distributions are plotted in Figure D5, and the similar results exhibit for the two cases of girder spacing. The damaged areas (elements) are shown in Figure D6. The transverse and longitudinal stress distributions are presented in Figures D7 and D8, respectively, and as expected, the narrower girder spacing of 8 ft. produces a better load transfer to the adjacent girders (see Figure D8(a)). The displacements along the horizontal (transverse) and vertical directions are shown in Figures D9 and D10, respectively. The transverse and longitudinal plastic strains are given in Figures D11 and D12, respectively, demonstrating the plastic strains concentrated around the loading point. In general, the girder spacing introduces 20 to 30% difference in terms of deflection and strain. The smaller the girder spacing, the less the deflection, displacement and plastic strain will be generated.

Also as shown in Table 8, with a lesser girder spacing (e.g., the 6 ft. or 8 ft. spacing), the maximal horizontal and vertical displacements are reduced. While the total damaged area and stress distributions become more complex due to the strengthening effect of closely spaced intermediate diaphragms, which could lead to increased damage areas and energy dissipation. In general, the close spacing of girders is beneficial in controlling deformation; however the stress distributions are much more complicated. Fortunately, all the bridges are designed to perform in elastic range. In the elastic range, the displacement has a direct proportion to the stress. Thus, when displacements are controlled, the stresses will be controlled as well.

The same situation is applicable to bridges with end intermediate diaphragms. The end intermediate diaphragms (IDs) as shown in most of existing bridge construction in the state of Washington reduce the displacements (see Table 8). But the end ID effect

(i.e., with and without end IDs) is not significant. In term of reduced damage with respect to the end IDs, it will more depend on the layout of bridges, loading applied position, and other factors.

All the numerical results for the bridge of 12 ft. girder spacing with and without the end intermediate diaphragms (IDs) are provided in Appendix I. In both the case of with and without the end IDs, the IDs are provided in the central span and at the location of applied load.

In summary, the girder spacing in the relationship to ID is not a critical factor in the bridge impact resistance (little difference between the total damaged area and the maximal plastic dissipative energy), when the impact load is around the location of ID. The narrower the girder spacing, the shorter the ID, leading to better load transfer of IDs from the girder to the subsequent girder as well as to the bridge deck.

Table 8. Effect of girder spacing under full designed load

Girder spacing	Totally damaged area (in^2)	Maximal horizontal displacement (in.)	Maximal vertical displacement (in.)	Maximal Principal plastic strain	Maximal tensile stress (psi)	Maximal plastic dissipative energy (lbs-in)
No IDs	> 700	> 8.800	> 6.000	> 0.0530	> 518.1	> 400,000.0
6 ft	60	0.256	0.0691	3.97E-3	483.6	14,832.5
8 ft	45	0.298	0.138	1.95E-4	443.8	6245.28
10 ft	48	0.384	0.158	2.08E-4	444.3	6128.29
12 ft	54	0.405	0.181	5.25E-3	460.4	5451.35
12 ft with end IDs	54	0.275	0.169	2.71E-3	395.0	4329.33

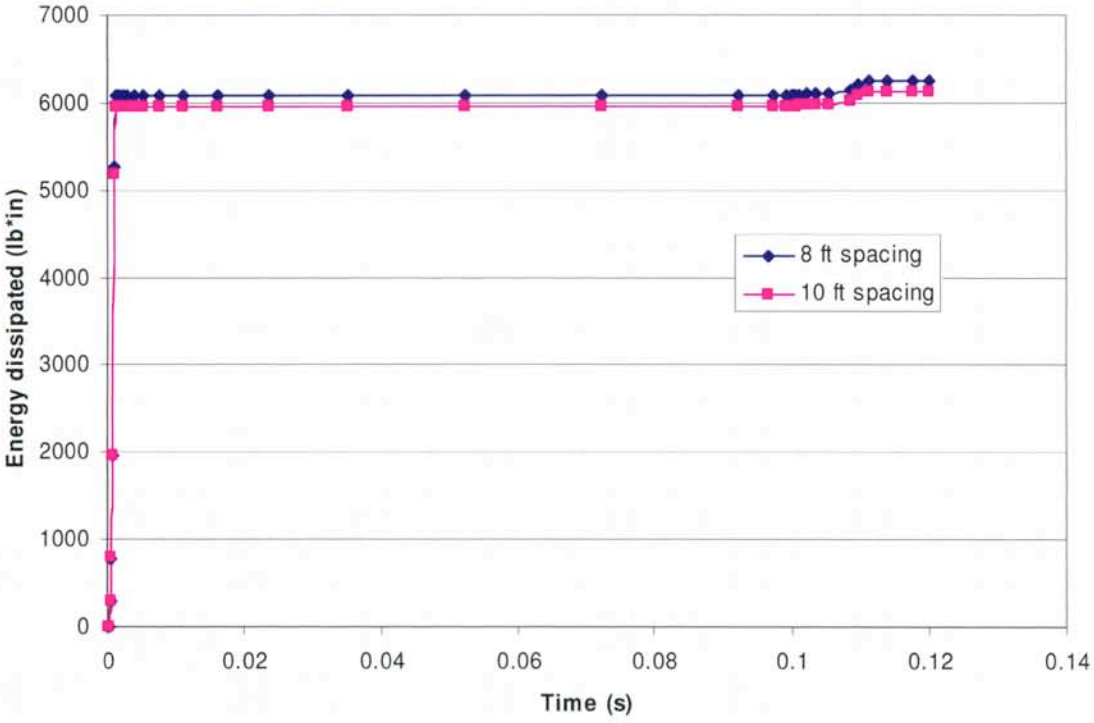

Figure 39. Energy dissipation of the bridges with 8 ft and 10 ft girder spacing

4.4 Girder Types

In this section and Appendix E, the effect of girder types on the responses of bridges under impact is investigated. The bridges with three different girder types of W42G, WF74G and WF42G are simulated, and the effect of flange width (e.g., W42G vs. WF42G and web depth (e.g., WF74G vs. WF42G) are considered. A concentrated impact load is still applied at the mid-span, and the span of 50 ft with a girder spacing of 8 ft. and a full depth ID of 8" thick located at the central span is considered. A summary of comparisons among three types of girders is given in Table 9.

Table 9. Effect of girder types under full designed load

Girder type	Totally damaged area (in^2)	Maximal horizontal displacement (in.)	Maximal vertical displacement (in.)	Maximal Principal plastic strain	Maximal tensile stress (psi)	Maximal plastic dissipative energy (lbs-in)
W42G	45	0.298	0.138	1.95E-4	443.8	6245.28
WF74G	0	0.557	0.312	9.67E-5	481.2	6290.47
WF42G	0	0.352	0.360	5.14E-5	424.5	2365.76

Comparing the results from the cases of different girder types, the case of W42G will generate more failed elements; however WF74G is better in spreading the energy

dissipation into large areas. While the maximal horizontal and vertical displacements are increased for the WF42G and WF74G girder type comparing with the girder case of W42G. In general, the girder types with wider flange will increase the vertical deflection of the deck due to the enhanced coupling between the girders and the deck. Increasing the web height of girders will increase the girder stiffness as well as the total bridge stiffness; however, the local displacement at the loading point is also increased due to the increase of web height.

In particular, the performance parameters of the bridges with the respective WF74G and WF42G girders are analyzed. The plastically-dissipated energy history for WF74G and WF42G girders are shown in Figure 40, and the large web height of WF74G girder dissipates more plastic energy than the small height of WF42G. The horizontal displacement of the bridges with two different girders is shown in Figure 41, and the WF74G exhibits a larger horizontal deformation compared to the WF42G. Similarly, the vertical displacement of the bridges is given in Figure 42, and both the points of the front and back of the bridges are plotted. As expected, due to a large bending stiffness of WF74G, the bridge with WF74G girders shows a smaller downward deflection in the front and upward deflection in the back than its counterpart (WF42G girder). The transverse plastic strain is shown in Figure 43, and due to large deformation induced in WF74G girder, the plastic strain is immediately picked up once the load makes the impact; while it takes time for WF42G to reach the plastic strain owning to its smaller deformation under impact.

All the additional numerical data for the bridge systems with WF74G and WF42G are given in Appendix E for the effect of girder type analysis. The von Mises, transverse, and longitudinal stress distributions are shown in Figures E1 to E3, respectively, and a high stress concentration at the loading point appears in the WF74G girder. The horizontal (transverse) and vertical displacement distributions are plotted in Figures E4 and E5, respectively, and it is shown that a larger horizontal displacement is prompted in the WF74G, due to its deeper web. The maximum principal, transverse, and longitudinal plastic strain distributions are given in Figures E6 to E8, respectively, and a larger plastic strain is shown for the bridge with WF74G girders. Finally, the transverse and longitudinal strain distributions are shown in Figures E9 and E10, respectively, and the strain spreads more around the loading point for the bridge with WF74G girders.

In summary, the girder types have some effect on the impact resistance of the bridge with consideration of IDs. A wider flange of the girder promotes a higher bending stiffness in the horizontal (transverse) direction (i.e., the direction of loading) and thus imparts a better impact resistance. The larger girder with a higher web induces more horizontal deformation, leading to more spread damage on the web.

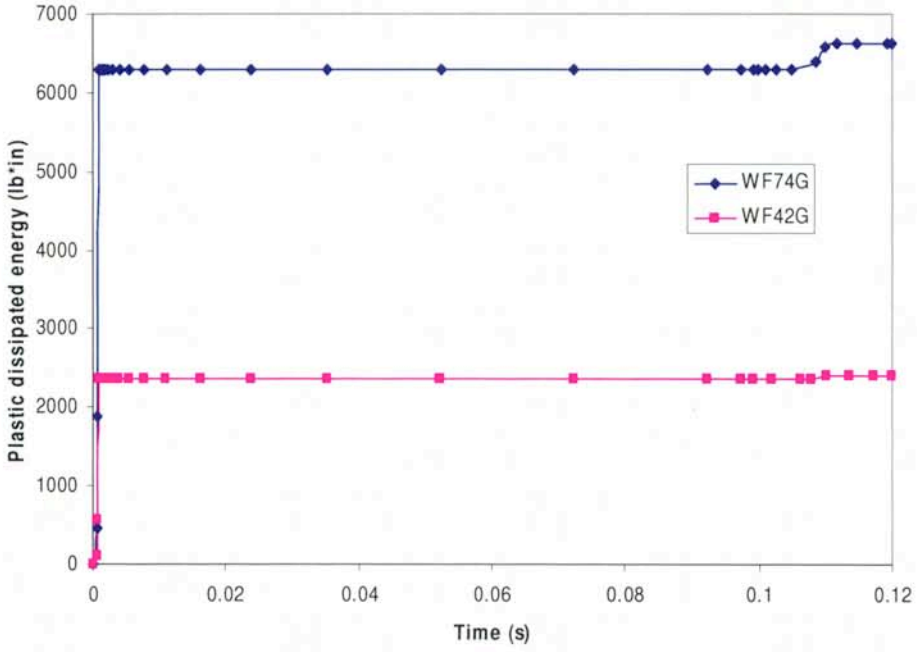

Figure 40. Comparison of plastic dissipated energy

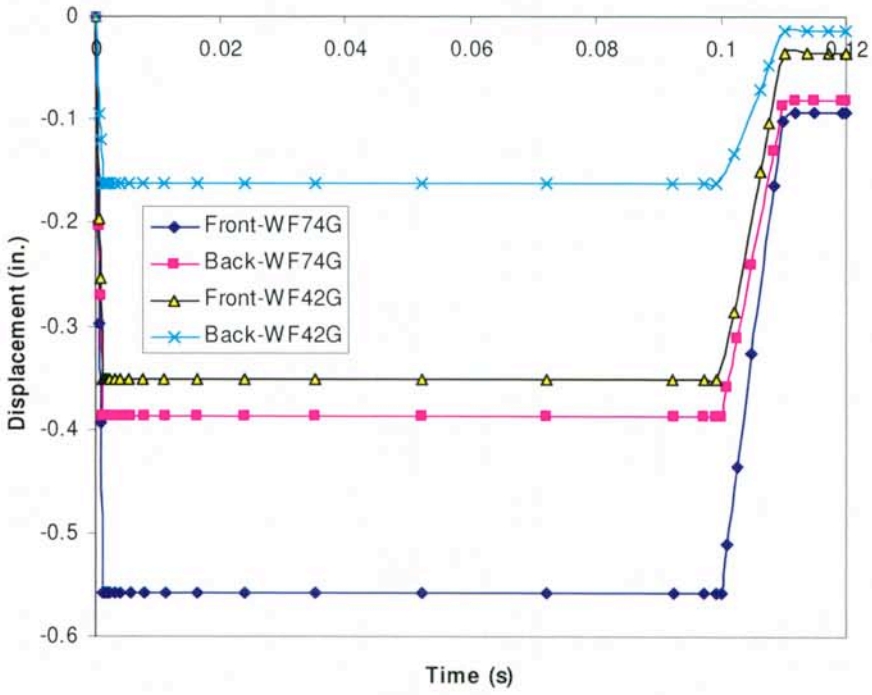

Figure 41. Comparison of horizontal displacement history at the front and back of the bridge girder corresponding to the loading location

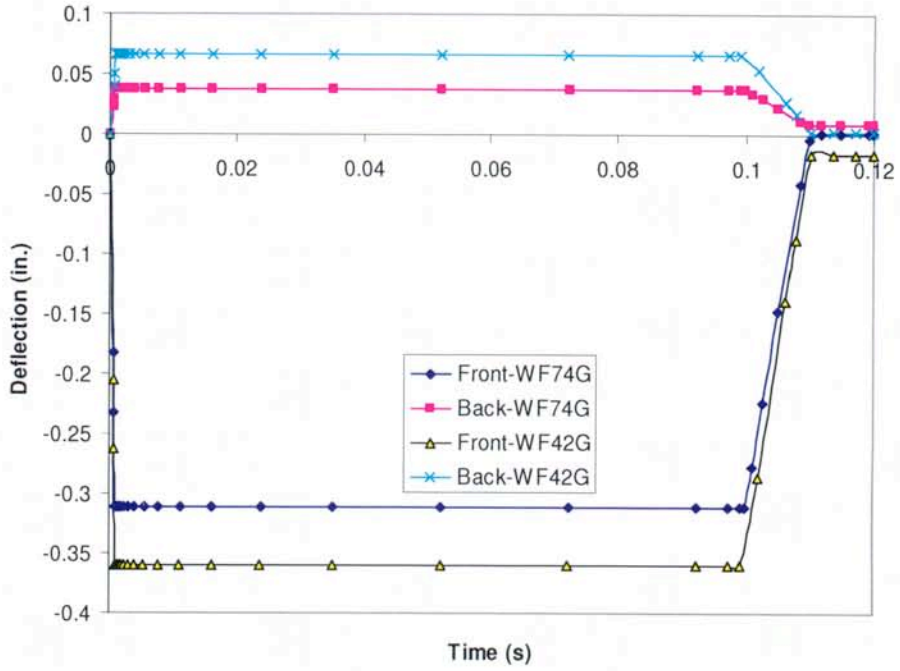

Figure 42. Comparison of vertical deflection history at the front and back of the bridge corresponding to the loading location

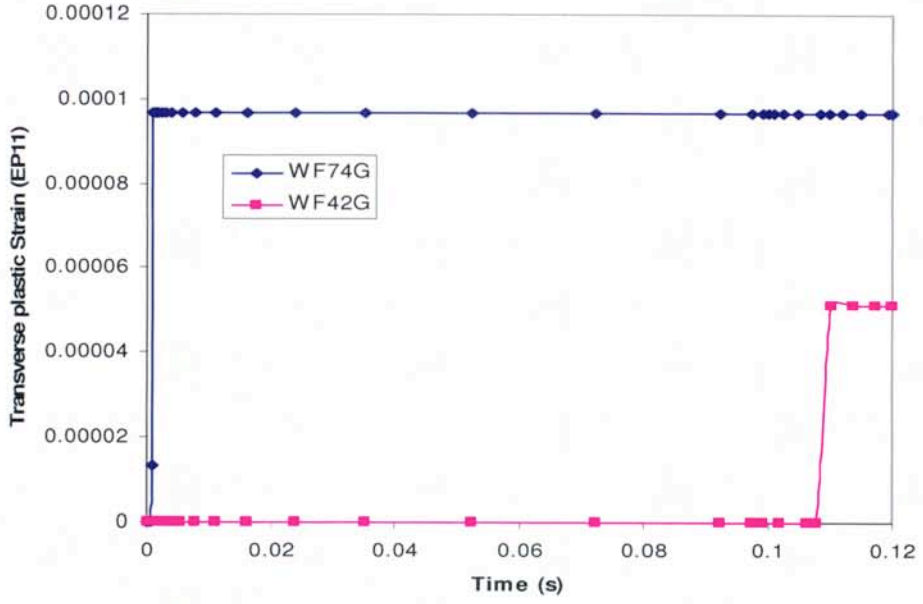

Figure 43. Comparison of transverse plastic strain history at the loading location

4.5 Framing Action: Aspect Ratio

In this section, the effect of framing action is evaluated, and two cases of a simple span bridge are considered and compared: one narrow bridge with 3 girders at 6 ft. spacing, and the other wide bridge with 10 girders at 6 ft. spacing. Apparently, the bridge with more girders is much stronger than that of fewer girders. Under the same impact load, the total damaged area is reduced to zero for the case of wide bridge of 10 girders; while the localized minor damage is induced in the bridge of 3 girders. A summary of the aspect ratio effect in term of narrow (3 girders with L/b = 50 ft/24 ft = 2.08; the width of the bridge = 6 ft x no. of girders + 6 ft) vs. wide (10 girders with L/b = 50/66 = 0.76) is provided in Table 10.

Table 10. Effect of aspect ratio on responses of the simple span bridge

No. of girders and aspect ratio	Totally damaged area (in^2)	Maximal horizontal displacement (in.)	Maximal vertical displacement (in.)	Maximal Principal strain	Maximal tensile stress (psi)	Maximal plastic dissipative energy (lbs-in)
No IDs 3 girders (L/b = 2.08)	> 700	> 8.800	> 6.000	> 0.0530	> 518.1	> 400,000.0
3 girders (L/b = 2.08)	26.25	0.56612	0.4187 in.	0.03553	524.4	15955.7
10 girders (L/b = 0.76)	0	0.04533	0.0036 in.	7.8311e-7	143.8	0.17

Since the data for the bridge of 3 girders is already presented in the previous sections, only the results for the bridge with 10 girders are provided in this section. The plastic dissipative energy history is shown in Figure 44, though only a small amount of plastic energy dissipation is observed. The displacement history at the front and back of the front (1^{st}) girder in the bridge is shown in Figure 45. The von Mises stress distribution is shown in Figure 46, showing a small area of stress concentration around and near the loading point. The horizontal and vertical displacement distribution contours are provided in Figures 47 and 48, respectively, and the only pronounced deformation of the 1^{st} (front) girder in the bridge of 10 girders is observed. The longitudinal and transverse strain distributions are shown in Figures 49 and 50, respectively, and the local concentrated area of strains near the loading point is observed. Different from the bridge with 3 girders, the bridge with 10 girders exhibits a significantly large stiffness in the horizontal direction (i.e., along the loading direction), and the local effect (e.g., the deformation and stress) is very pronounced in the first girders, especially the 1^{st} girder in the front.

As expected, the small aspect ratio (i.e., for the cases with more girders) results in a larger stiffness of the bridge system which is significantly larger than the stiffness of individual girder, leading to pronounced local concentration at the front girder near the loading point. While the bridge with few girders more exhibits a global response (i.e., the front and back girders in the bridge system have comparable deformation magnitude), and the load is better transferred from the front to the back girder with aid of IDs.

In summary, the aspect ratio in term of the number of the girders with an equal spacing in a bridge has a significant effect on the impact resistance of the bridge in association with IDs. The larger the aspect ratio, the more important the IDs in the load transfer and the bridge composite action with the effect of IDs.

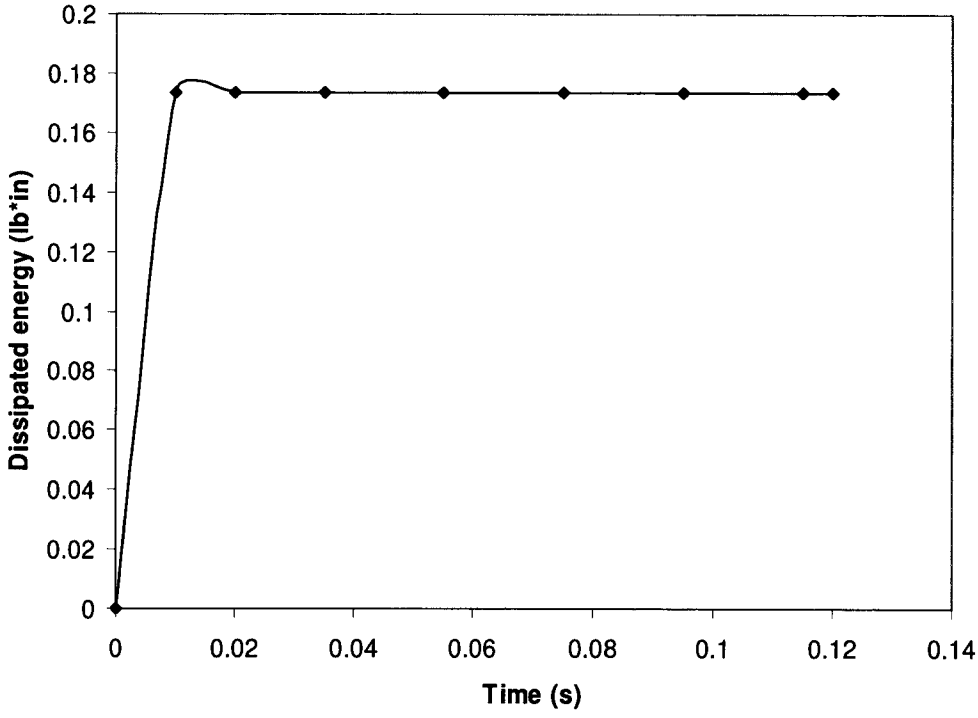

Figure 44. Plastic dissipated energy in the bridge with 10 girders

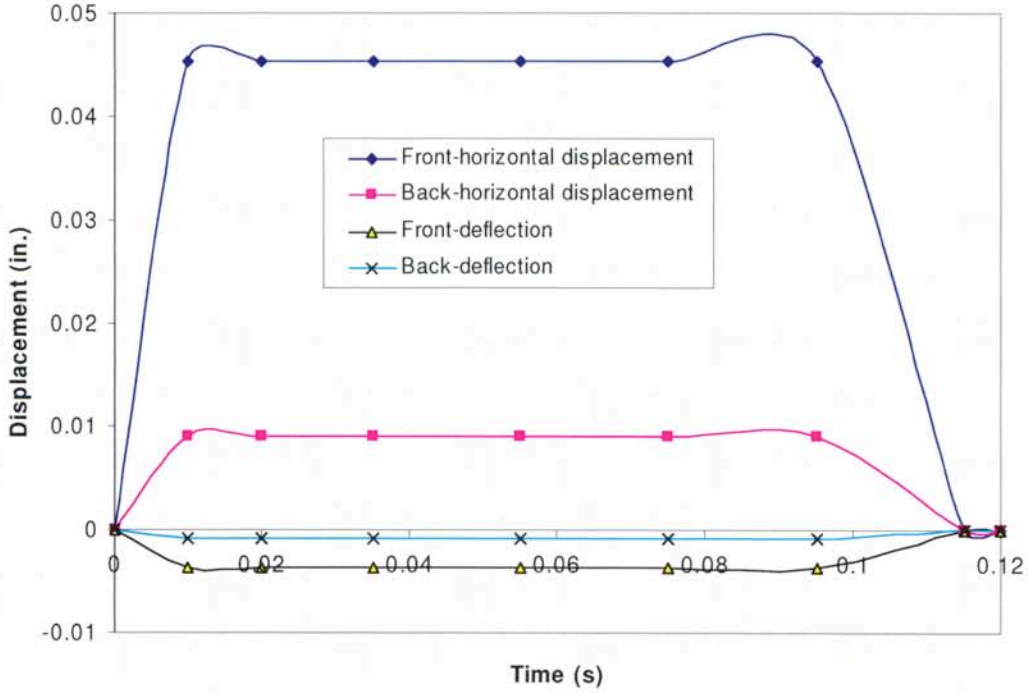

Figure 45. Comparison of horizontal displacement and vertical deflection at the loading point and at the opposite side girder location for the bridge with 10 girders

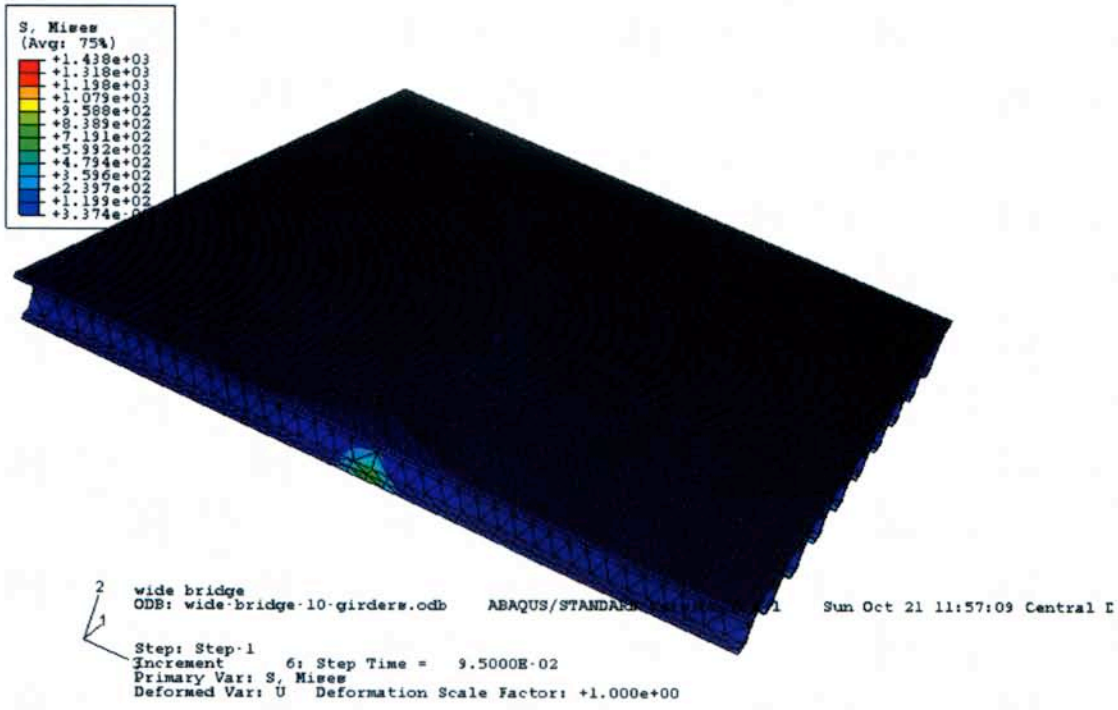

Figure 46. Von Mises stress distribution of the bridge with 10 girders

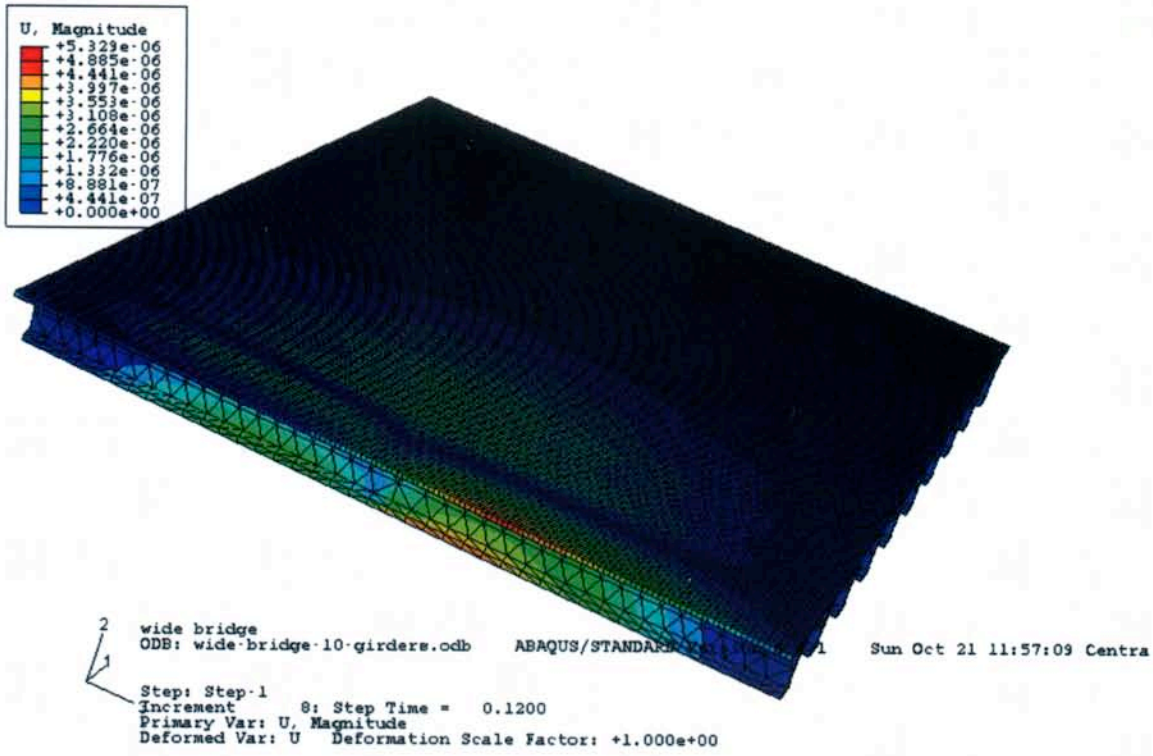

Figure 47. Horizontal displacement distribution for the bridge with 10 girders

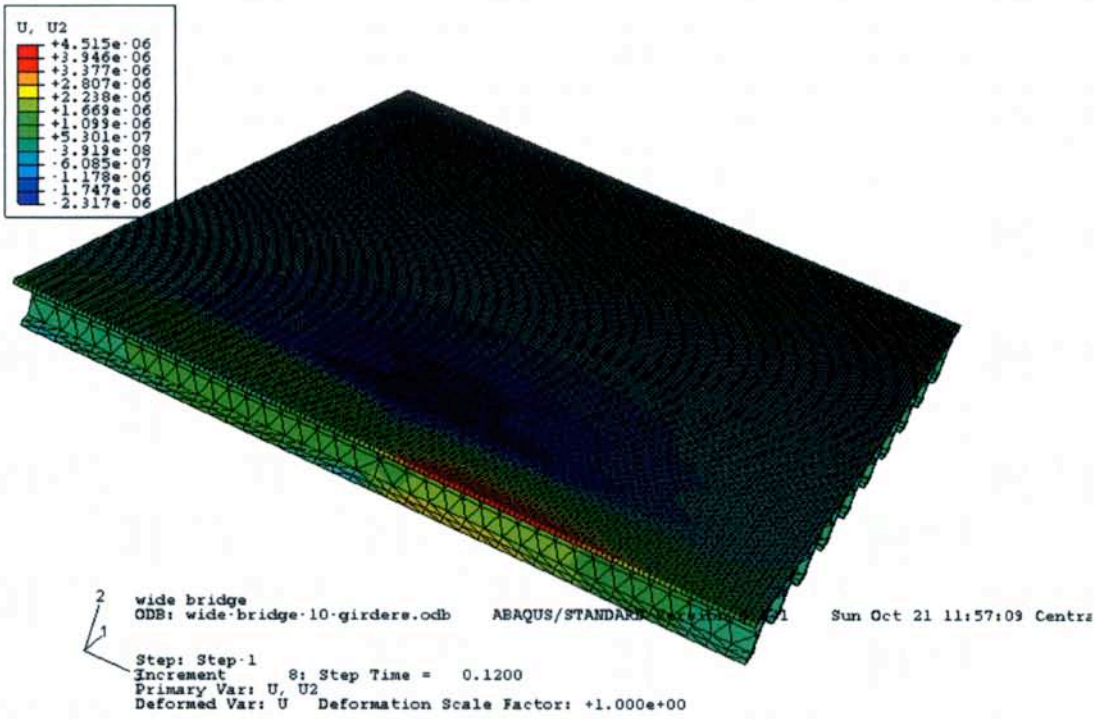

Figure 48. Vertical deflection of the bridge with 10 girders

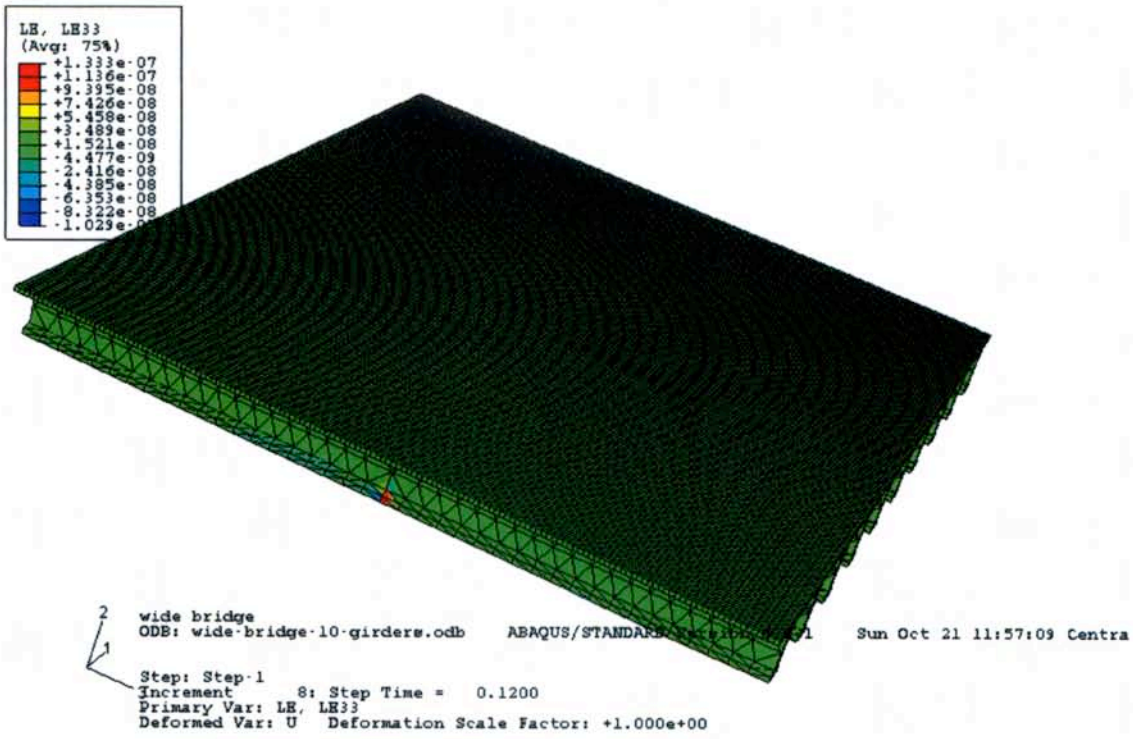

Figure 49. Longitudinal strain distribution of the bridge with 10 girders

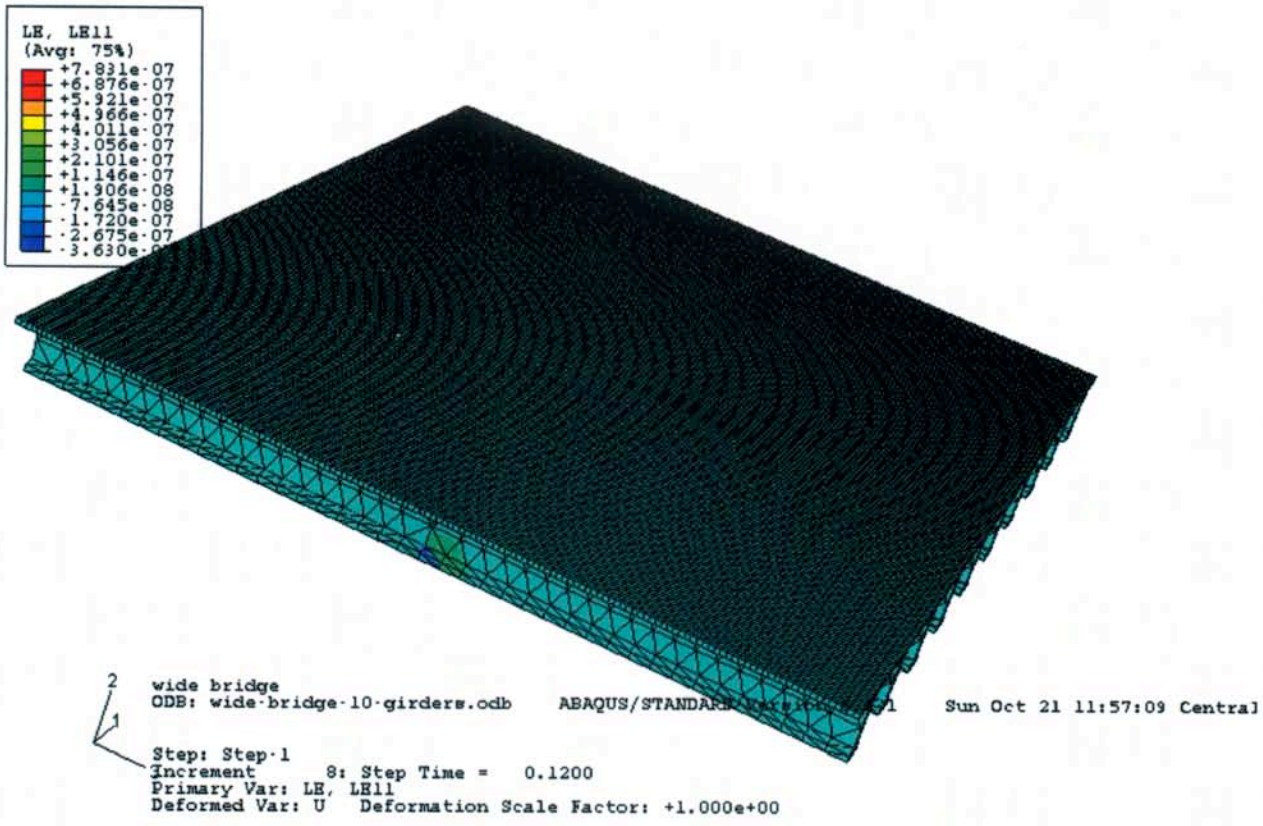

Figure 50. Transverse strain distribution along the loading direction for the bridge with 10 girders

4.6 Impact Types and Contact Interface

Both the impact types (e.g., quasi-static vs. fully dynamic) and contact interface (e.g., concentrated load vs. distributed load) may have some influence on the IDs to promote the impact protection for the bridge girders, and they are hereby evaluated.

4.6.1 Concentrated load vs. distributed load

The effect of concentrated point load vs. distributed wide load on the responses of bridge is analyzed and compared in this section. The bridge with span 100 ft. of three girders with spacing of 6 ft. and two full depth intermediate diaphragms (IDs) at 1/3 and 2/3 with thickness of 8" are considered. The full design load is applied at the mid span, and it is considered as either a concentrated load at one point or a distributed wide load acting over an area of 12 in^2 near the bottom flange of the girder at the mid span.

A summary of the comparison between the concentrated and distributed load cases is provided in Table 11. As expected, the concentrated load case produces more damage to the girder than the one of distributed load, since the bridge and its IDs are better utilized to transfer load when the applied load is more uniformly distributed (spread). More plastic energy is dissipated for the distributed load case (see Figure 51) than the concentrated load one. The horizontal displacement of the front and back sides of the front girder for the two loading cases are shown in Figure 52, and the displacement in the distributed load case is larger than the one with the concentrated load. Also, the difference of deformation between the front and back girders is quite significant, indicating a more pronounced local effect in the front girder. It is primarily caused by the location of the loading which is not directly at the location of the IDs. Thus, the IDs play an important role in transferring the impact load from the front to the back girders and secure a better composite action of the bridge in the horizontal direction (in the direction of impact loading). The longitudinal plastic strain history is shown in Figure 53, and a significantly large plastic strain is present in the case of concentrated load, leading to large plastic dissipative energy.

All the numerical analysis results for the bridge under distributed load case are given in Appendix F. From the results compared with the case of concentrated loading, the case of distributed load generates few failed elements (Figure F1) and spread the energy dissipation into large areas, as shown in the von Mises stress distribution (Figure F2). The longitudinal strain, the transverse and longitudinal plastic strain distributions are presented in Figures F3 to F5, respectively. While the transverse and longitudinal stress distributions are shown in Figures F6 and F7, respectively. Finally, the transverse and vertical displacement distributions are shown in Figures F8 and F9, respectively. The maximal horizontal and vertical displacements are increased for the distributed load comparing with the concentrated loading case, due to the plasticity involved. In general, the loading type introduces 20 to 30% difference in terms of deflection and strain; however, the distributed loading does reduce the total damaged area.

In summary, a concentrated load at a point prompts more damage in the bridge; while a distributed impact load over a certain area better spread the load and results less damage, though it dissipates more plastic energy in the system.

Table 11. Effect of impact loading distribution

Load action type	Totally damaged area (in^2)	Maximal horizontal displacement (in.)	Maximal vertical displacement (in.)	Maximal Principal strain	Maximal tensile stress (psi)	Maximal plastic dissipative energy (lbs-in)
Distributed load	18.0	5.46	1.59	1.44E-4	478.3	143830.0
Concentrated load	180.0	4.38	1.45	9.15E-4	494.0	120663.0

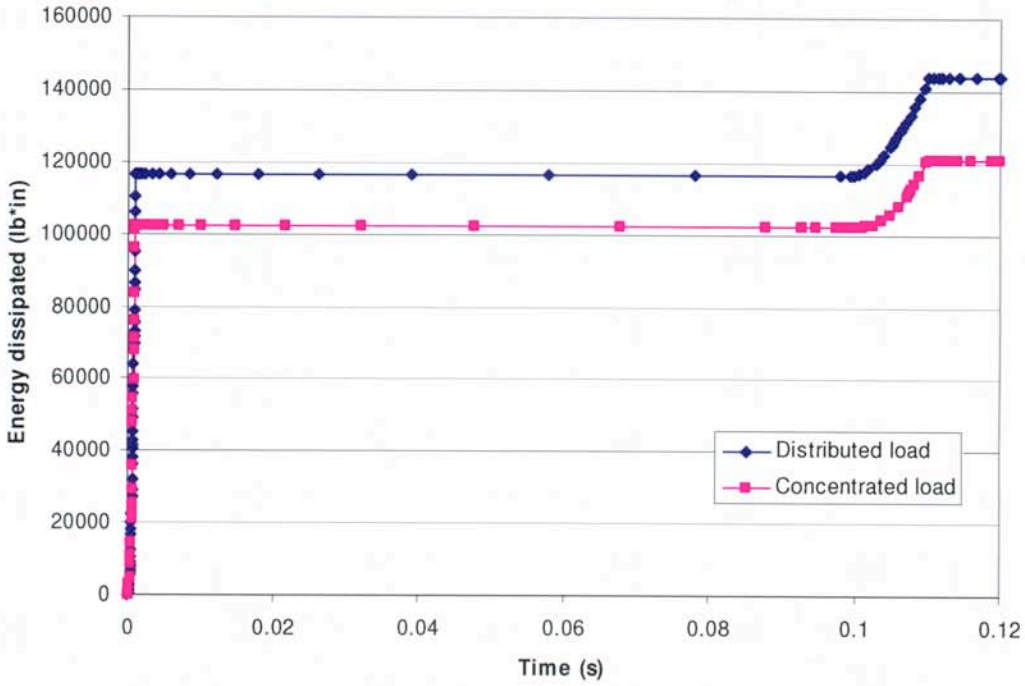

Figure 51. Energy dissipated via the plasticity of concrete

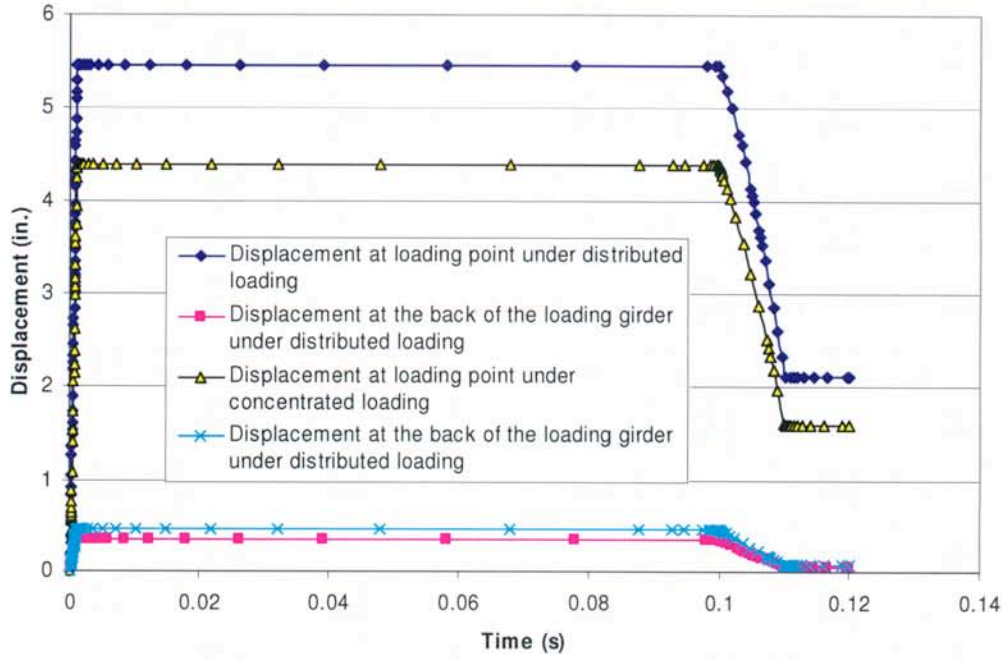

Figure 52. Comparison of horizontal displacement history at the center of loading

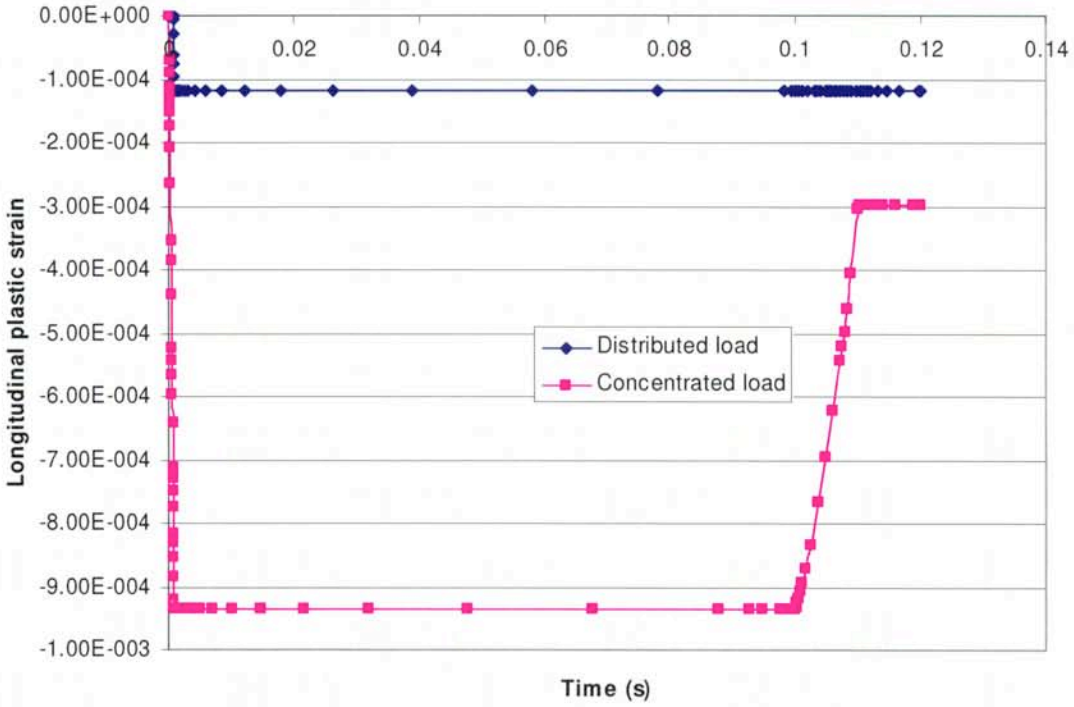

Figure 53. Comparison of longitudinal plastic strain history at the loading location

4.6.2 Dynamic impact load vs. quasi-static load

In all the above analysis, a quasi-static pulse impact load of 0.1-second duration and 120-kips magnitude (considered as a full design load) (see Figure 17) is considered to simulate the impact effect of overheight truck to the birdge. While to better mimic the transient dynamic effect and to capture the effect of inertial mass of the bridge, the explicit simulation of the bridge is adopted. A 150 ft. span bridge with three WF47G girders at 8 ft spacing and with intermediate diaphragms of 8" thick and full depth at quarter (¼) points is considered. A summary of comparison between the dynamic and quasi-static loads is presented in Table 12. As shown in Table 12 and also all the comparisons of dynamic vs. quasi-static impact cases given in Appendix G, the total displacement and strain are reduced with consideration of the mass inertia of the bridge. Using the quasi-static solution only produces the design in the safe side since this case is more conservative. Therefore, the solution based on the quasi-static simulations provides validated results for the impact analysis.

Table 12. Effect of dynamic impact on responses of the simple span bridge

Load type	Totally damaged area (in^2)	Maximal horizontal displacement (in.)	Maximal vertical displacement (in.)	Maximal Principal strain	Maximal tensile stress (psi)	Maximal plastic dissipative energy (lbs-in)
Dynamic	0	1.35	0.75	1.00e-4	482.3	25,000
Quasi-static	16.0	2.62	1.02	1.02e-3	482.3	44,000

The energy components in the dynamic analysis is shown in Figure 54, and the energy conservation is observed, i.e., the external applied work equals to the sum of total kinetic energy, plastically-dissipated energy, and total strain energy. The horizontal and vertical displacement history at the front and back girders at the loading point is shown in Figure 55, and due to the bending effect of the bridge, the front girder is bent downward and the back girder is bent upward, leading to a positive vertical deflection. However, for the horizontal displacement, all the girders are pushed along the loading direction, and the displacements in the front and back girders are all negative. The plastic strain energy is presented in Figure 56, and it is interesting to observe that the horizontal and longitudinal plastic strain at the front and back girders are only produced at a later time of higher loading. In comparison, the damage elements and plastic strain distribution of the bridge under quasi-static load are shown in Figures 57 and 58, respectively.

Additional comparisons between the dynamic and quasi-static analyses are provided in Appendix G. The von Mises, transverse and longitudinal stress distributions are shown in Figures G1 to G3, respectively, and the stress concentration is more pronounced in the quasi-static analysis. While the horizontal and vertical displacement distributions are presented in Figures G4 and G5, respectively, and the deformation produced by the quasi-static analysis is larger than the one in the dynamic analysis. Similarly, the longitudinal strain distribution is shown in Figure G6, and a large strain and its distribution are observed in the quasi-static analysis.

In summary, the quasi-static impact analysis provides conservative results and thus promotes a safer design in all the associated analyses. Though it may deviate from the real dynamic scenario, the quasi-static load provides a simple analysis and more easy-to-interpret results.

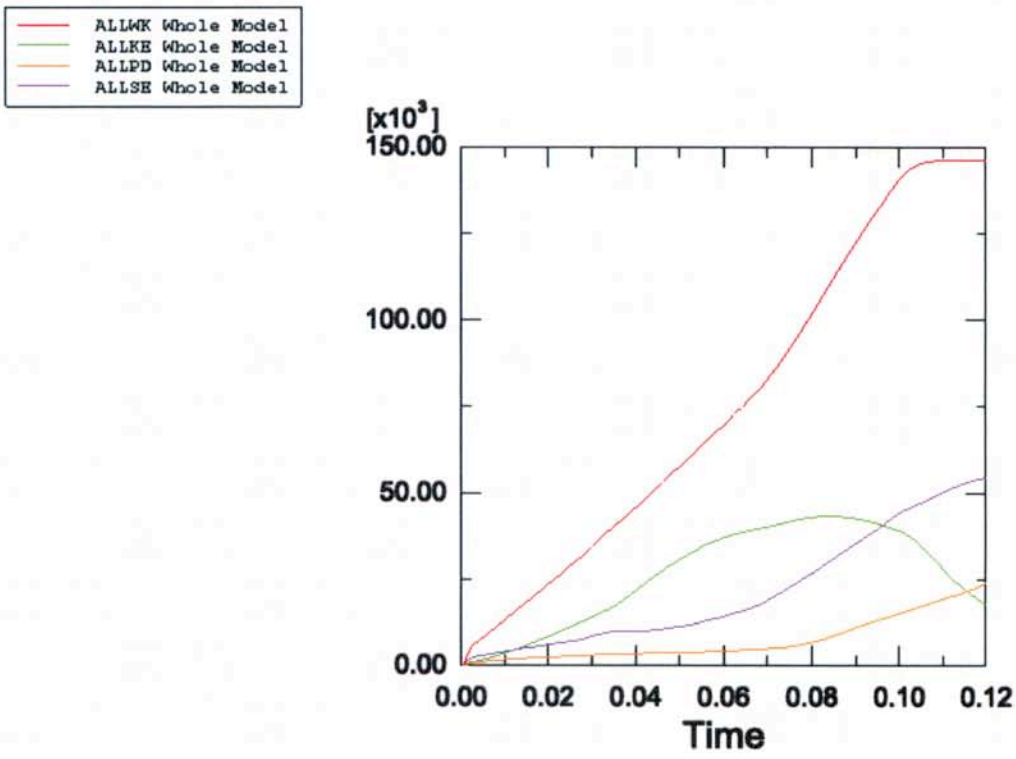

Figure 54. Energy composition of the bridge under dynamic loading case (ALLWK stands for the total external work, ALLKE stands for the total kinetic energy, ALLPD stands for the plastically-dissipated energy and ALLSE stands for the total strain energy)

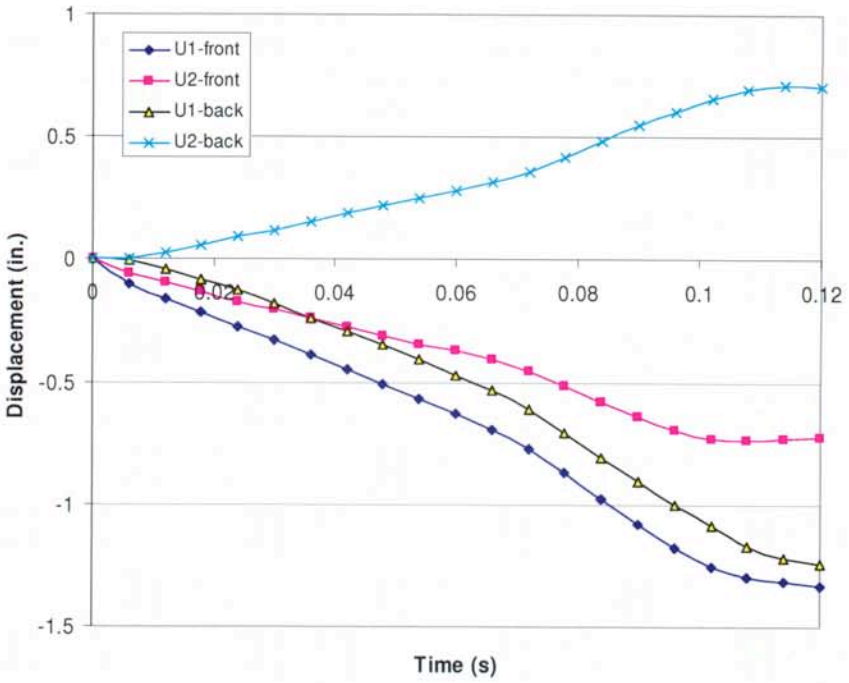

Figure 55. Comparison of all displacements under dynamic loading case (U1 - horizontal displacement, U2 - vertical deflection)

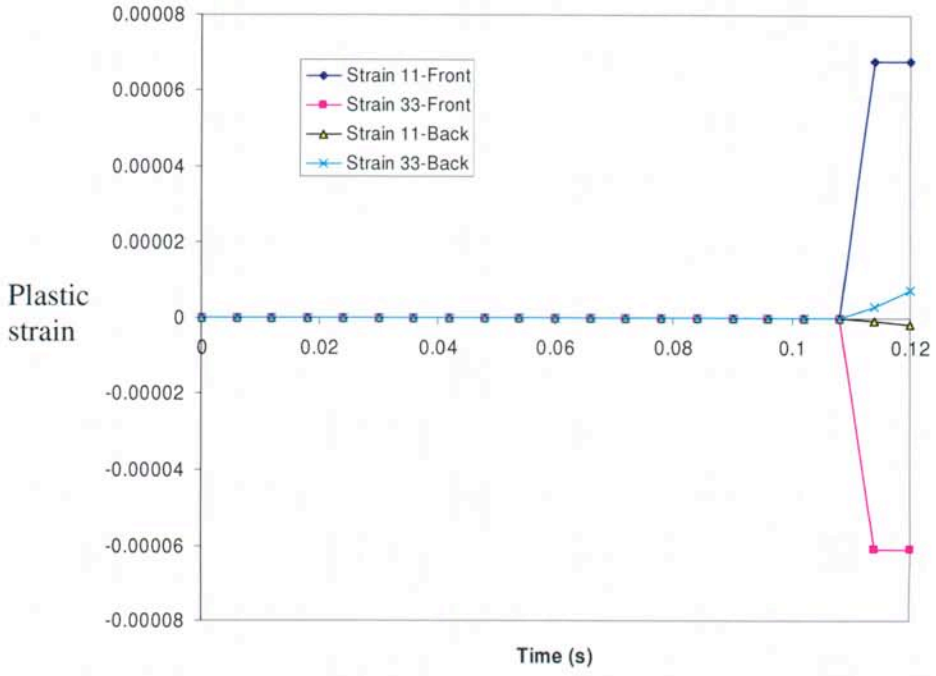

Figure 56. Comparison of plastic strains under dynamic loading case (The plastic strain component 11 (horizontal) and 33 (longitudinal))

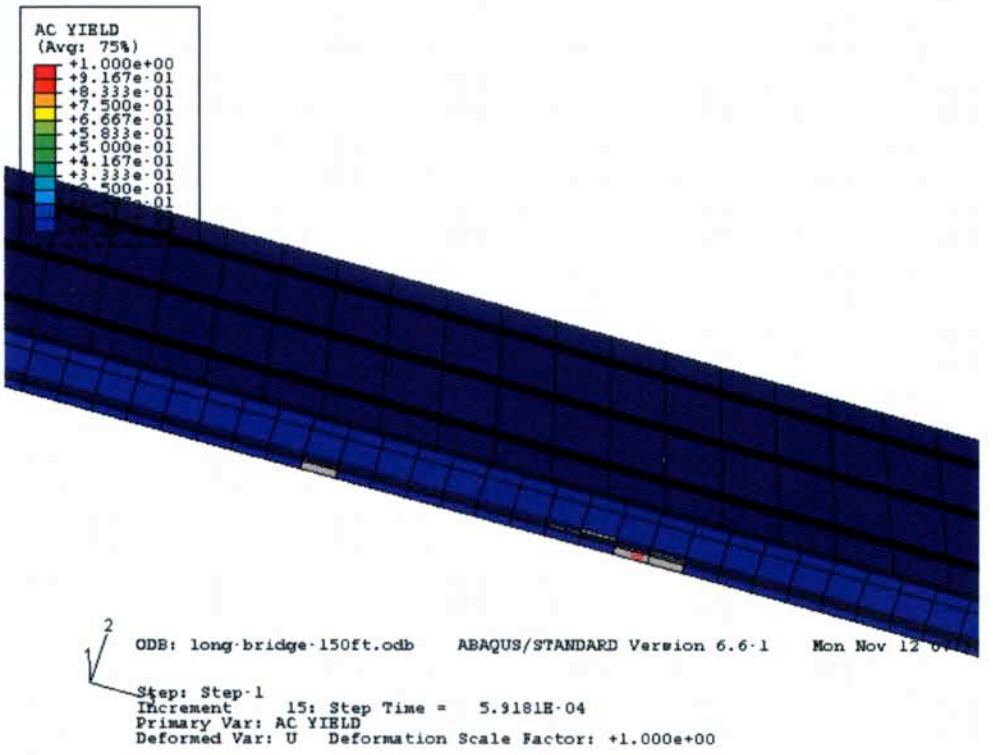

Figure 57. Failed element distribution of the bridge under quasi-static loading case

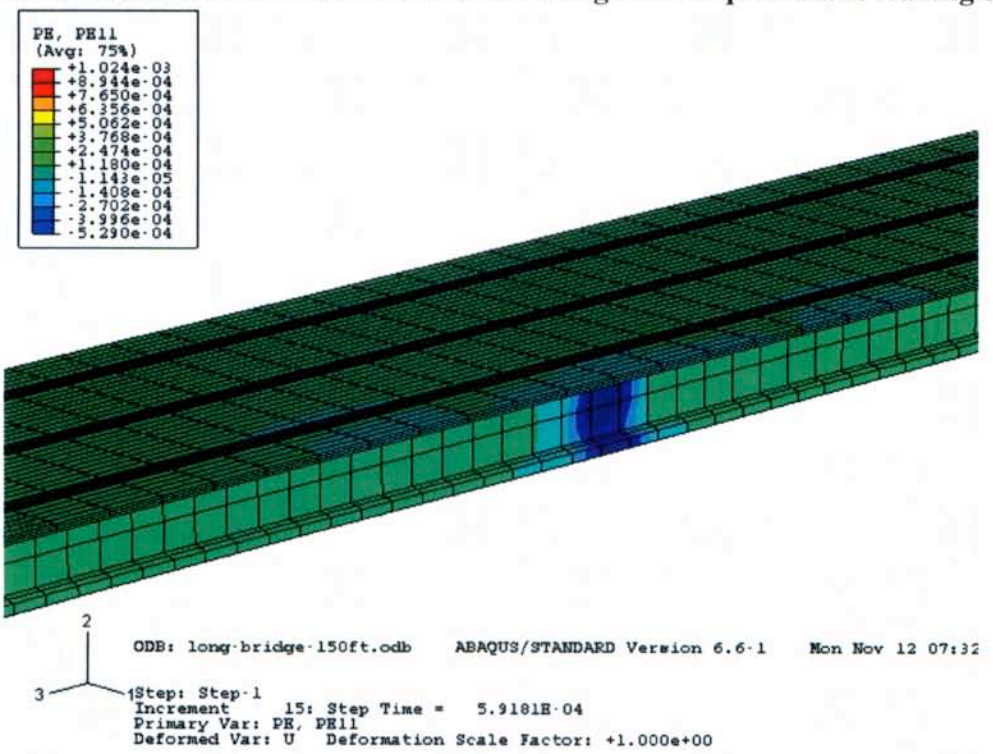

Figure 58. Plastic strain distribution of the bridge under quasi-static loading case

5. RECOMMENDATIONS AND GUIDELINE

Based on the numerical parametric study conducted in Section 4, the effects of studied factors associated with the role of intermediate diaphragms (IDs) are summarized and discussed, and recommendations of intermediate diaphragm design for improving impact protection and resistance is provided. A step-by-step design guideline useful for decision making and practice of the prestressed concrete girder bridge construction is proposed.

5.1 Discussions and Recommendations

Quasi-static and explicit dynamic numerical finite element analyses of prestressed concrete girder bridges with intermediate diaphragms (IDs) are conducted, and the key factors (i.e., location and size of ID, spacing and types of girders, frame action and dynamic load types) involving the role of IDs in the impact protection are evaluated. For the bridge without the IDs at all, the bridge is not capable of sustaining the full design load of 120 kips, thus demonstrating the important role of IDs in impact protection and performance enhancement of the bridges under impact. Thus, it is worth investigating the role of IDs in collision protection of PC bridges. The following discussions and recommendations for the effects of these key factors and their corresponding design in impact resistance are provided:

- **Location and spacing of IDs**: A single span bridge of 100 ft. span with the ID at ½ span and at 1/3 span is analyzed, and the location and spacing of IDs within the span has an influential effect on impact protection. For the relatively long span bridge, multiple and distributed IDs resist impact better by effectively transferring large deformations to other girders and decks, reducing the damaged areas and absorbing more kinetic energy. Based on the observation from the simulation, a suitable distance of ID spacing can be determined for a particular loading, and it is recommended that a spacing of IDs of 25 to 40 feet for 100 ft. or longer span of the bridge is better in impact protection.

- **Thickness and axial stiffness of IDs**: The thickness effect of the IDs is studied, in which the axial stiffness of the ID increases with the increase of the ID thickness. The thickness of IDs has minor effect on the impact protection of the PC girder bridge from impact. So does the axial stiffness of ID. The axial stiffness of the ID is proportional to the thickness of ID, and the ID is usually under axial loading during the horizontal impact event to transfer the load to the adjacent girders. The increase of the axial stiffness could also be realized by adding more steel reinforcement. Though the effect of steel reinforcement ratio in IDs is not investigated in the present study, it can be analogously concluded that the axial stiffness of ID does not much influence the capacity of ID in impact protection, based on the observation from the ID thickness effect analysis. In conclusion, a moderate thick ID (e.g., 8") is adequate for the function of ID to impact protection.

- **Depth of IDs**: The effect of depth of IDs on impact protection is quite detrimental, and the deeper the ID, the less rotation of the girder and the better the impact protection to the bridge system. It thus recommends that a full-depth ID (the depth of ID to the top edge of the bottom flange of girder, see Figure 3) should be implemented in construction to maximize the capacity of ID in the impact protection.

- **Girder spacing**: The spacing of girder in the relationship to ID design (i.e., the length of ID) is not a critical factor in the bridge impact resistance when the impact load is around the location of ID. As expected, the narrower the girder spacing, the shorter the ID, leading to better load transfer of IDs from the girder to the subsequent girders as well as to the bridge deck. Though the spacing of girder is not an important factor in the ID design, it recommends that a bridge with closer girders connected by the IDs has a better composite action and load transfer in the loading (horizontal) direction, thus leading to higher impact resistance. With a smaller girder spacing (e.g., the 6 ft. or 8 ft. spacing), the maximal horizontal and vertical displacements are reduced. While the total damaged area and stress distributions become more complex due to the strengthening effect of closely spaced IDs, which could lead to increased damage areas and energy dissipation. In general, the closer spacing of girders is beneficial in controlling deformation; however the stress distributions are much more complicated. Fortunately, all the bridges are designed to perform in elastic range. In the elastic range, the displacement has a direct proportion to the stress. Thus, when displacements are controlled, the stresses will be controlled as well.

- **Girder types**: The types of girders in the bridge system have some noticeable effect on the impact resistance of the bridge with consideration of IDs. A wider flange type of girder promotes a higher bending stiffness in the horizontal (transverse) direction (i.e., the direction of loading) and improved composite action with the bridge deck, and it thus results in better impact resistance. The higher web type of girder induces more horizontal deformation in the girder, leading to more spread damage on the web. A girder type with a wider flange and a moderately deep web is thus recommended, when the IDs are considered to transfer and resist the bottom girder horizontal impact loading.

- **Frame action**: The aspect ratio in term of the number of the girders with an equal spacing in a bridge has a significant effect on the impact resistance of the bridge in association with IDs. The larger the aspect ratio, the more important the IDs in the load transfer and the bridge composite action. Thus, the IDs play an important role in impact protection, particularly when the global response of the bridge system is significant.

- **Types of applied impact loads**: A concentrated load at a point prompts more damage in the bridge; while a distributed impact load over a certain area better spreads the load and results in less total damaged elements, and it dissipates more plastic energy in the system. Thus, the girder bridge system with IDs is better in resisting the distributed impact than a concentrated point load impact.

- **Types of impact analysis**: Both the quasi-static impact and dynamic impact analyses are considered and compared. The quasi-static impact analysis offers larger performance predictions than the explicit dynamic impact analysis. The conservative nature of quasi-static analysis thus promotes a safer design in all the associated analysis of ID effects. Though it may deviate from the real dynamic scenario, the quasi-static load provides a simple and conservative analysis procedure and is recommended in the ID design analysis.

- **Effect of end IDs**: As demonstrated for the bridge cases of 12 ft. girder spacing with and without the end IDs, the effect of end IDs to the bridge performance under impact is not significant, though the end IDs help reduce stress and deformation in the bridge.

5.2 Step-by-step Design Guideline

Based on the above discussions and recommendations, the following step-by-step design guideline for implementing the intermediate diaphragms (IDs) in impact resistance and protection of the prestressed concrete girder bridges is provided:

(1) **Site investigation of girder types, spacing and span length**: Girder types, spacing and span length shall be first determined based on the site and construction requirements.

(2) **Design of ID size**: The size of the IDs shall be then designed. A full depth of IDs (to the top edge of the bottom flange of the PC girders) should be chosen, and the thickness of IDs can be selected as the minimum allowed. Even though reinforcement ratio is not critical, a standard reinforcement ratio shall be followed for the ID design.

(3) **Design of ID location and placement**: The IDs should be placed with a spacing of 20 to 40 ft. within a span of 100 ft. or longer. For a short span of less than 50 ft., one ID at the center is sufficient. For the bridge with a small aspect ratio (i.e., the width to length ratio), the IDs placed among the first three or four rows of girders facing the traffic are adequate in load transfer and impact protection.

(4) **Protection of girder flanges**: In order to significantly reduce the dynamic contact effect from the impact of over-height trucks (not the inertia effect of bridge itself), a soft buffer layer (for example, a foam or sandwich material), is suggested for exterior girders.

6. CONCLUSIONS

In this study, the numerical finite element model for impact analysis of prestressed concrete girder bridges with inclusion of intermediate diaphragms (IDs) is first developed and validated with the existing experimental data. The numerical model is then

implemented in analyzing the effects of IDs on several key performance parameters in the impact event. The effects of ID size and location, girder spacing and types, frame action, applied load, and analysis types are investigated, and the impact resistance reflected in term of damaged area and plastically-dissipated energy are compared. Based on the analysis and observation from the numerical results, several conclusions and recommendations of ID design and analysis with aim to improve impact protection of PC girder bridges are made.

The developed dynamic numerical modeling and analysis and resulting findings reveal the intriguing behavior of the bridges under impact, shed light on impact protection provided by intermediate diaphragms (IDs), and provide recommendations and guideline for ID design. They can also be used to aid the American Association of State Highway and Transportation Officials (AASHTO), the Federal Highway Administration (FHWA), or the Washington State Department of Transportation (WSDOT) (particularly, WSDOT's Bridge Office) in their design and construction practice. The findings of this study assist in developing the specific standard of practice (such as, amendments to AASHTO standard specifications, WSDOT standard specifications, policy directives, implementation manuals, or operating procedures) for design of prestressed concrete bridge girders with intermediate diaphragms. More importantly, the proposed recommendations and guideline help the bridge engineers to make better design decision for prestressed concrete bridges.

REFERENCES

AASHTO (2002). "Standard specifications for highway bridges," Washington, DC.

AASHTO (2004). "LRFD bridge design specifications," Washington, DC.

Abendroth, R., and Fanous, F., (2003). "Lateral impacts to PC girders in bridges with intermediate diaphragms," Proceedings of the 2003 mid-continent transportation research symposium, Ames, Iowa, August 2003, Iowa State University Press.

Abendroth, R., Fanous, F., and Andrawes, B.O. (2004). "Steel diaphragms in prestressed concrete girder bridges," Final report to Iowa Department of Transportation, Iowa State Univeristy, Ames, IA.

Andrawes, B.O. (2001). "Laterial impact response for prestressed concrete girder bridges with intermediate diaphragms," MS Thesis, Iowa State University, Ames, Iowa.

Garcia, T.M. (1999). "IDs for precast prestressed concrete bridges," Proc. Of Western Bridge Engineer's Seminar, Seattle, WA.

Green, T.M., Yazdani, N., and Spainhour, L. (2004). "Contribution of intermediate diaphragms in enhancing precast bridge performance," Journal of Performance of Constructed Facilities, ASCE, 18(3): 142-146.

Shanafelt, G.O., and Horn, W.B., (1980). "Damage evaluation and repair methods for prestressed members," Transportation Research Board, NCHRP Report 226, Washington, DC.

APPENDICES

Appendix A. Effect of Location of Intermediate Diaphragms within Span

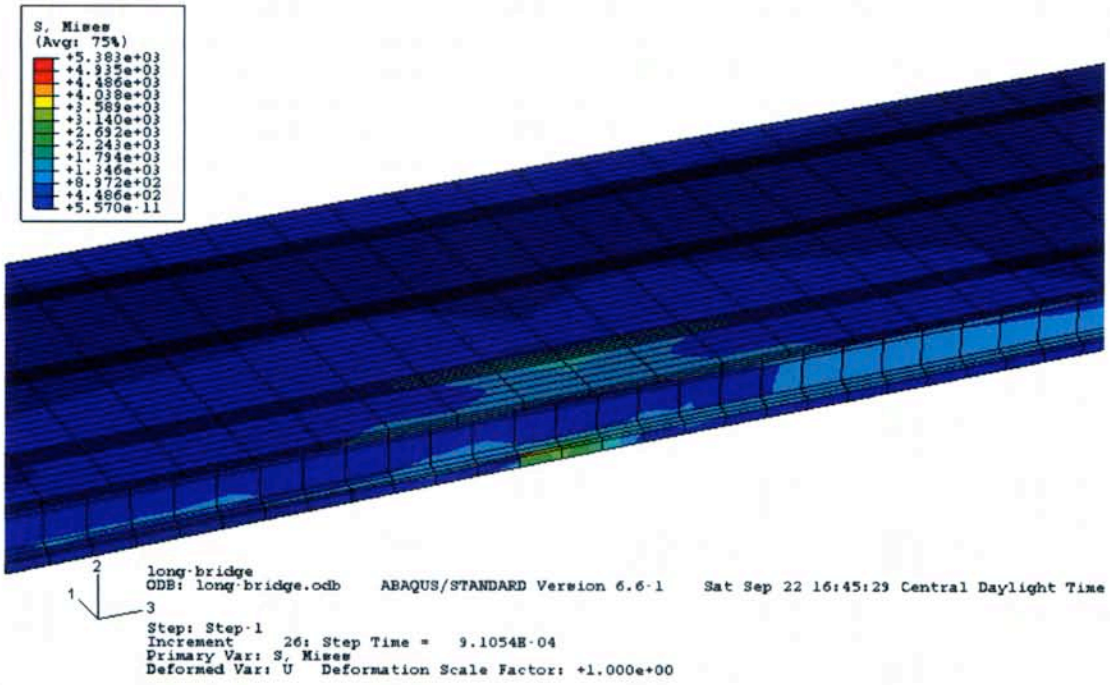

(a) Bridge with intermediate diaphragms at mid-span (1/2 span)

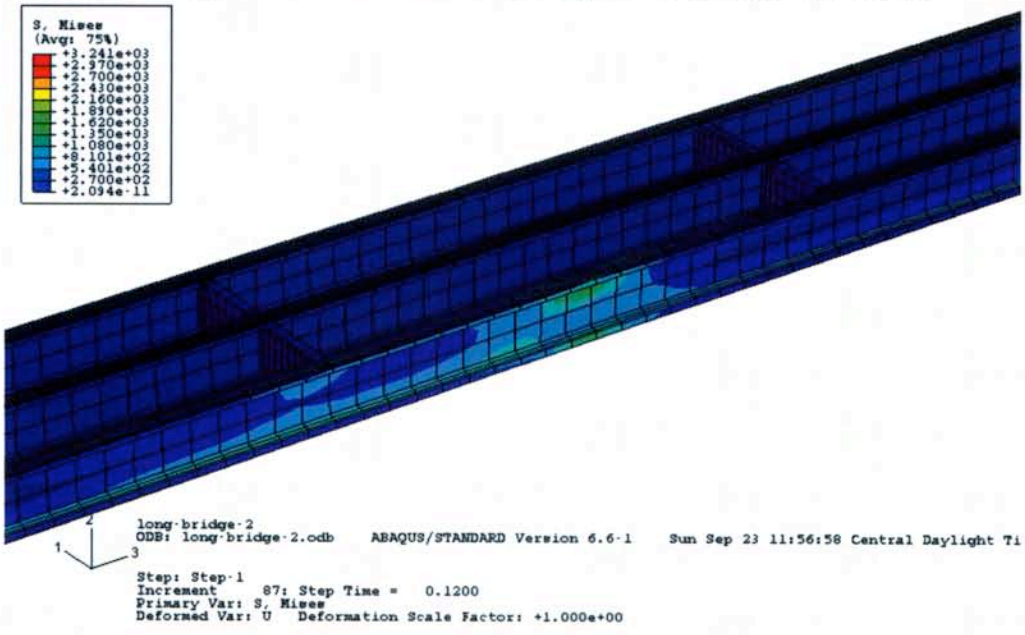

(b) Bridge with intermediate diaphragms at one-third-span (1/3 and 2/3 span)

Figure A1. Von Mises stress distributions of the 100-ft span bridge around the loading point

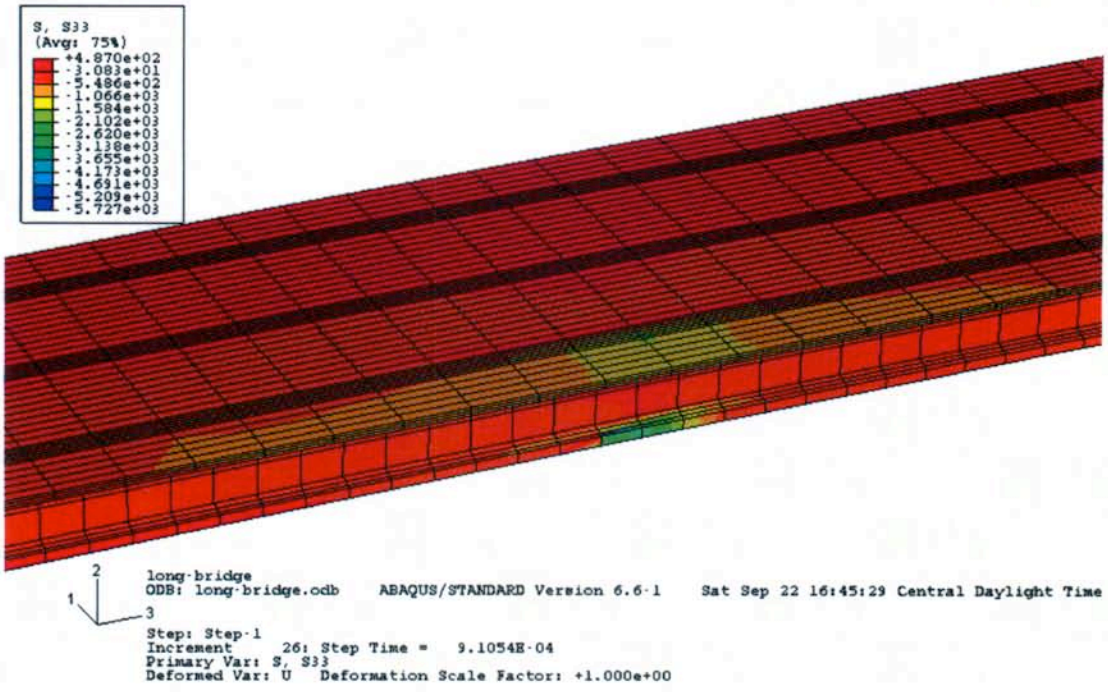

(a) Bridge with intermediate diaphragms at mid-span (1/2 span)

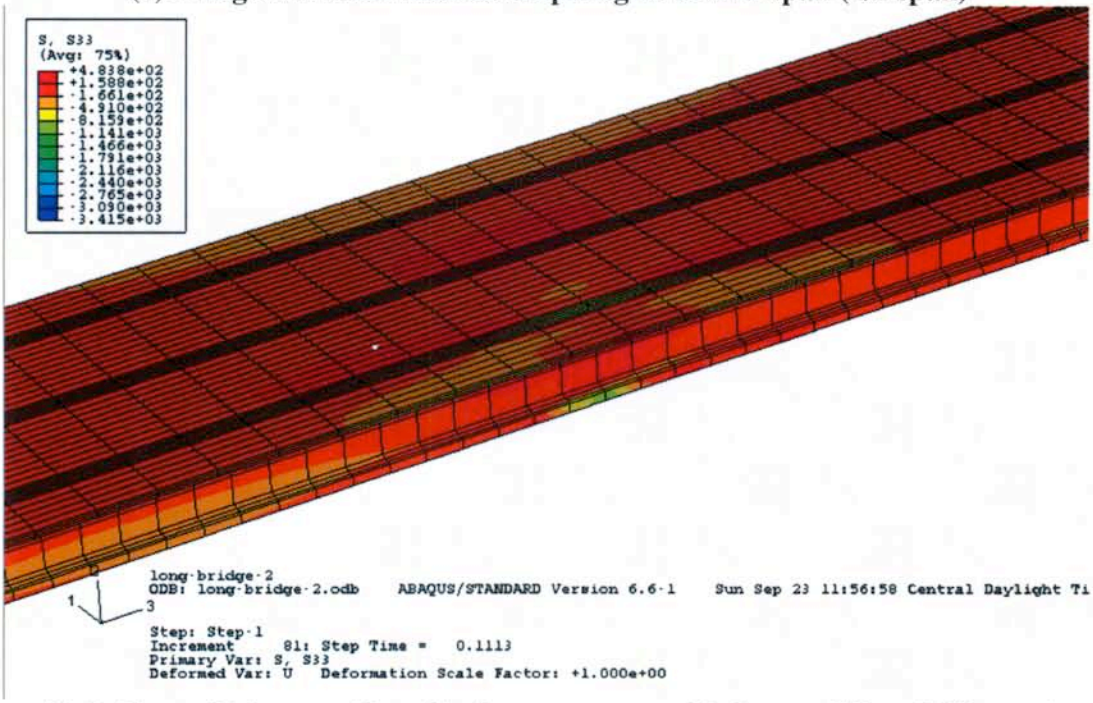

(b) Bridge with intermediate diaphragms at one-third-span (1/3 and 2/3 span)

Figure A2. Longitudinal stresses distributions in the girders

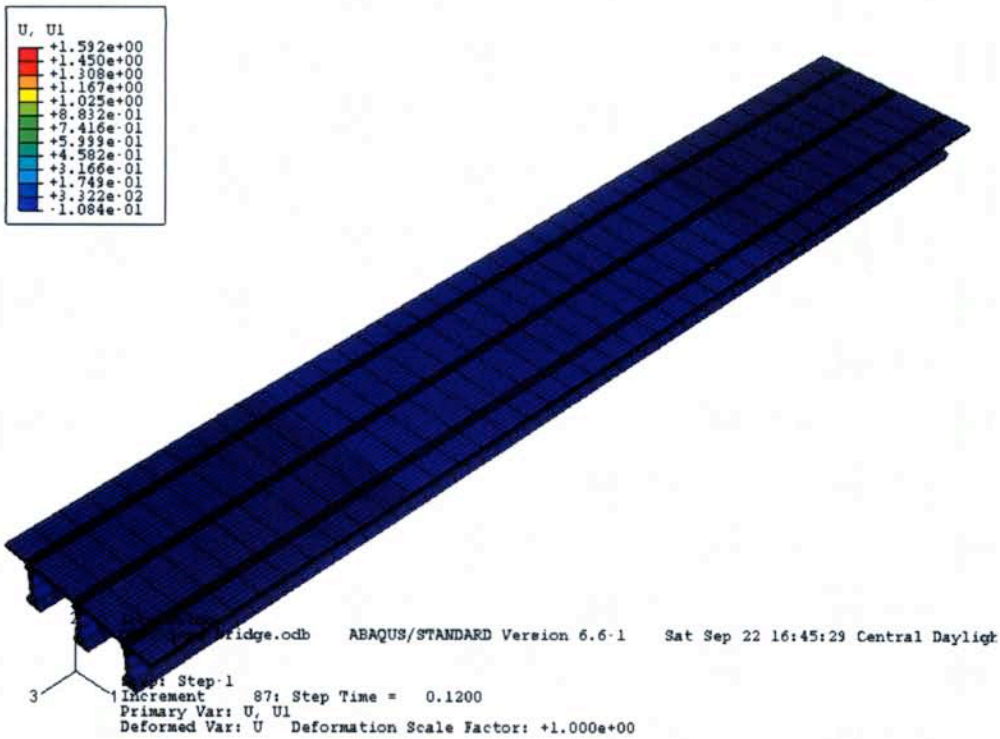

(a) Bridge with intermediate diaphragms at mid-span (1/2 span)

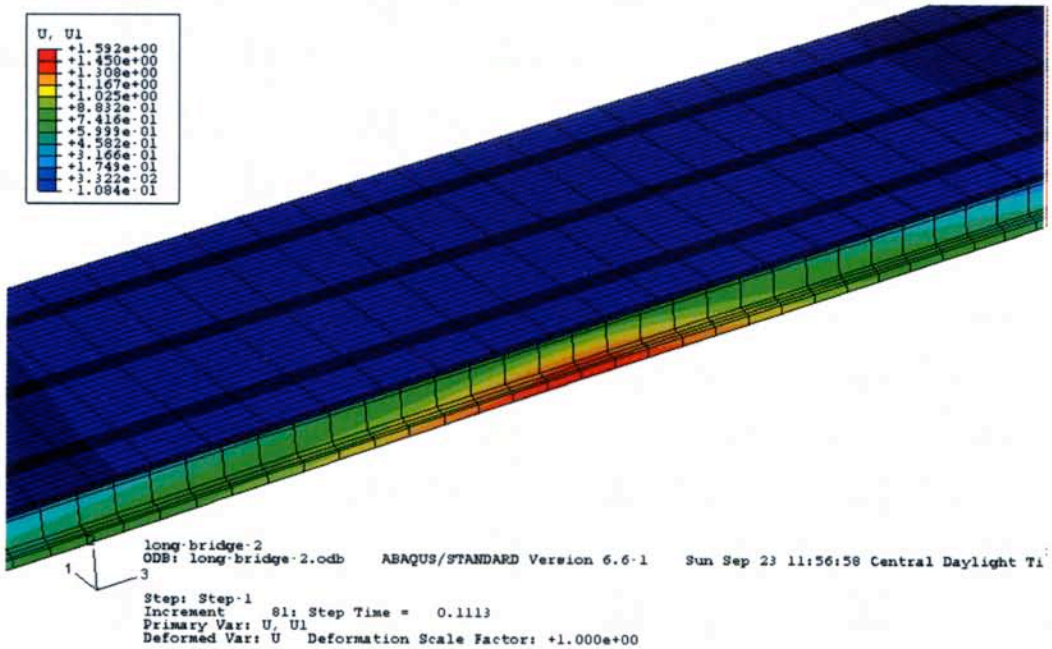

(b) Bridge with intermediate diaphragms at one-third-span (1/3 and 2/3 span)

Figure A3. Transverse displacement distribution (along the loading direction) of the bridge

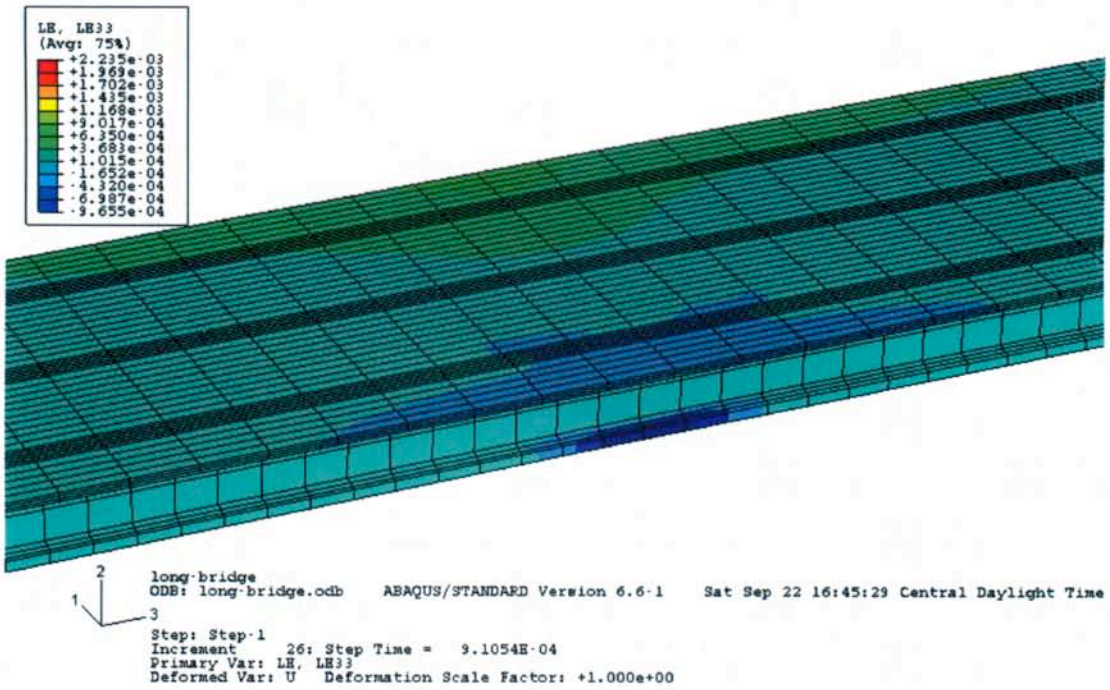

(a) Bridge with intermediate diaphragms at mid-span (1/2 span)

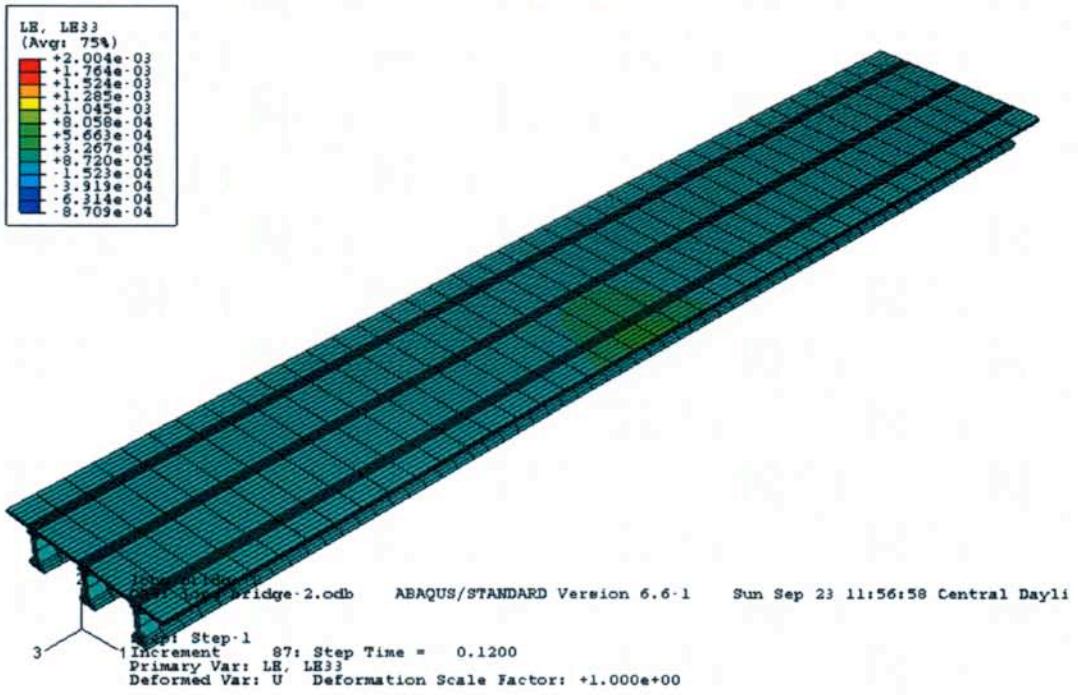

b) Bridge with intermediate diaphragms at one-third-span (1/3 and 2/3 span)

Figure A4. Longitudinal plastic strain distribution of the bridge under the given pulse loading with duration of 0.1 s.

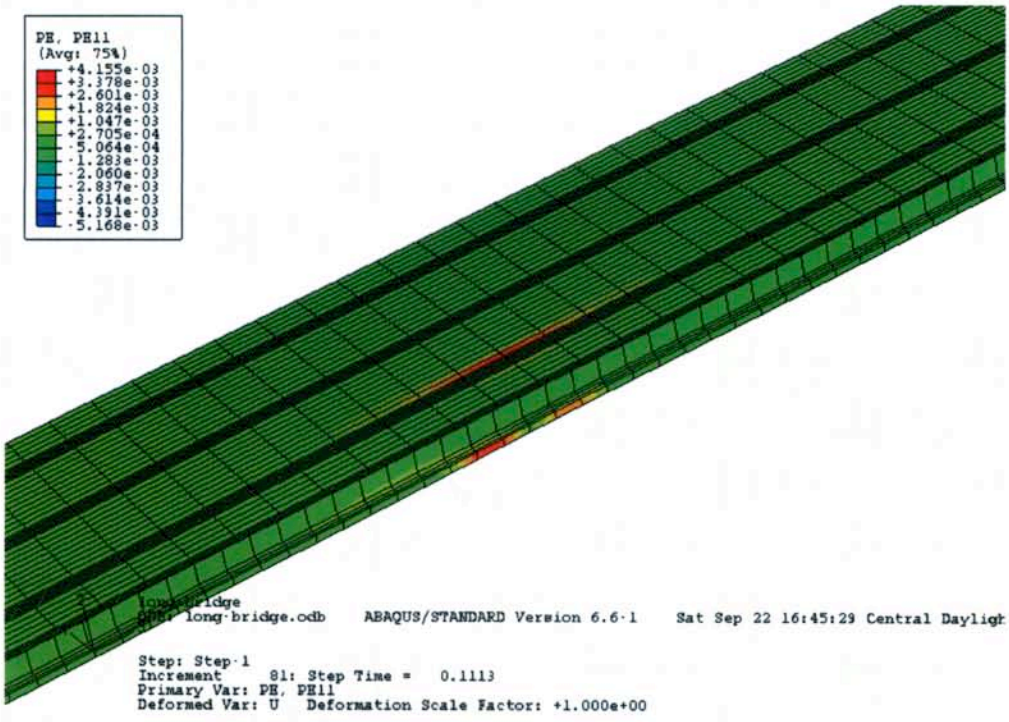

(a) Bridge with intermediate diaphragms at mid-span (1/2 span)

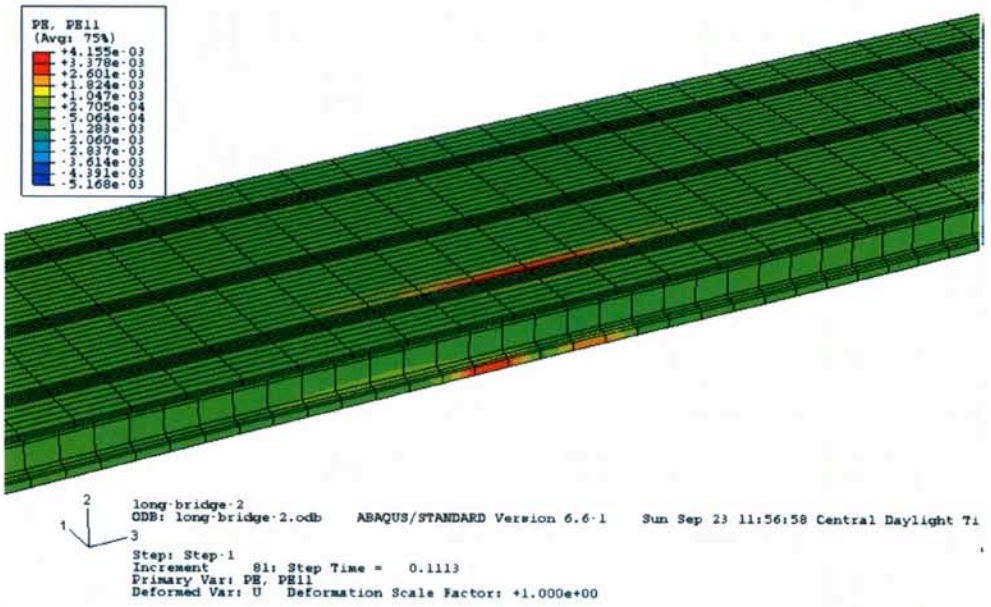

(b) Bridge with intermediate diaphragms at one-third-span (1/3 and 2/3 span)

Figure A5. Transverse plastic strain distribution (along the loading direction) of the 100 ft. bridge under the given pulse loading with duration of 0.1 s

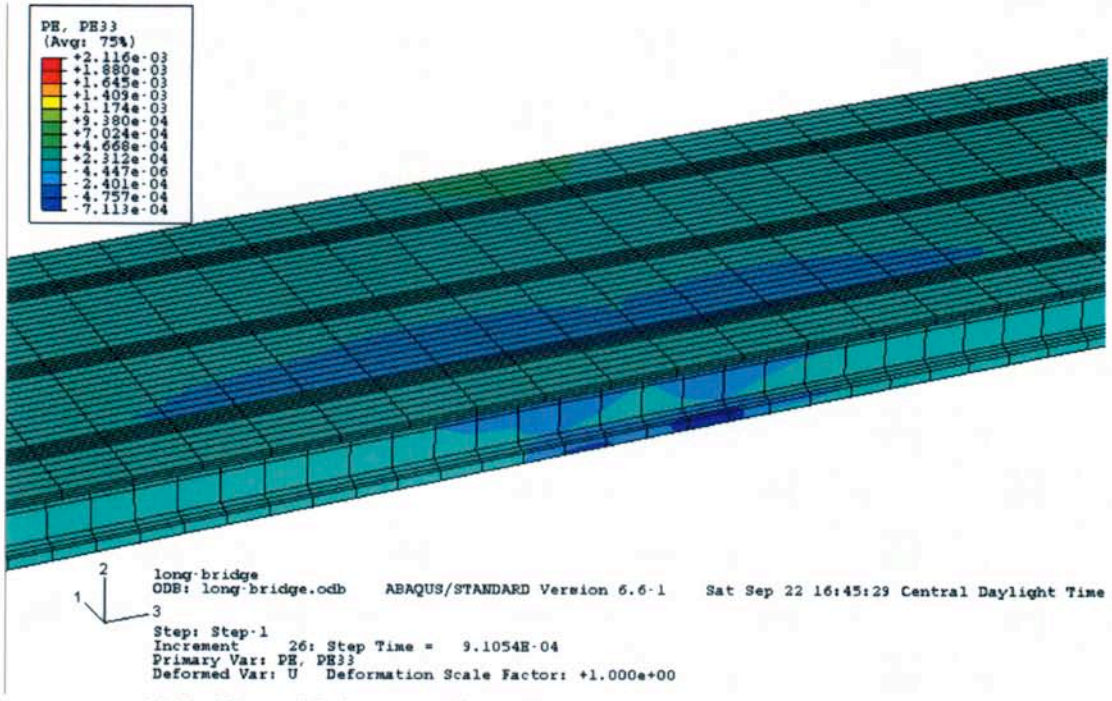

(a) Bridge with intermediate diaphragms at mid-span (1/2 span)

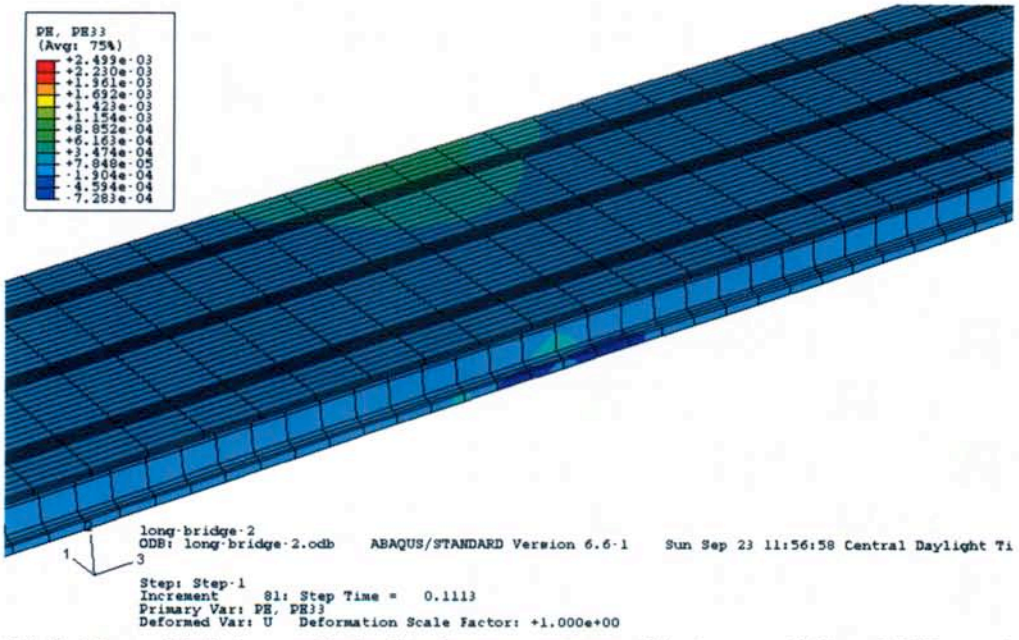

(b) Bridge with intermediate diaphragms at one-third-span (1/3 and 2/3 span)

Figure A6. Longitudinal plastic strain distribution for the 100 ft. span bridge under the given pulse loading with duration of 0.1 s

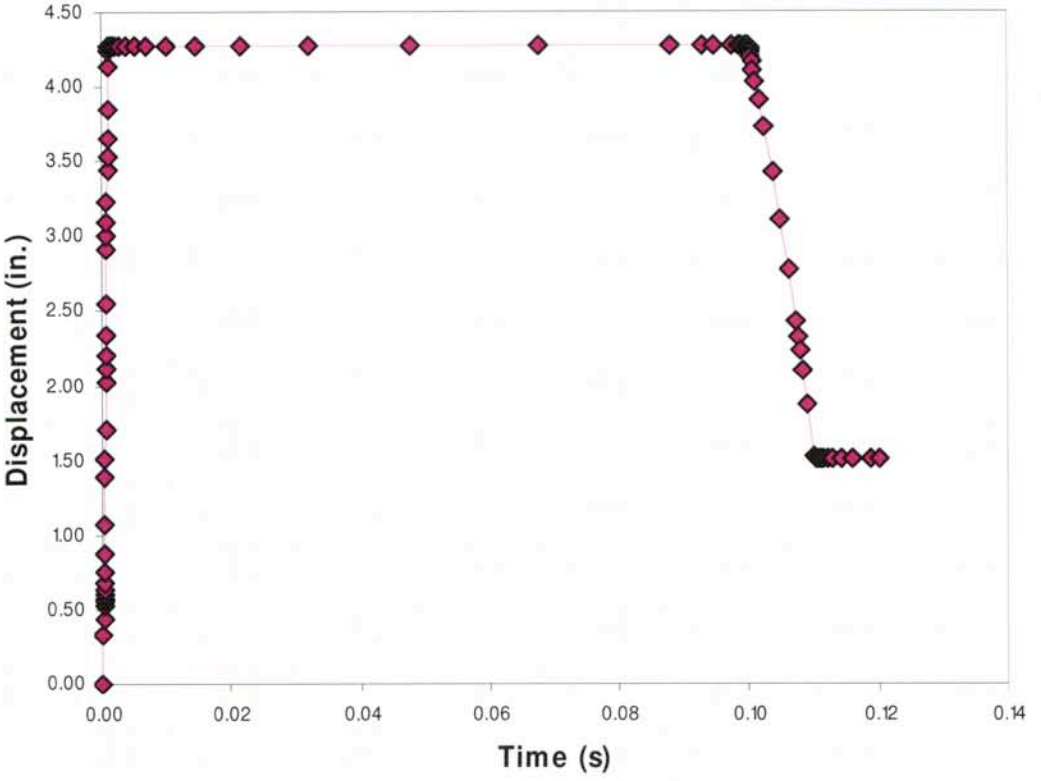

(a) Bridge with intermediate diaphragms at mid-span (1/2 span)

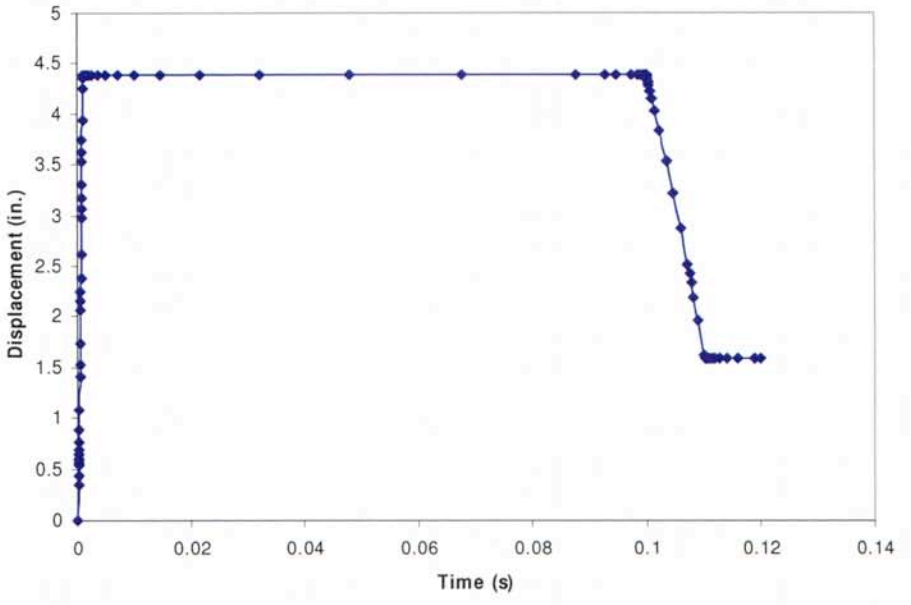

(b) Bridge with intermediate diaphragms at one-third-span (1/3 and 2/3 span)

Figure A7. Transverse displacement history of the bridge at the loading position

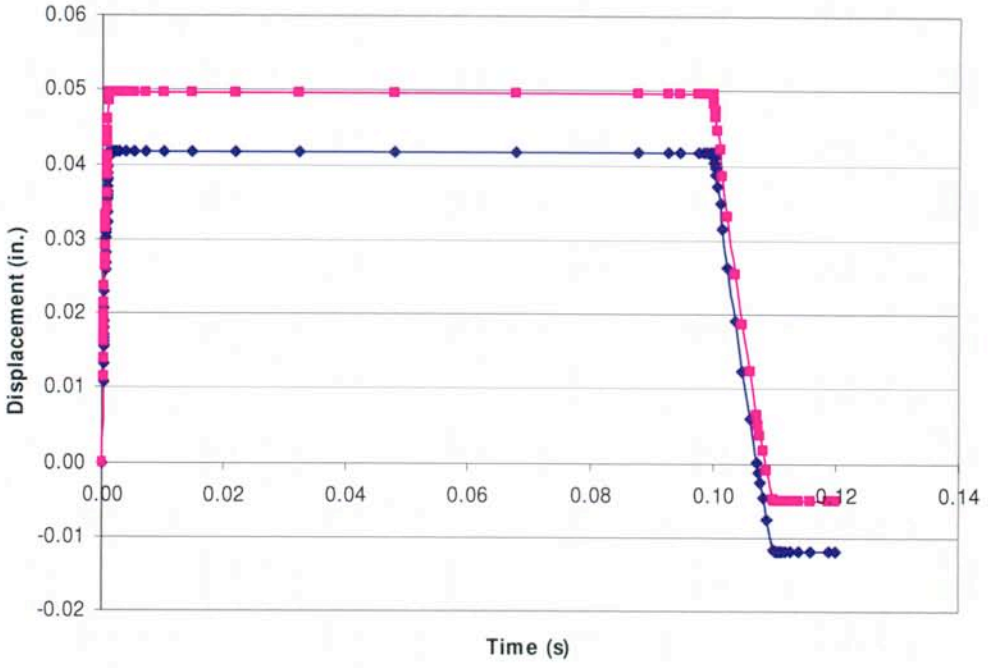

(a) Bridge with intermediate diaphragms at mid-span (1/2 span) (the blue and pink line is the two node displacement at the bottom flange of the 3st girder, respectively)

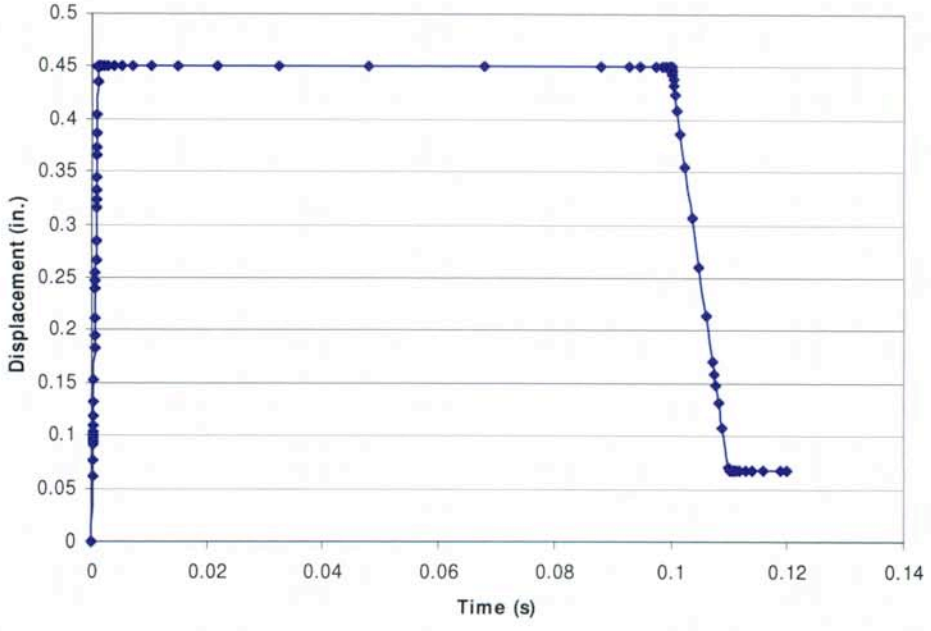

(b) Bridge with intermediate diaphragms at one-third-span (1/3 and 2/3 span)
Figure A8. Transverse displacement history of the bottom flange of the outside girder opposite to the loading position (the displacement history of the back (3rd) girder)

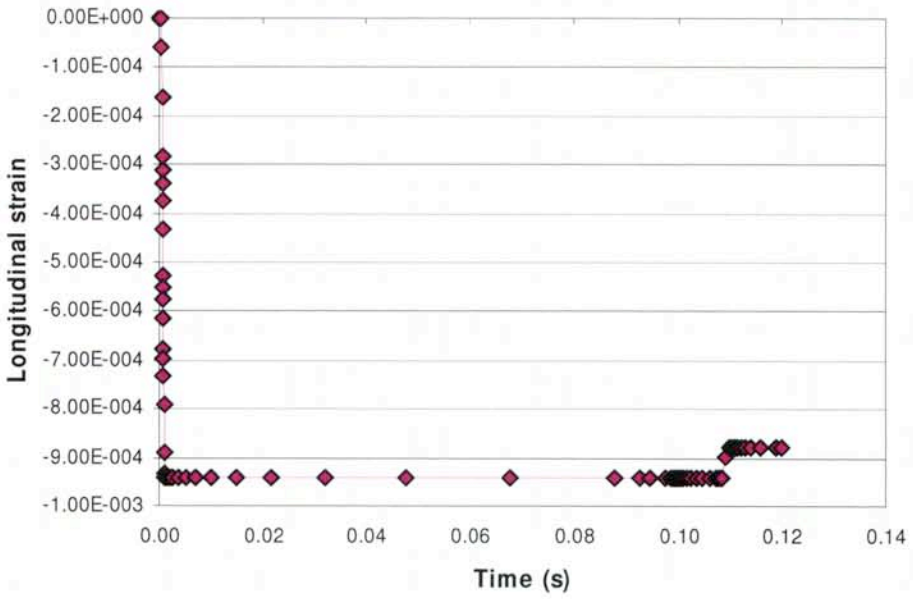

(a) Bridge with intermediate diaphragms at mid-span (1/2 span)

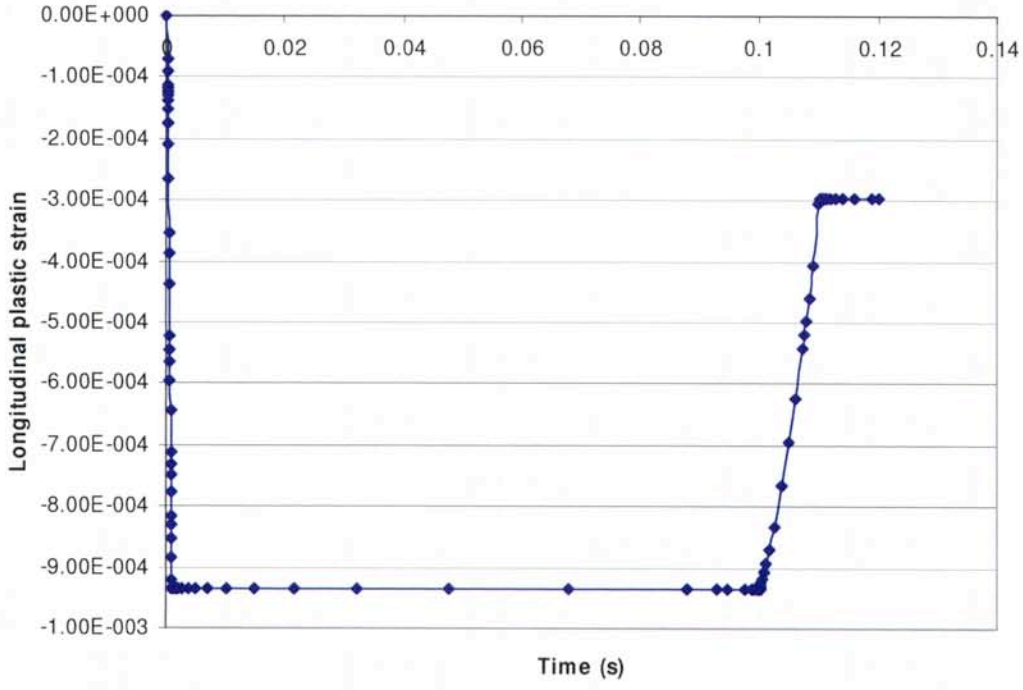

(b) Bridge with intermediate diaphragms at one-third-span (1/3 and 2/3 span)

Figure A9. Longitudinal plastic strain history at the loading position

Appendix B. Effect of Size of Intermediate Diaphragms – Thickness Effect

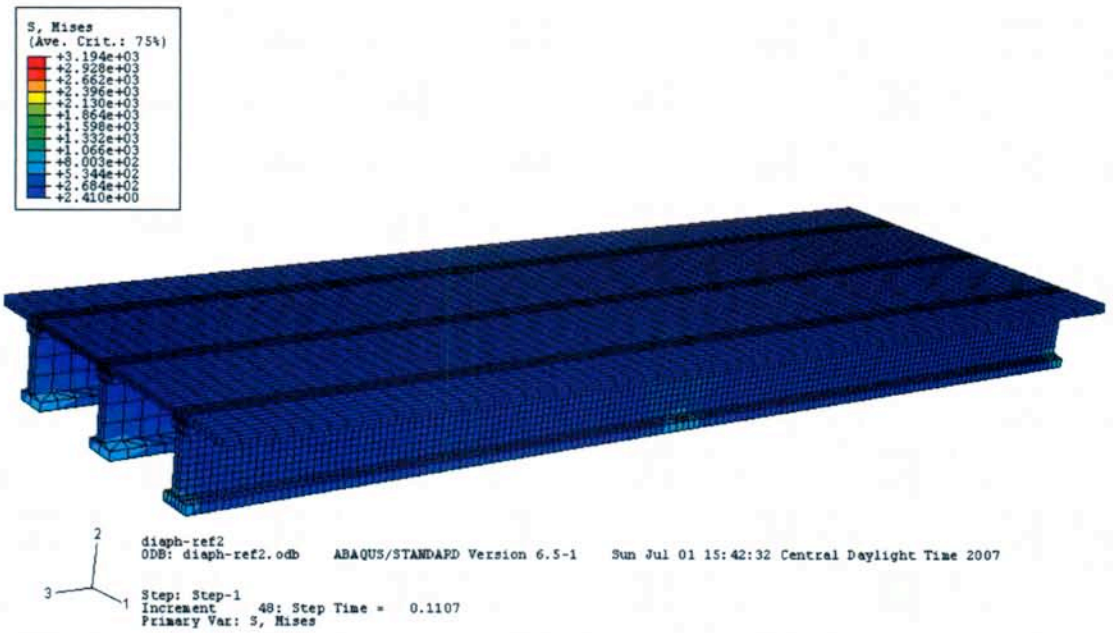

(a) 8 in. thick intermediate diaphragms

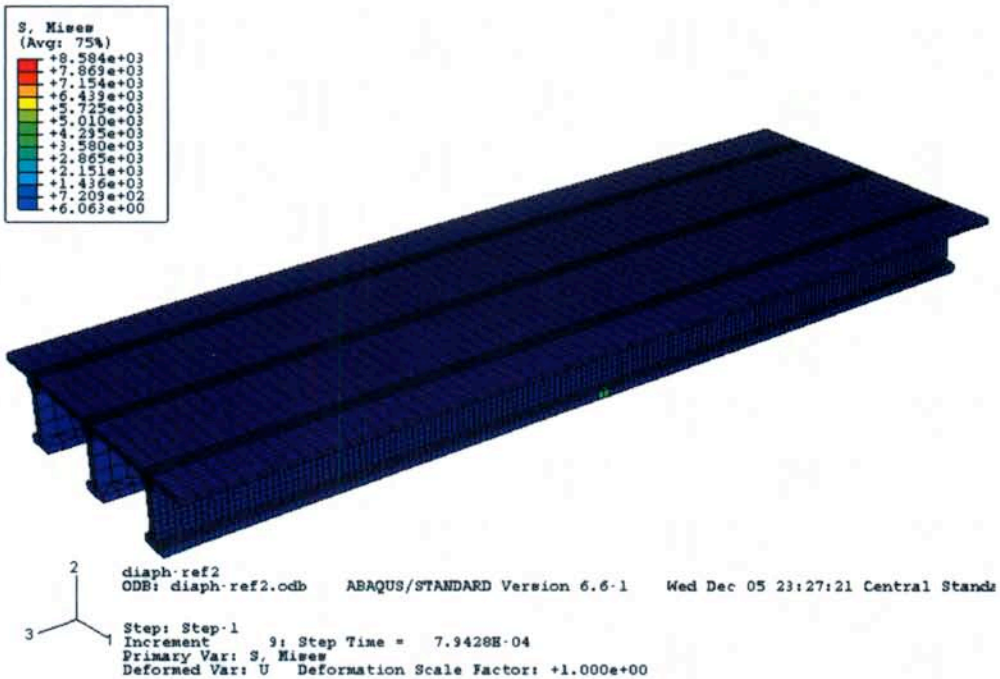

(b) 12 in. thick intermediate diaphragms

Figure B1. von Mises stress distribution in the girder bridge system

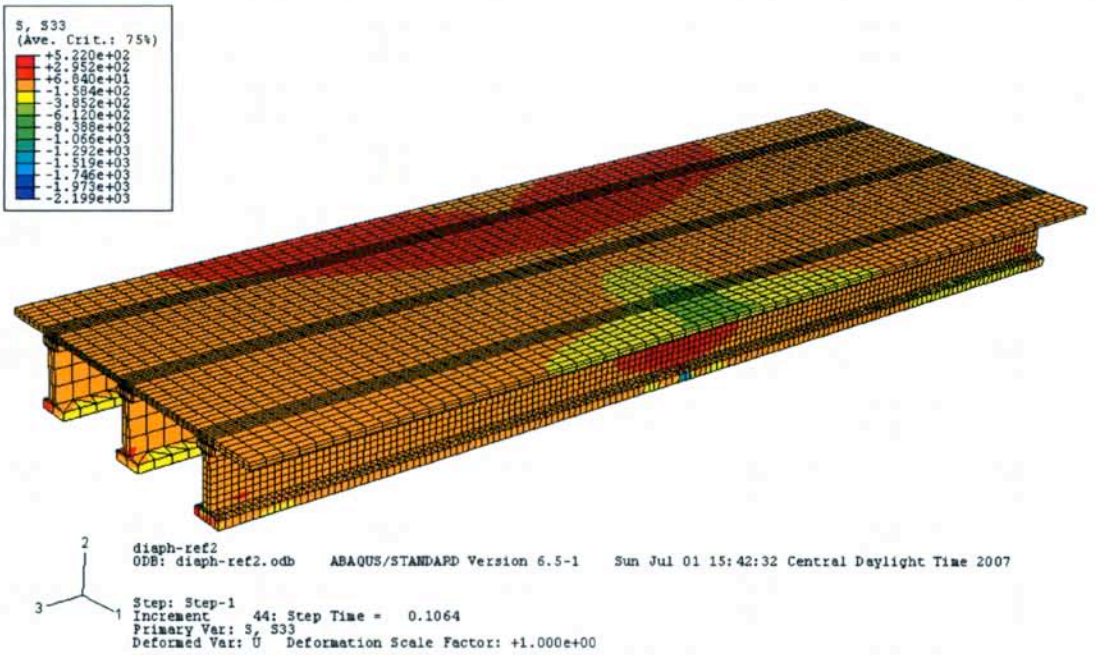

(a) 8 in. thick intermediate diaphragms

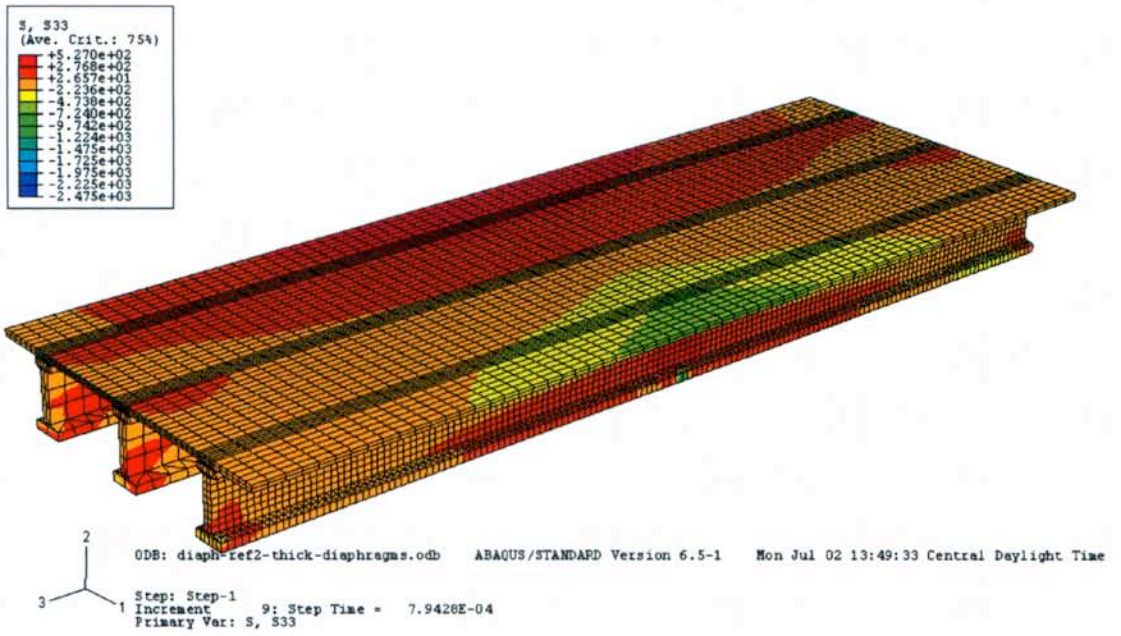

(b) 12 in. thick intermediate diaphragms

Figure B2. Longitudinal stress distribution in the girder bridge system

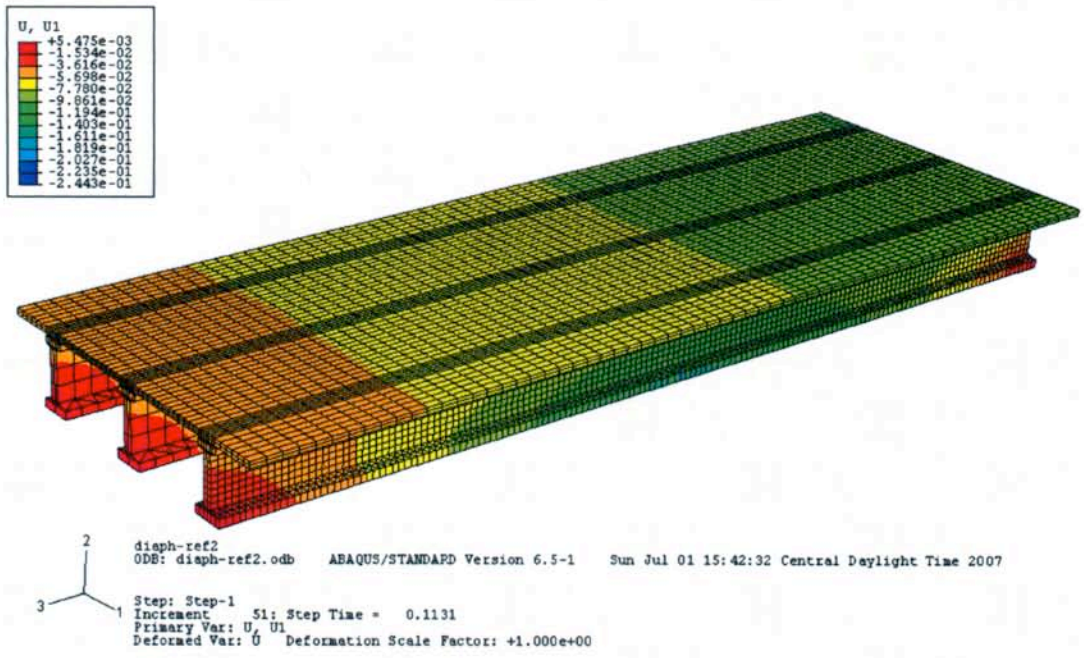

(a) 8 in. thick intermediate diaphragms

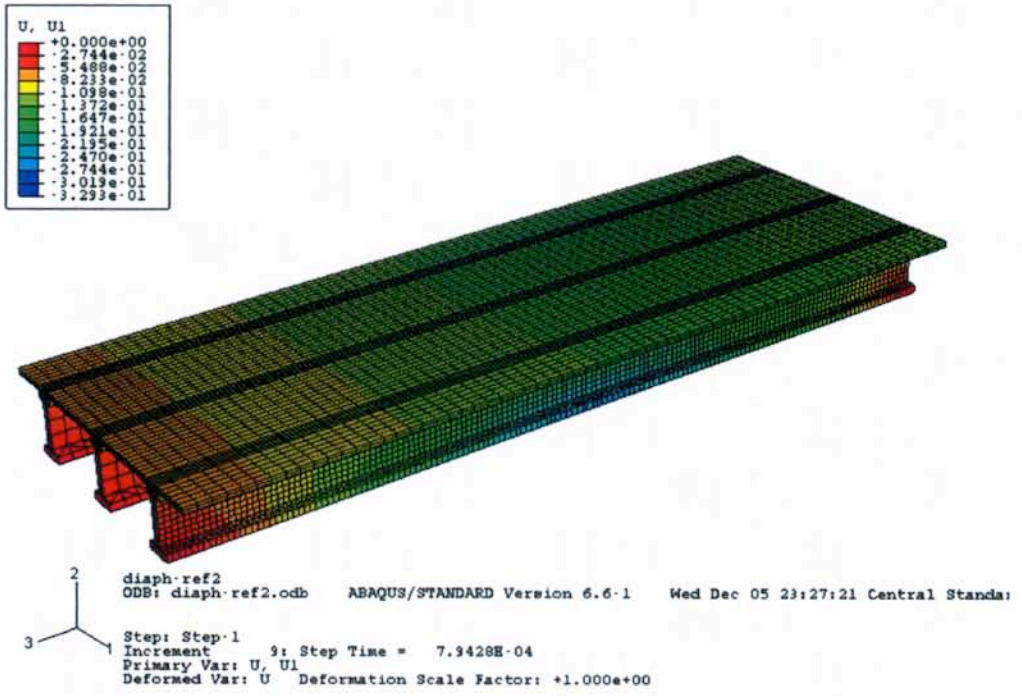

(b) 12 in. thick intermediate diaphragms

Figure B3. Transverse displacement distribution with the full depth of ID

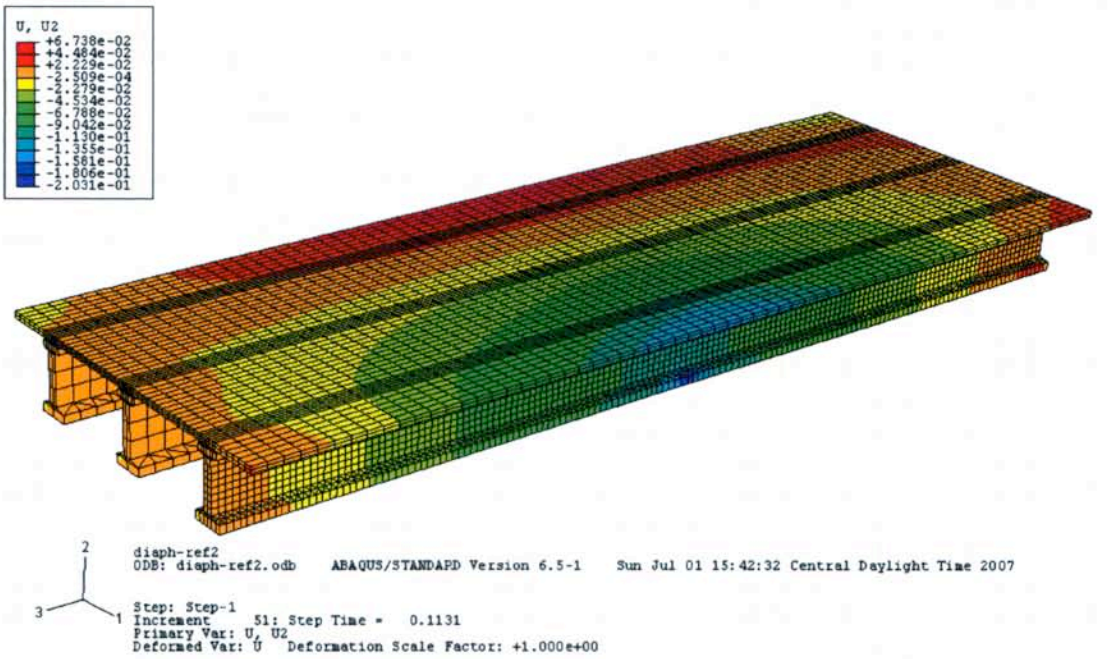

(a) 8 in. thick intermediate diaphragms

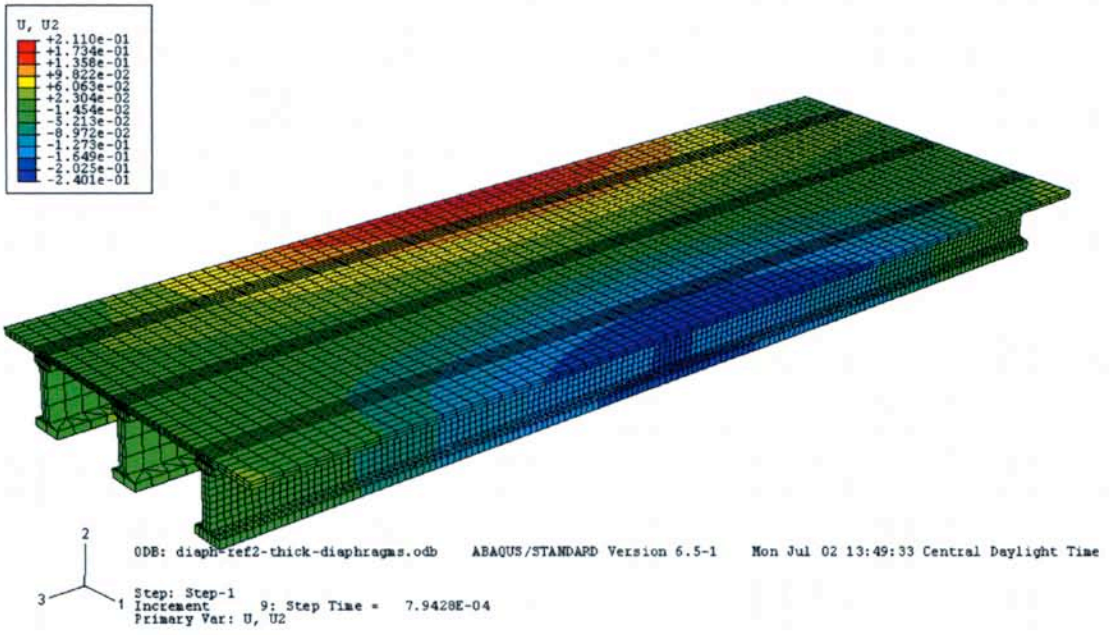

(b) 12 in. thick intermediate diaphragms

Figure B4. Vertical deflection distribution with the full depth of ID

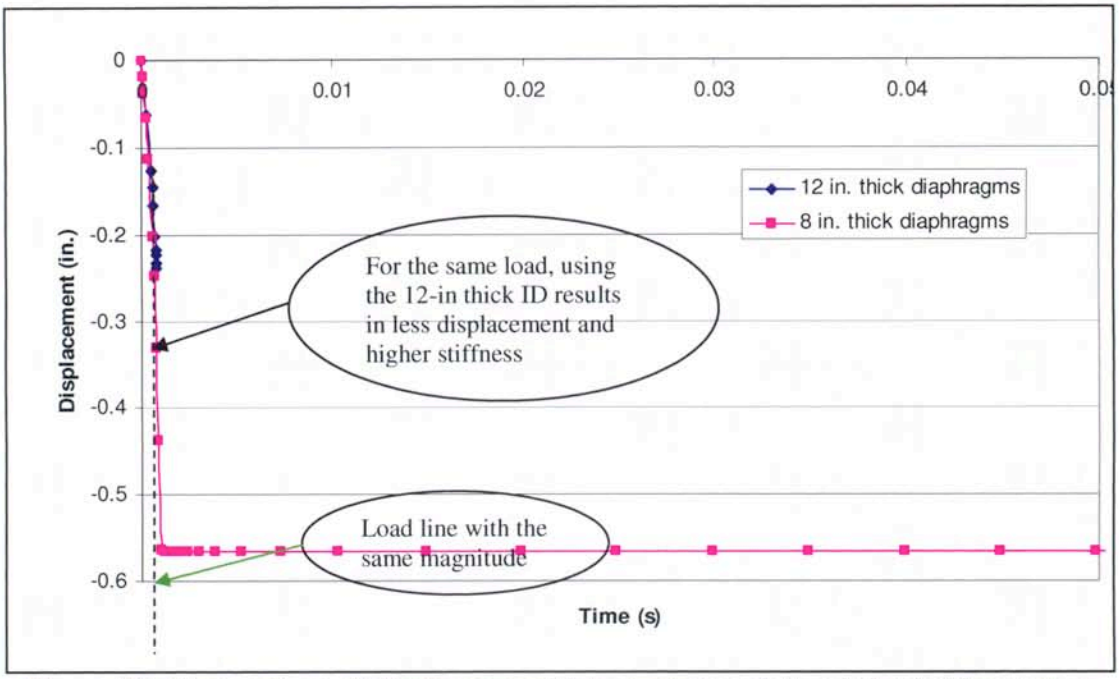

Figure B5. Comparison of displacement history curves of the girder bridge system with two different thicknesses of IDs at loading point 1

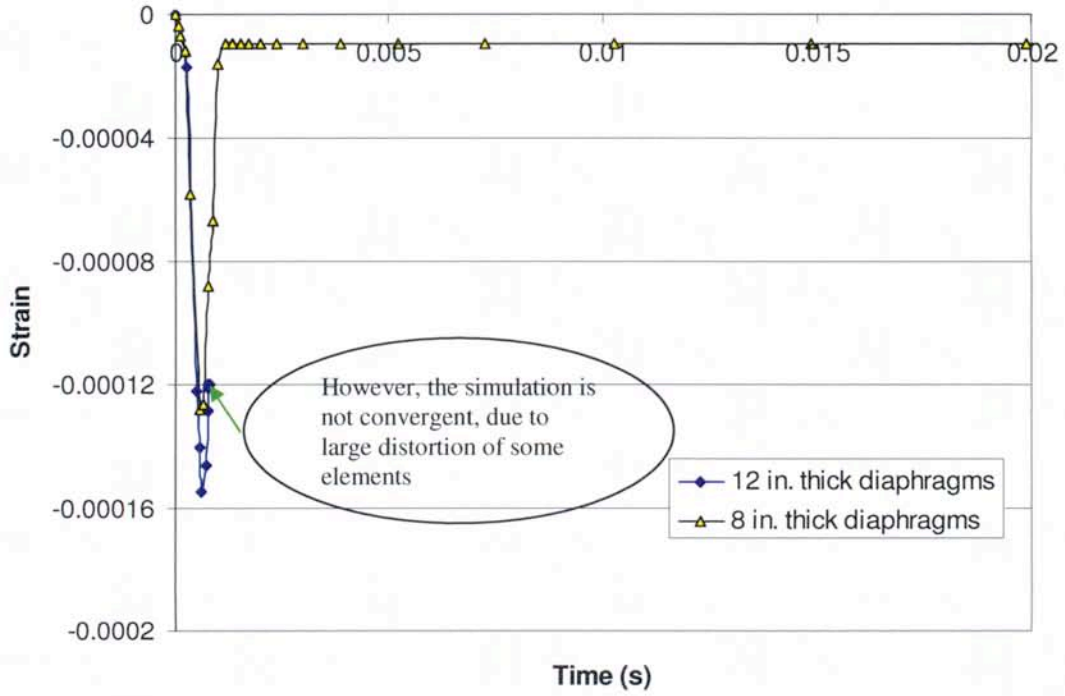

Figure B6. Comparison of strain history curve of the girder bridge system with two different thicknesses of IDs at loading point 1

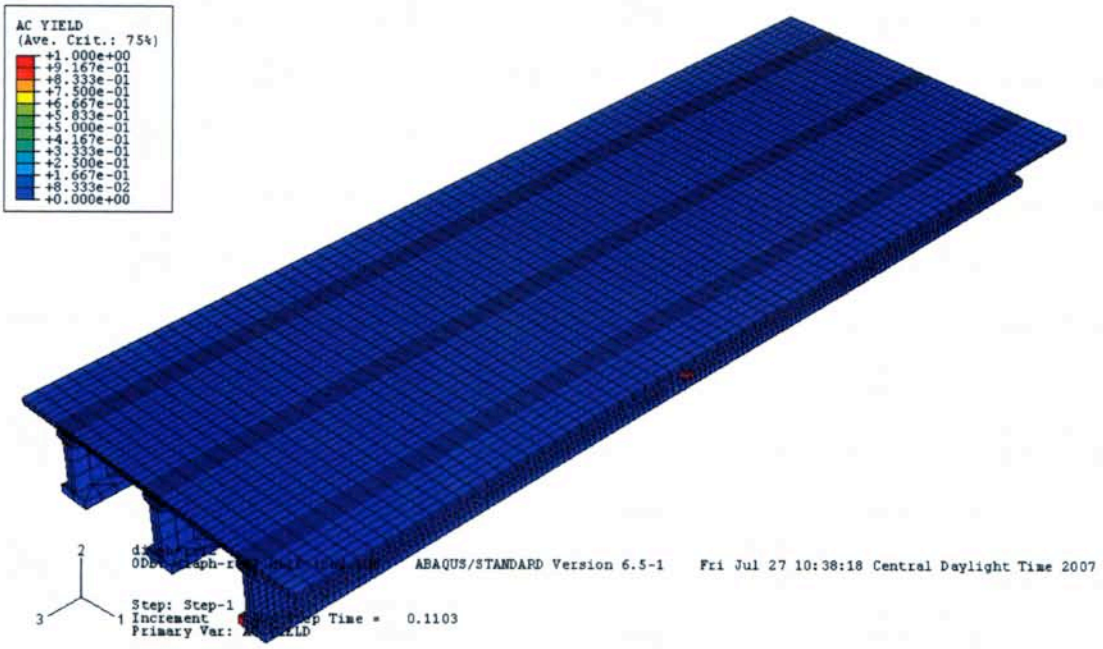

(a) 8 in. thick intermediate diaphragms

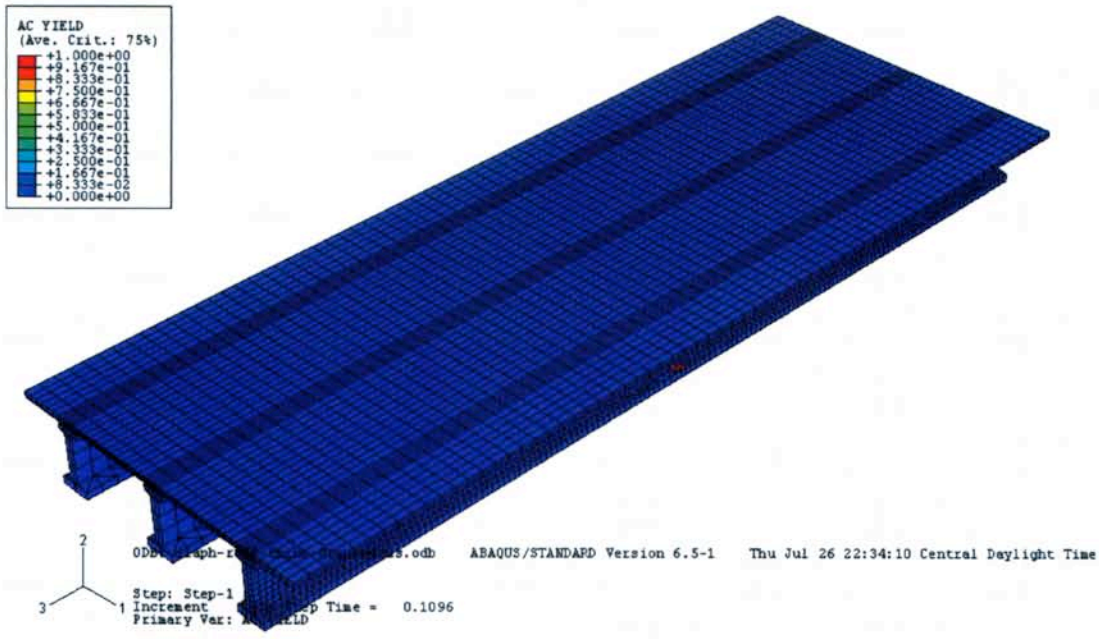

(b) 12 in. thick intermediate diaphragms

Figure B7. Failed elements in the bridge systems under half design load

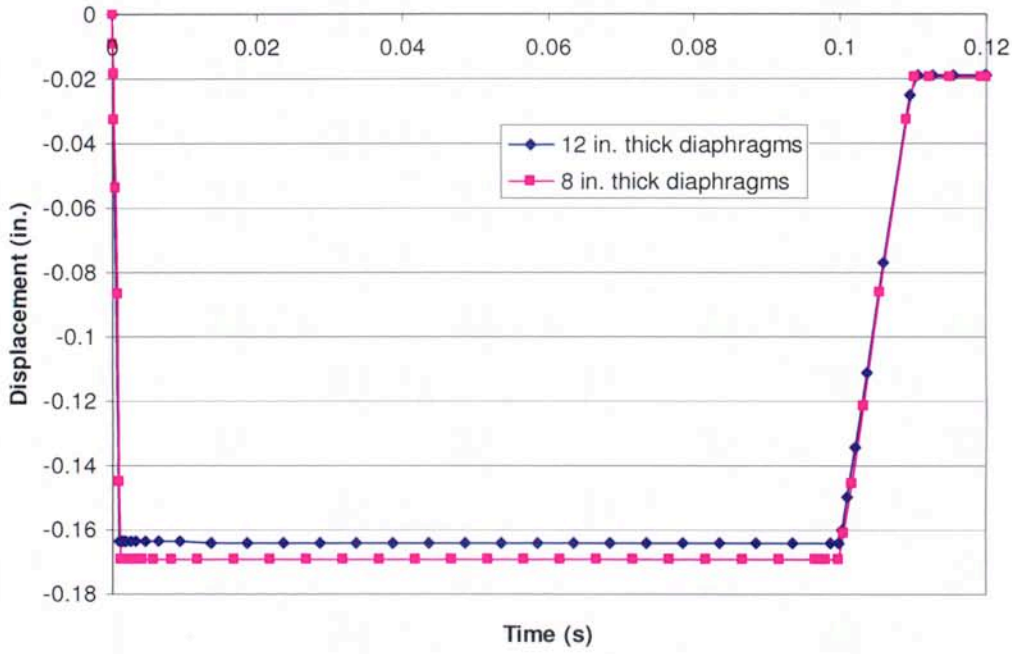

Figure B8. Comparison of horizontal displacements at the loading point with different thickness of IDs

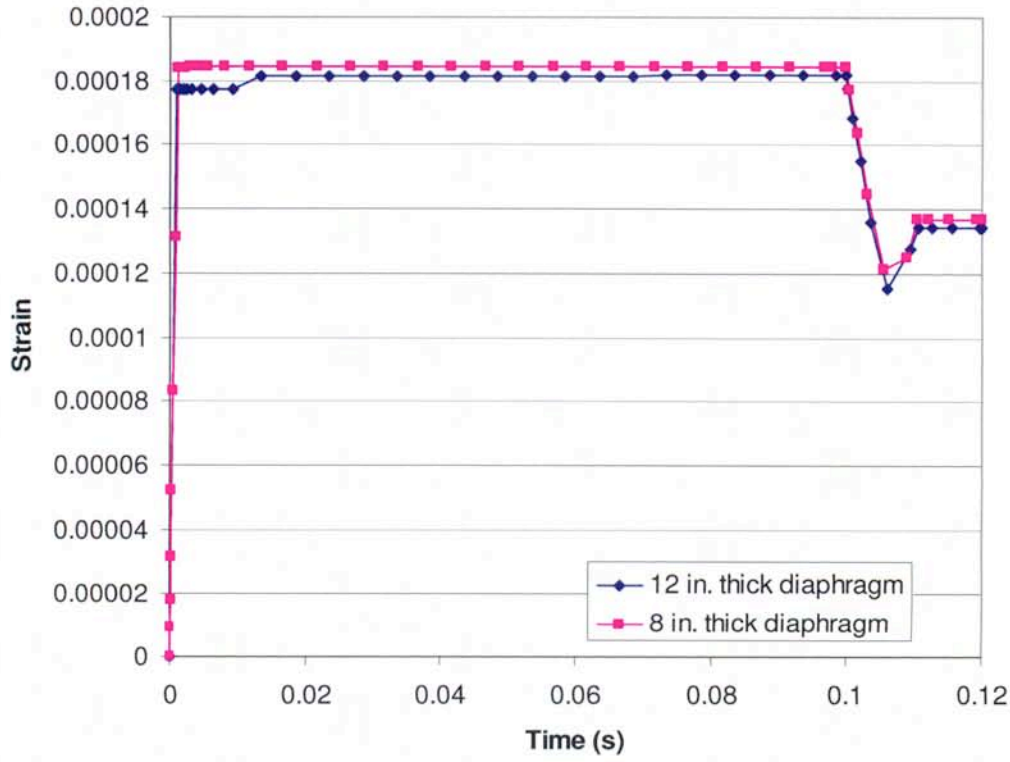

Figure B9. Comparison of strain at the loading point with different thickness IDs

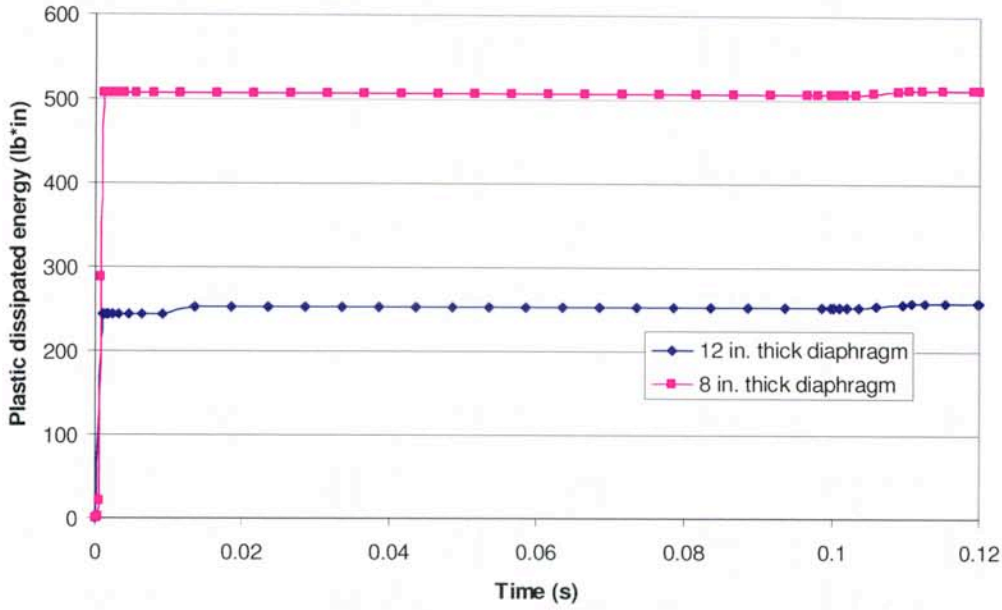

Figure B10. Comparison of plastically-dissipated energy with different thickness of IDs

Appendix C. Effect of Size of Intermediate Diaphragms – Depth Effect

The numerical analysis data for the ID of full depth (i.e., the depth of the ID to the top edge of the bottom flange, see Figure 3) is provided in Appendix B. In this section, the cases of (a) partial depth (ID of the depth to the bottom of web) and (b) 2/3 web depth (ID of the depth to 2/3 of web) are presented, as some comparison between the cases of full and partial ID depth.

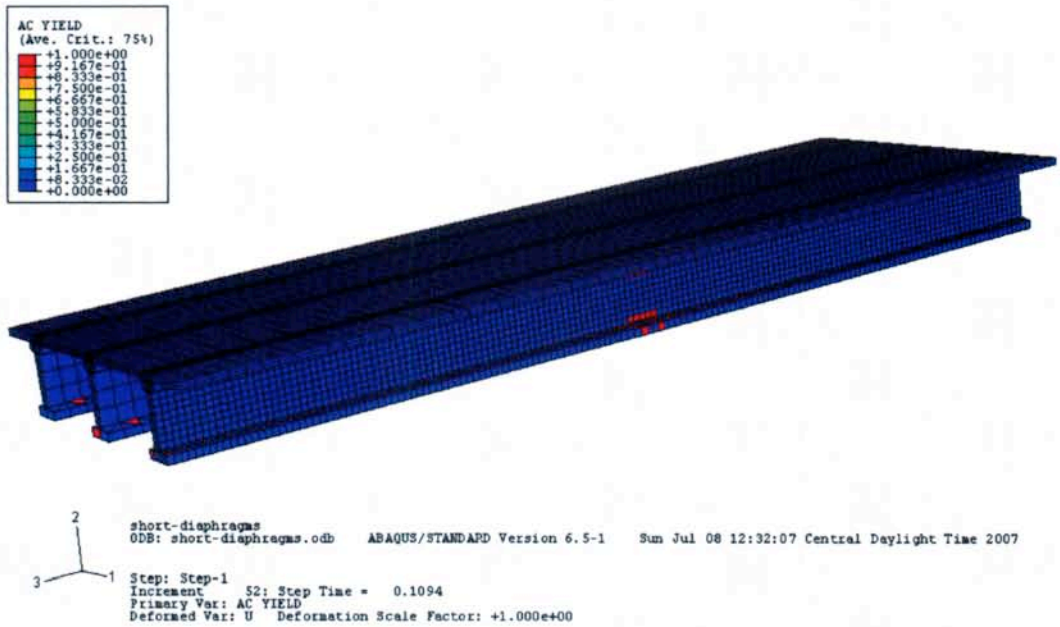

(a) Partial depth

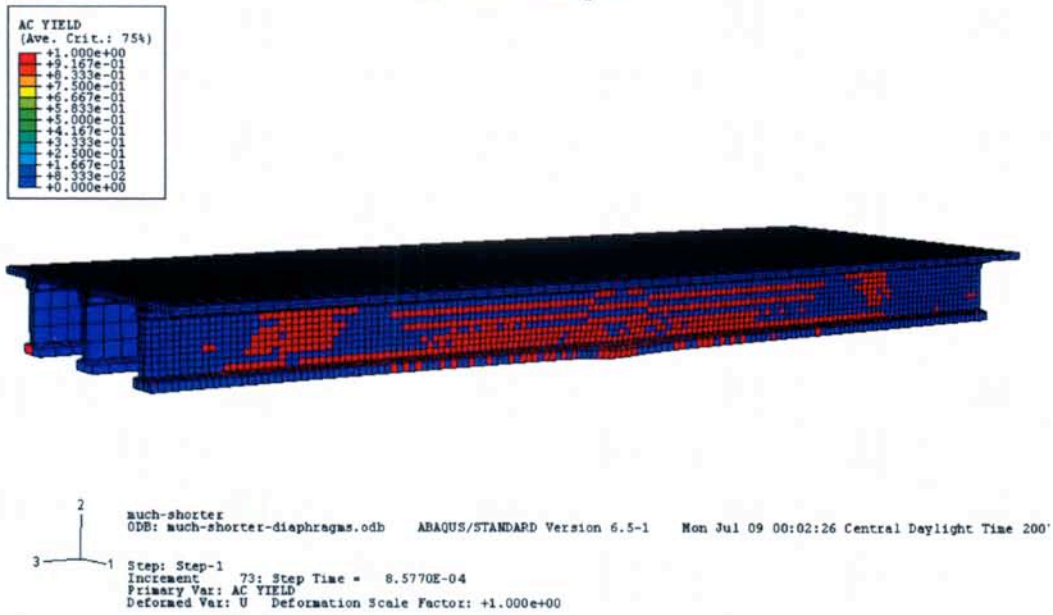

(b) 2/3 web depth

Figure C1. Failure area of the bridge system

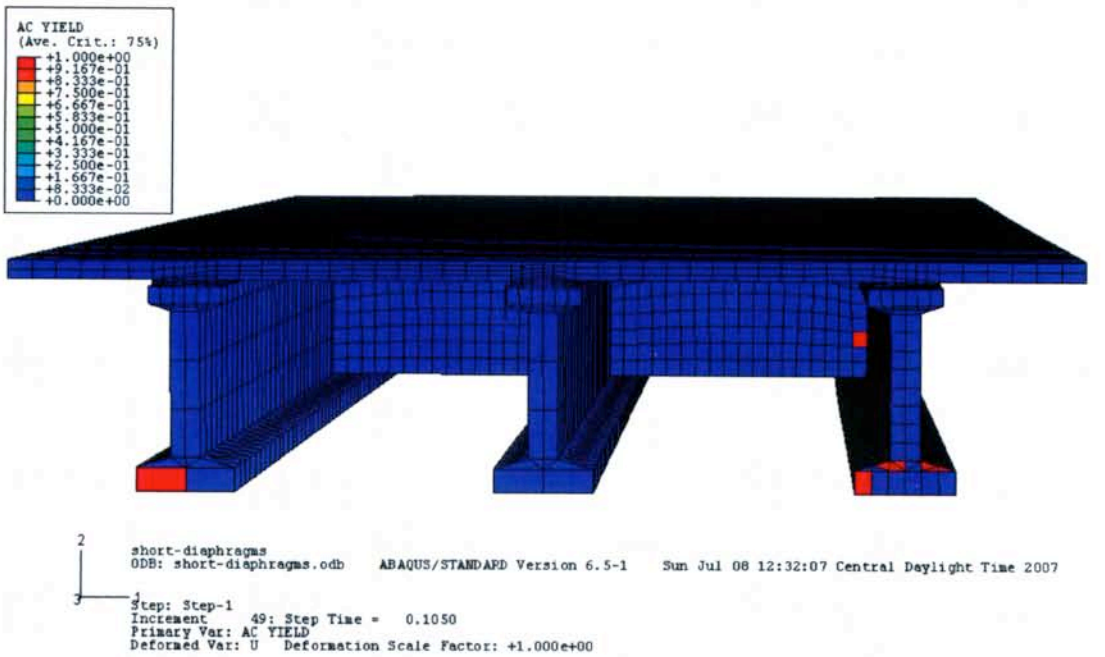

(a) Partial depth

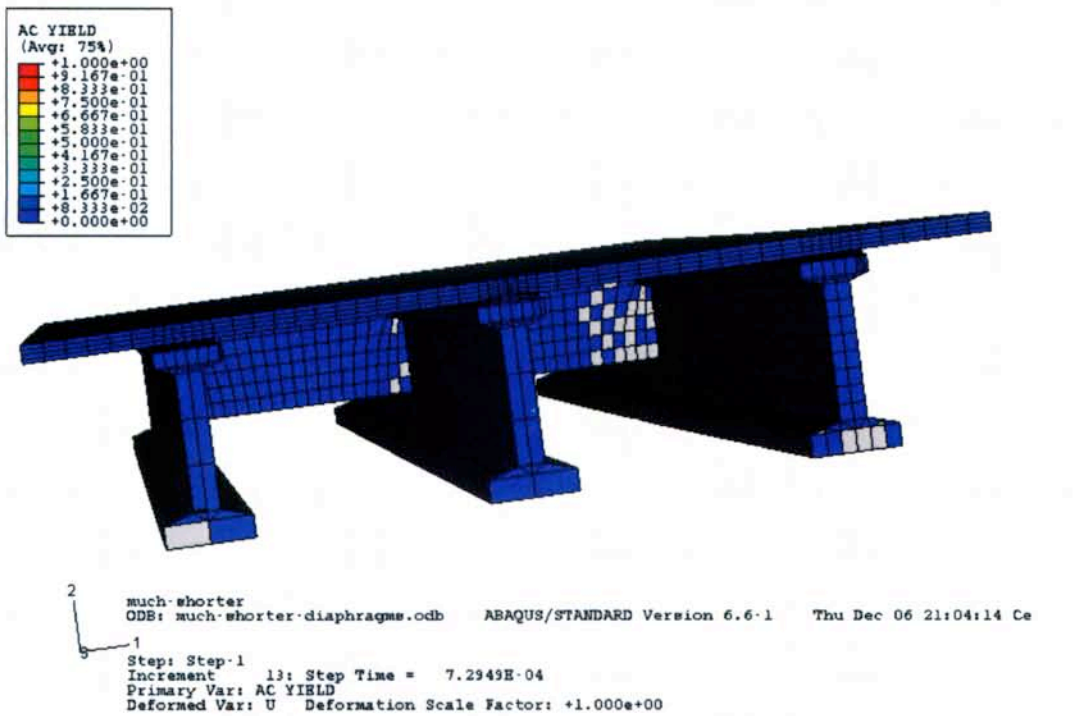

(b) 2/3 web depth

Figure C2. Side view of failure areas due to the decreasing depth of diaphragms

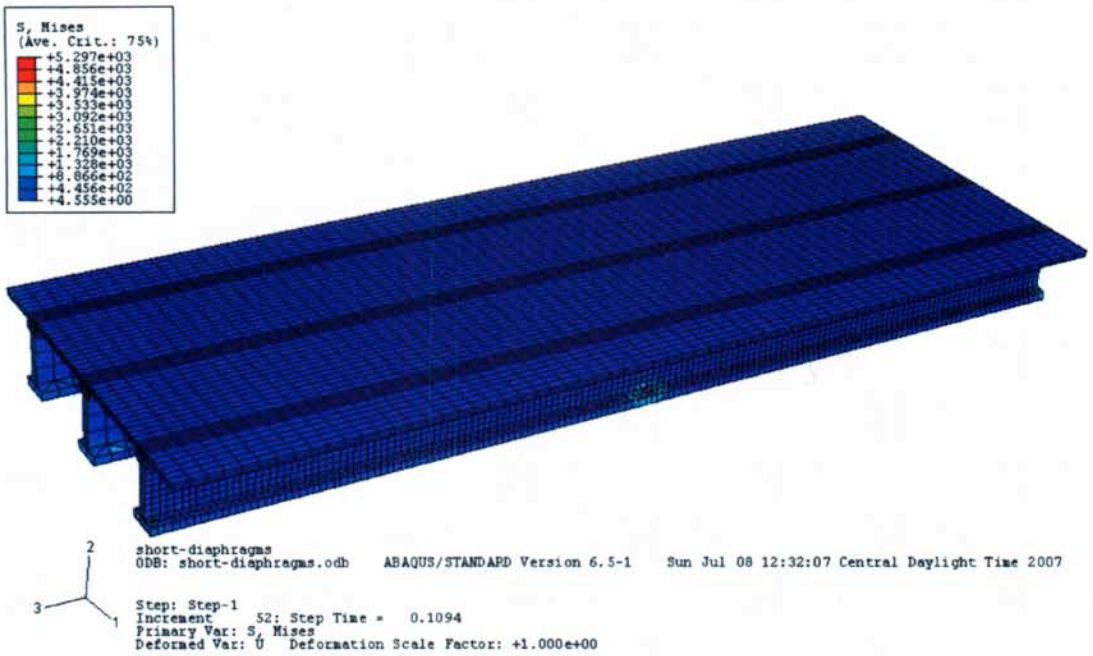

(a) Partial depth

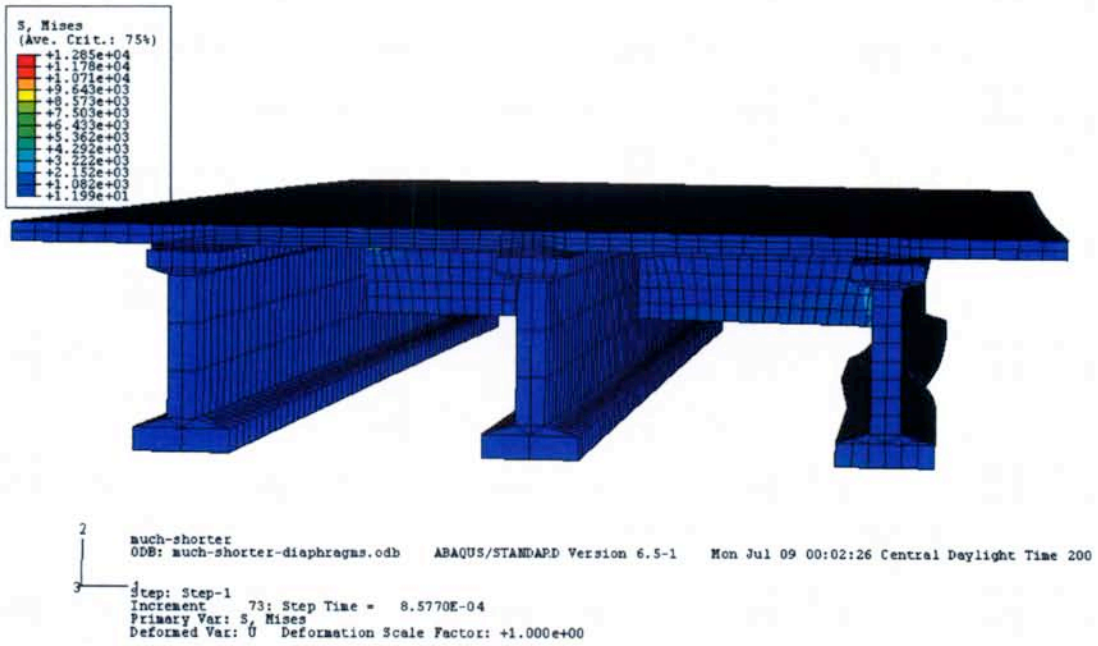

(b) 2/3 web depth

Figure C3. Von Mises stress concentrated along the loading point and the two supporting areas

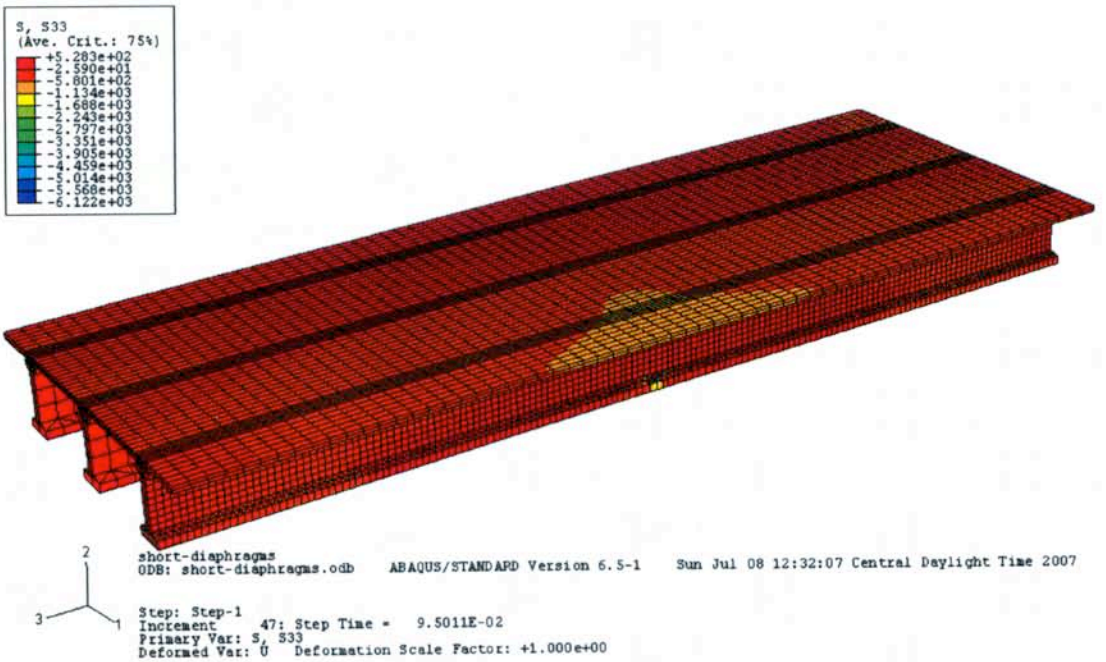

(a) Partial depth

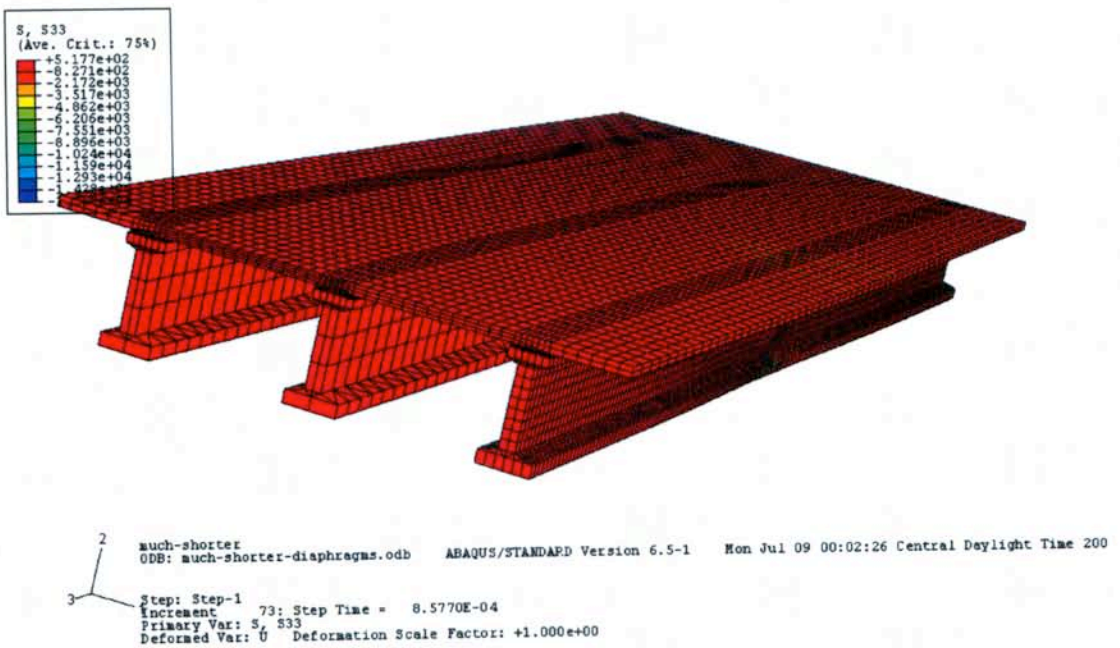

(b) 2/3 web depth

Figure C4. Tensile longitudinal stresses generated over large area of the bridge system due to the impact generated loading

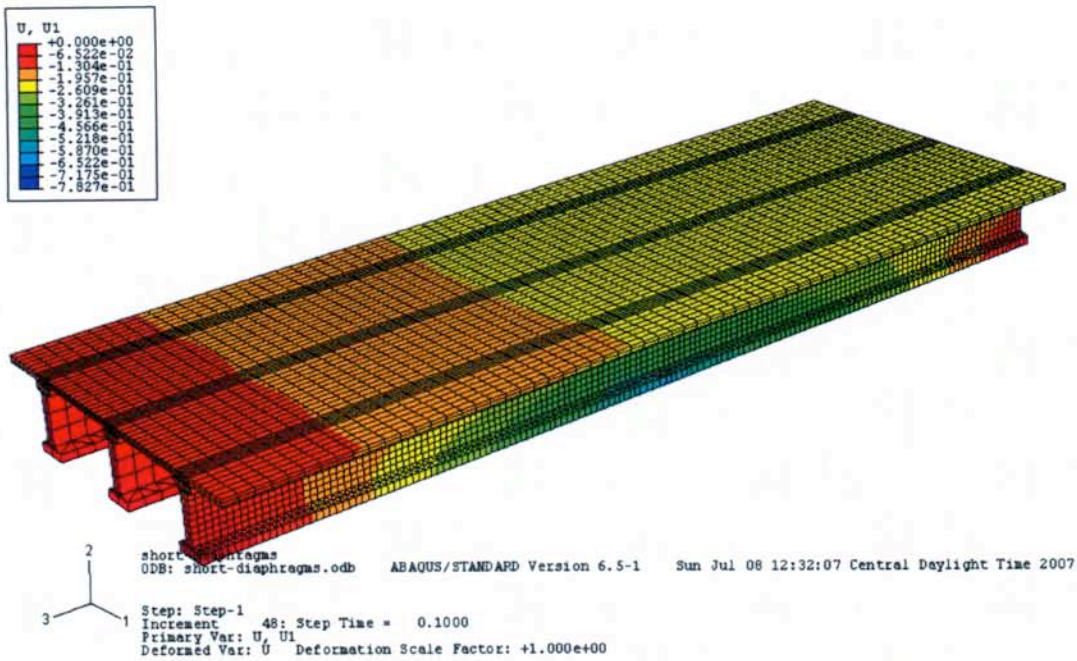

(a) Partial depth

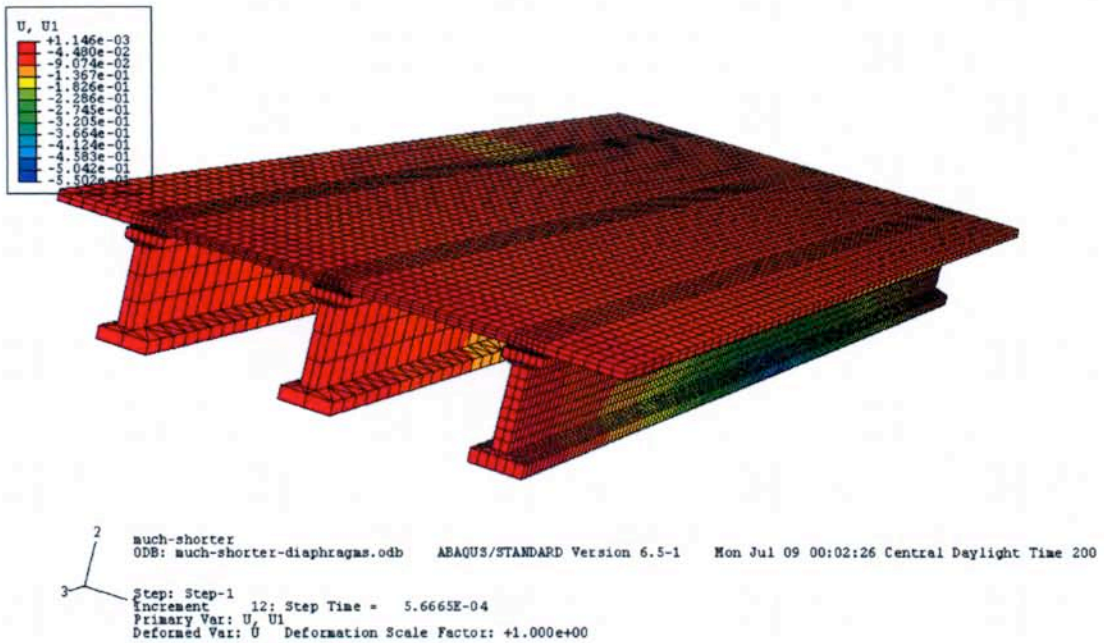

(b) 2/3 web depth

Figure C5. Horizontal displacement distribution

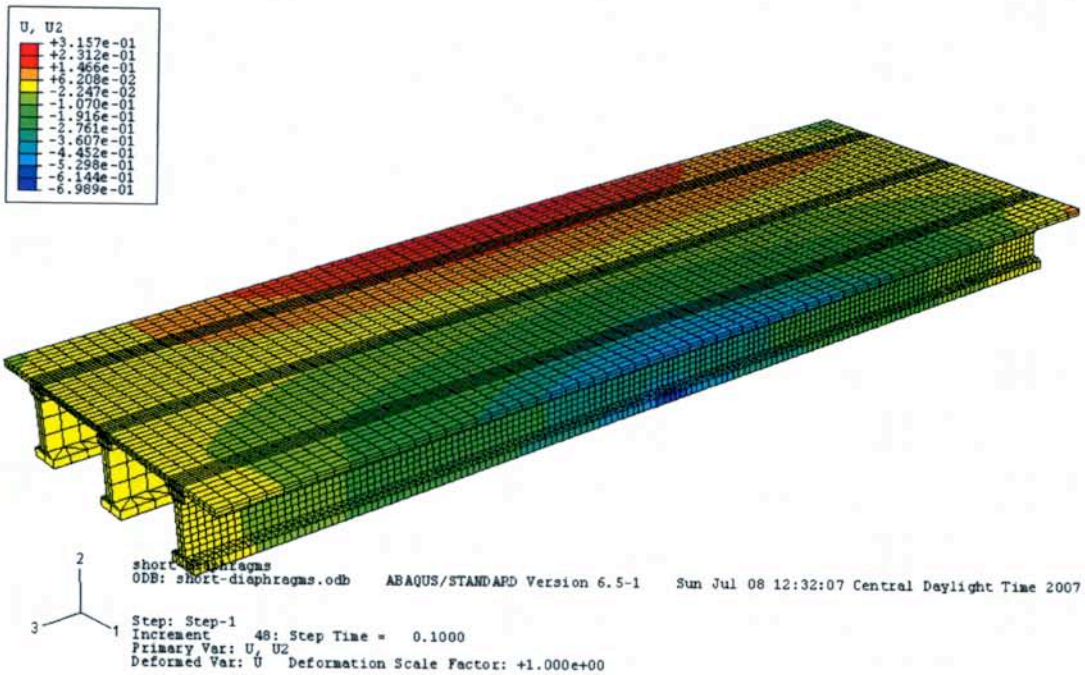

(a) Partial depth

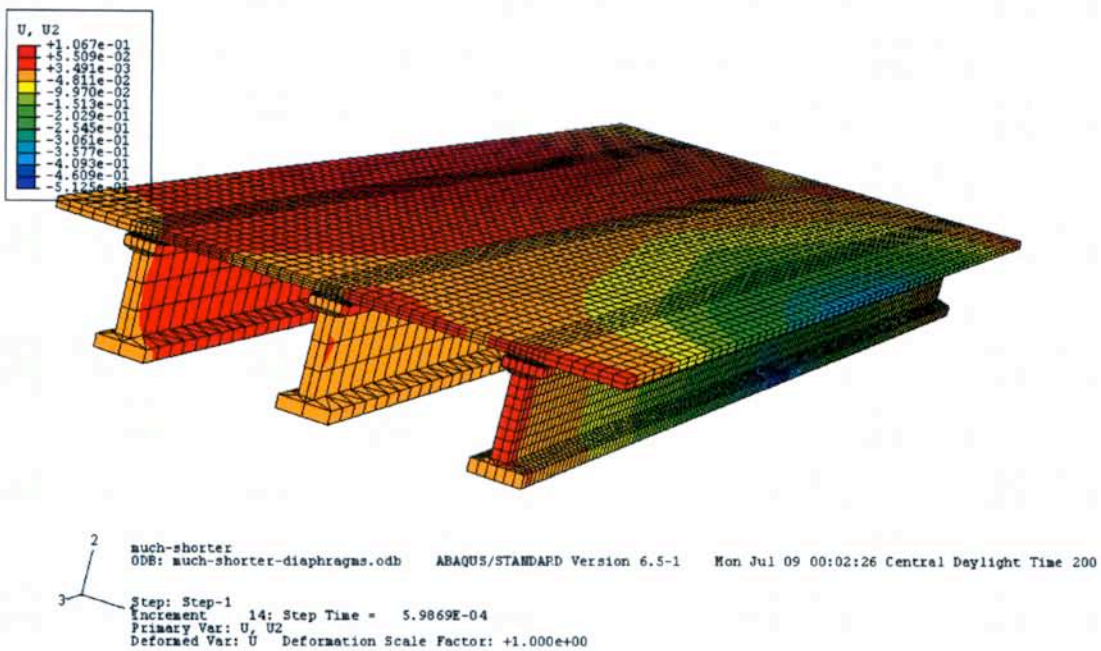

(b) 2/3 web depth

Figure C6. Vertical displacement distribution

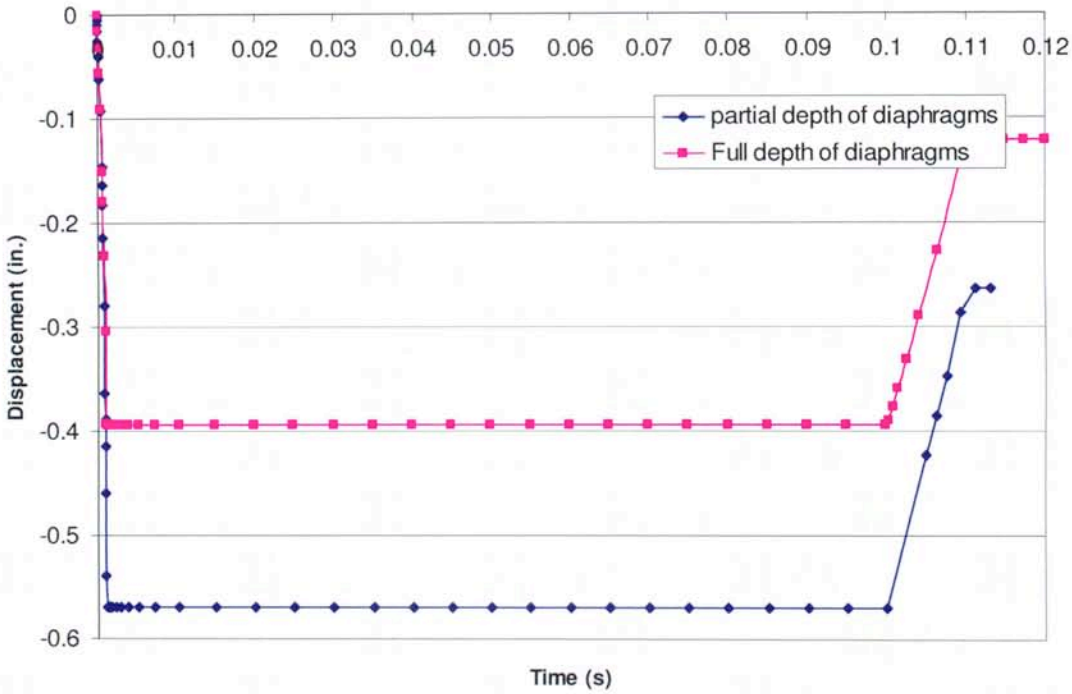

Figure C7. Comparison of the maximal horizontal displacement at the loading point between the full depth and partial depth of IDs

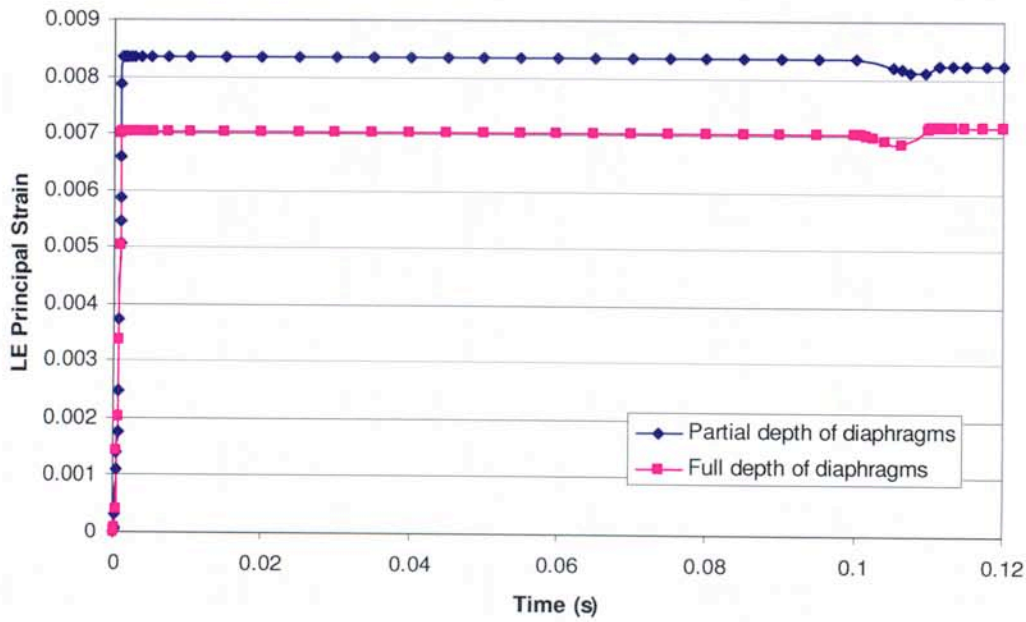

Figure C8. Comparison of the maximal strain at the loading point between the full depth and partial depth of IDs

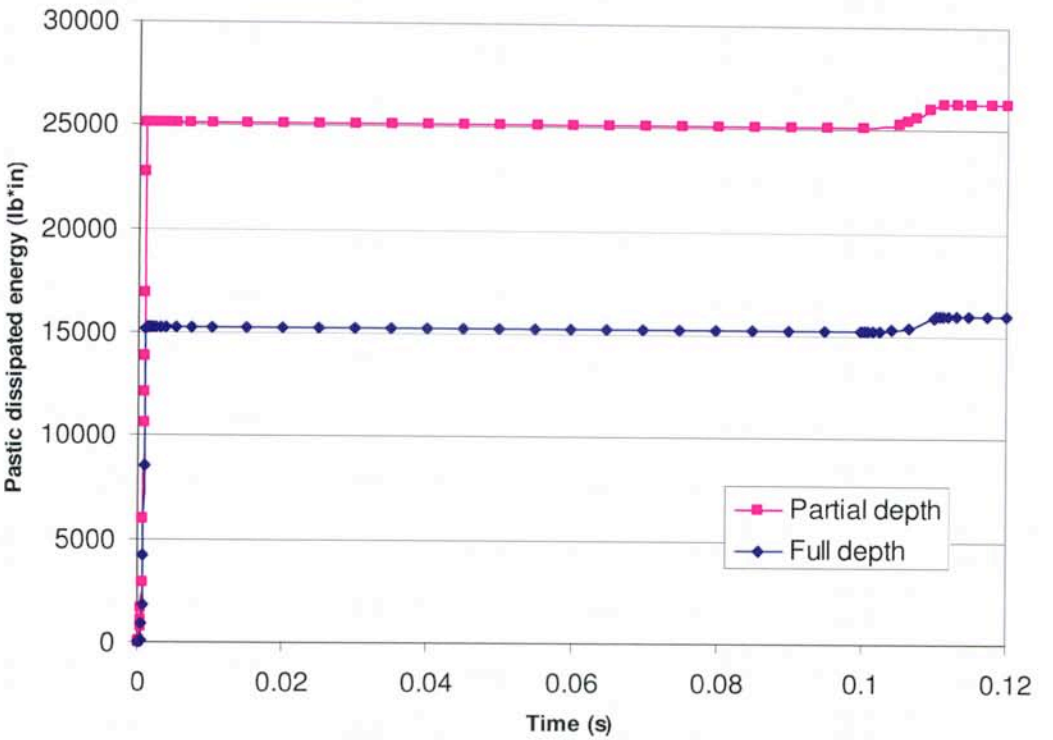

Figure C9. Comparison of the plastically energy dissipation at the loading point between the full depth and partial depth of IDs

Appendix D. Effect of Girder Spacing

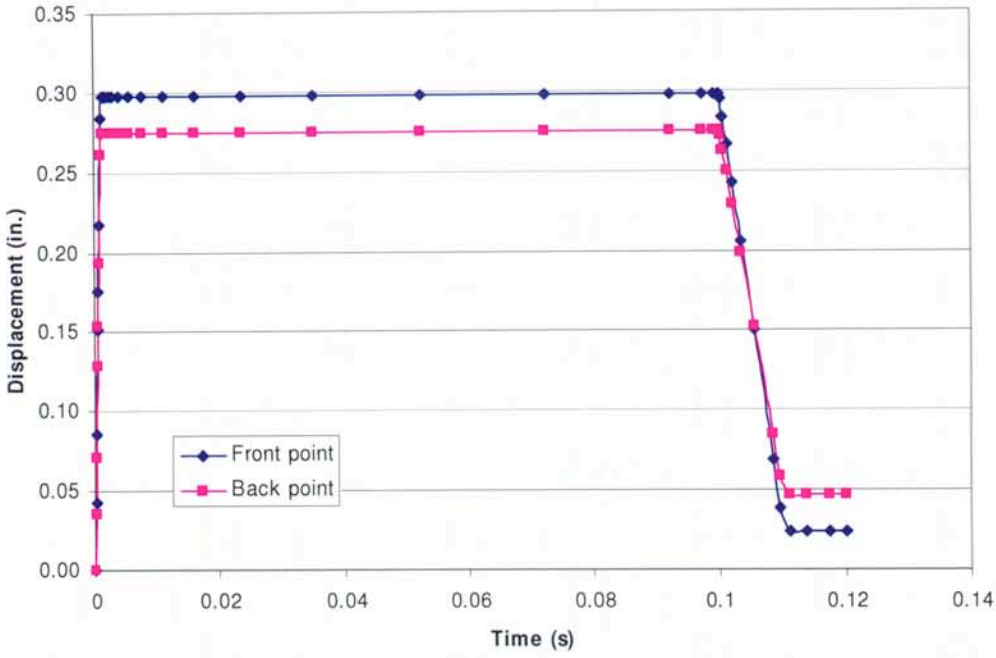

(a) 8 ft. girder spacing

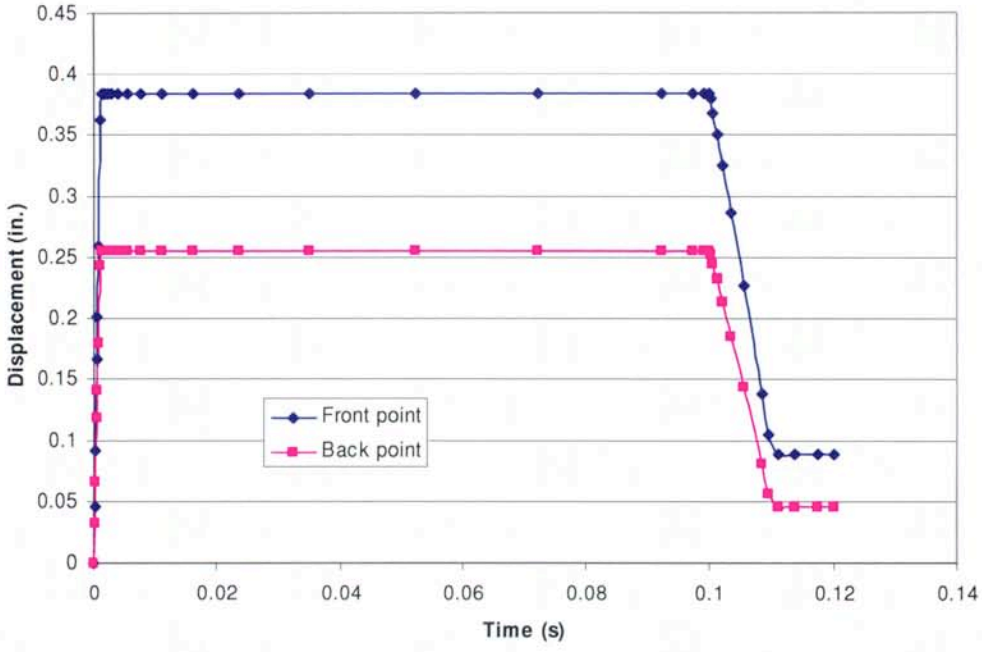

(b) 10 ft. girder spacing

Figure D1. Horizontal displacement of the bridge girder at the loading point and at the opposite girder point along the loading direction

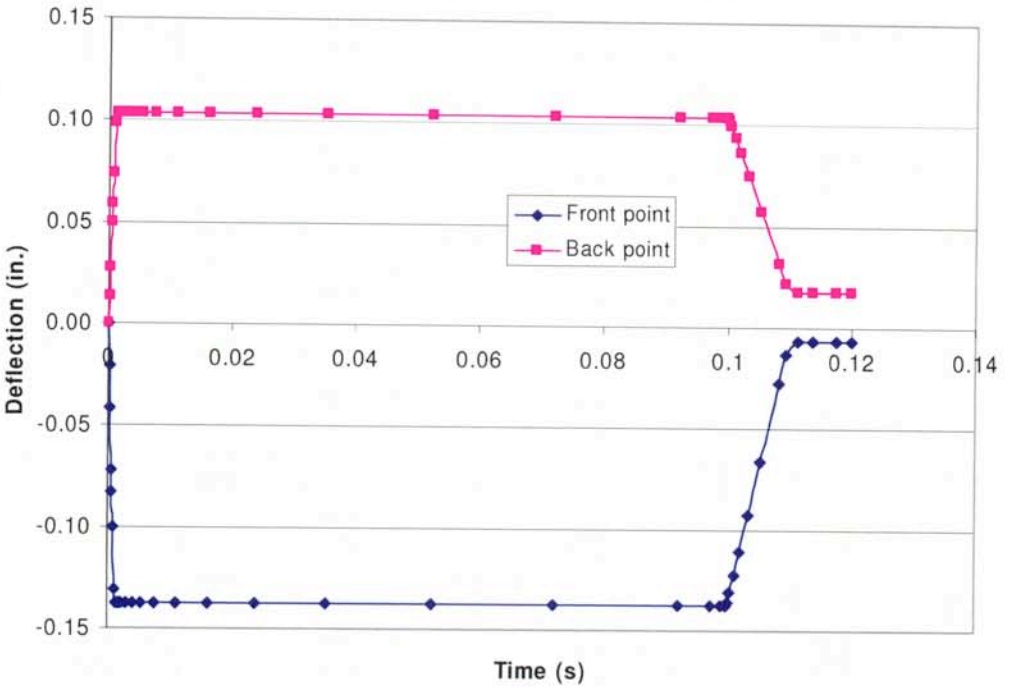

(a) 8 ft. girder spacing

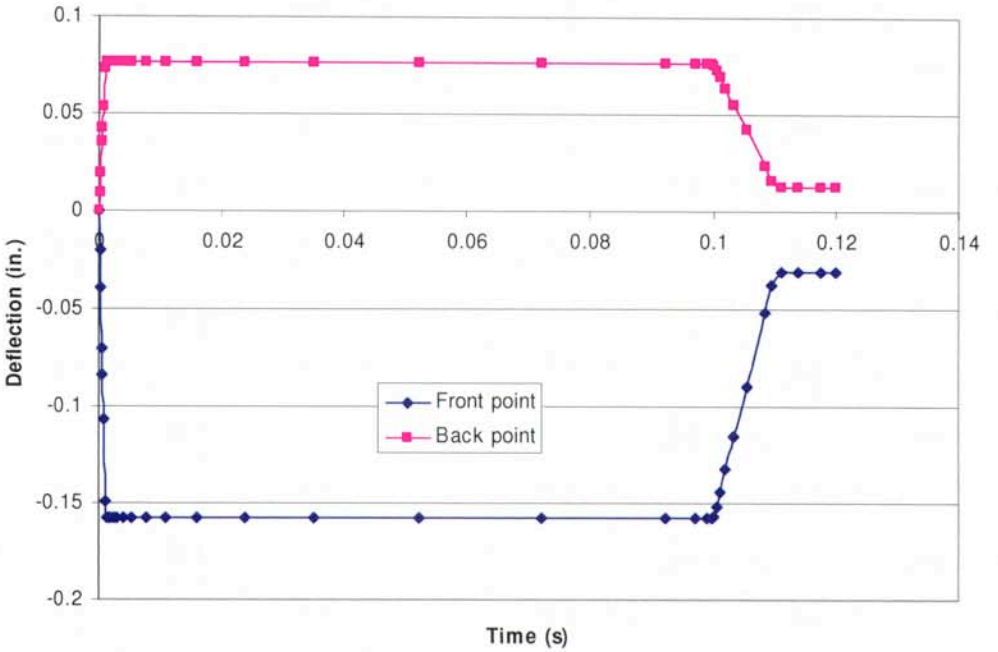

(b) 10 ft. girder spacing

Figure D2. Vertical deflection of the bridge at the loading point and at the opposite girder point along the loading direction (the front portion bended downward, while the back portion bended upward)

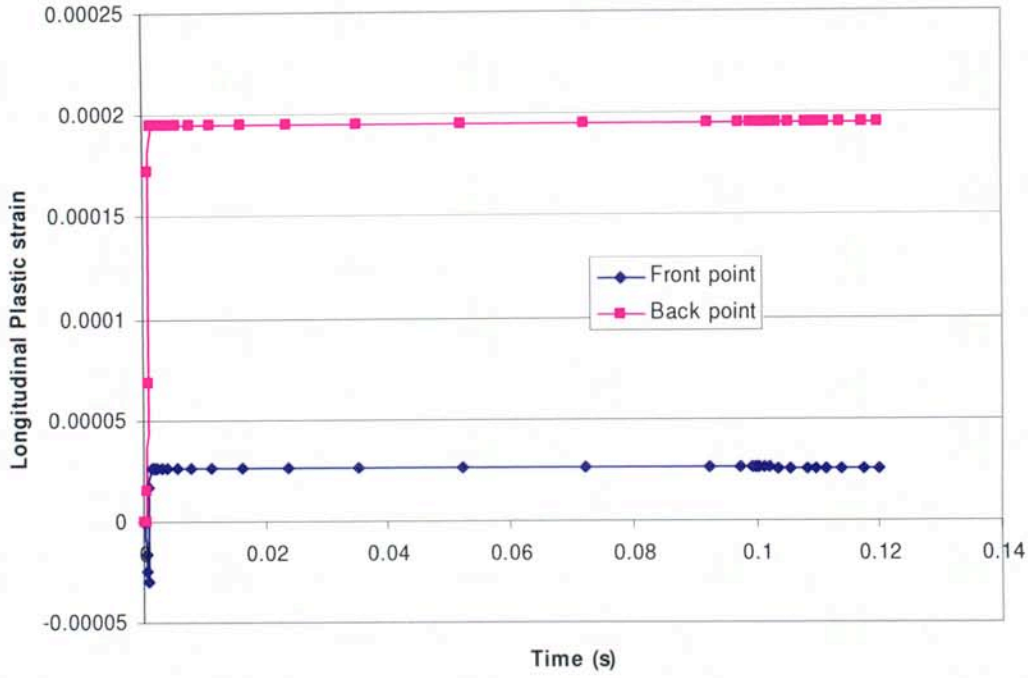

(a) 8 ft. girder spacing

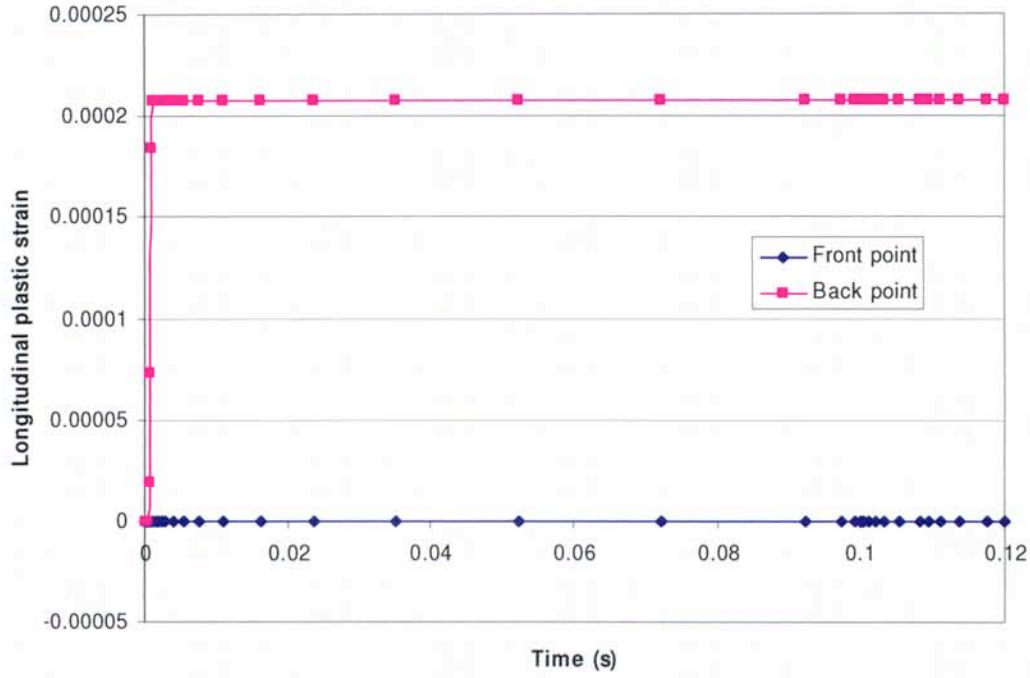

(b) 10 ft. girder spacing

Figure D3. Longitudinal plastic strain of the bridge at the loading point and at the opposite girder point

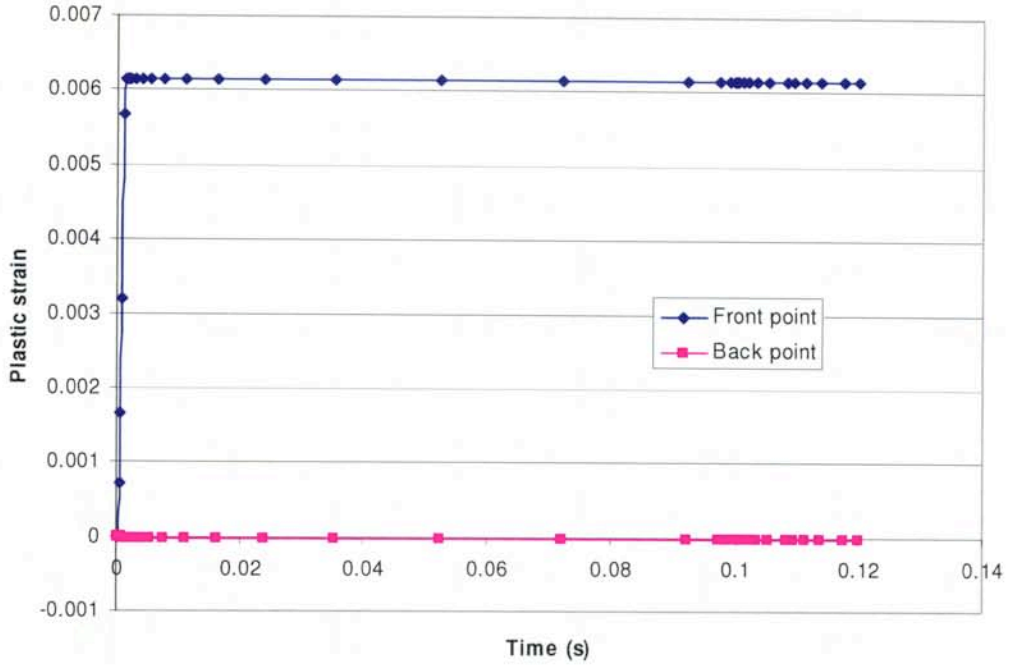

(a) 8 ft. girder spacing

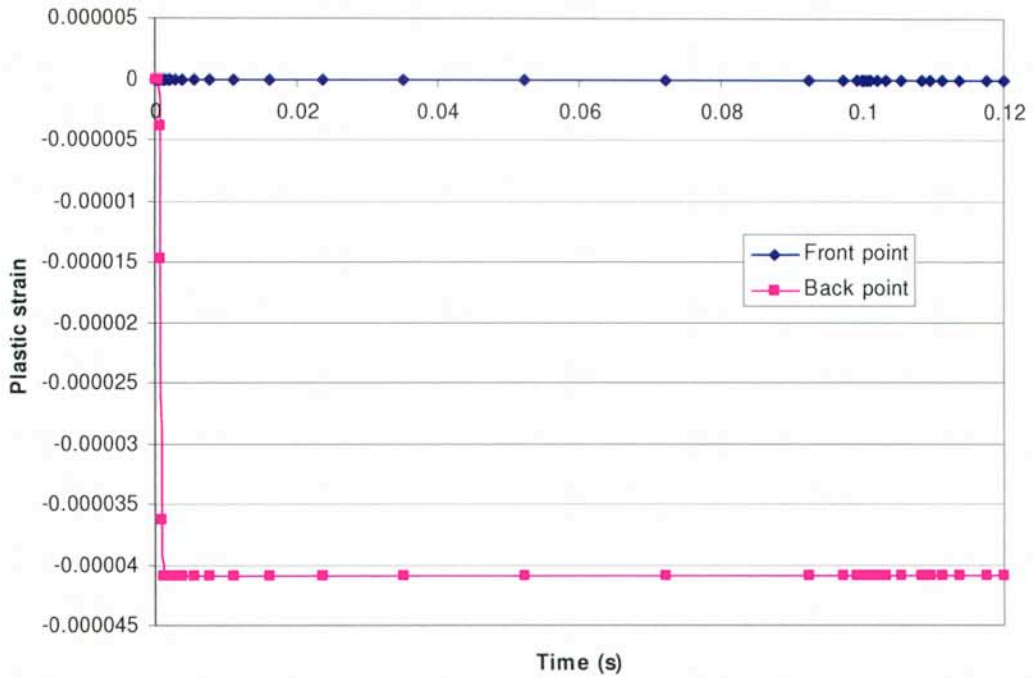

(b) 10 ft. girder spacing

Figure D4. Transverse plastic strain of the bridge at the loading point and at the opposite girder point along the loading direction

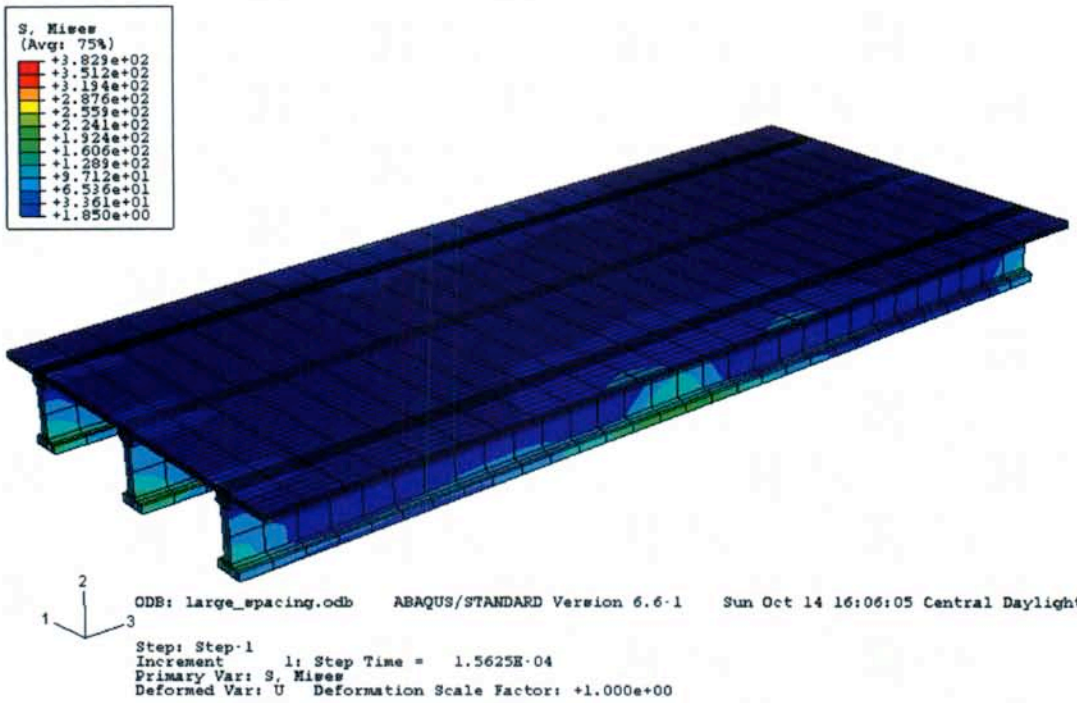

(a) 8 ft. girder spacing

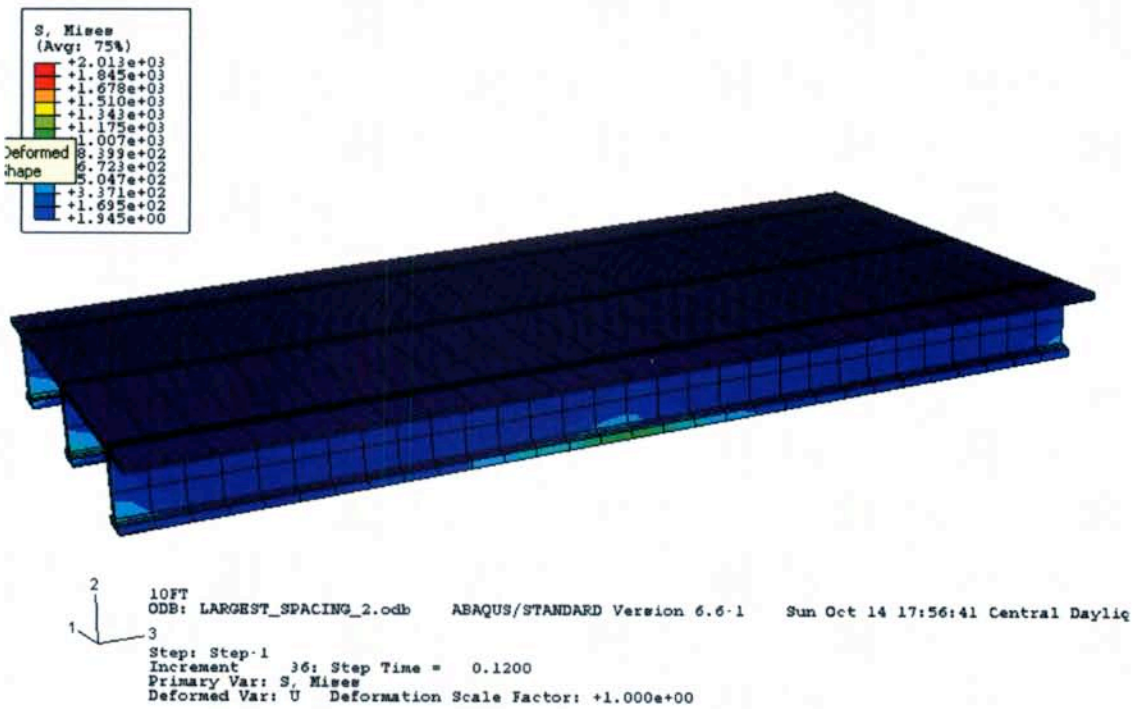

(b) 10 ft. girder spacing

Figure D5. Von Mises distributions of the bridge

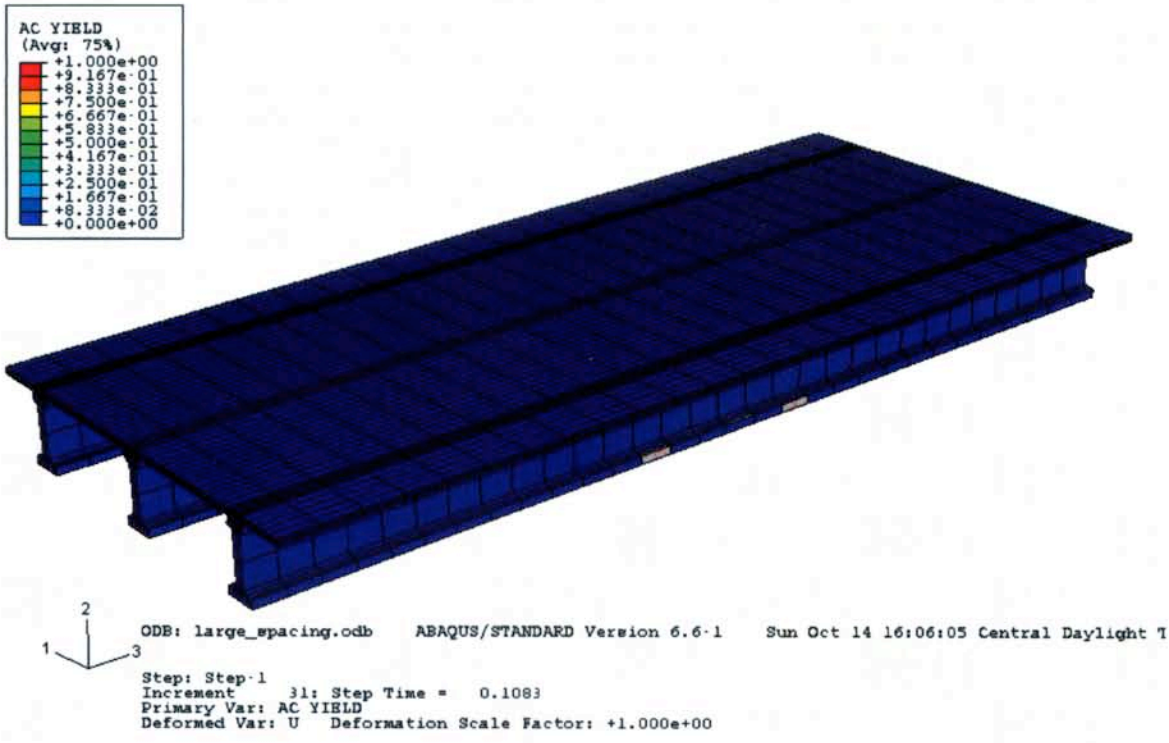

(a) 8 ft. girder spacing

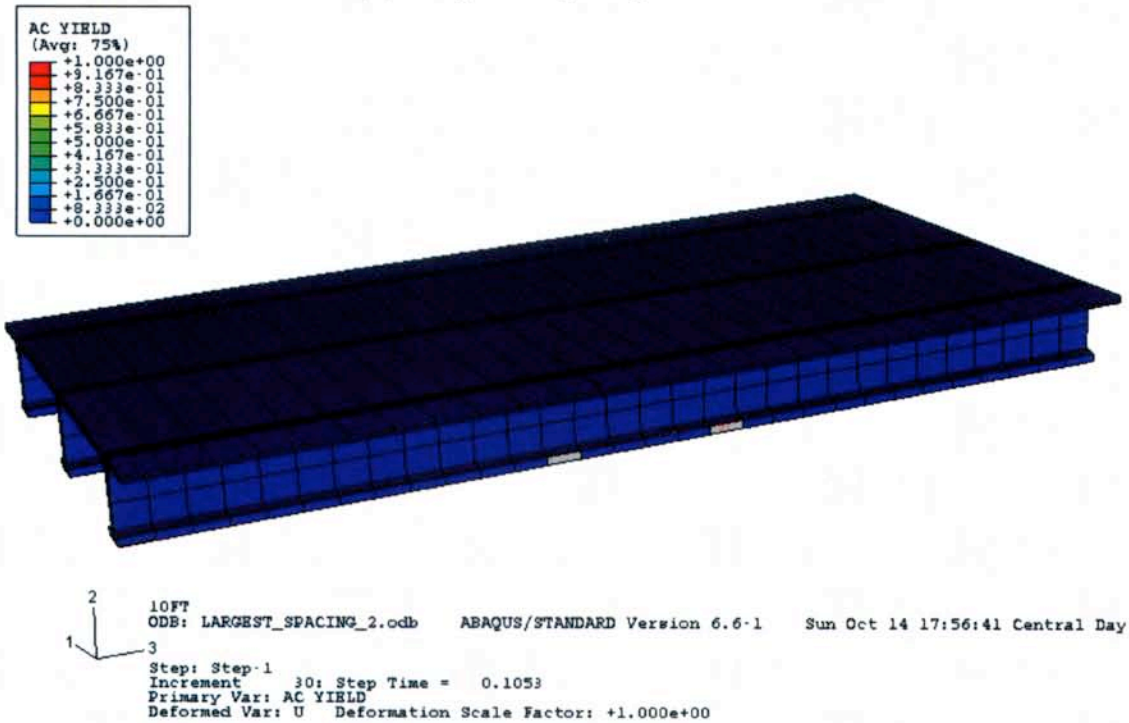

(b) 10 ft. girder spacing

Figure D6. Failed elements of the bridge

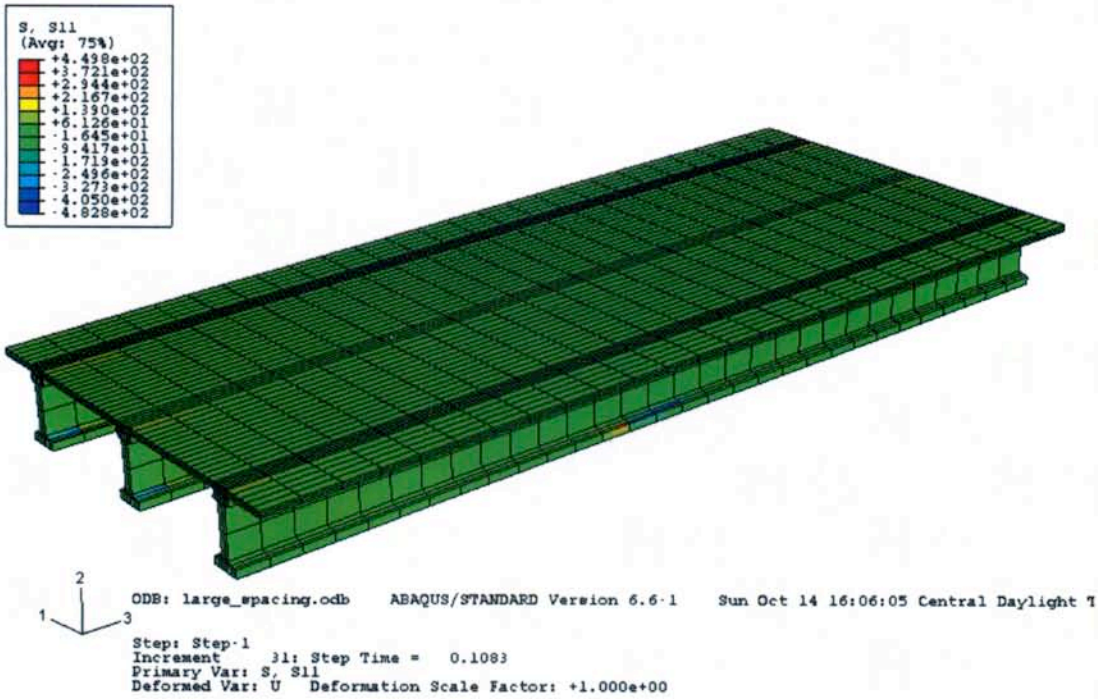

(a) 8 ft. girder spacing

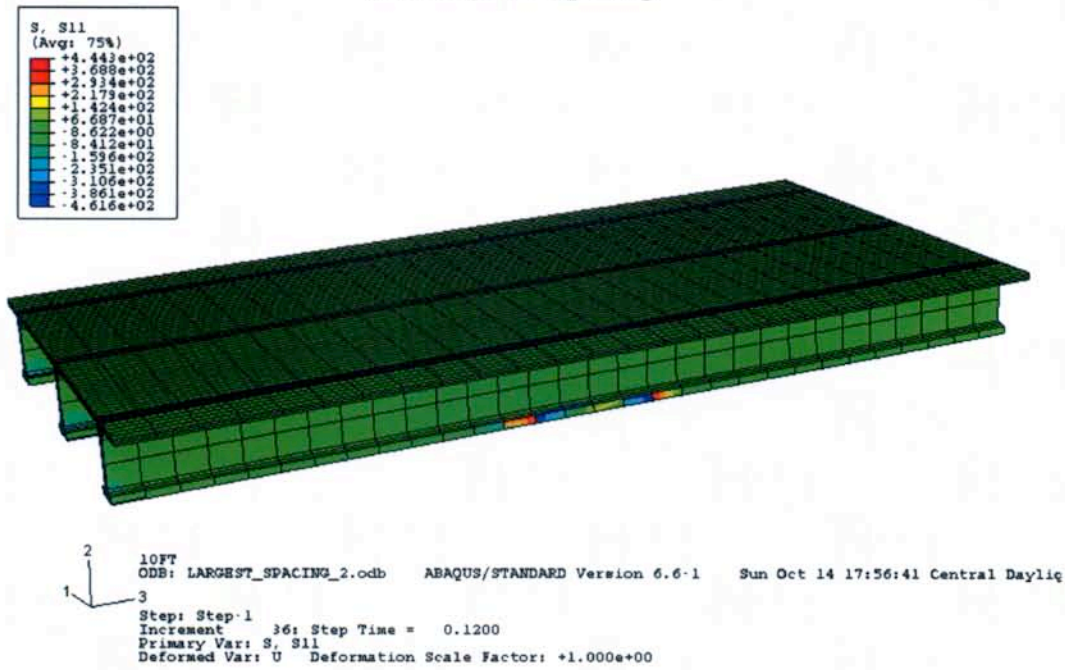

(b) 10 ft. girder spacing

Figure D7. Transverse stress distribution of the bridge system along the loading direction

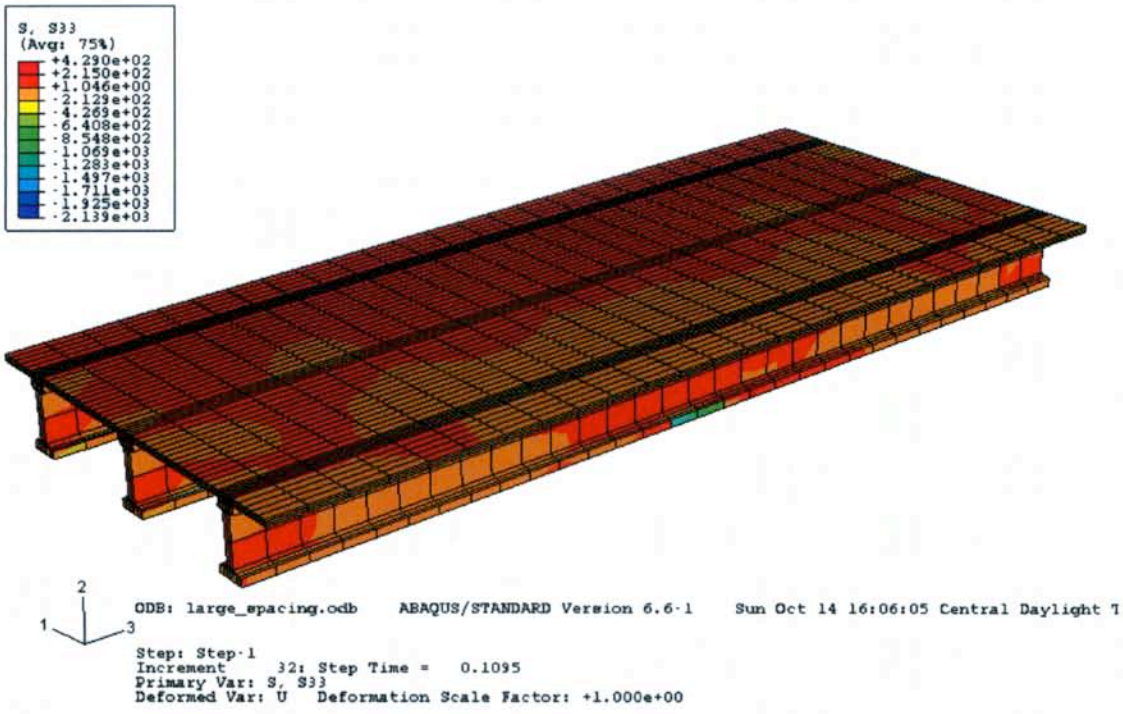

(a) 8 ft. girder spacing

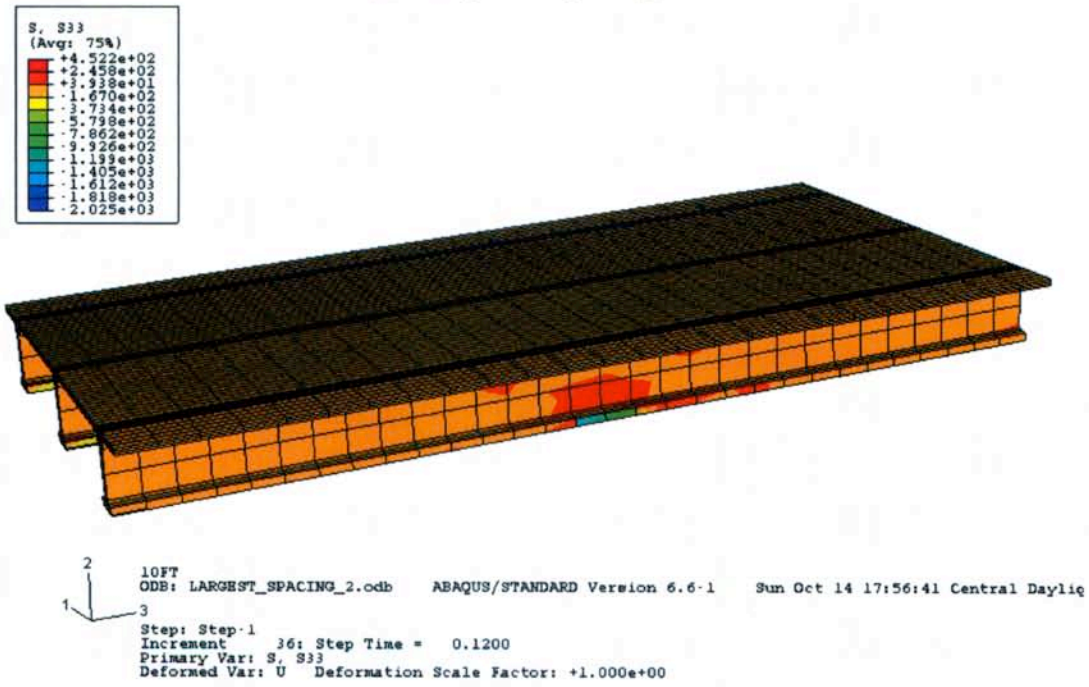

(b) 10 ft. girder spacing

Figure D8. Longitudinal stress distribution of the bridge

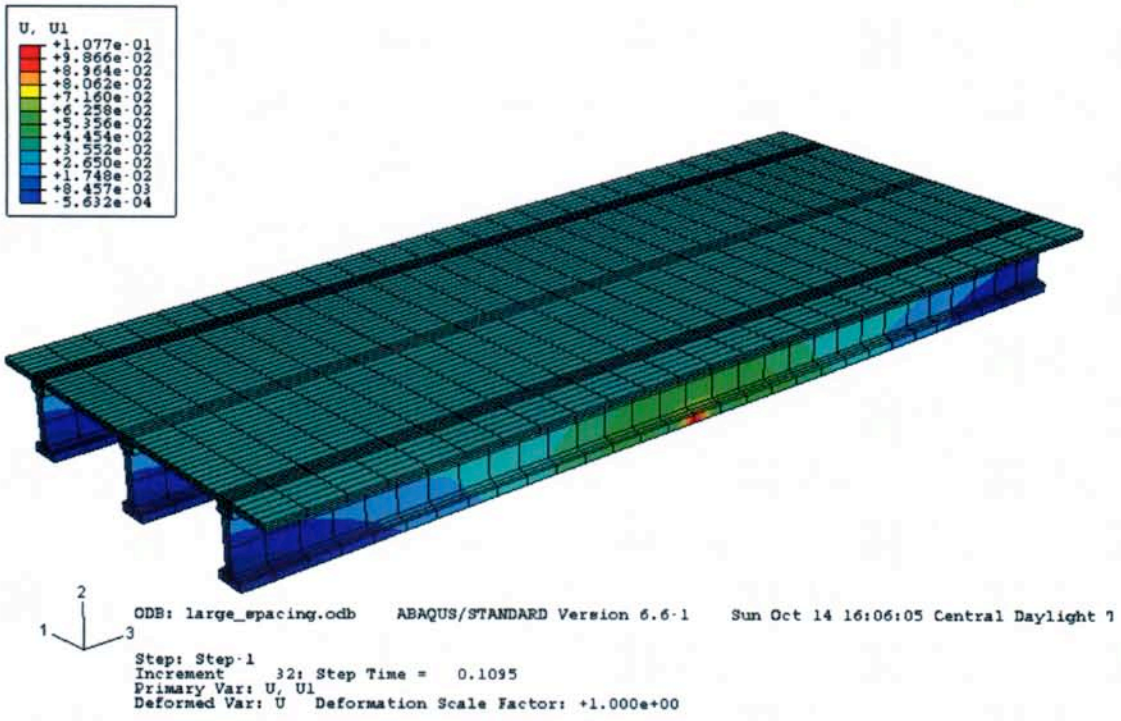

(a) 8 ft. girder spacing

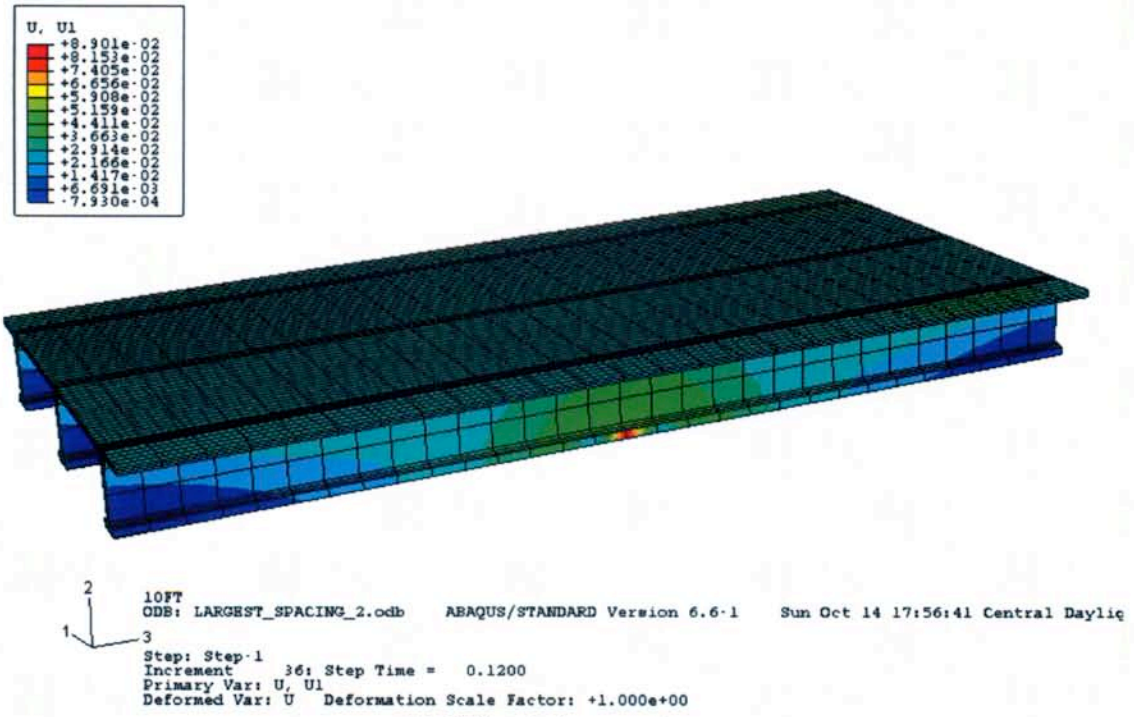

(b) 10 ft. girder spacing

Figure D9. Horizontal displacement distribution along the loading direction

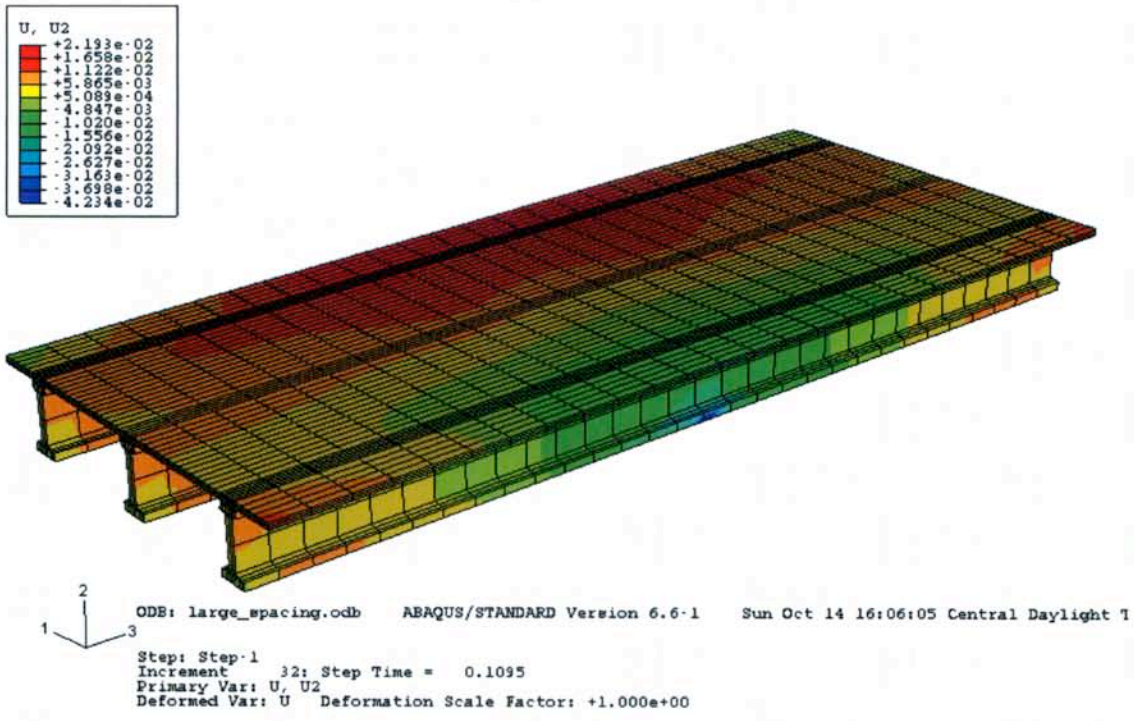

(a) 8 ft. girder spacing

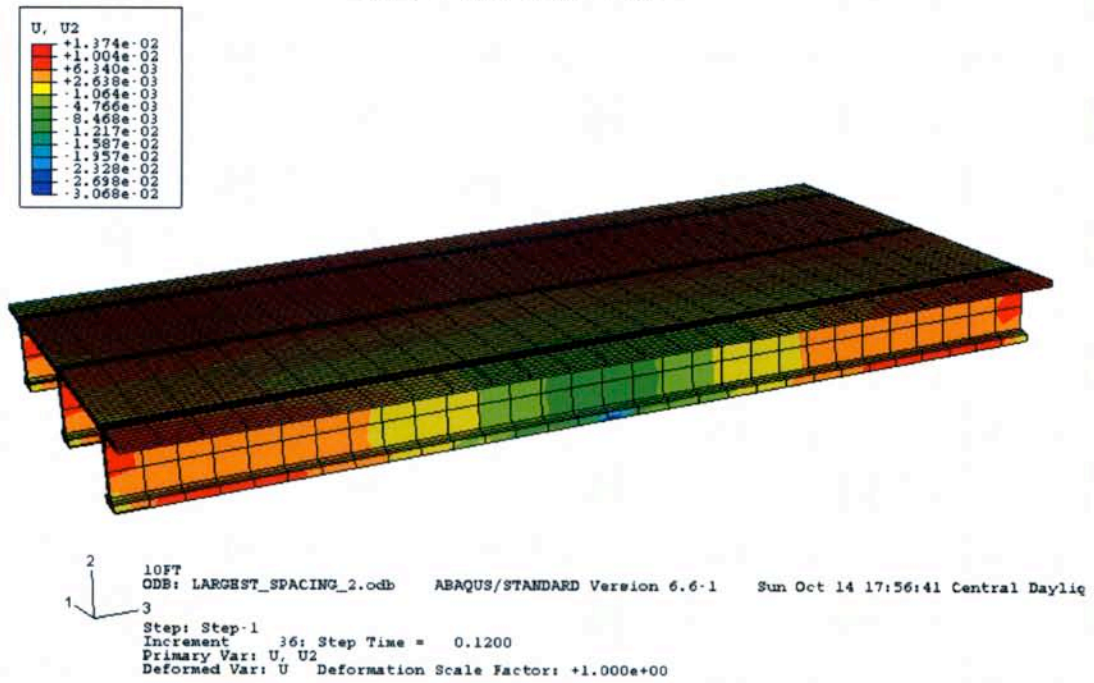

(b) 10 ft. girder spacing

Figure D10. Vertical deflection distribution of the bridge

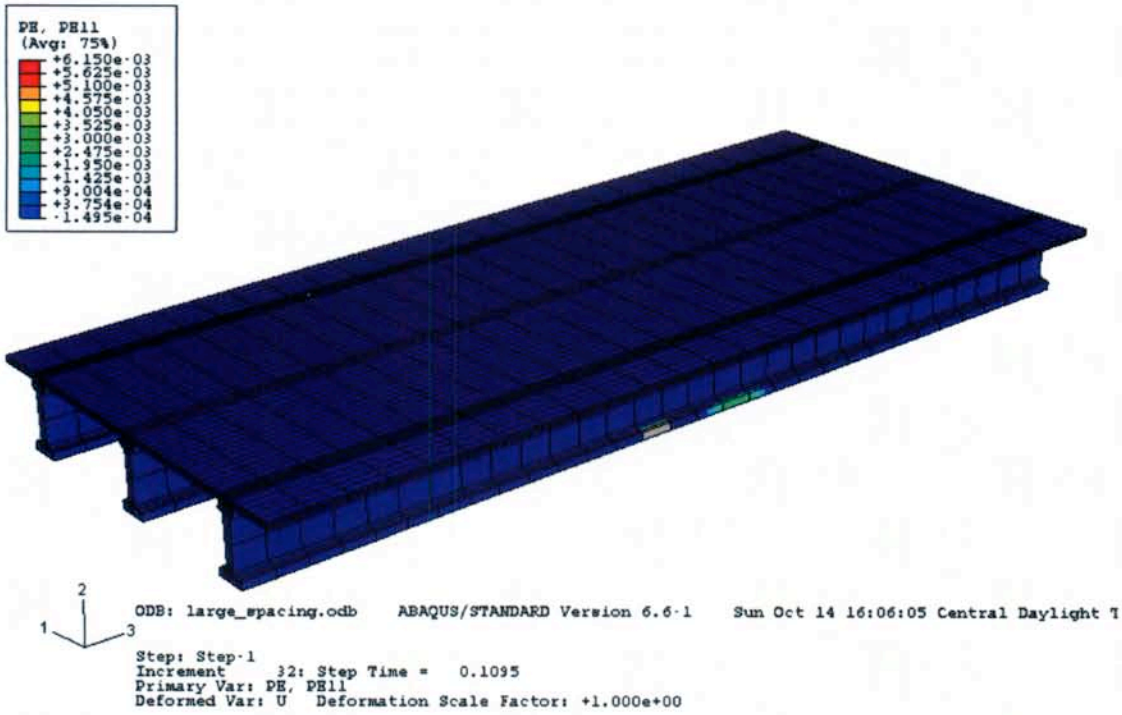

(a) 8 ft. girder spacing

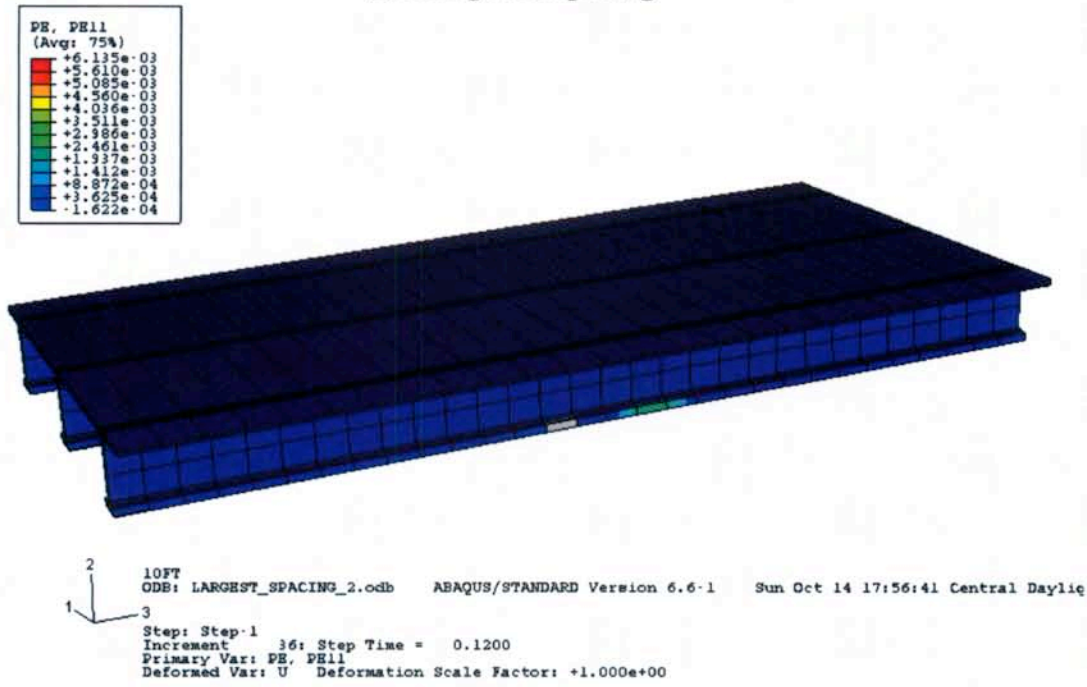

(b) 10 ft. girder spacing

Figure D11. Plastic strain distribution of the bridge along the loading direction (PE11 stands for the plastic strain in the 11 (transverse) direction)

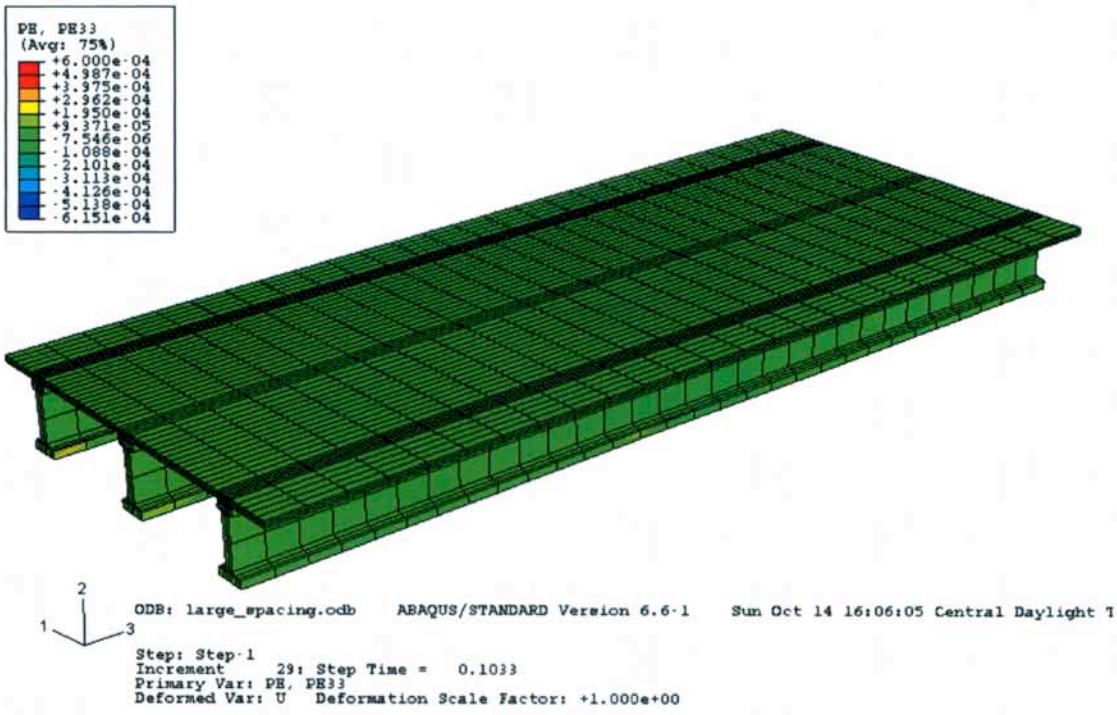

(a) 8 ft. girder spacing

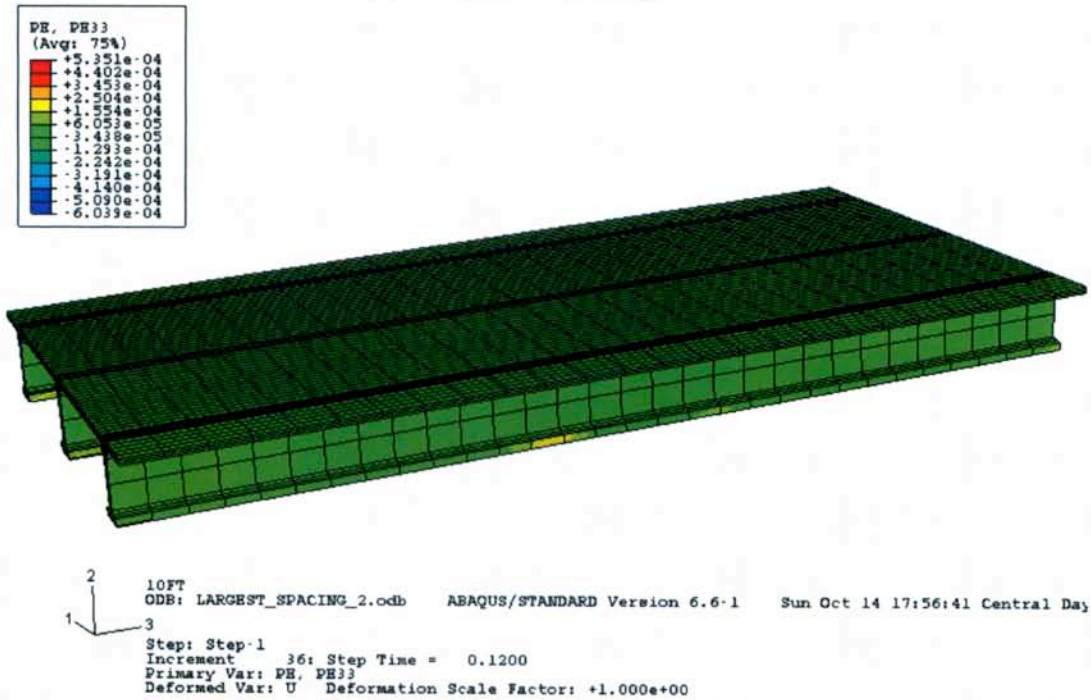

(b) 10 ft. girder spacing

Figure D12. Longitudinal plastic strain distribution (PE33 stands for the plastic strain in the 33 (longitudinal) direction)

Appendix E. Effect of Girder Types

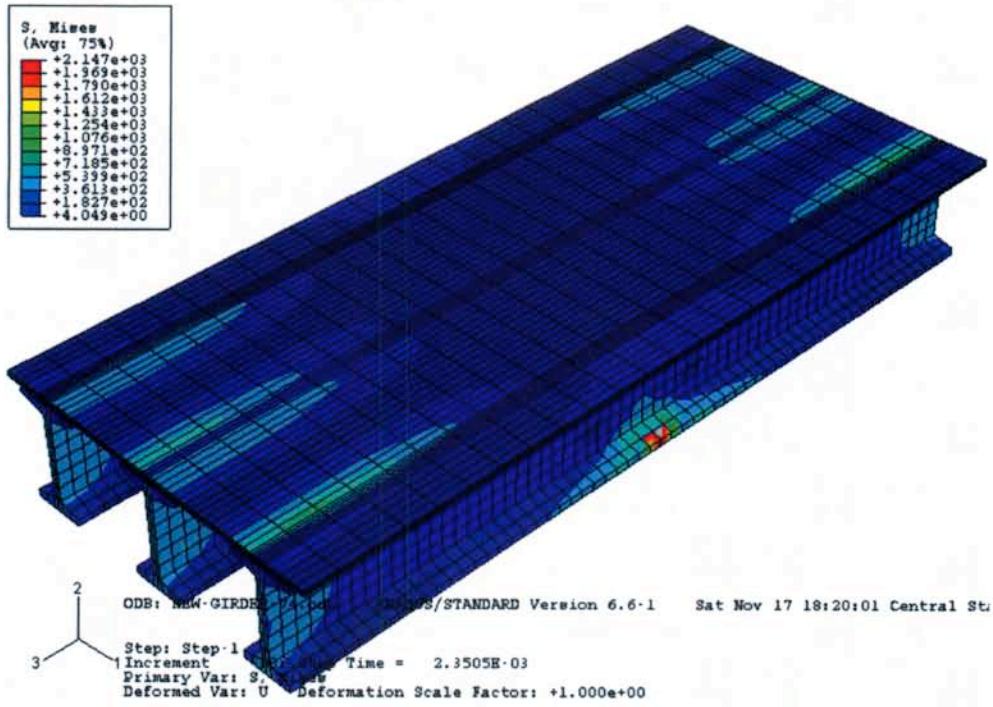

(a) WF74G

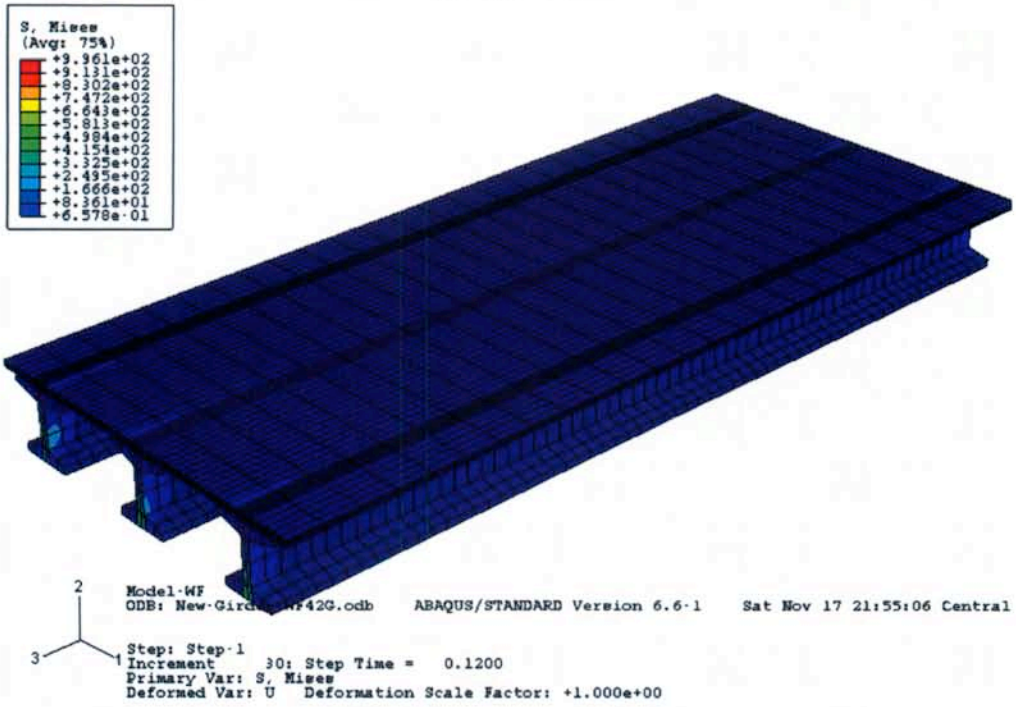

(b) WF42G

Figure E1. Von Mises stress distribution under the full design loading

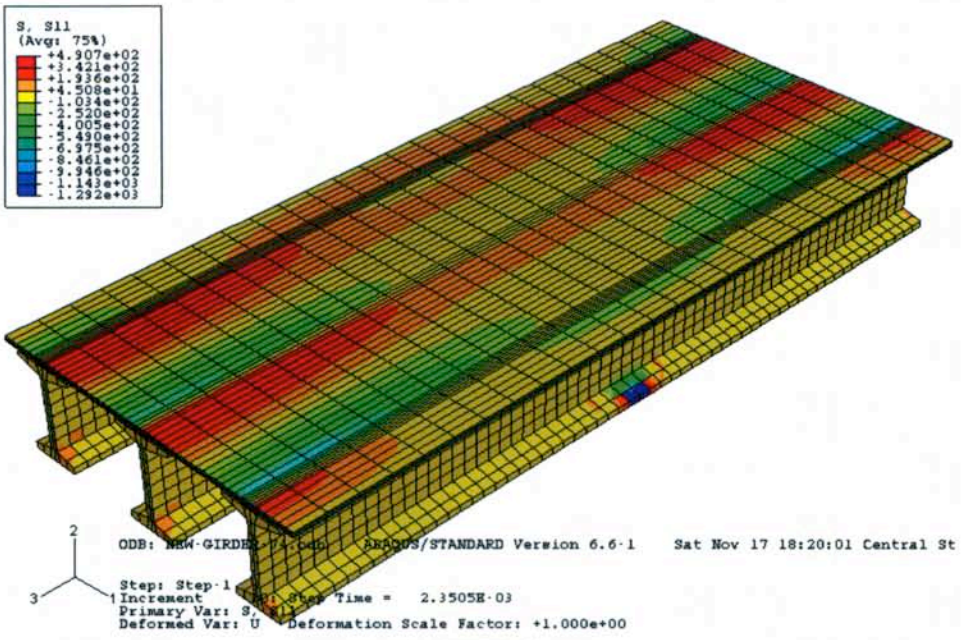

(a) WF74G

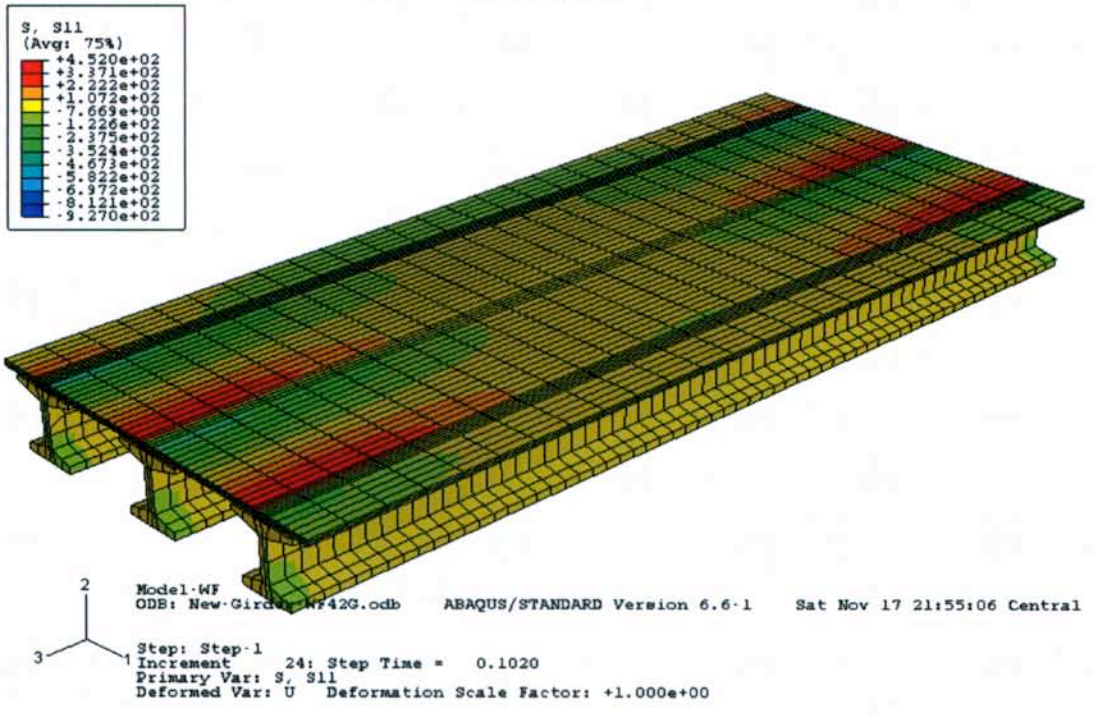

(b) WF42G

Figure E2. Transverse stress distribution along the loading direction

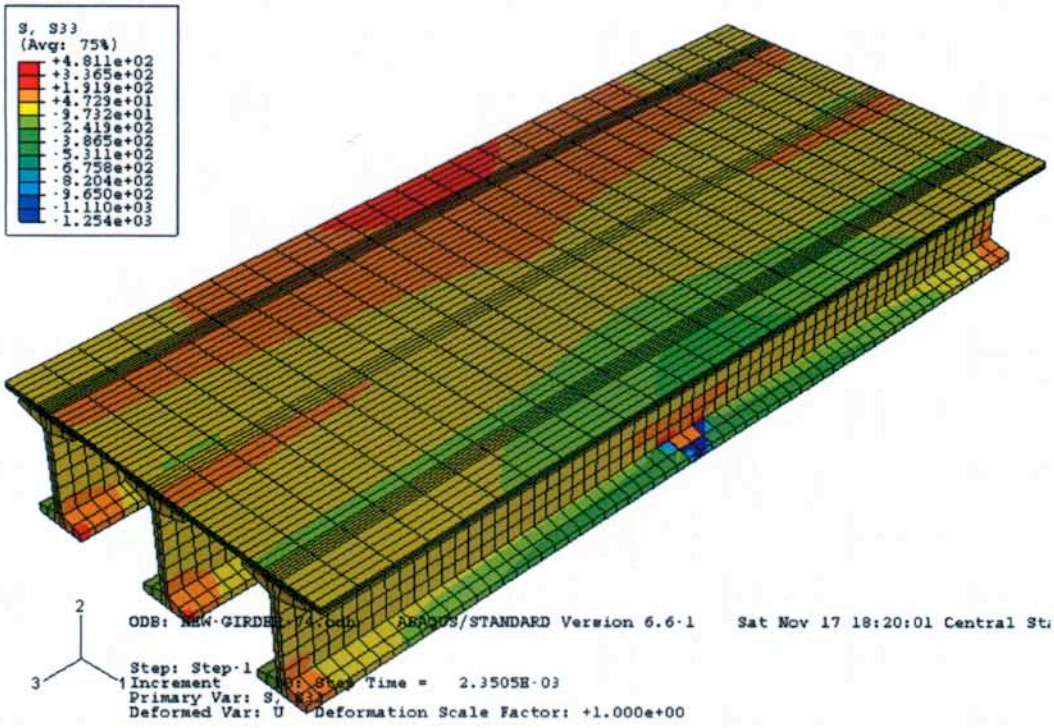

(a) WF74G

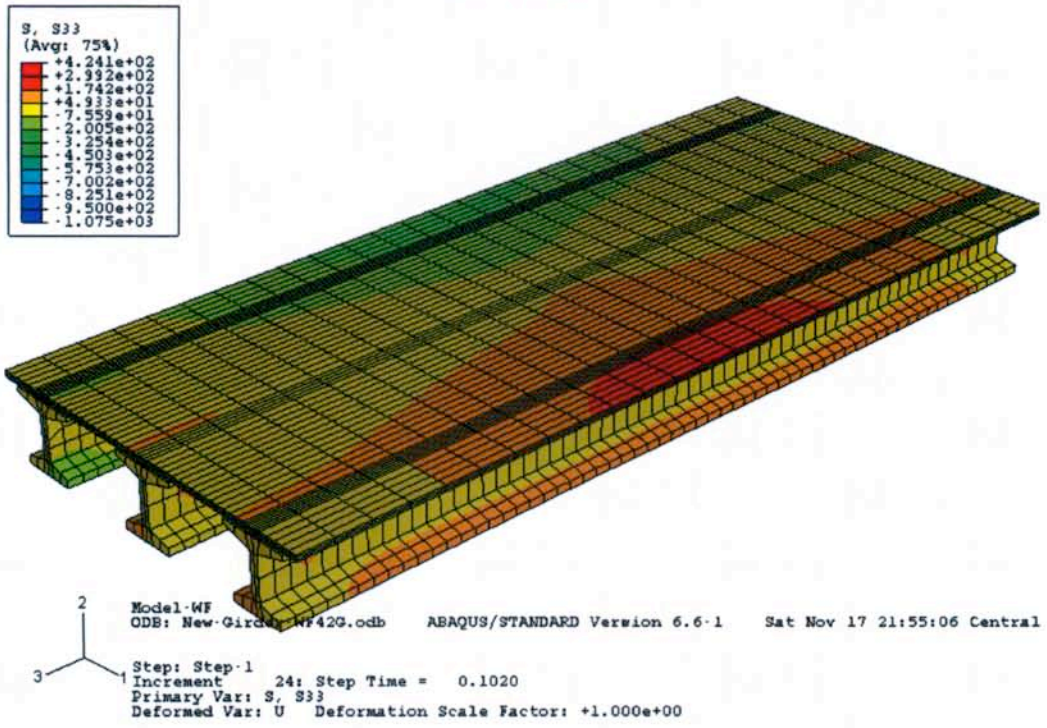

(b) WF42G

Figure E3. Longitudinal stress distribution

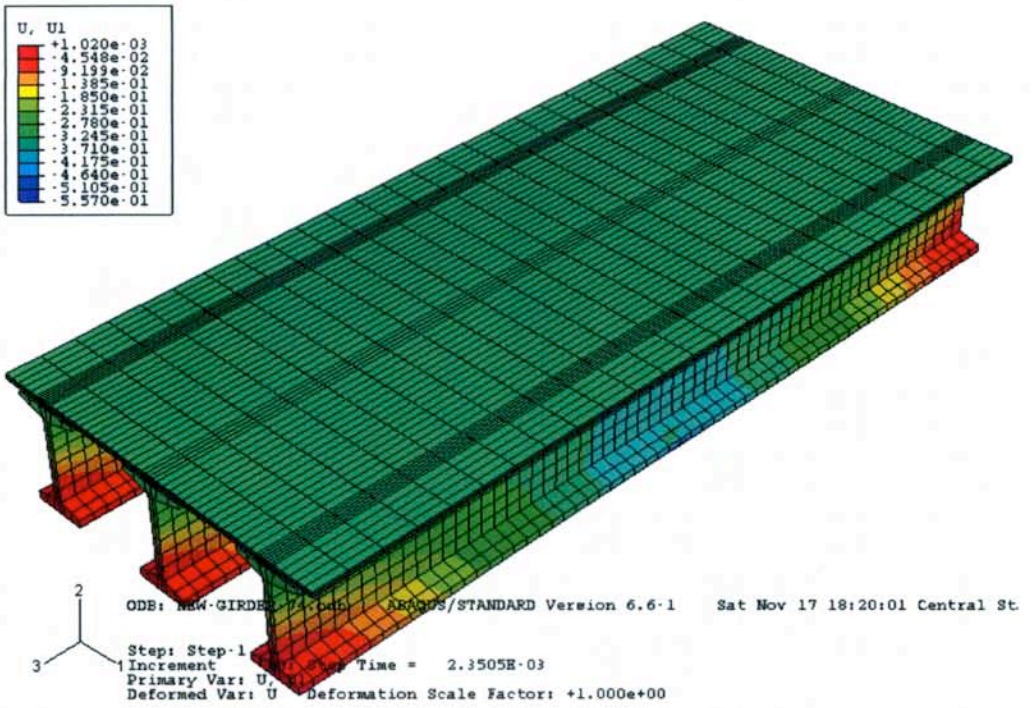

(a) WF74G

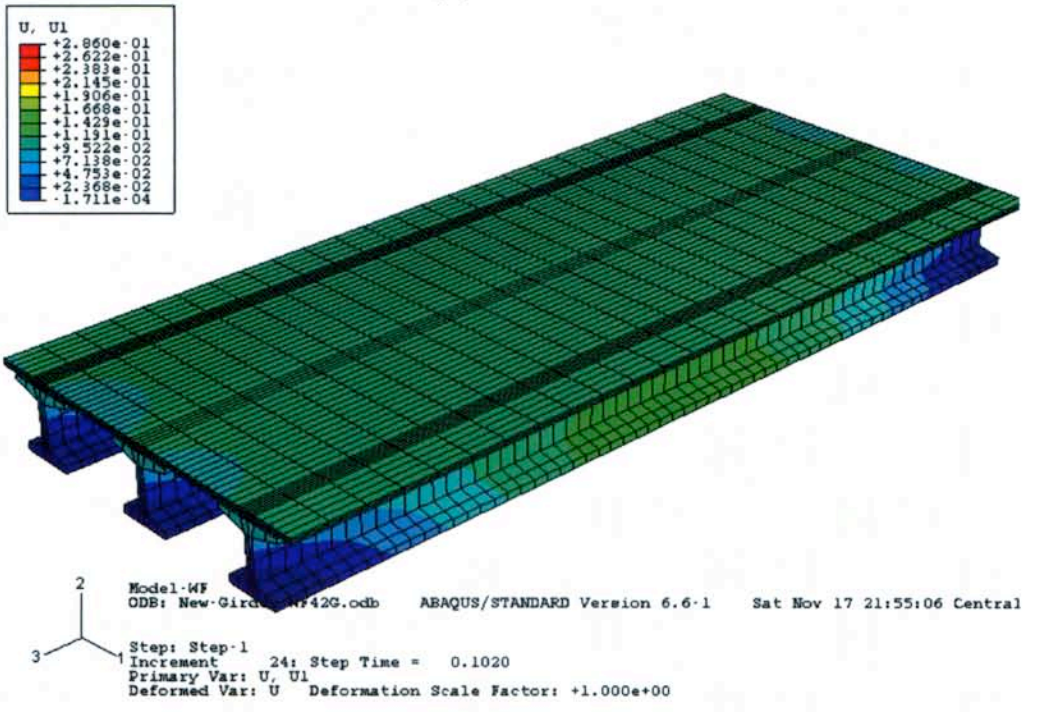

(b) WF42G

Figure E4. Transverse displacement distribution along the loading direction

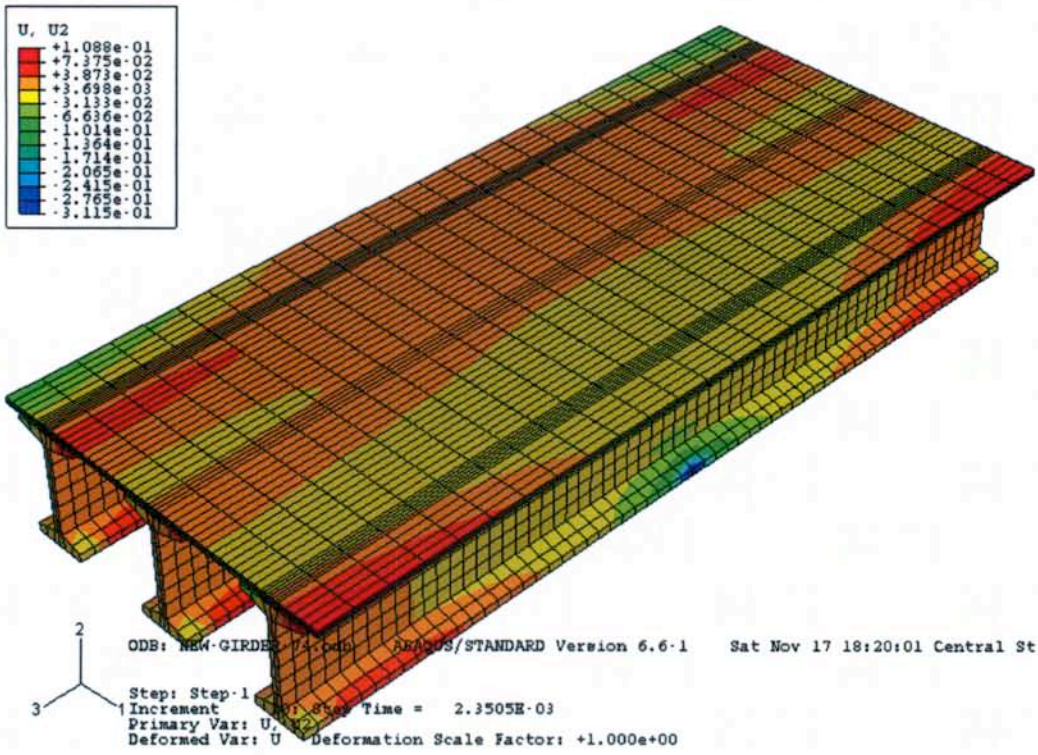

(a) WF74G

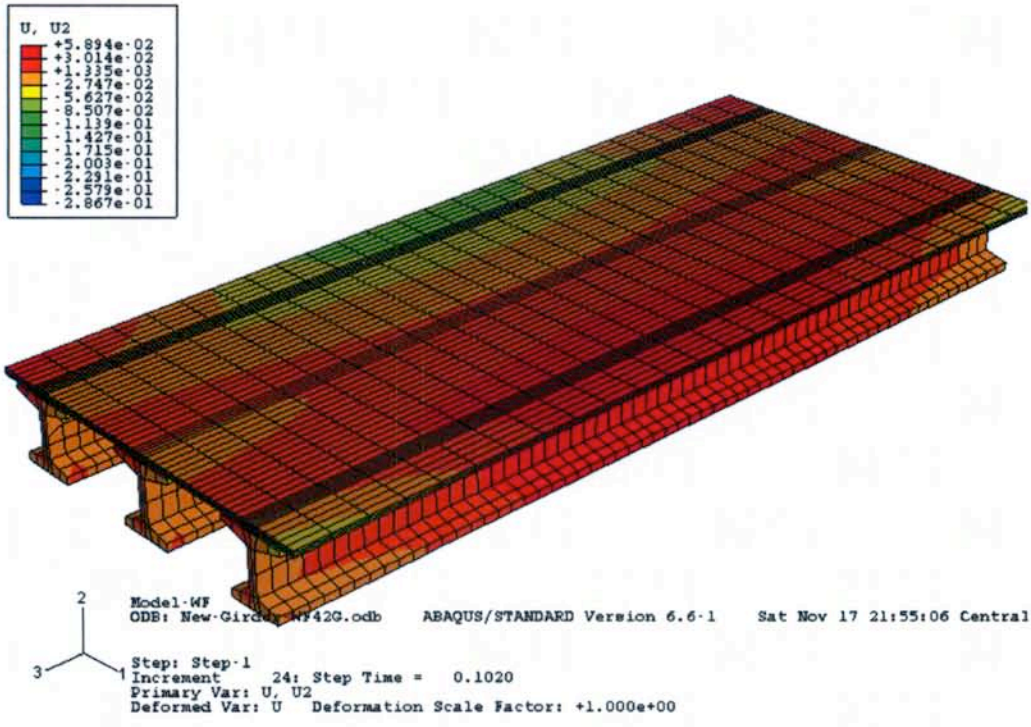

(b) WF42G

Figure E5. Vertical deflection distribution

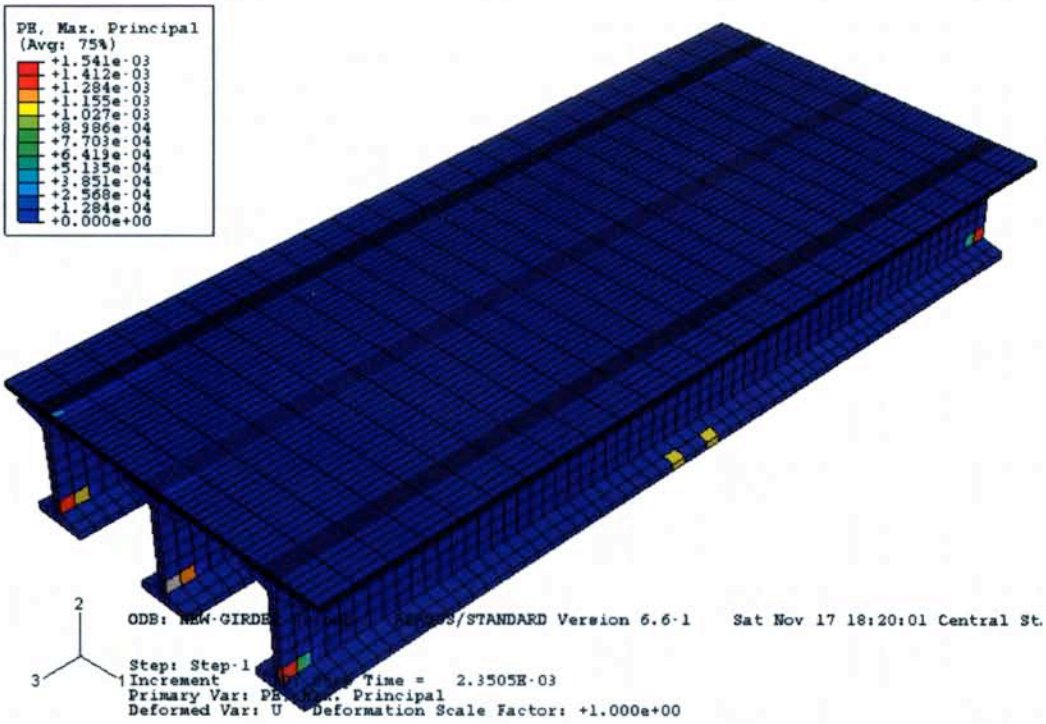

(a) WF74G

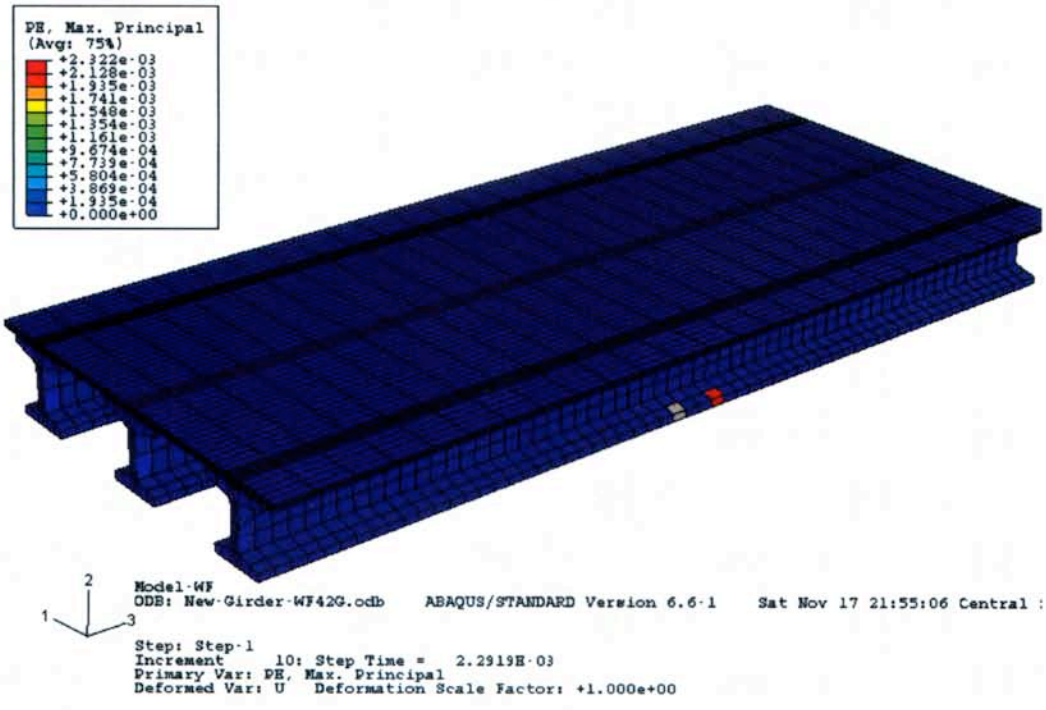

(b) WF42G

Figure E6. Maximal principal plastic strain distributions

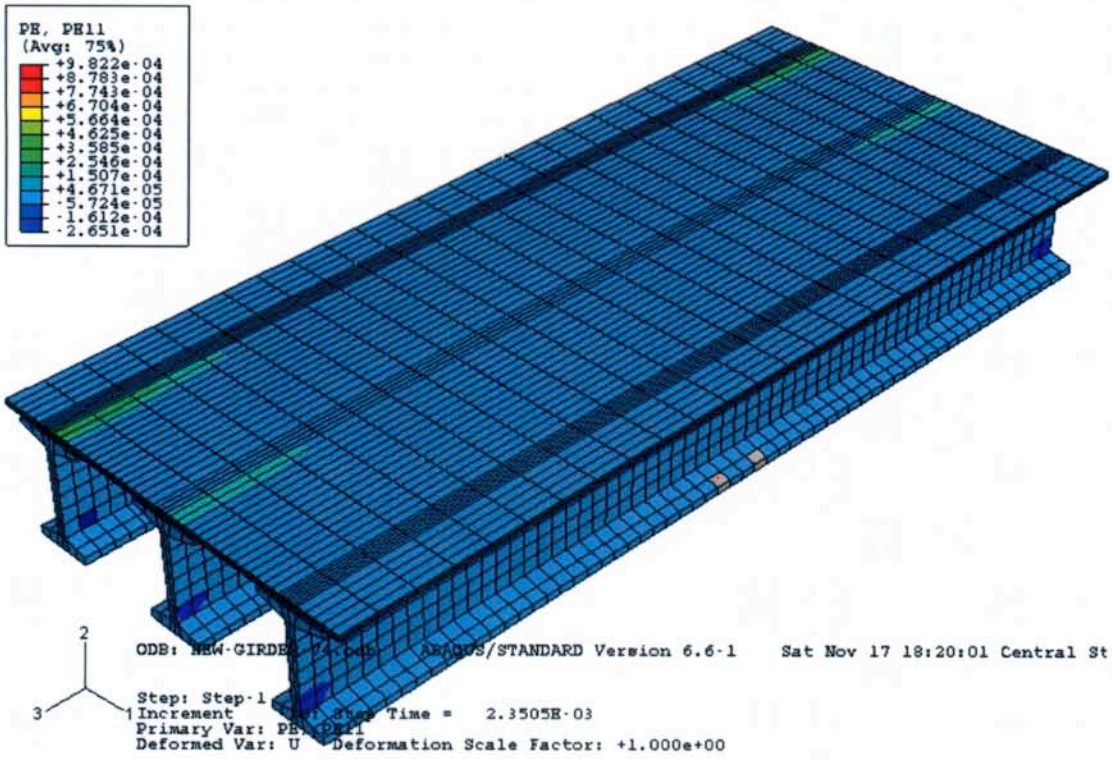

(a) WF74G

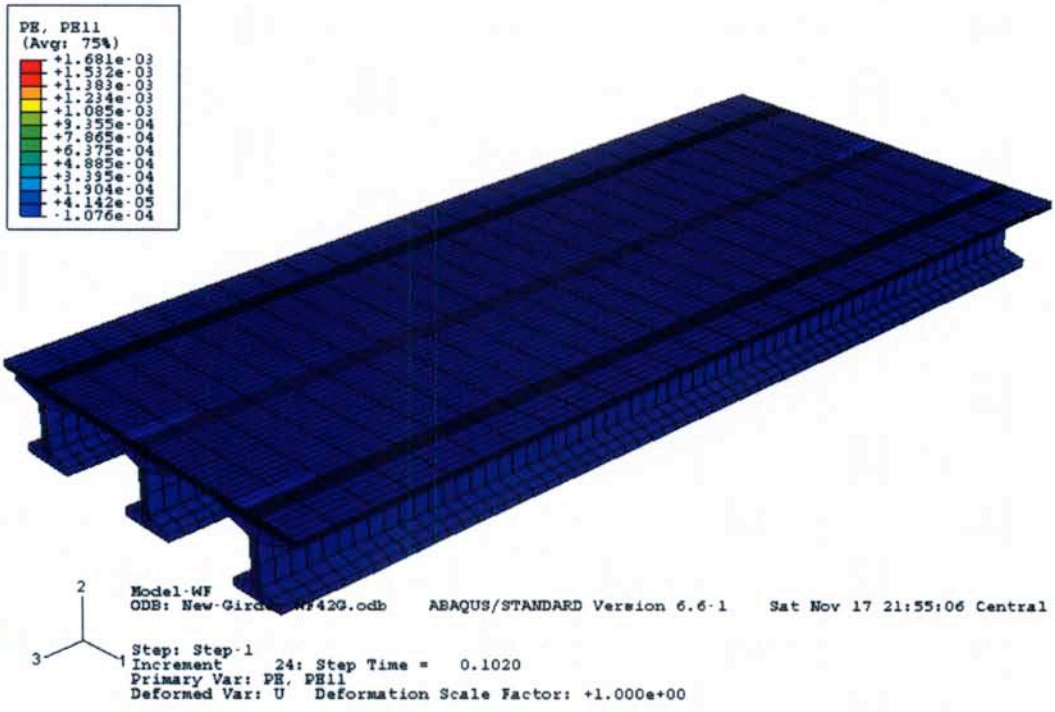

(b) WF42G

Figure E7. Transverse plastic strain distribution

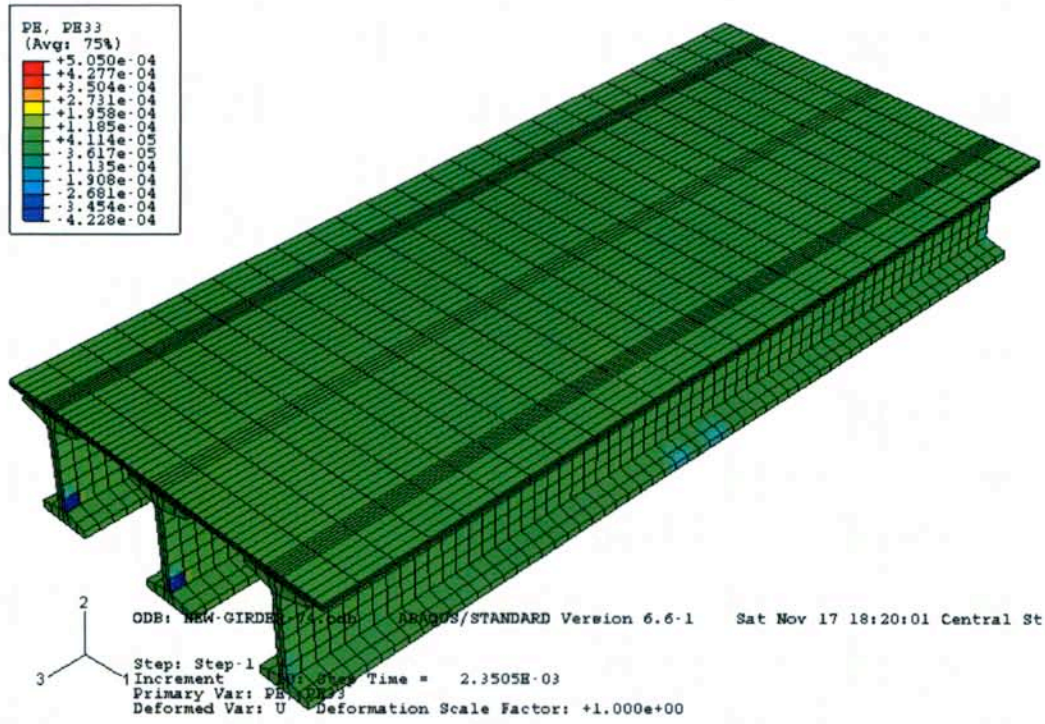

(a) WF74G

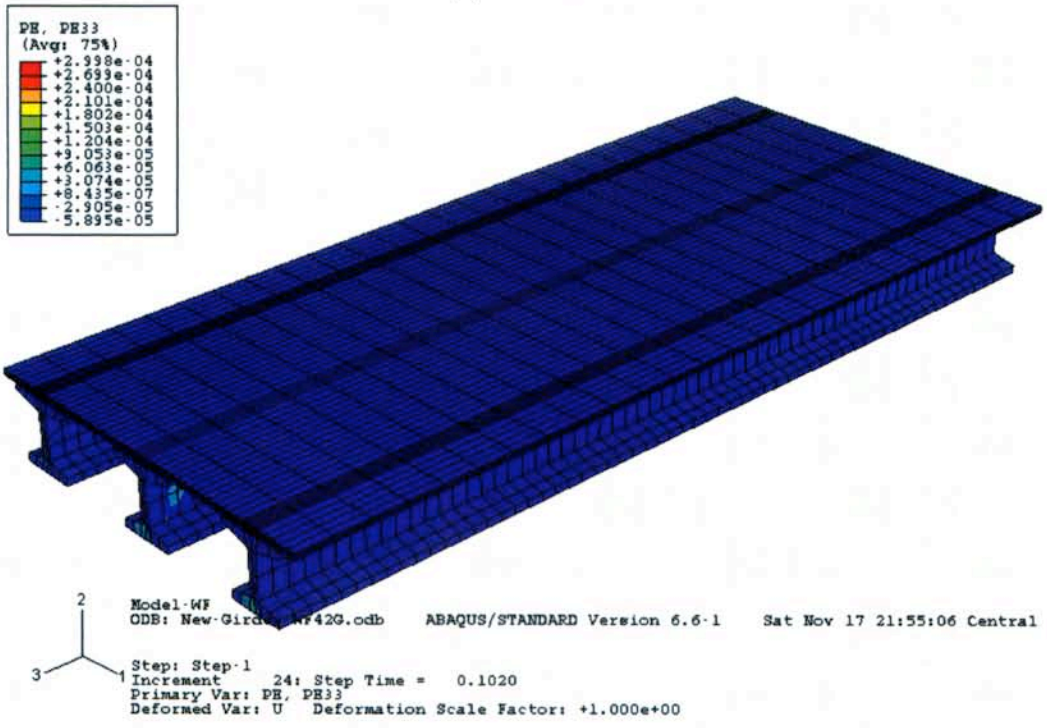

(b) WF42G

Figure E8. Longitudinal plastic strain distributions

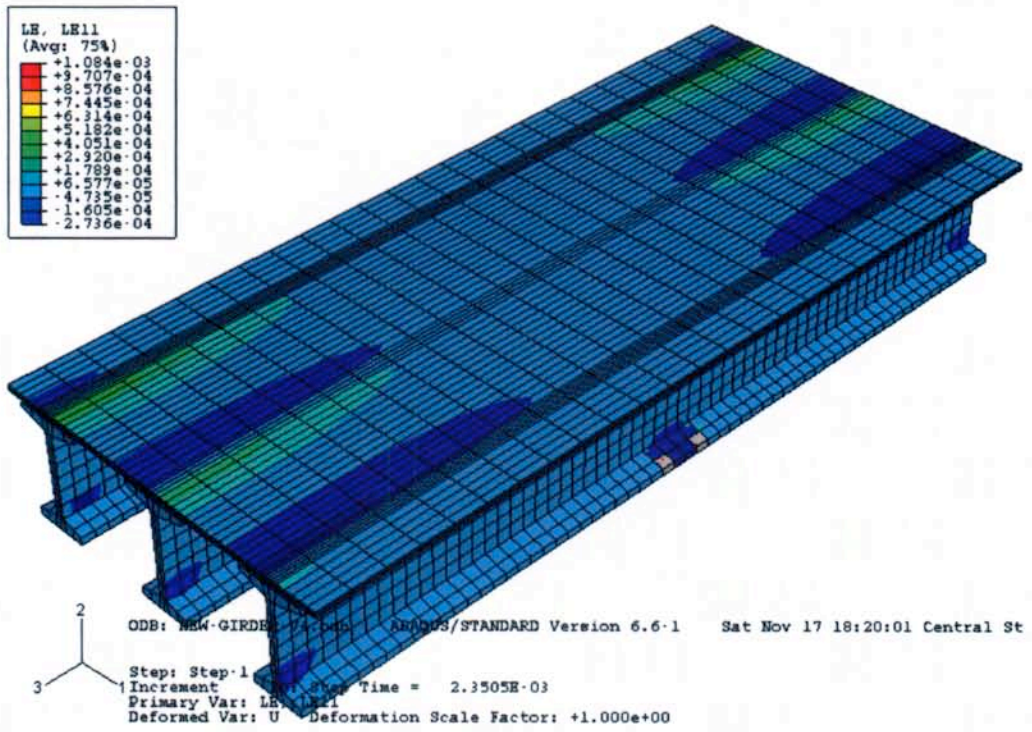

(a) WF74G

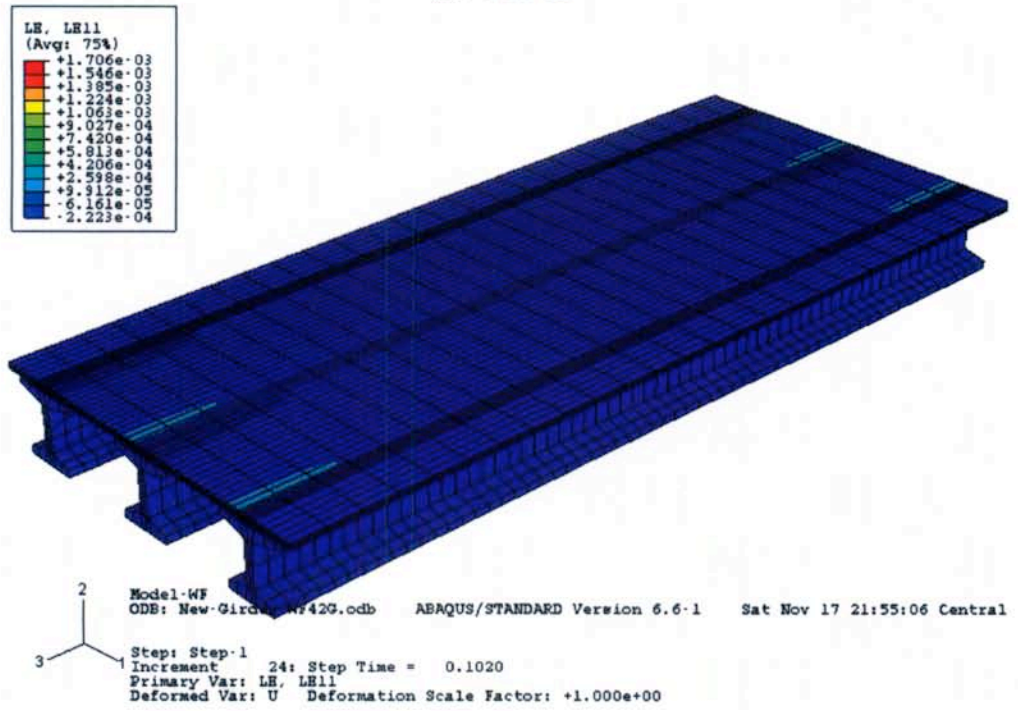

(b) WF42G

Figure E9. Transverse strain distributions

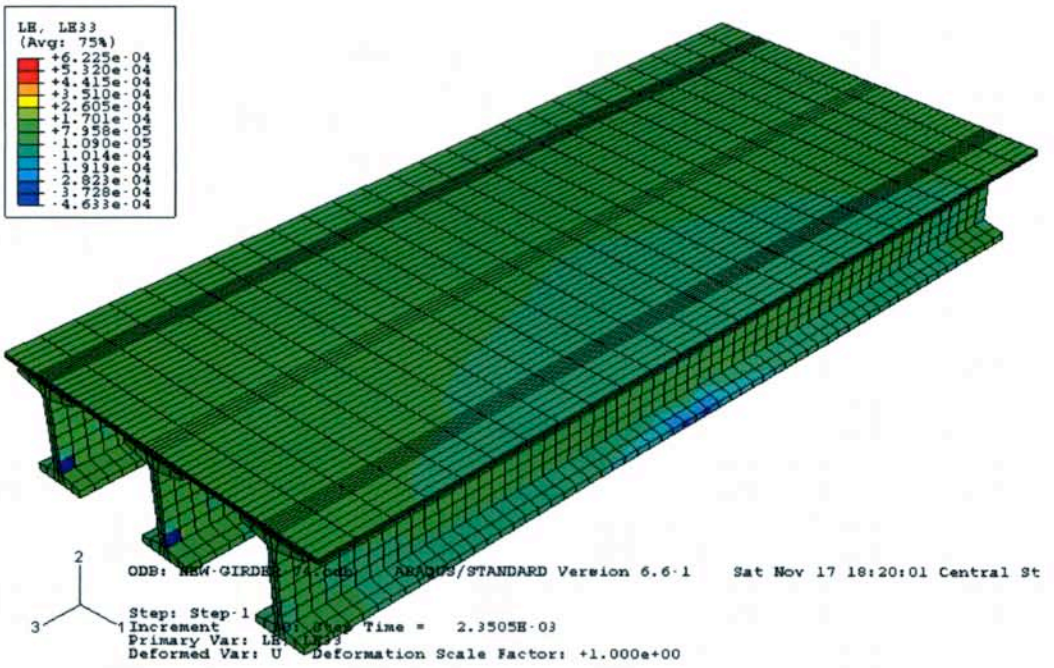

(a) WF74G

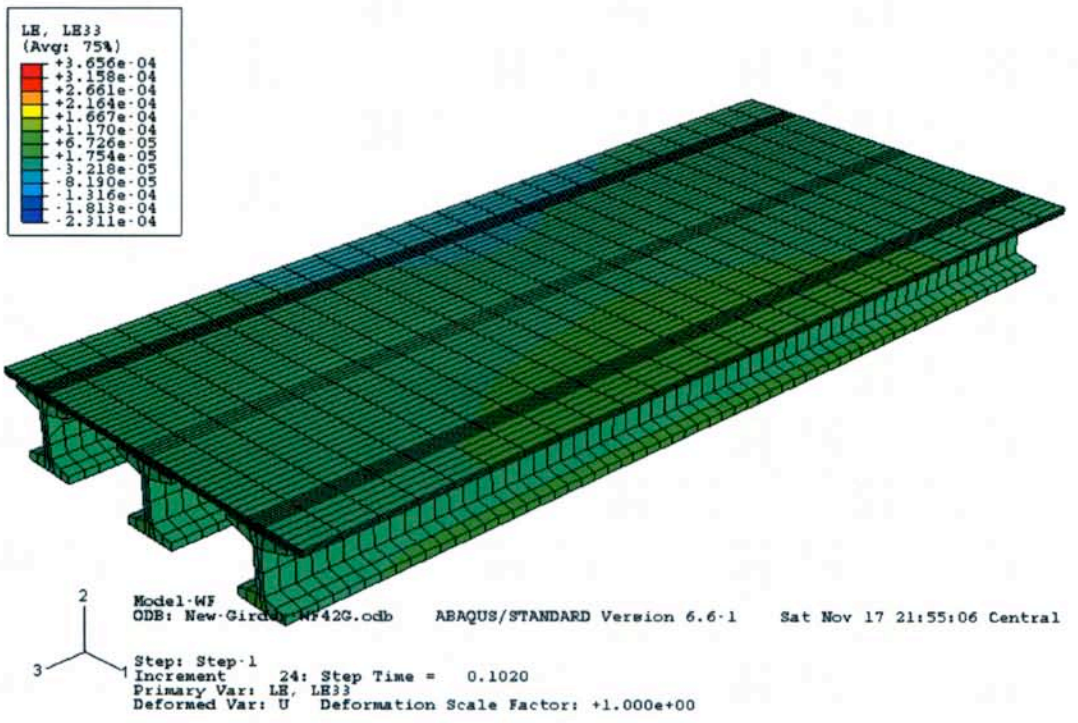

(b) WF42G

Figure E10. Longitudinal strain distribution

Appendix F. Effect of Impact Types and Contact Interface

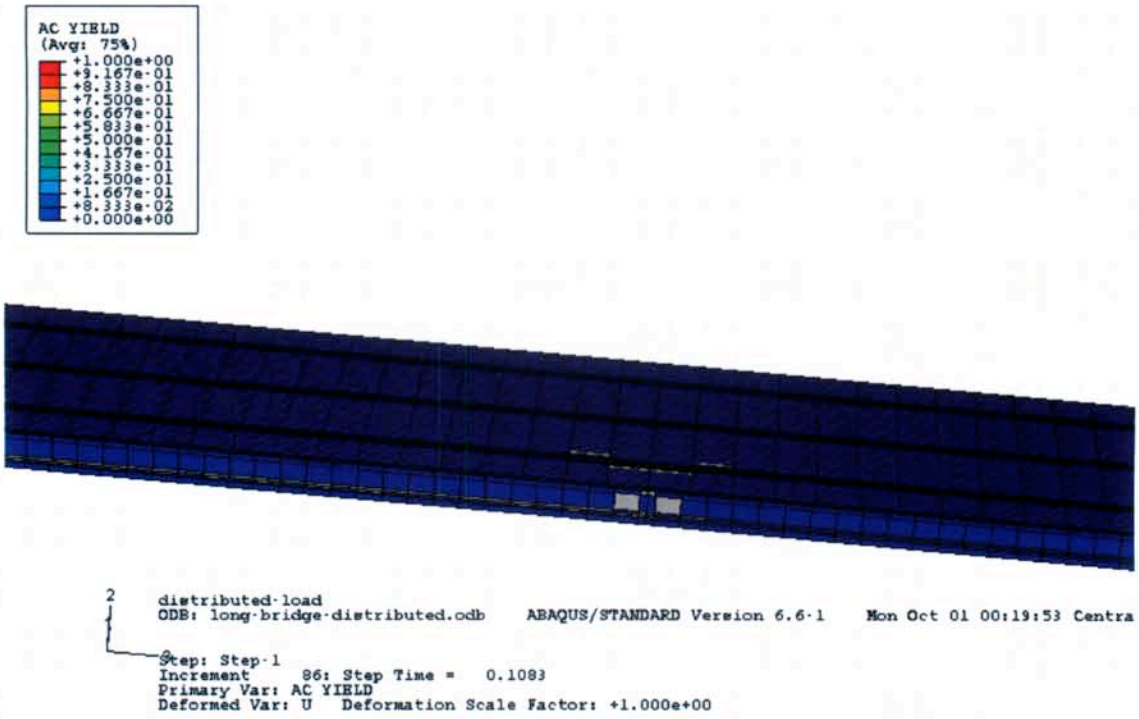

Figure F1. Failed element distribution of the bridge under distributed loads

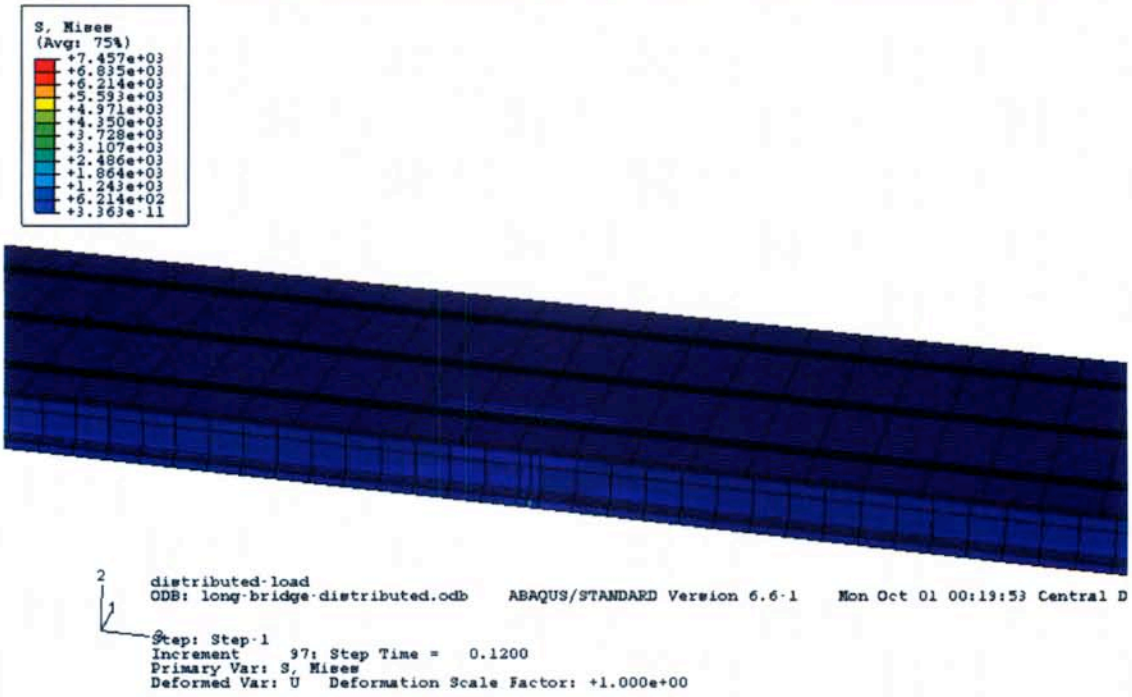

Figure F2. Vons Mises stress distribution of the bridge under distributed loads

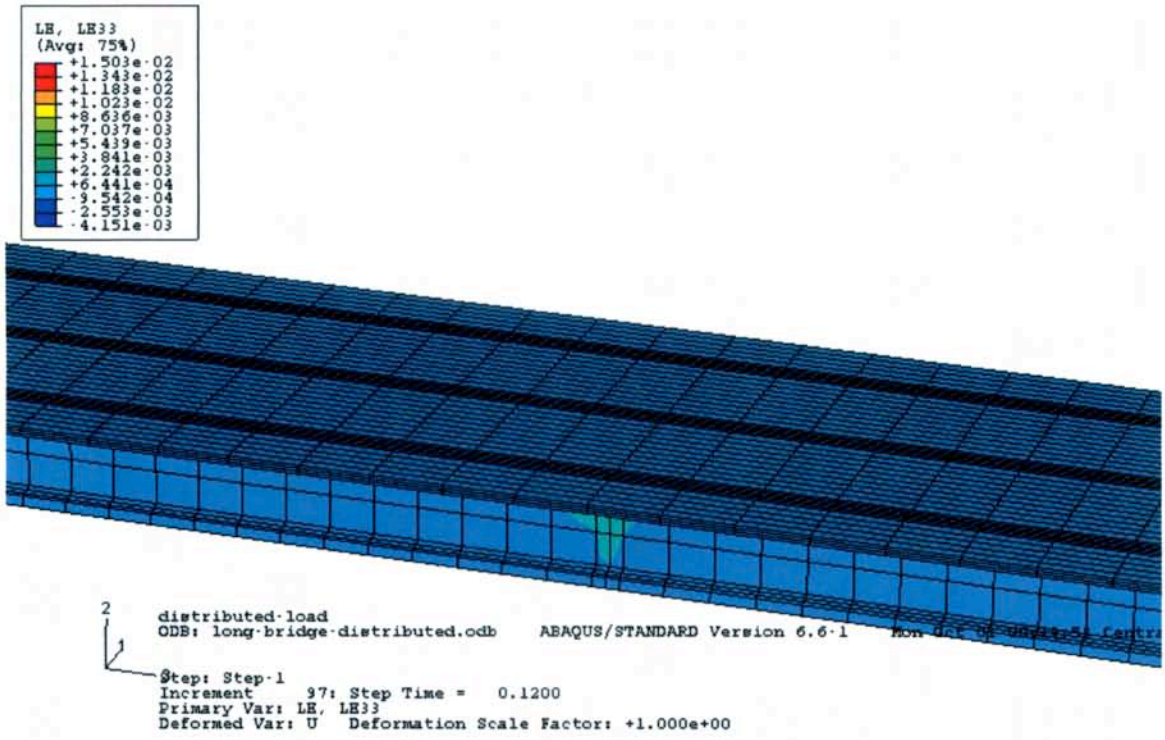

Figure F3. Longitudinal strain distribution of the bridge under distributed loads

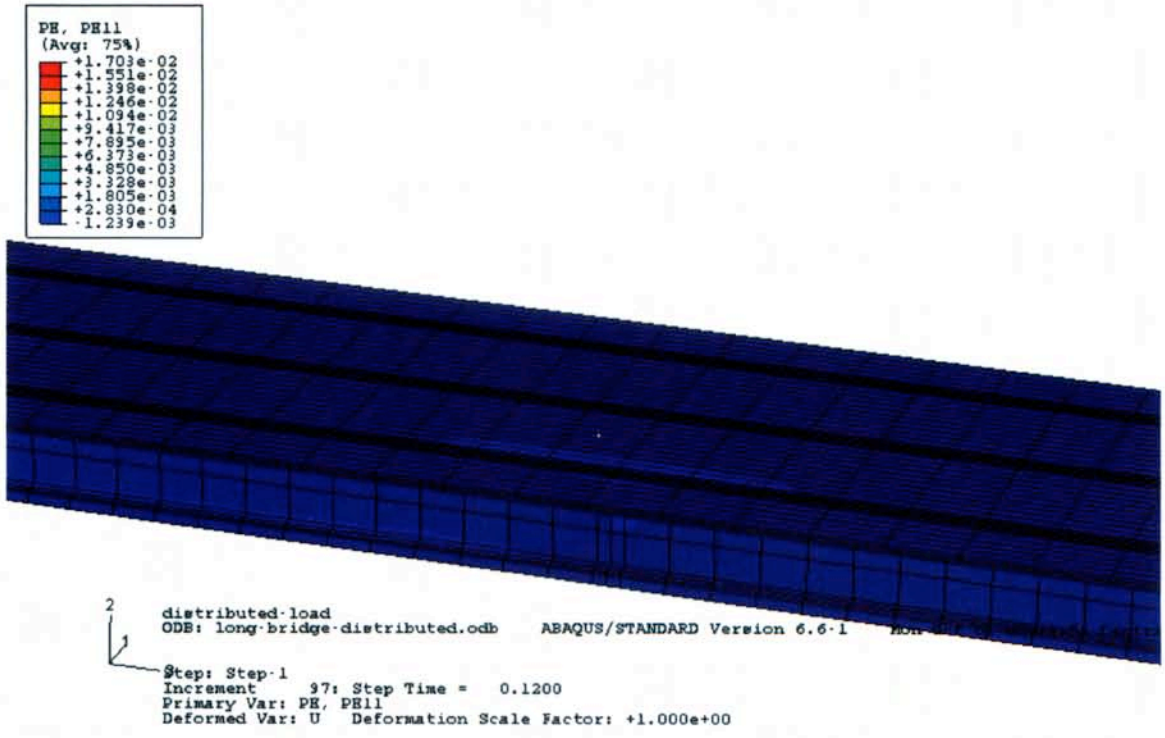

Figure F4. Transverse plastic strain distribution of the bridge under distributed loads

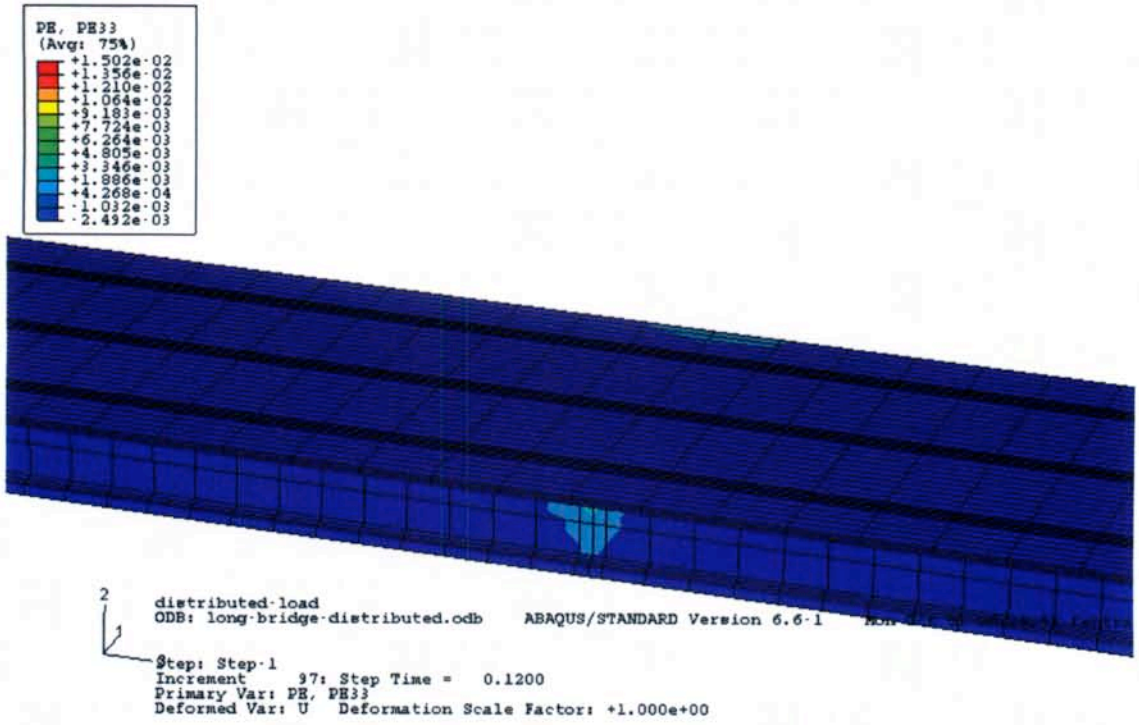

Figure F5. Longitudinal plastic strain distribution of the bridge under distributed loads

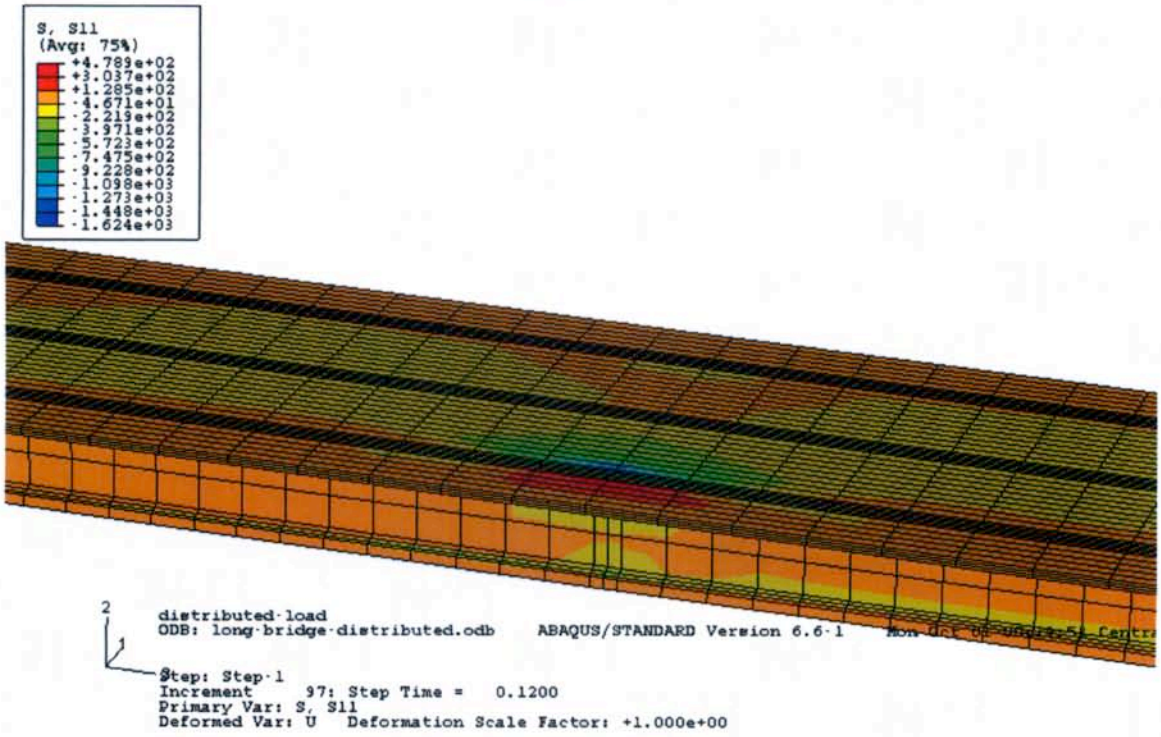

Figure F6. Transverse stress distribution of the bridge under distributed loads

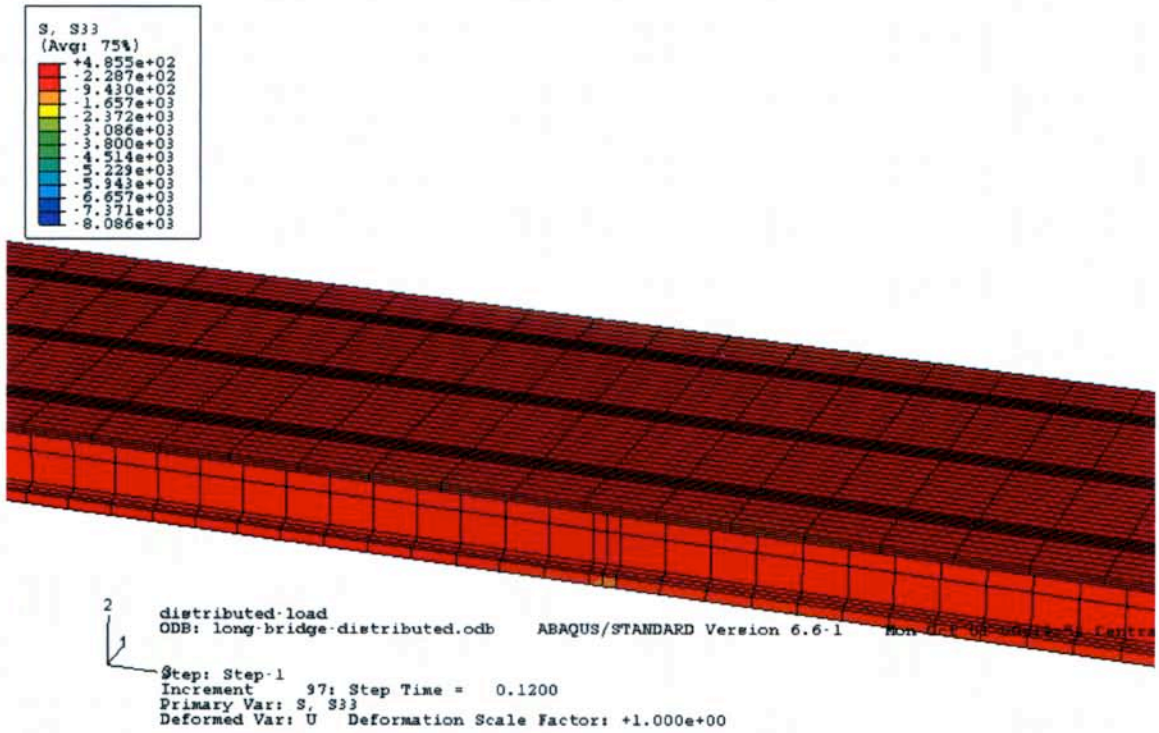

Figure F7. Longitudinal stress distribution of the bridge under distributed loads

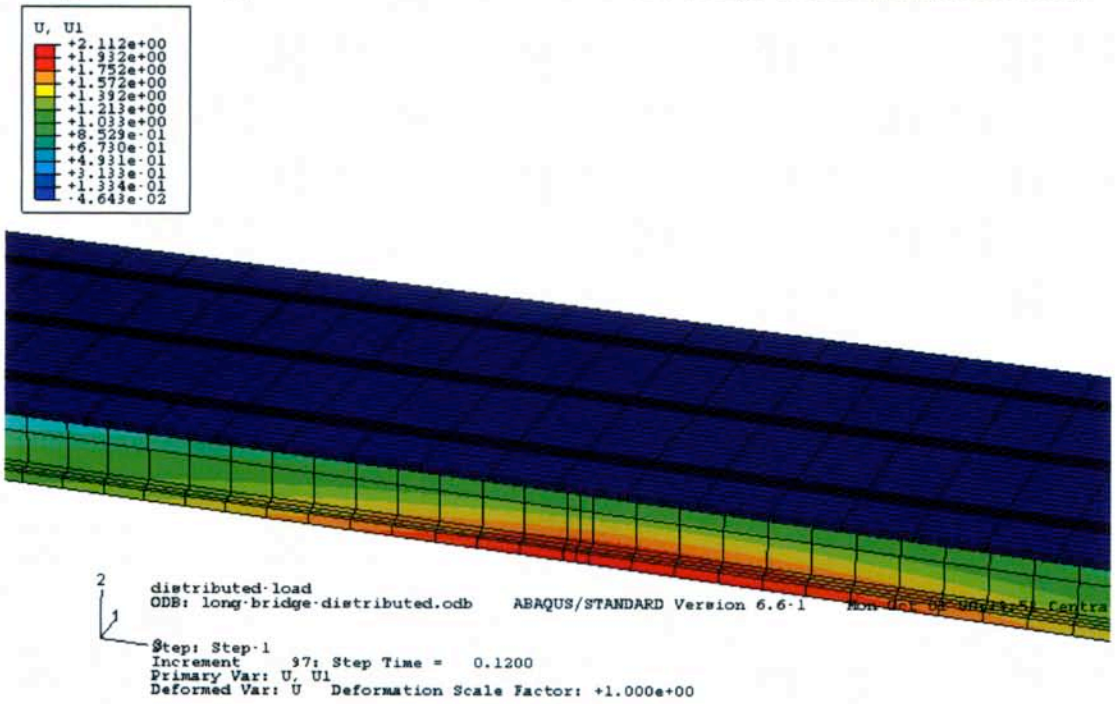

Figure F8. Transverse displacement distribution of the bridge under distributed loads

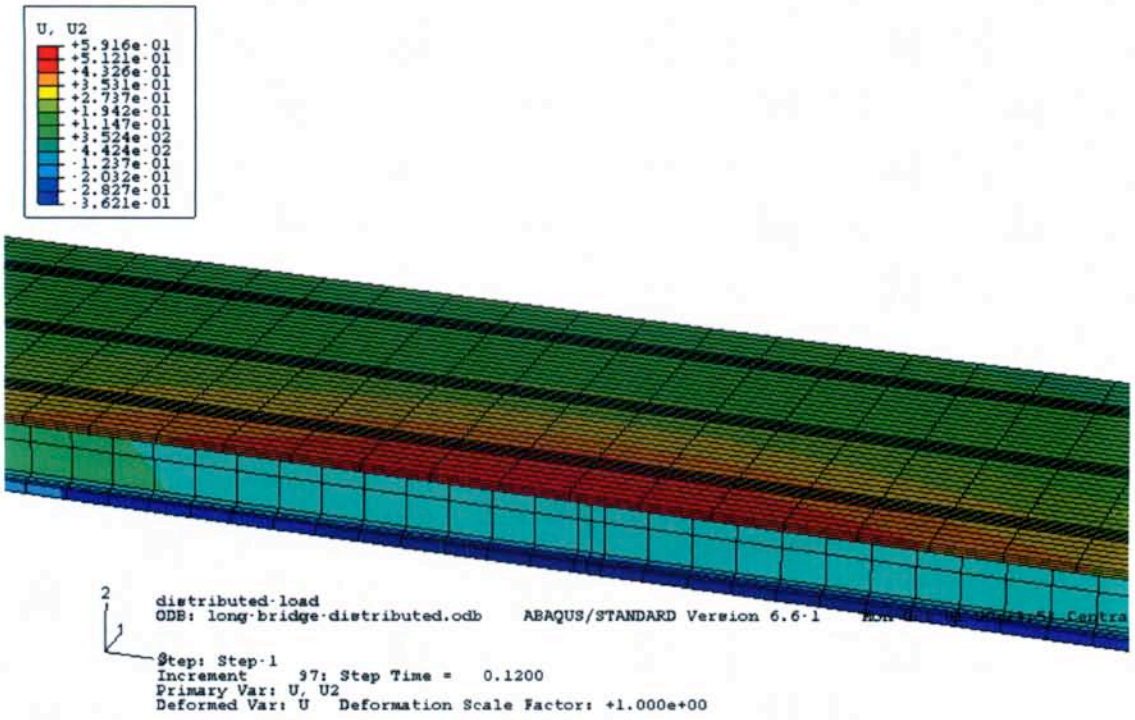

Figure F9. Vertical deflection distribution of the bridge under distributed loads

Appendix G. Effect of Dynamic Load vs. Quasi-static Load

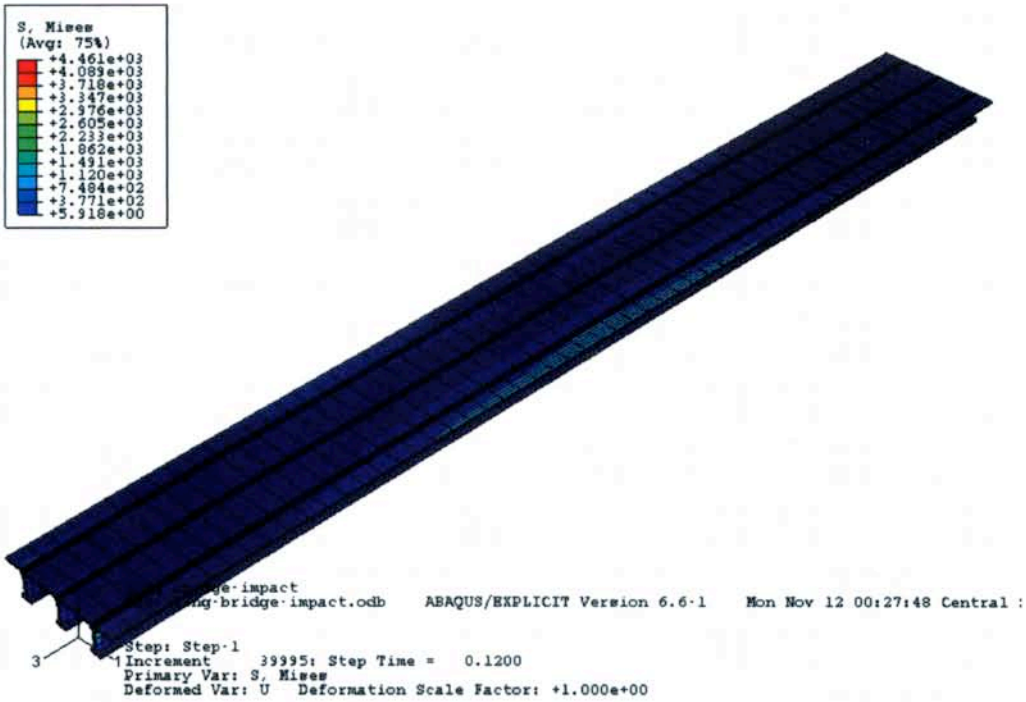

(a) Dynamic simulation

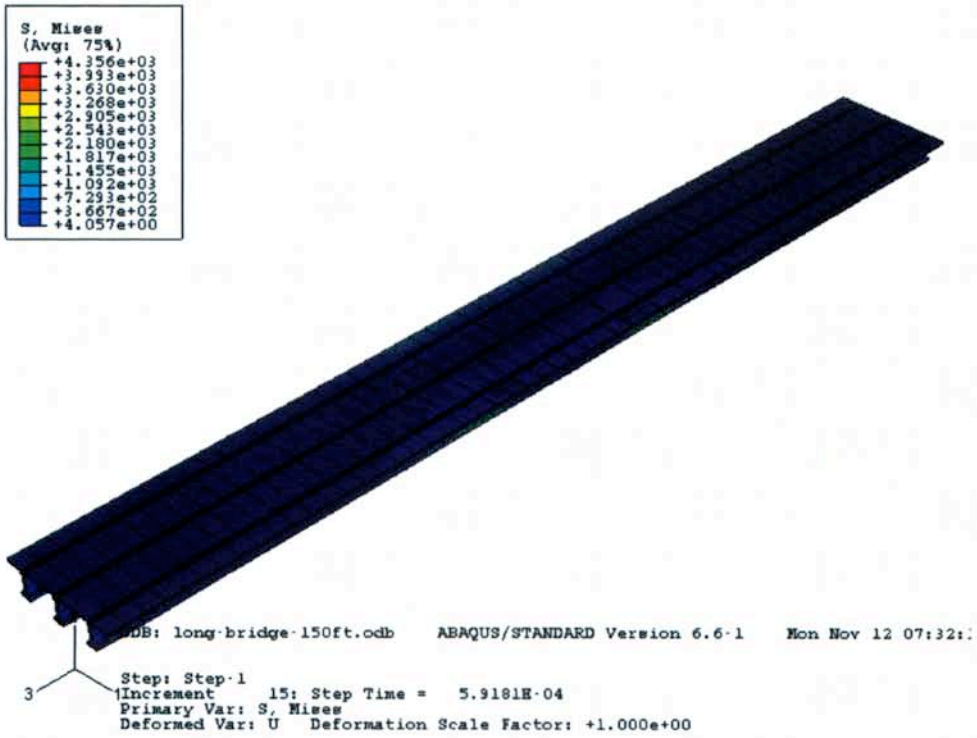

(b) Quasi-static load simulation

Figure G1. Von Mises stress distribution

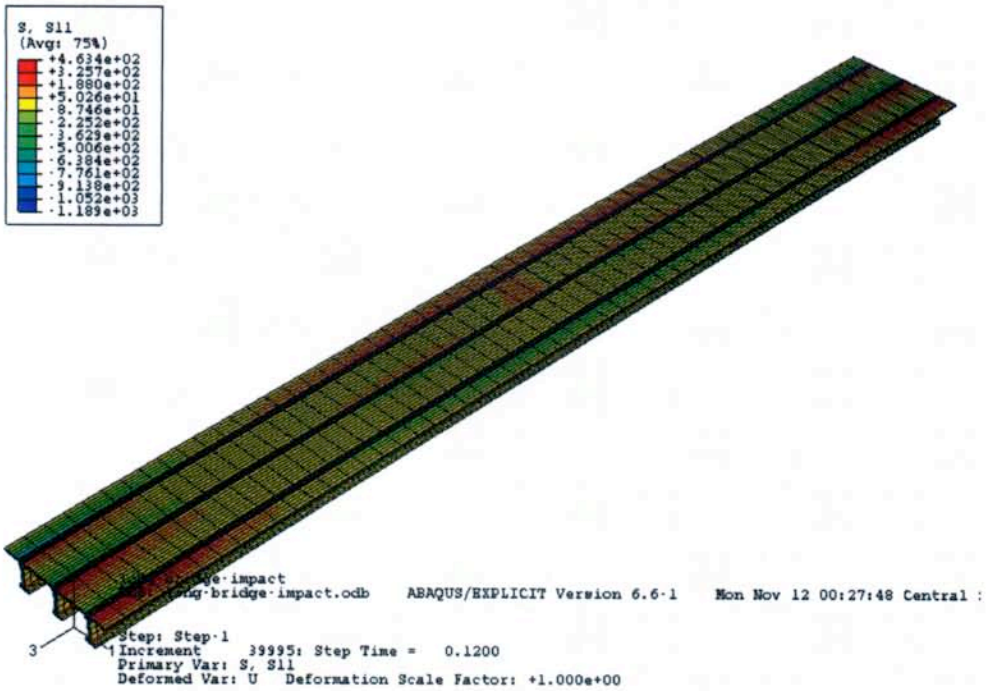

(a) Dynamic simulation

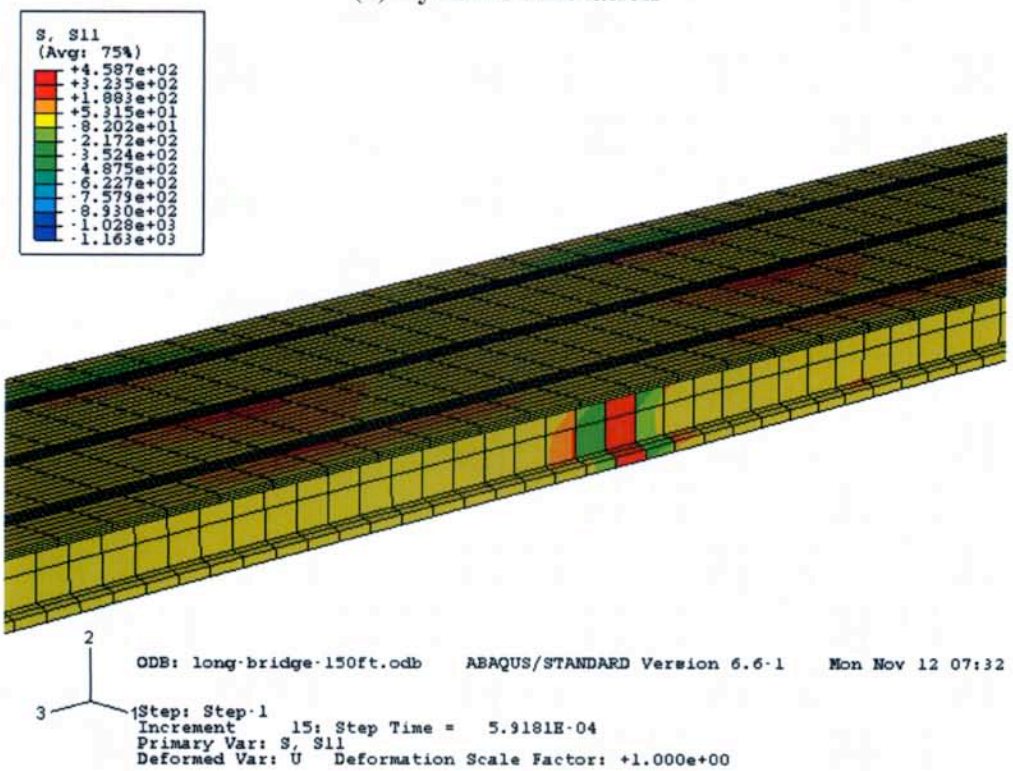

(b) Quasi-static load simulation

Figure G2. Transverse stress distribution along the loading direction

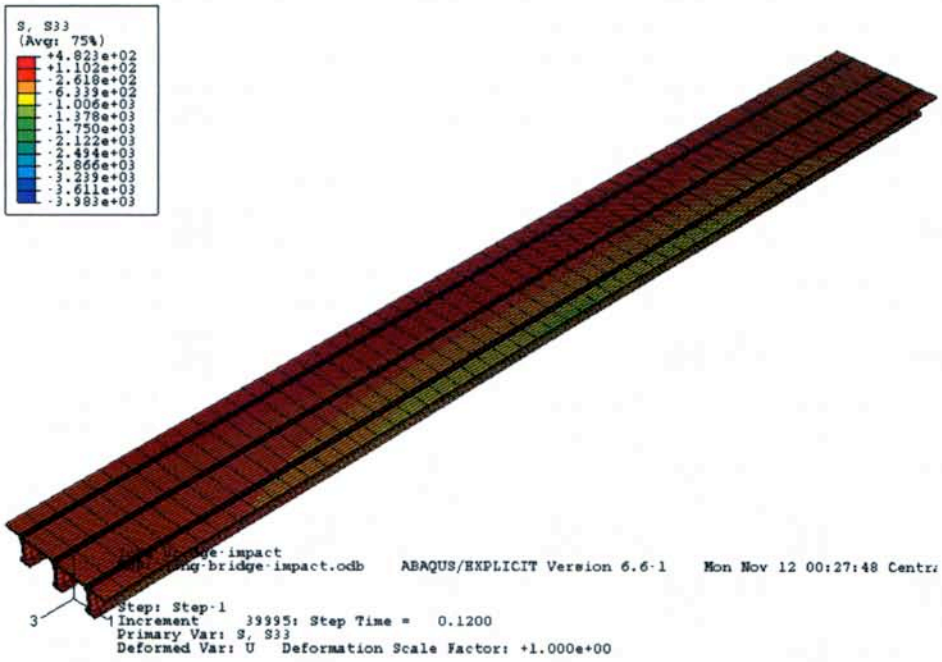

(a) Dynamic simulation

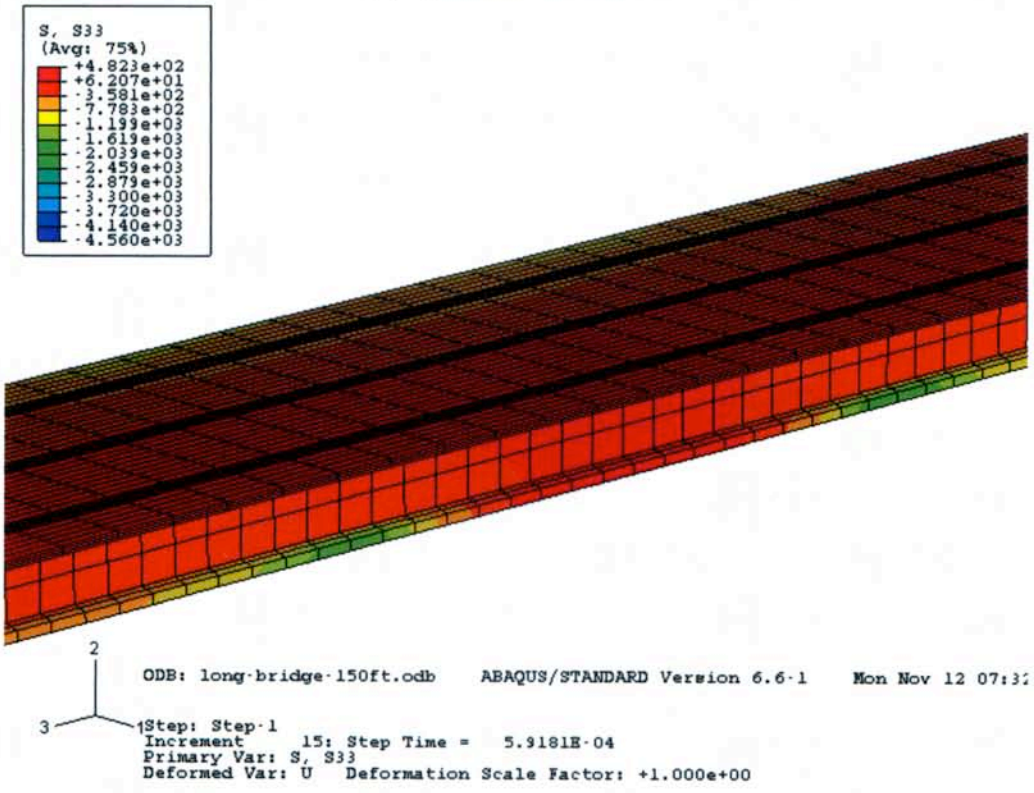

(b) Quasi-static load simulation

Figure G3. Longitudinal stress distribution

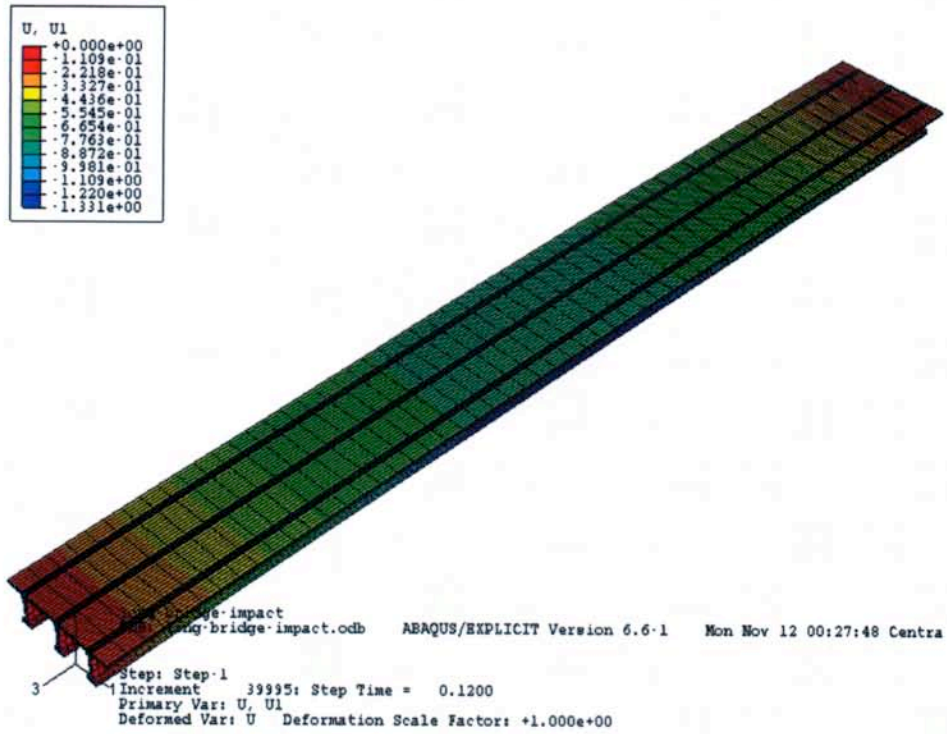

(a) Dynamic simulation

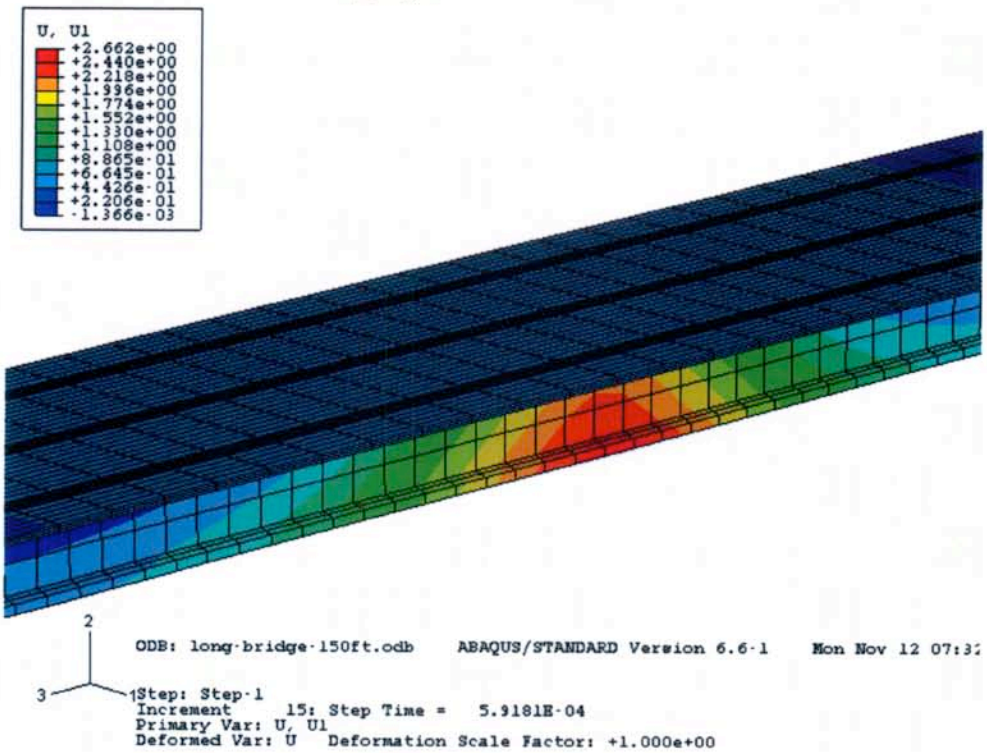

(b) Quasi-static load simulation

Figure G4. Horizontal displacement distribution along the loading directions

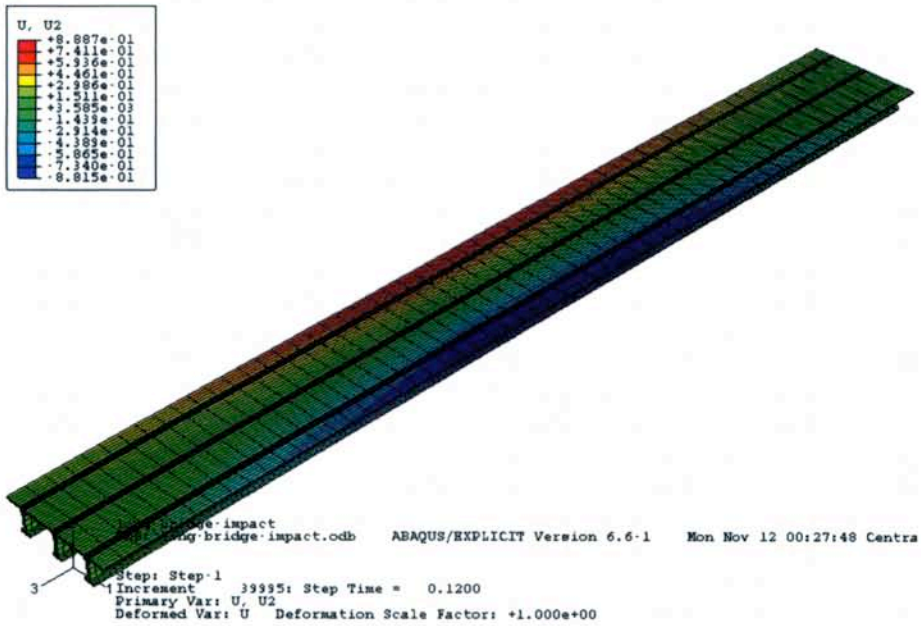

(a) Dynamic simulation

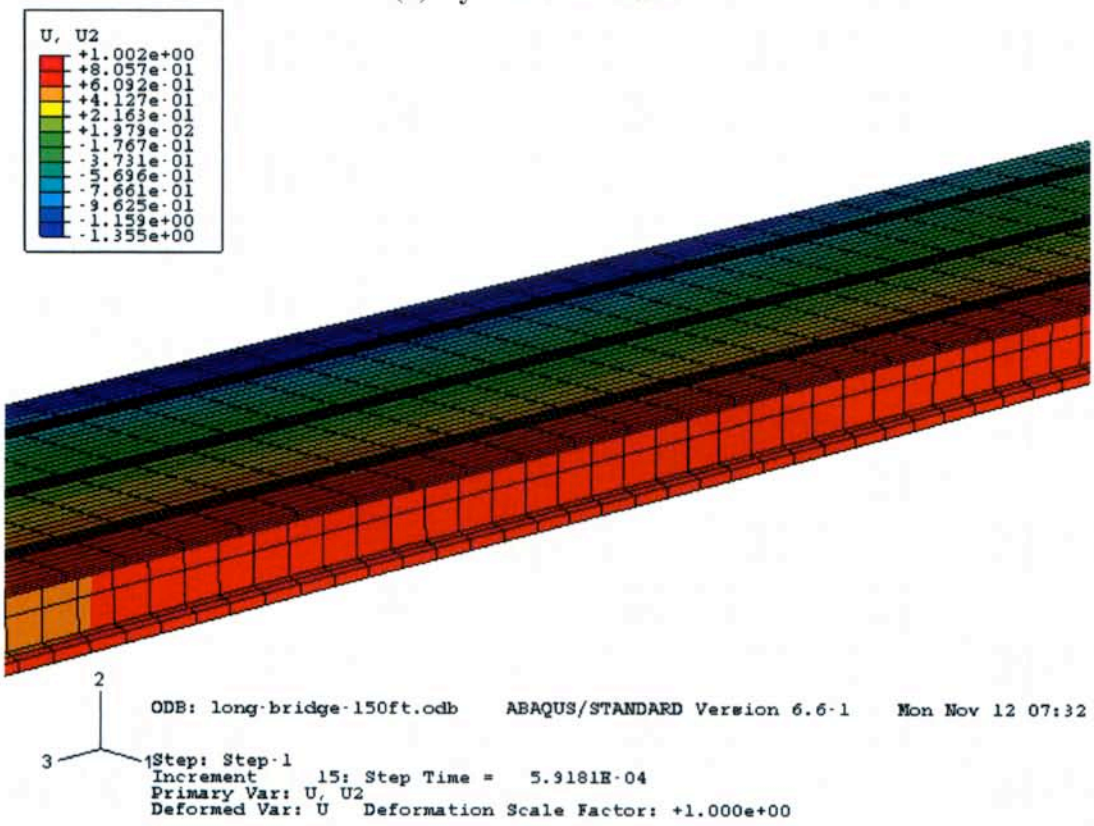

(b) Quasi-static load simulation

Figure G5. Vertical deflection distribution along the bridge

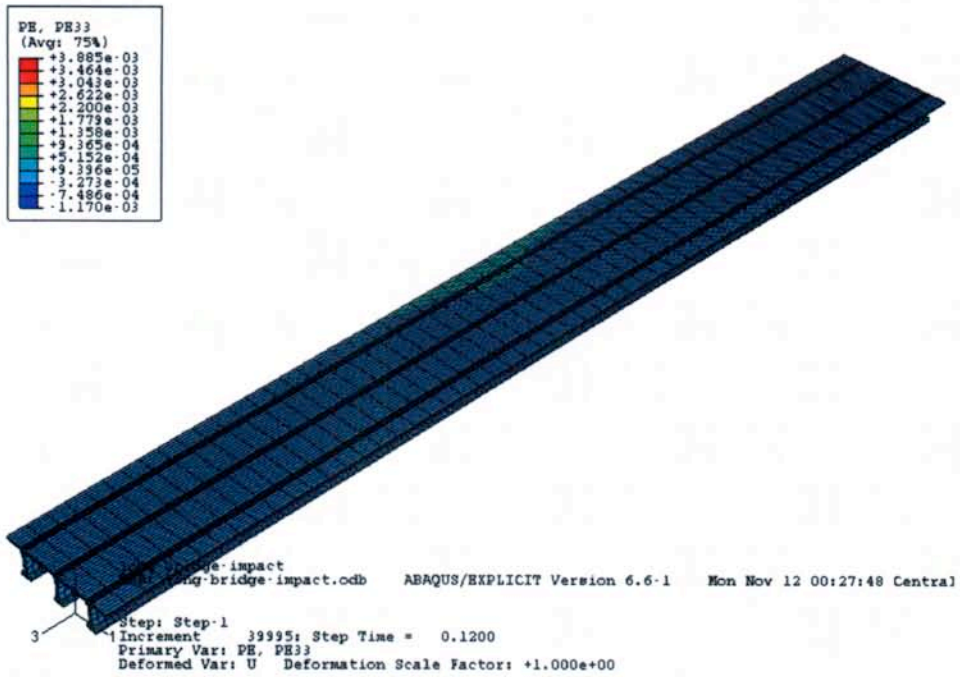

(a) Dynamic simulation

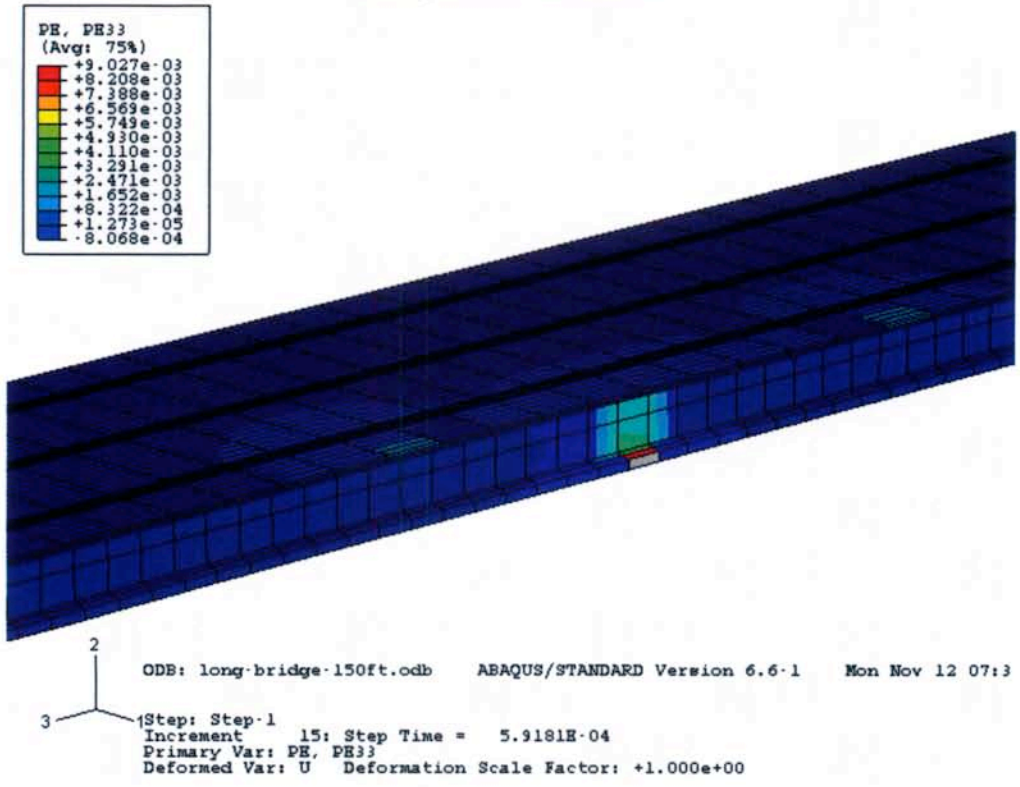

(b) Quasi-static load simulation

Figure G6. Longitudinal strain distribution along the bridge

Appendix H. Analysis of Bridge without Intermediate Diaphragms

Bridge of 6 ft girder spacing without IDs

The numerical analysis results for the bridge with a girder spacing of 6 ft. without the intermediate diaphragms (IDs) are given in Figures H1 to H10. While as a comparison, the corresponding results for the case of the bridge of 6 ft. girder spacing but with the IDs in the central span and at the location of the applied load are also provided in Figures H11 to H20. The damage area in the bridge without IDs is significantly increased, so are their displacements and strains.

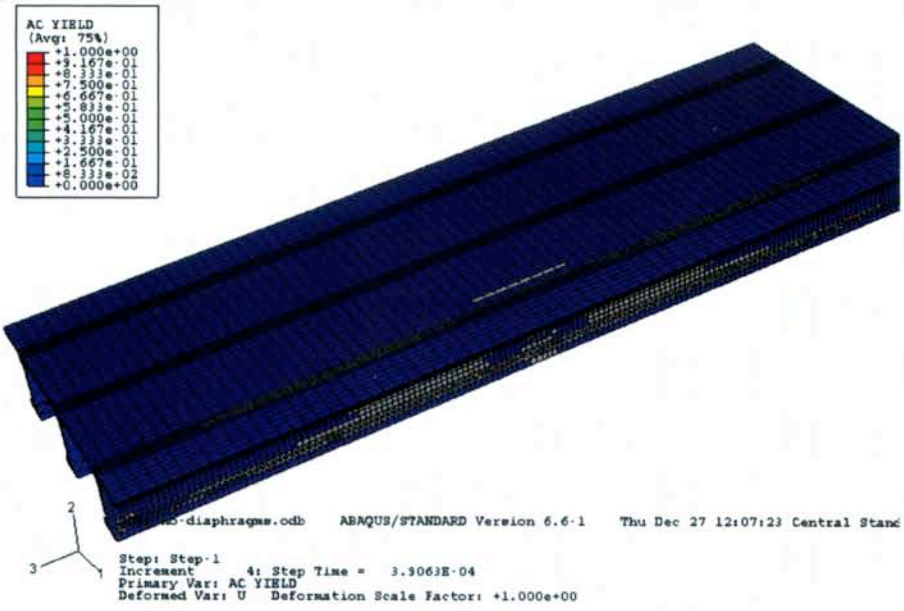

Figure H1. Damage area in the bridge of 6 ft girder spacing without IDs

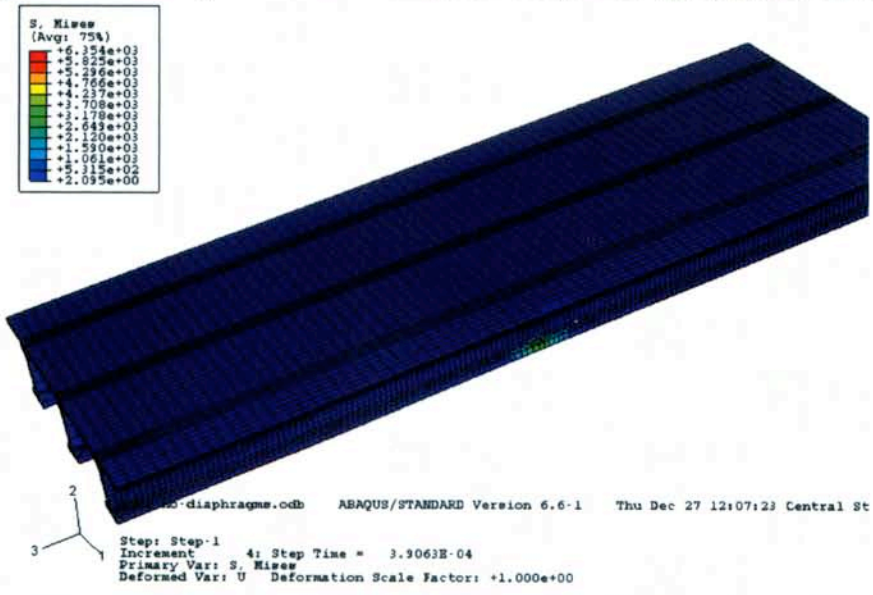

Figure H2. von-Misses stress of the bridge of 6 ft girder spacing without IDs

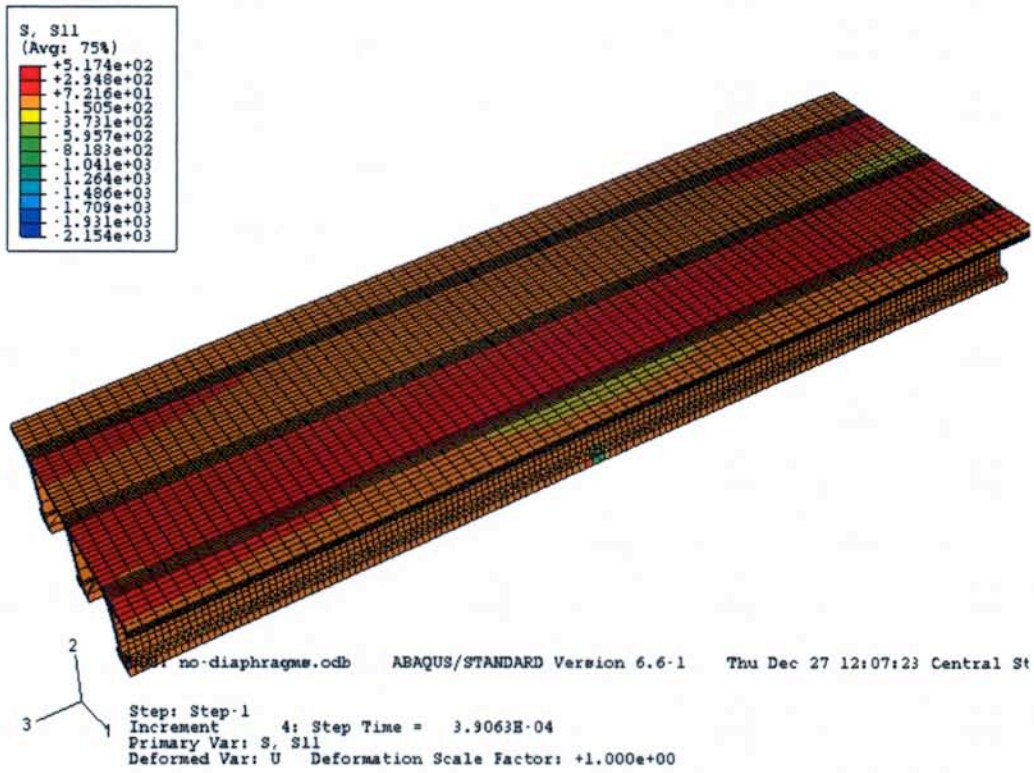

Figure H3. Transverse stress distribution of the bridge of 6 ft girder spacing without IDs

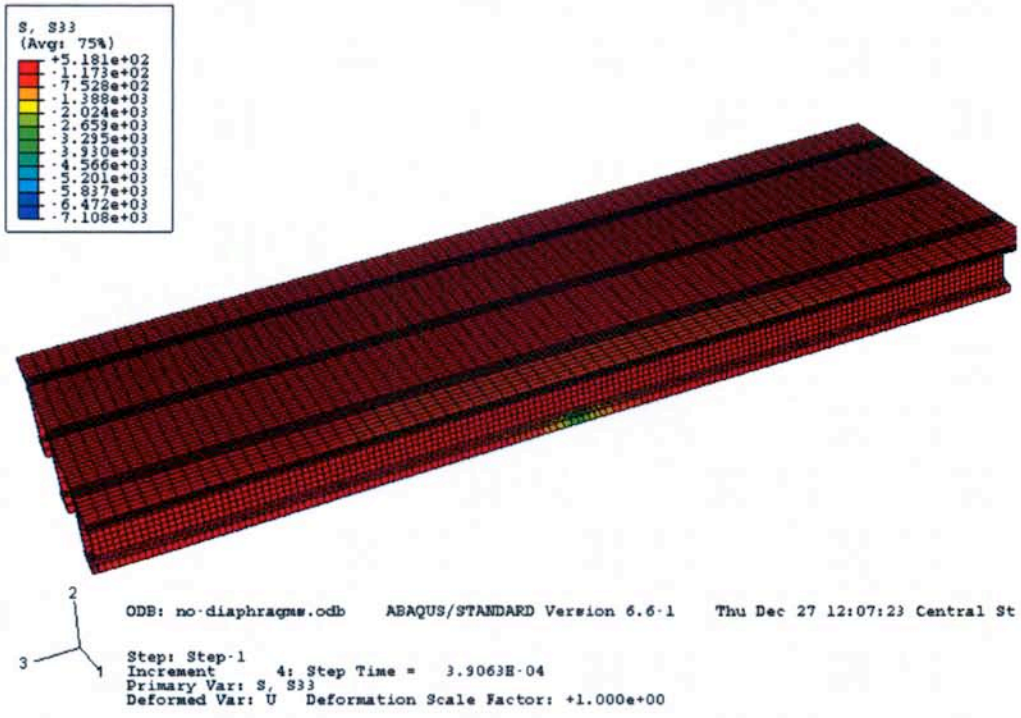

Figure H4. Longitudinal stress distribution of the bridge of 6 ft girder spacing without IDs

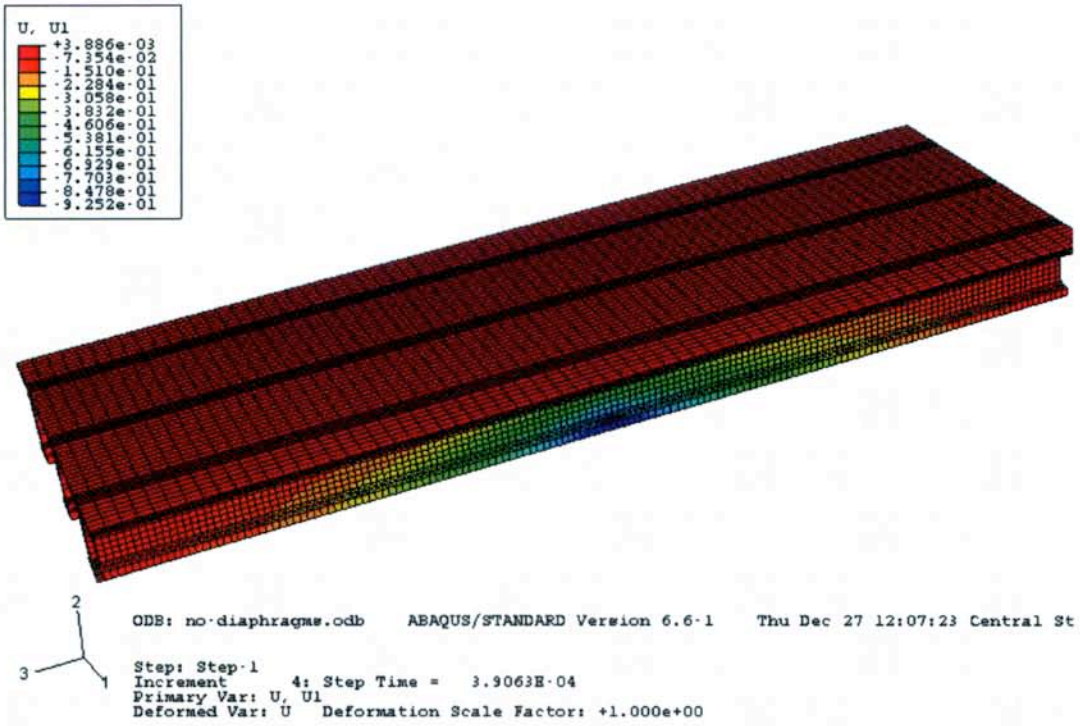

Figure H5. Transverse displacement distribution of the bridge of 6 ft girder spacing without IDs

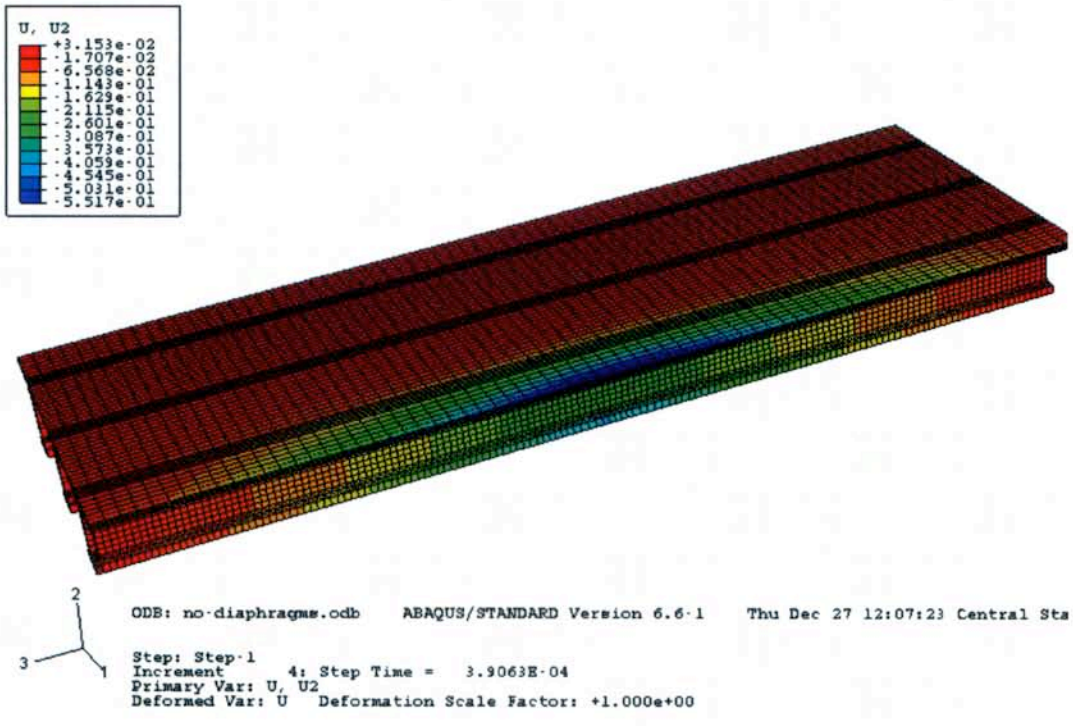

Figure H6. Vertical deflection of the bridge of 6 ft girder spacing without IDs

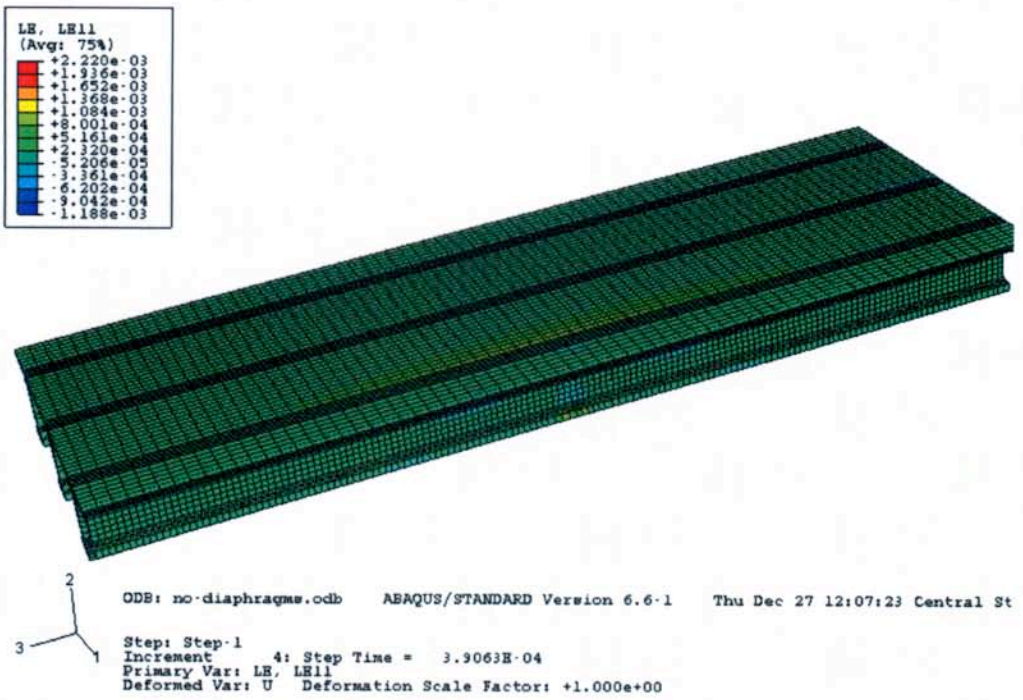

Figure H7. Logarithm transverse strain of the bridge of 6 ft girder spacing without IDs

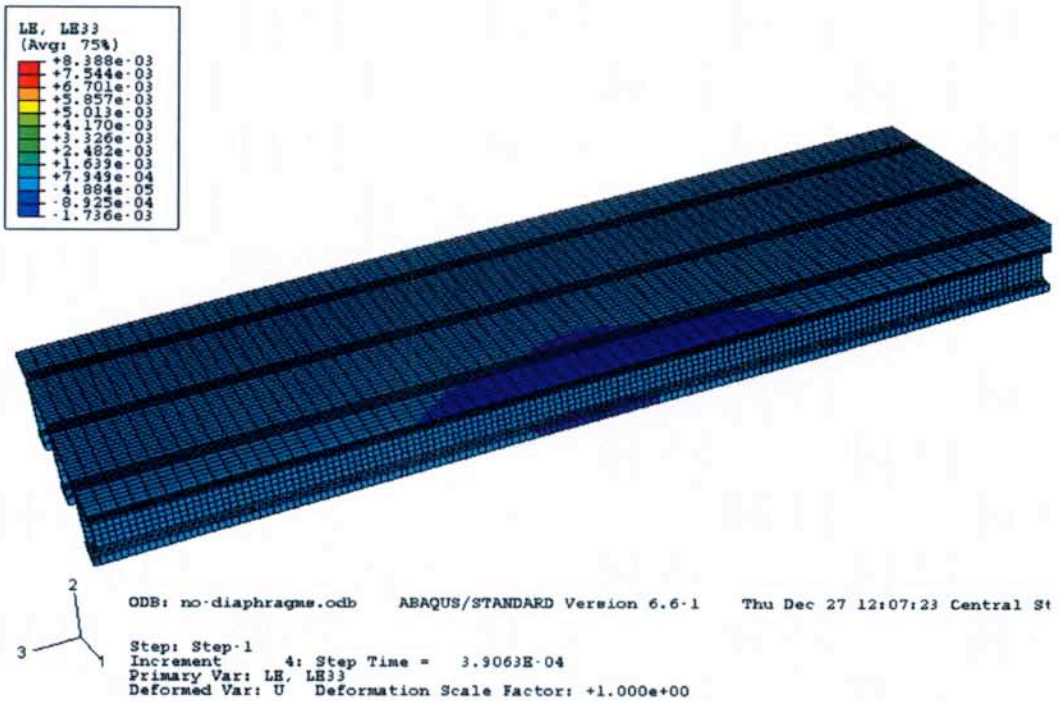

Figure H8. Logarithm longitudinal strain of the bridge of 6 ft girder spacing without IDs

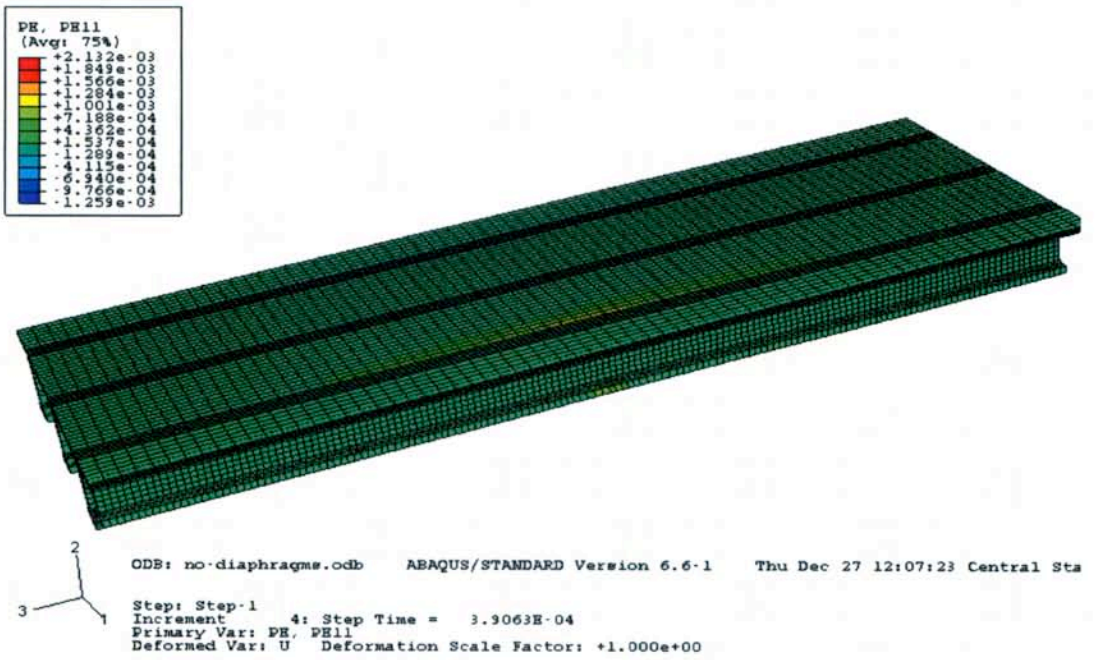

Figure H9. Transverse plastic strain of the bridge of 6 ft girder spacing without IDs

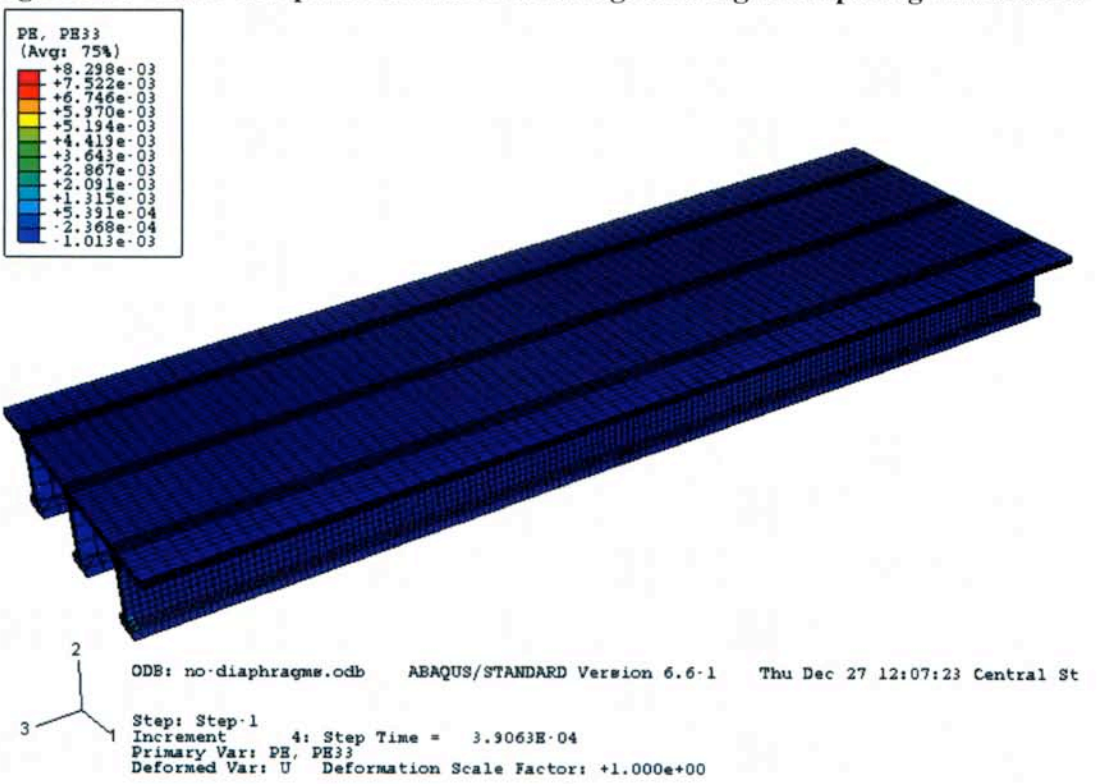

Figure H10. Longitudinal plastic strain of the bridge of 6 ft girder spacing without IDs

Bridge of 6 ft girder spacing with IDs at central span

In comparison, the numerical results for the bridge of 6 ft girder spacing with IDs at the central span and location of the applied load are shown in Figures H11 to H20, and they correspond to Figures H1 to H10 for the case of the bridge without IDs.

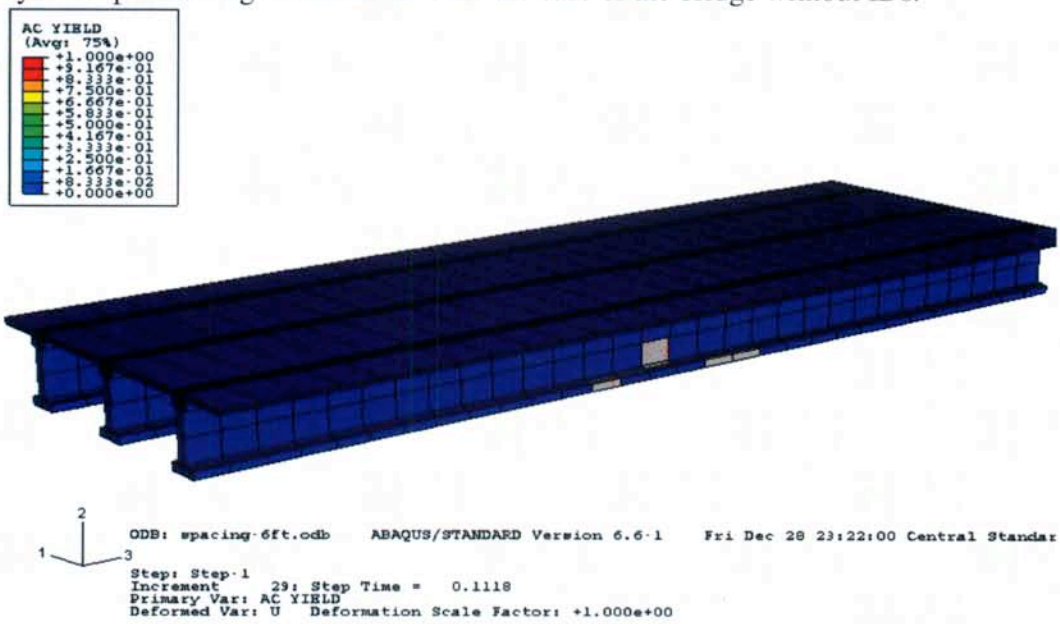

Figure H11. Damage area of the bridge of 6 ft girder spacing with IDs

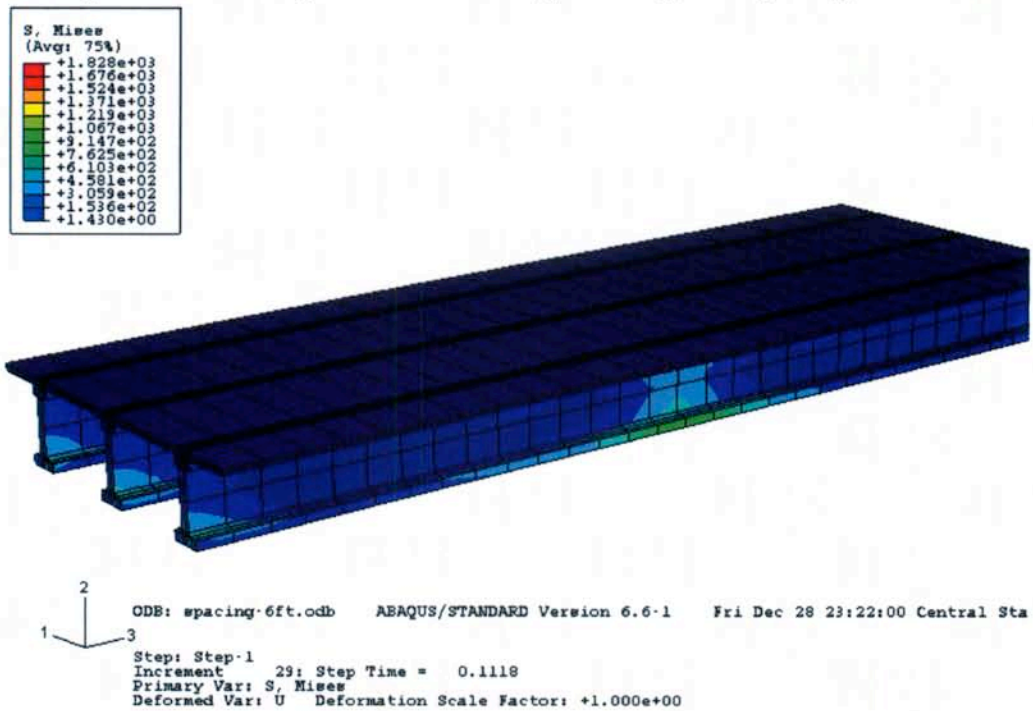

Figure H12. von Misses stress distribution of the bridge of 6 ft girder spacing with IDs

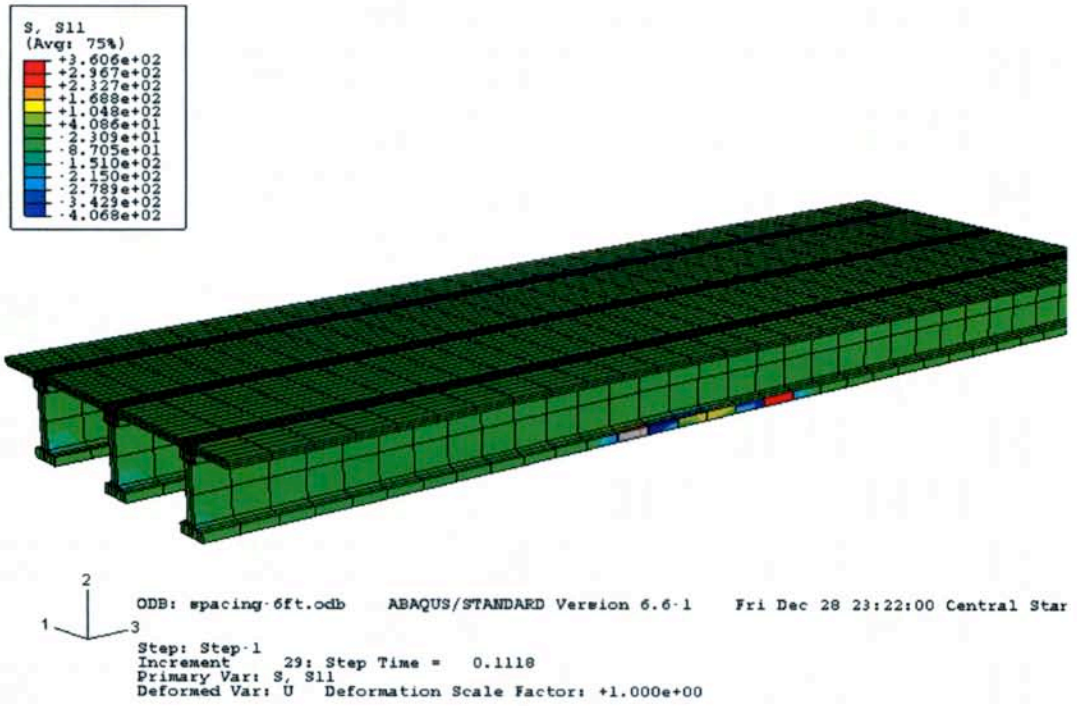

Figure H13. Transverse stress distribution of the bridge of 6 ft girder spacing with IDs

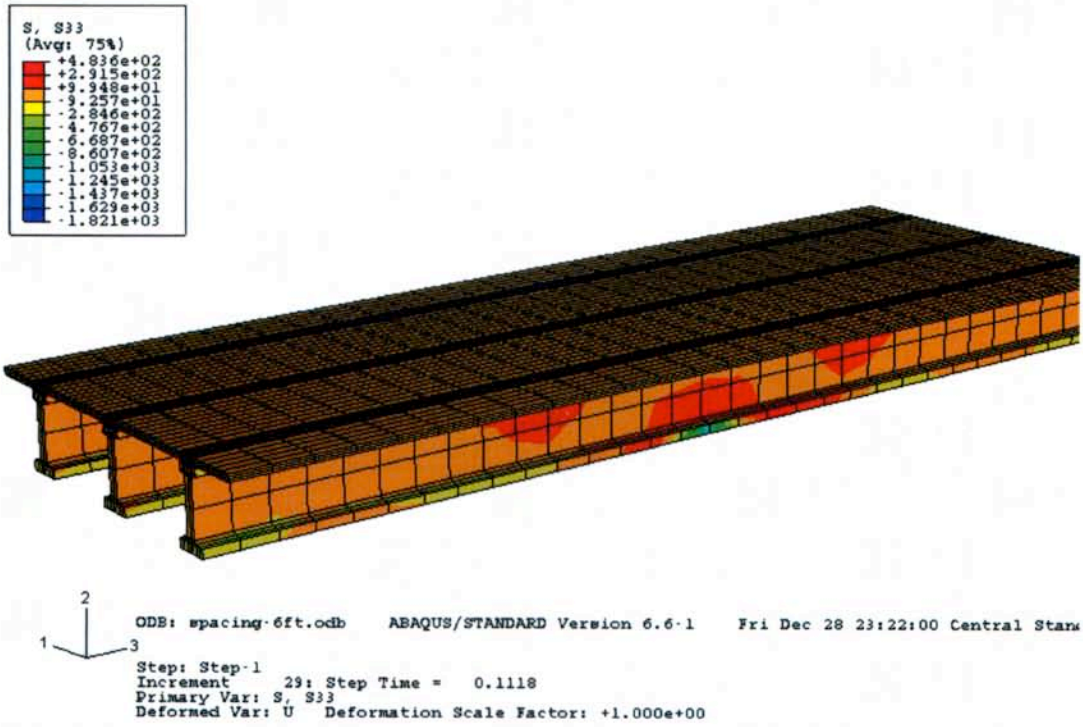

Figure H14. Longitudinal stress distribution of the bridge of 6 ft girder spacing with IDs

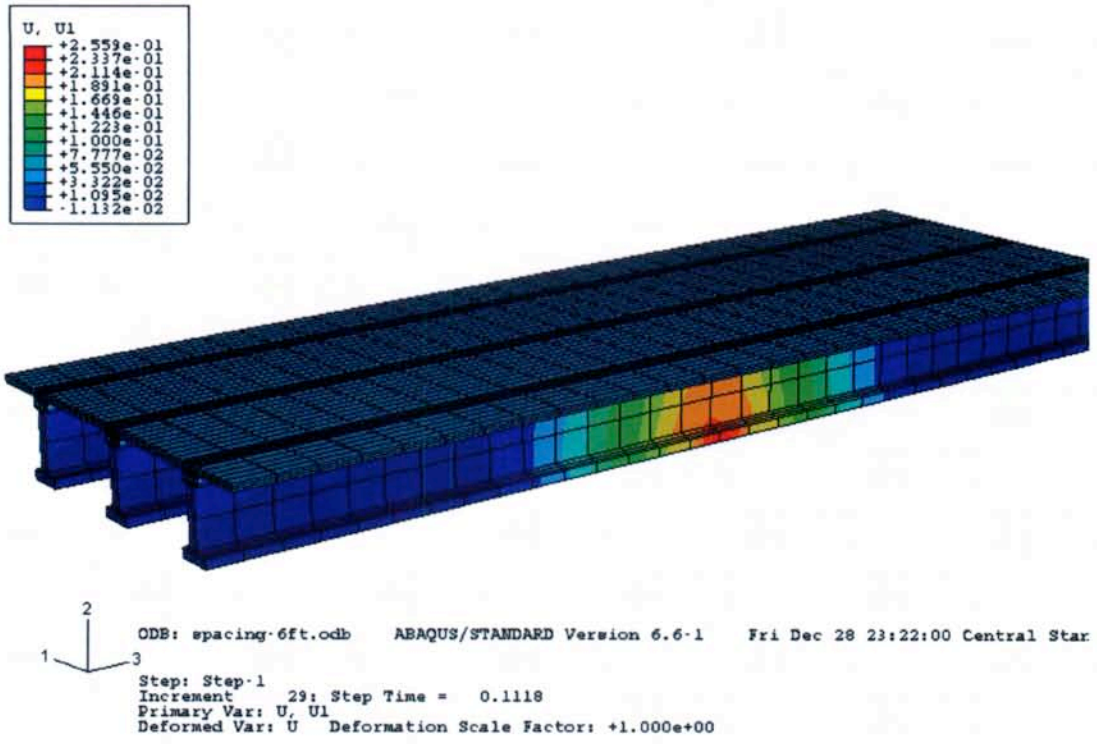

Figure H15. Transverse displacement distribution of the bridge of 6 ft girder spacing with IDs

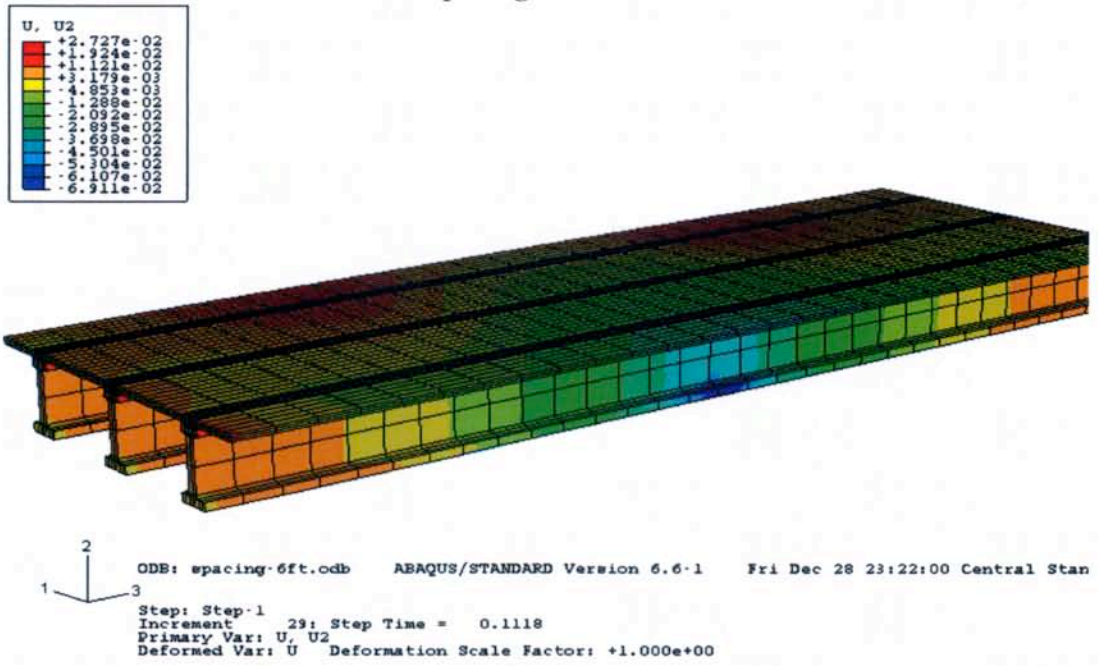

Figure H16. Vertical deflection distribution of the bridge of 6 ft girder spacing with IDs

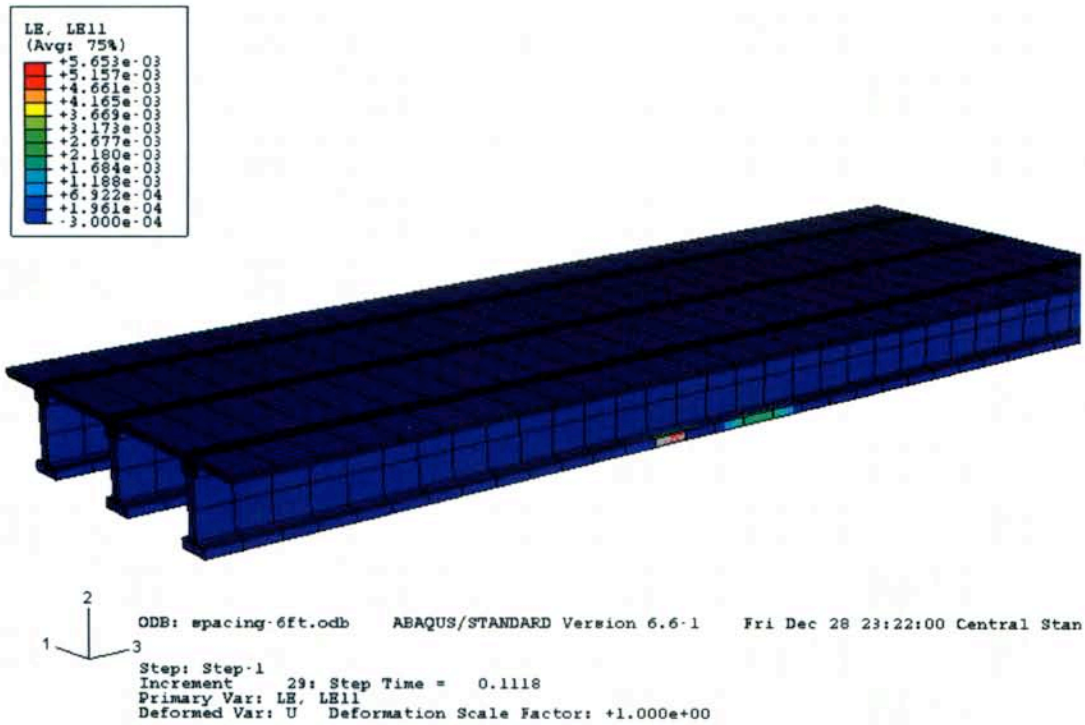

Figure H17. Transverse strain distribution of the bridge of 6 ft girder spacing with IDs

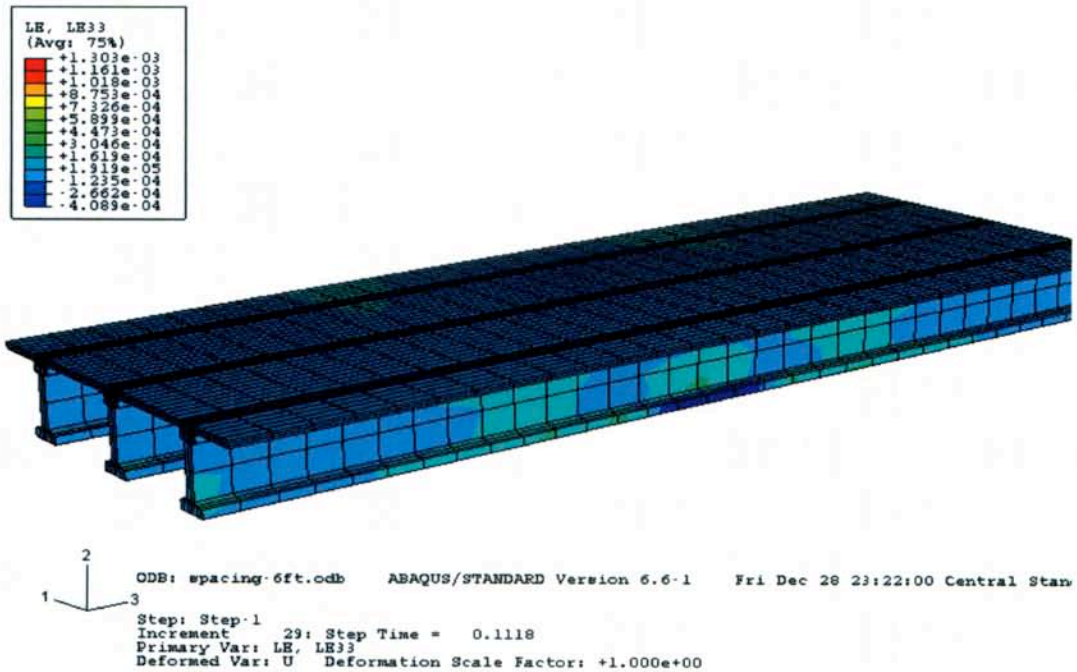

Figure H18. Longitudinal strain distribution of the bridge of 6 ft girder spacing with IDs

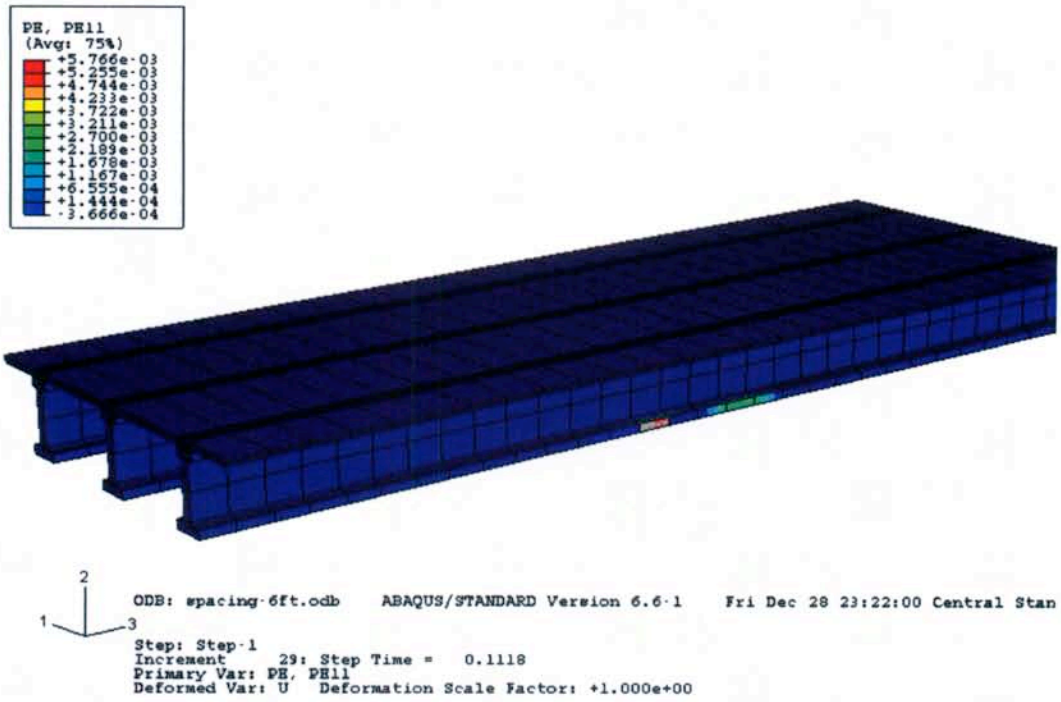

Figure H19. Transverse plastic strain distribution of the bridge of 6 ft girder spacing with IDs

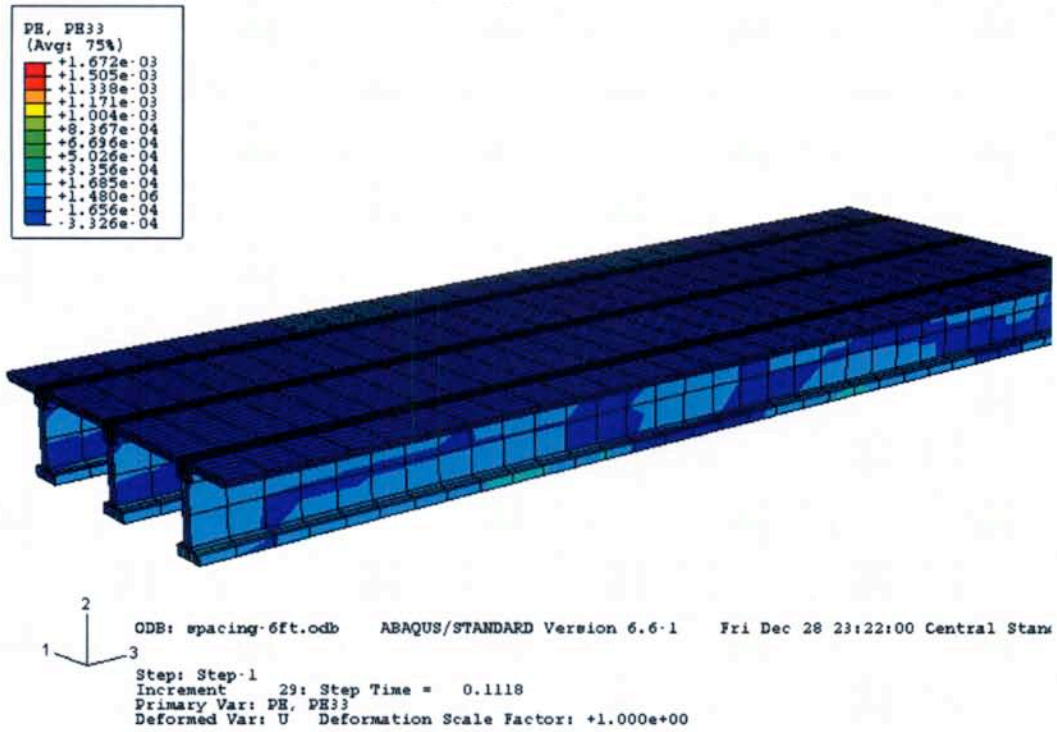

Figure H20. Longitudinal plastic strain distribution of the bridge of 6 ft girder spacing with IDs

Appendix I. Effect of the End Intermediate Diaphragms

Case without end IDs

The numerical analysis results for the bridge of 12 ft. girder spacing of 6 ft. without the end intermediate diaphragms (IDs) are given in Figures I1 to I10. While as a comparison, the corresponding results for the case of the bridge of 12 ft. girder spacing but with the end IDs are also provided in Figures I11 to I20. For both the case, the intermediate diaphragms (IDs) in the central span and at the location of the applied load are included. The purpose of the analysis is to study the effect of the end IDs. The bridge with the end IDs shows a reduced damage area as the bridge is strengthened with the end IDs; but the effect of the end IDs to the bridge performance under impact is not significant.

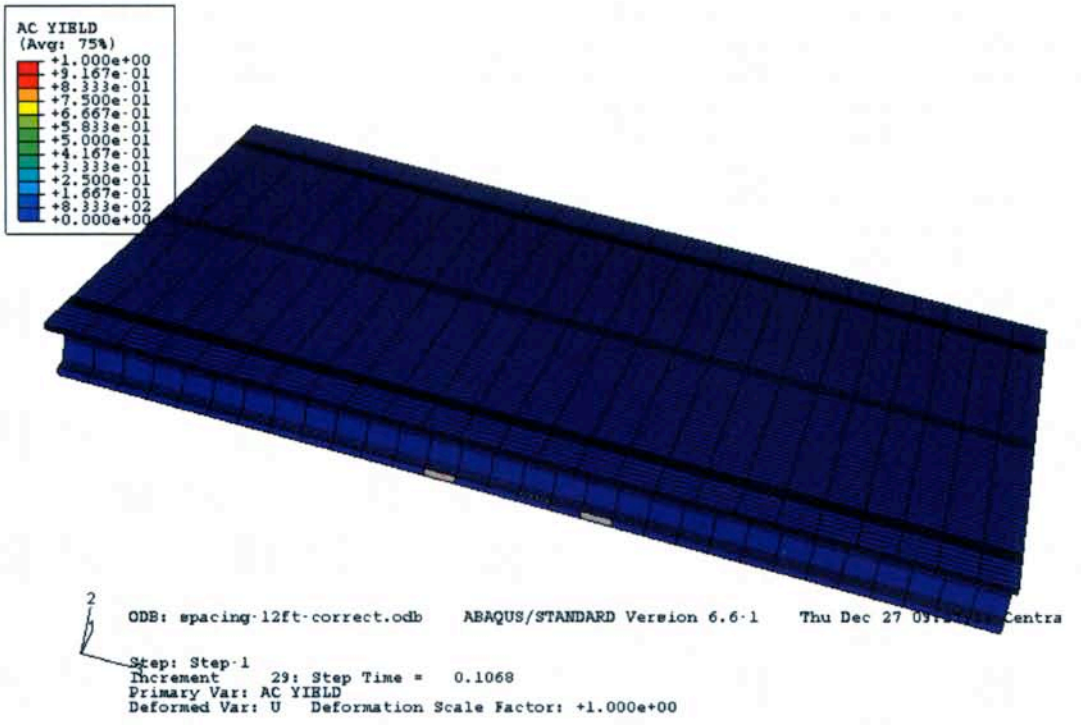

Figure I1. Damage area of the bridge of 12 ft girder spacing without end IDs

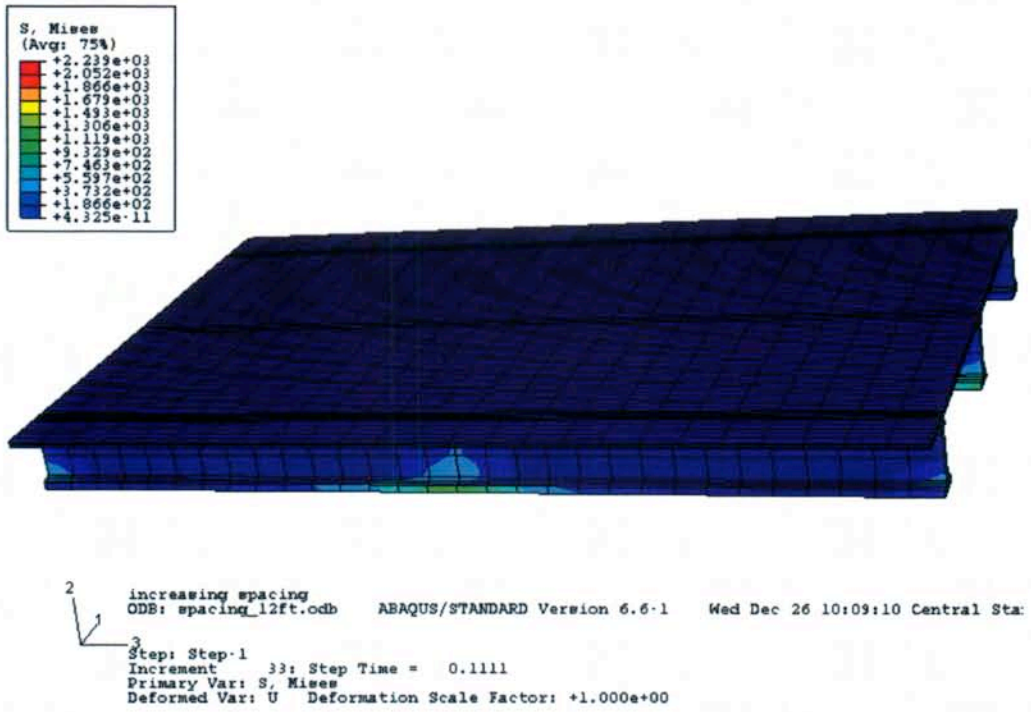

Figure I2. von Misses stress distribution of the bridge of 12 ft girder spacing without end IDs

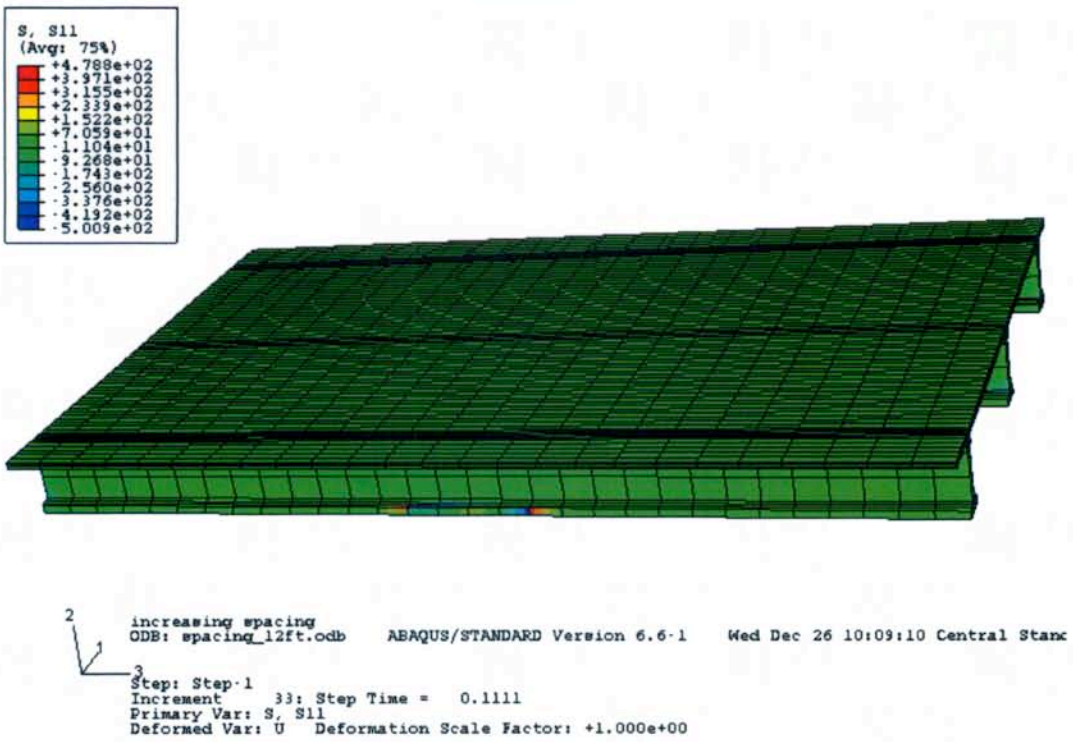

Figure I3. Transverse stress distribution of the bridge of 12 ft girder spacing without end IDs

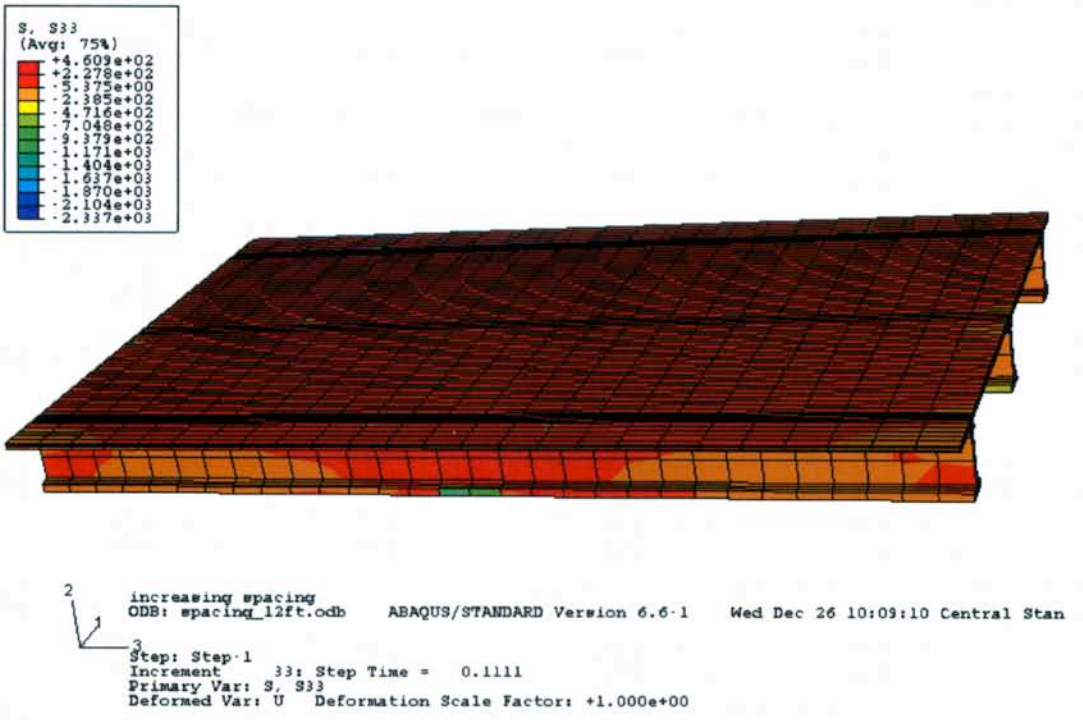

Figure I4. Longitudinal stress distribution of the bridge of 12 ft girder spacing without end IDs

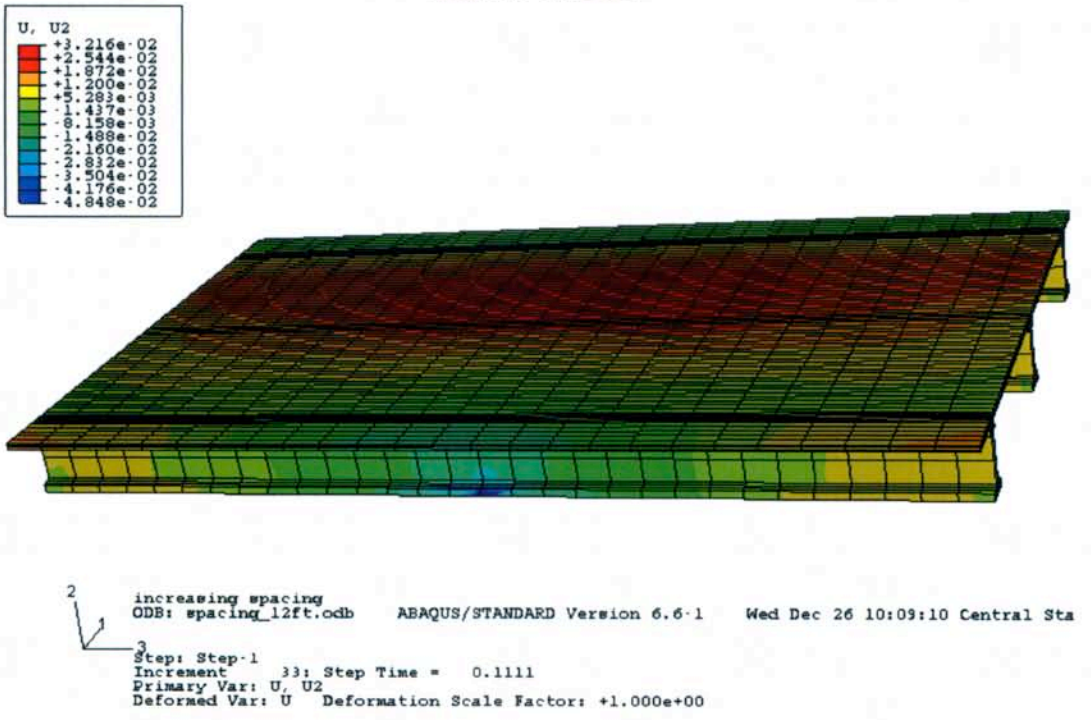

Figure I5. Vertical deflection distribution of the bridge of 12 ft girder spacing without end IDs

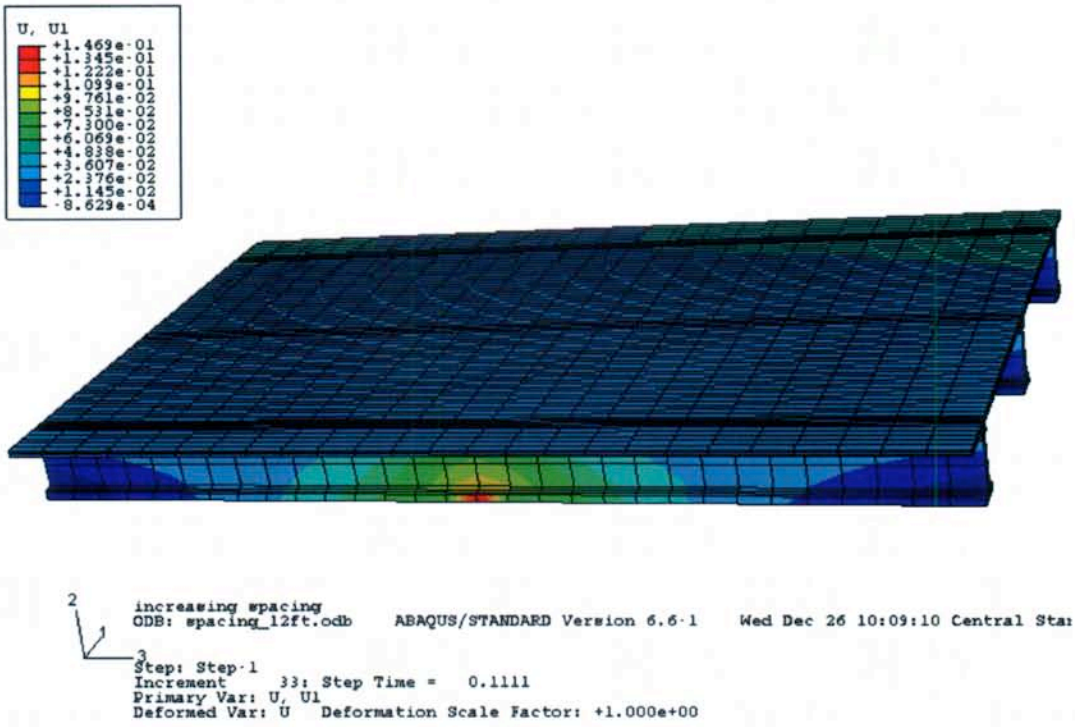

Figure I6. Longitudinal deflection distribution of the bridge of 12 ft girder spacing without end IDs

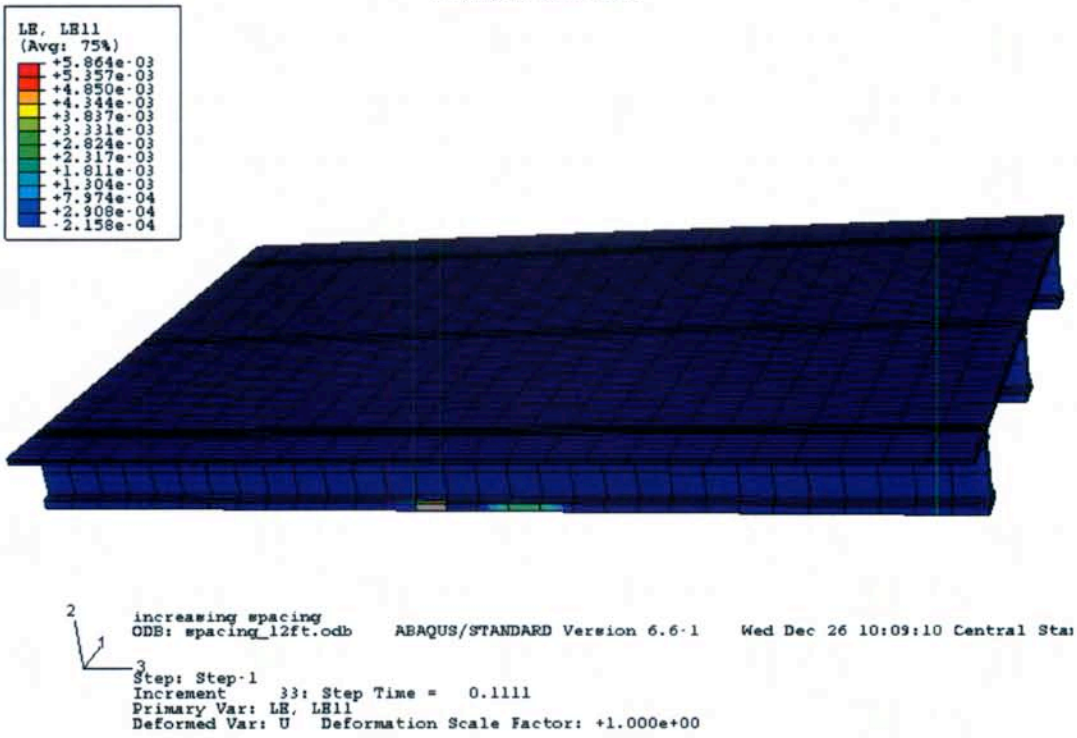

Figure I7. Transverse strain distribution of the bridge of 12 ft girder spacing without end IDs

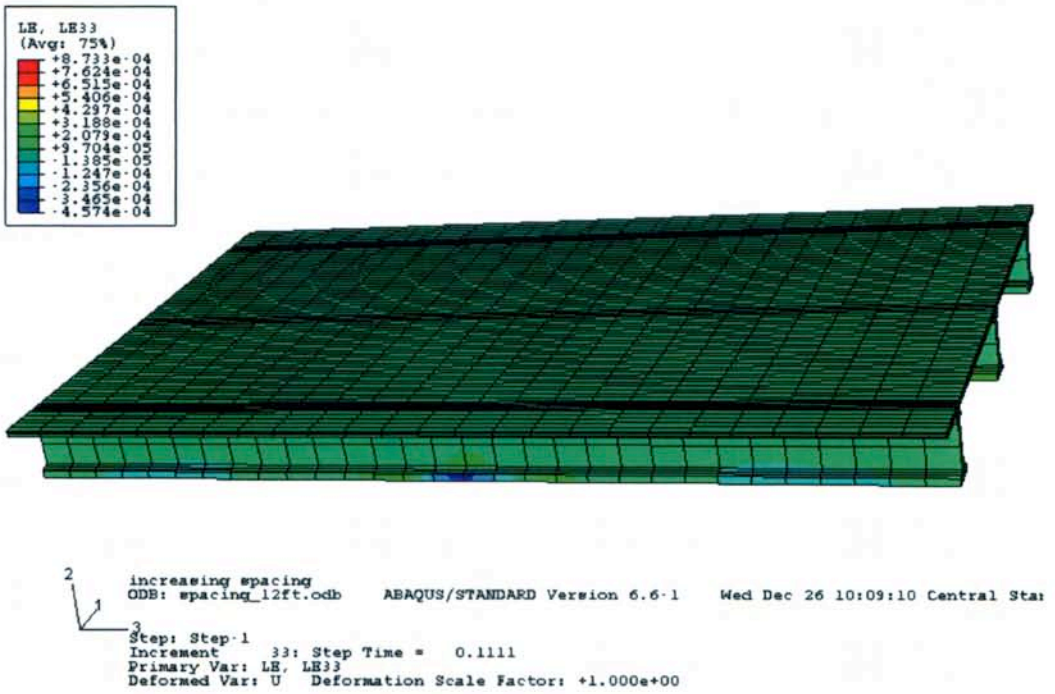

Figure I8. Longitudinal strain distribution of the bridge of 12 ft girder spacing without end IDs

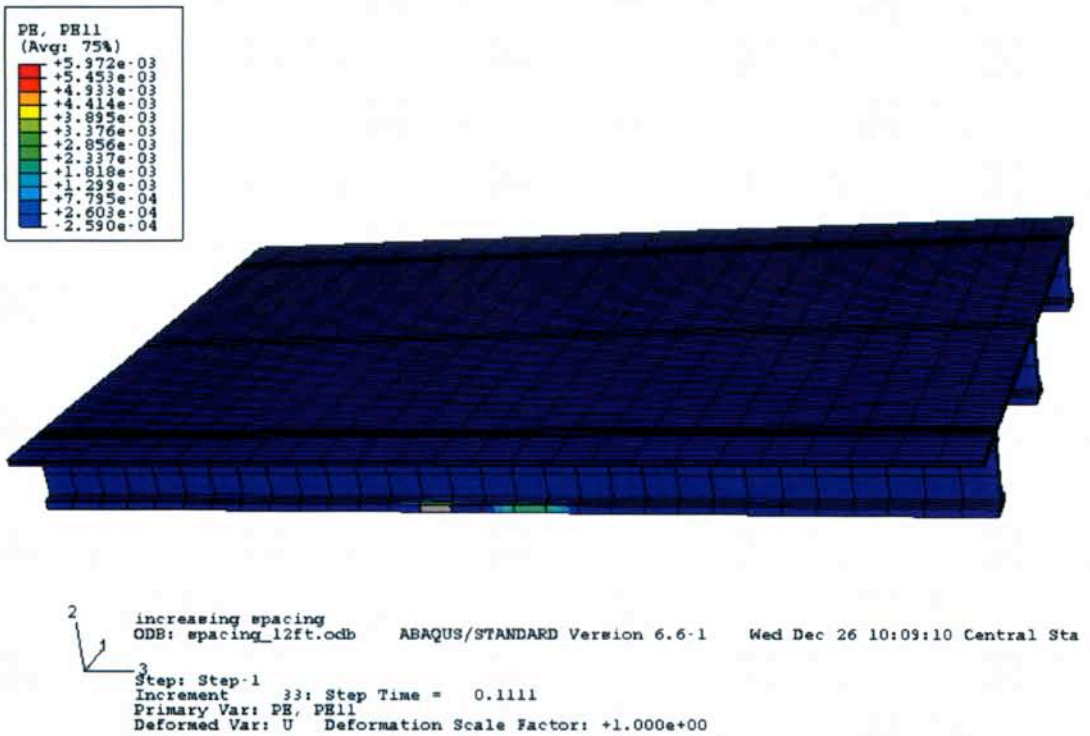

Figure I9. Transverse plastic strain distribution of the bridge of 12 ft girder spacing without end IDs

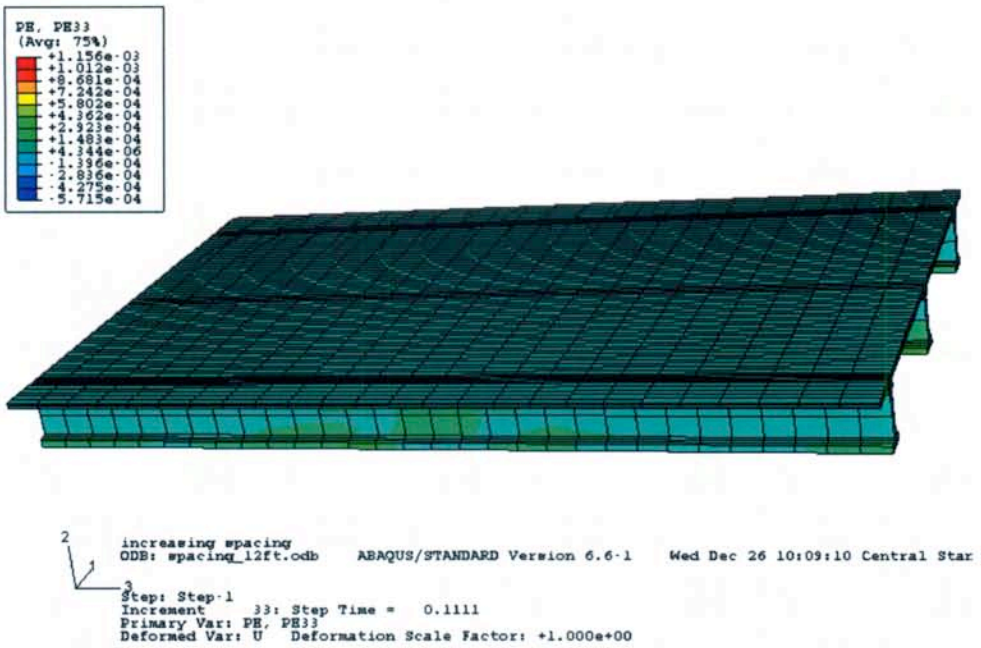

Figure I10. Longitudinal plastic strain distribution of the bridge of 12 ft girder spacing without end IDs

Case with end IDs

While for the case of the bridge of 12 ft. girder spacing with the end intermediate diaphragms (IDs), the numerical results are presented in Figures I11 to I20. Though the damage area is slightly reduced, the effect of the end IDs to the bridge performance under impact is not obvious.

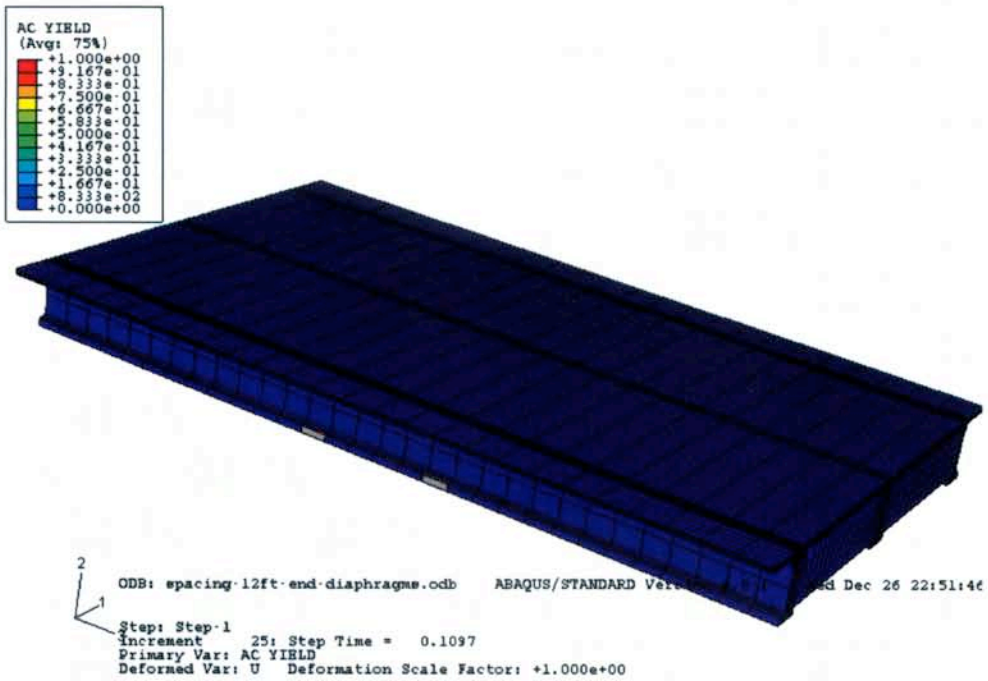

Figure I11. Damage area of the bridge of 12 ft girder spacing with end IDs

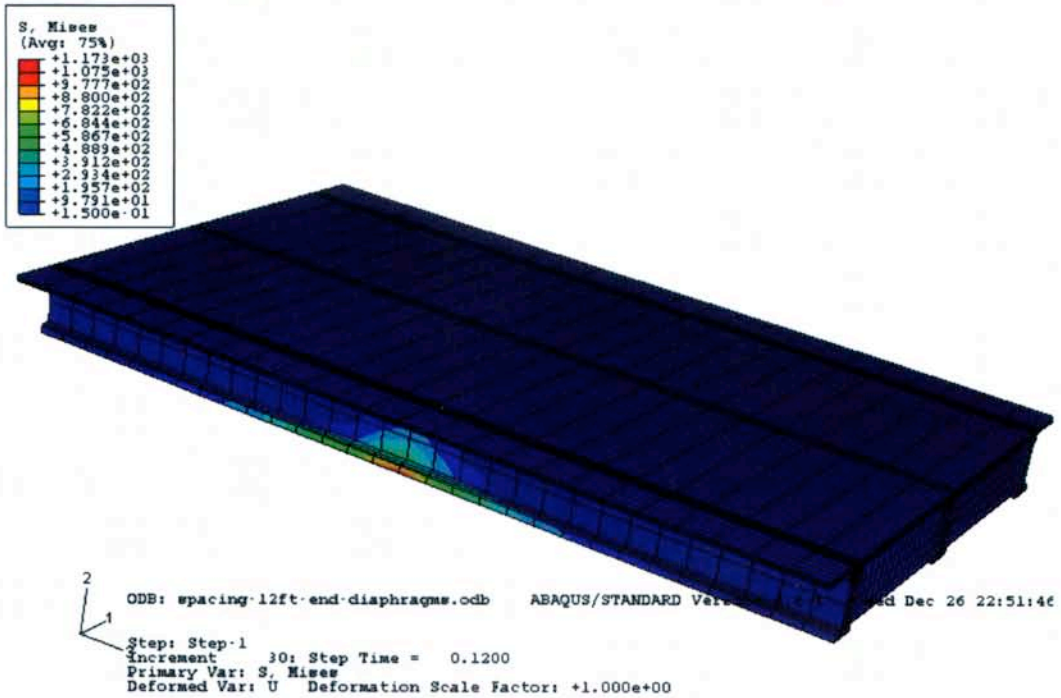

Figure I12. von Misses stress distribution of the bridge of 12 ft girder spacing without end IDs

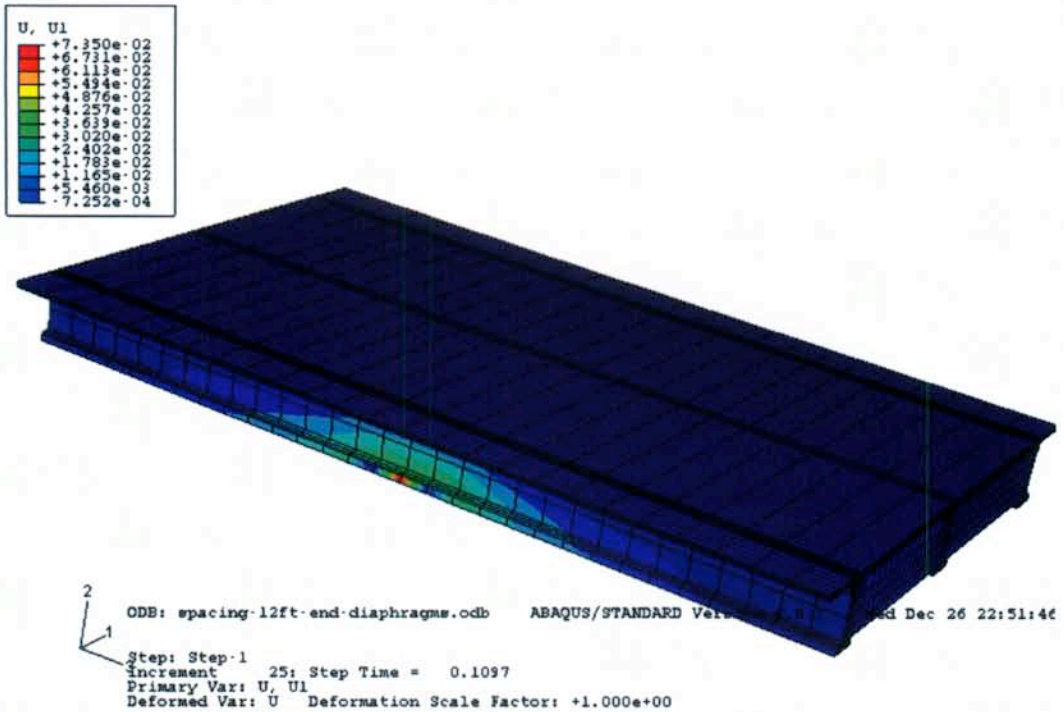

Figure I13. Transverse displacement distribution of the bridge of 12 ft girder spacing without end IDs

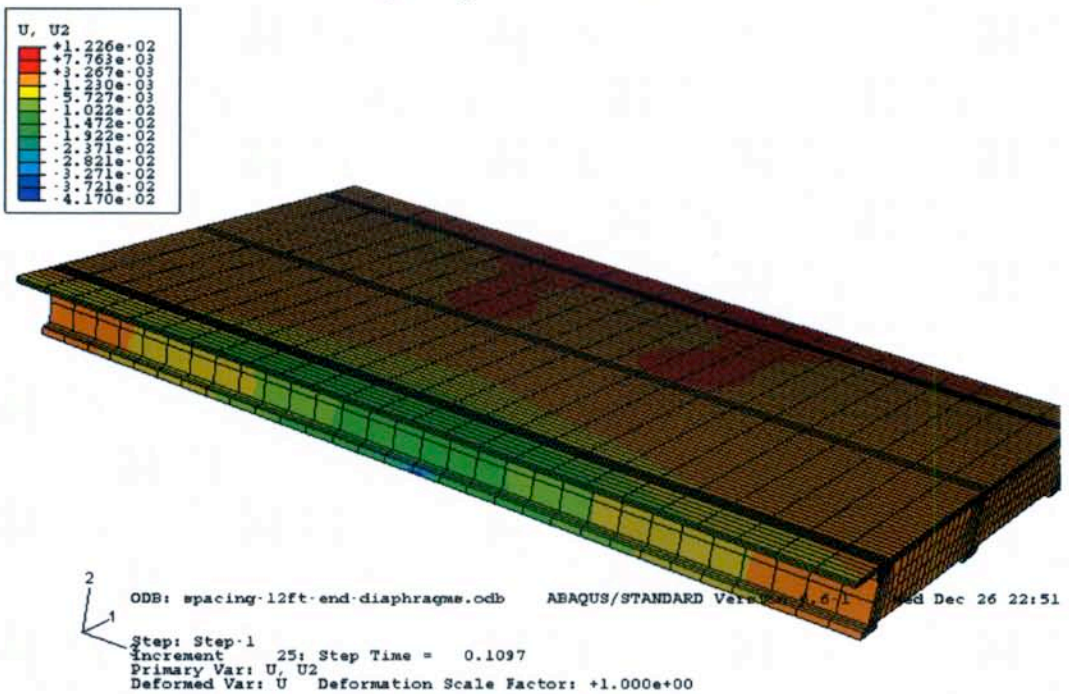

Figure I14. Vertical displacement distribution of the bridge of 12 ft girder spacing without end IDs

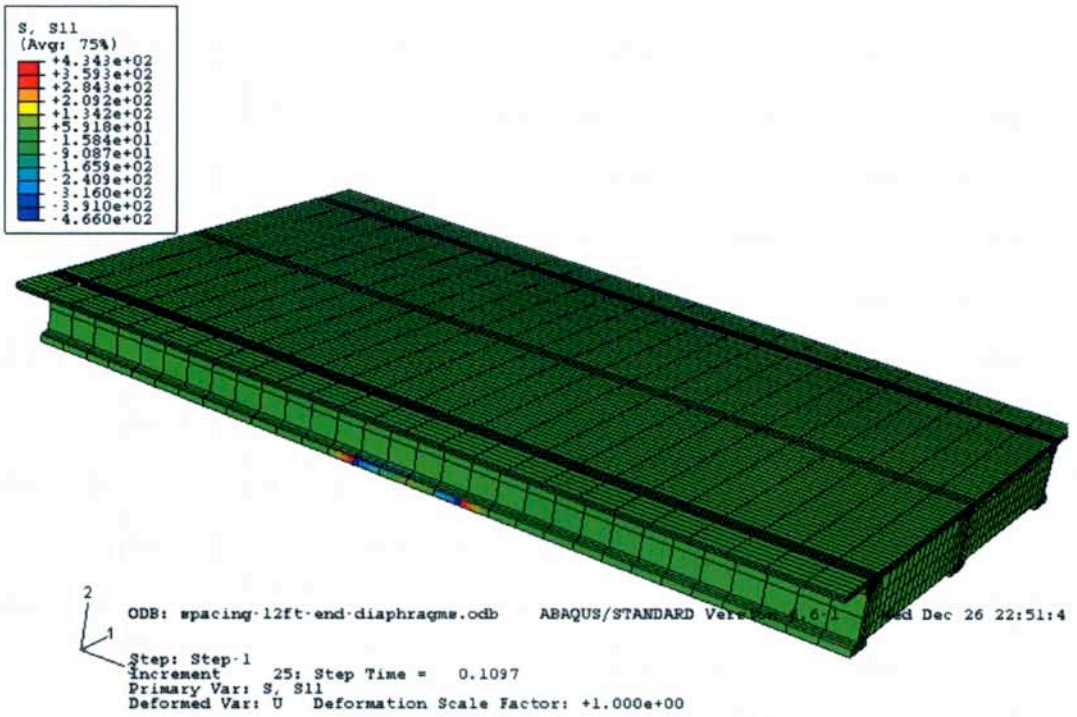

Figure I15. Transverse stress distribution of the bridge of 12 ft girder spacing without end IDs

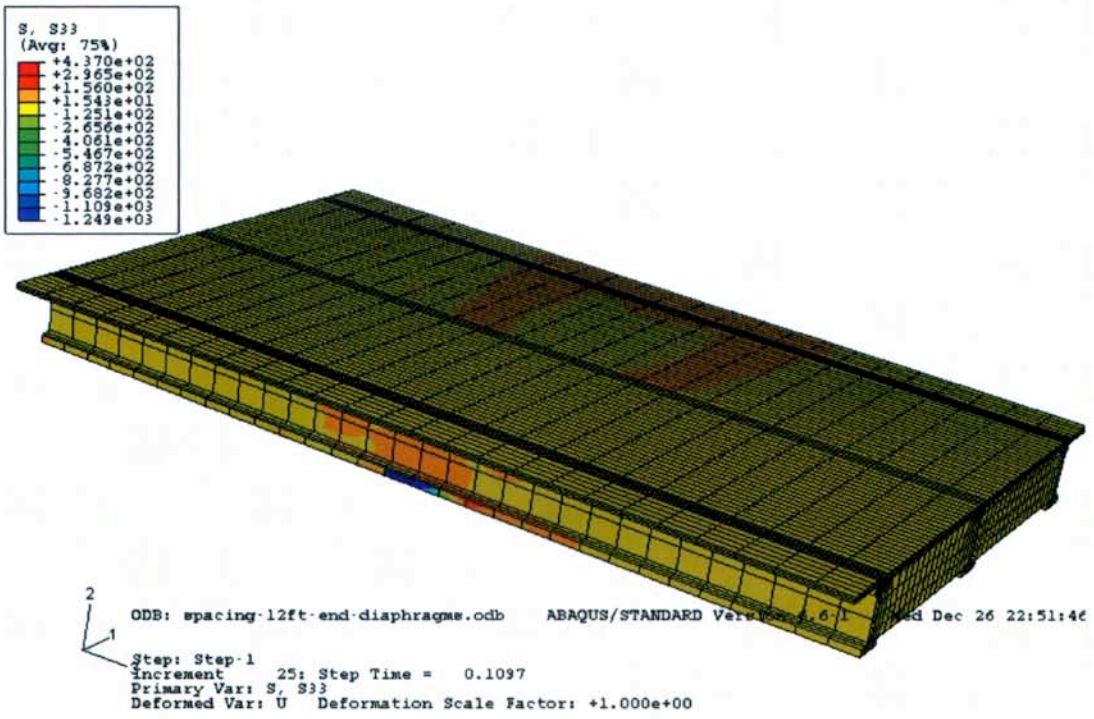

Figure I16. Longitudinal stress distribution of the bridge of 12 ft girder spacing without end IDs

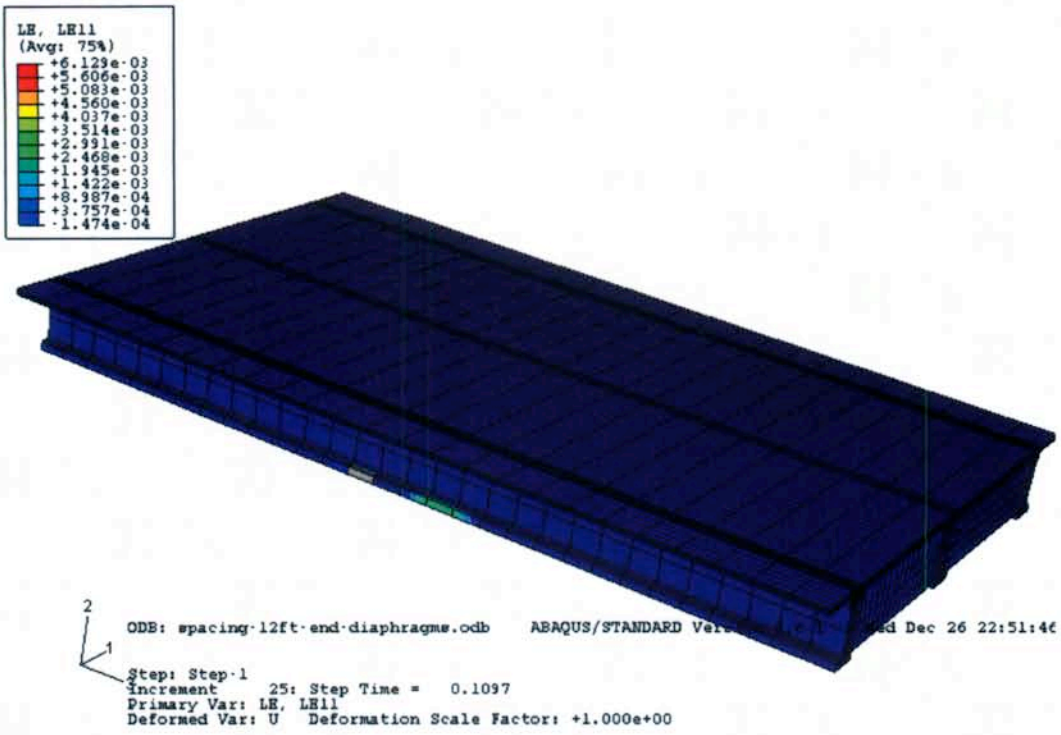

Figure I17. Transverse strain distribution of the bridge of 12 ft girder spacing without end IDs

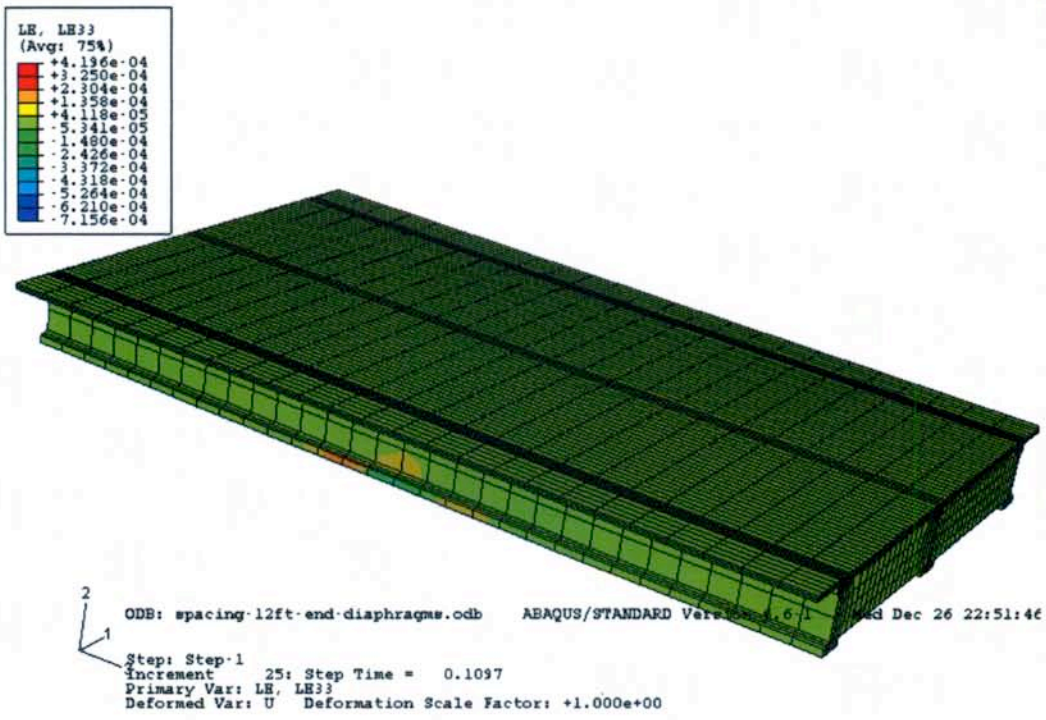

Figure I18. Longitudinal stress distribution of the bridge of 12 ft girder spacing without end IDs

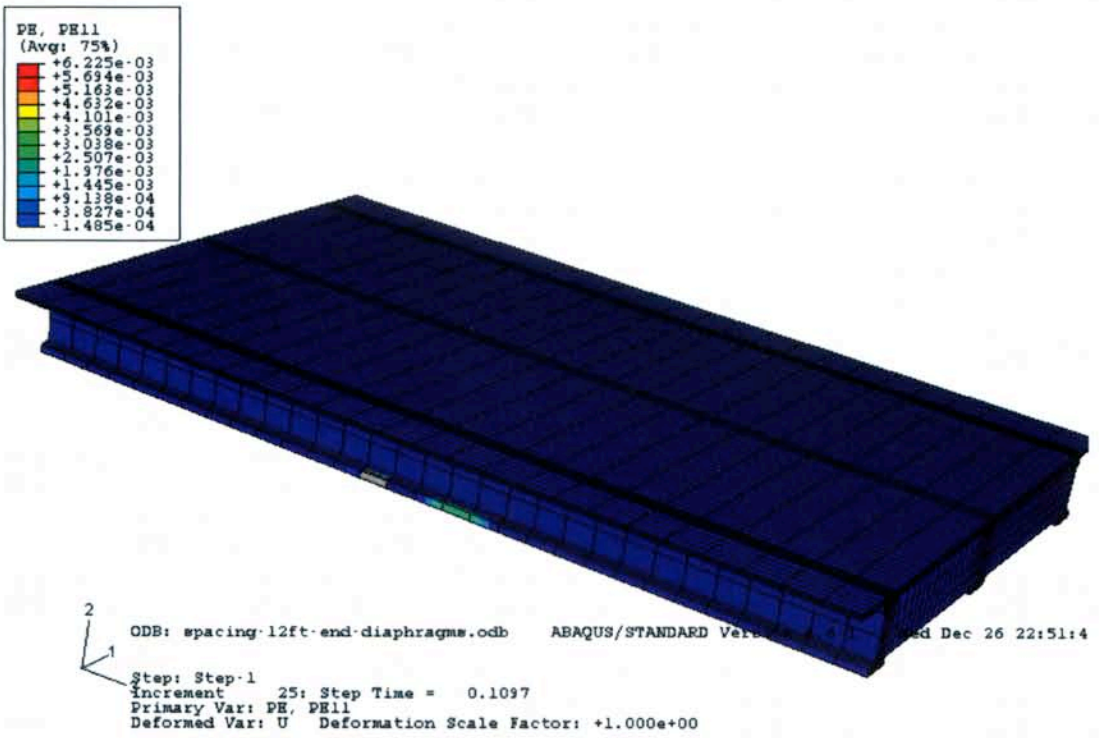

Figure I19. Transverse plastic strain distribution of the bridge of 12 ft girder spacing without end IDs

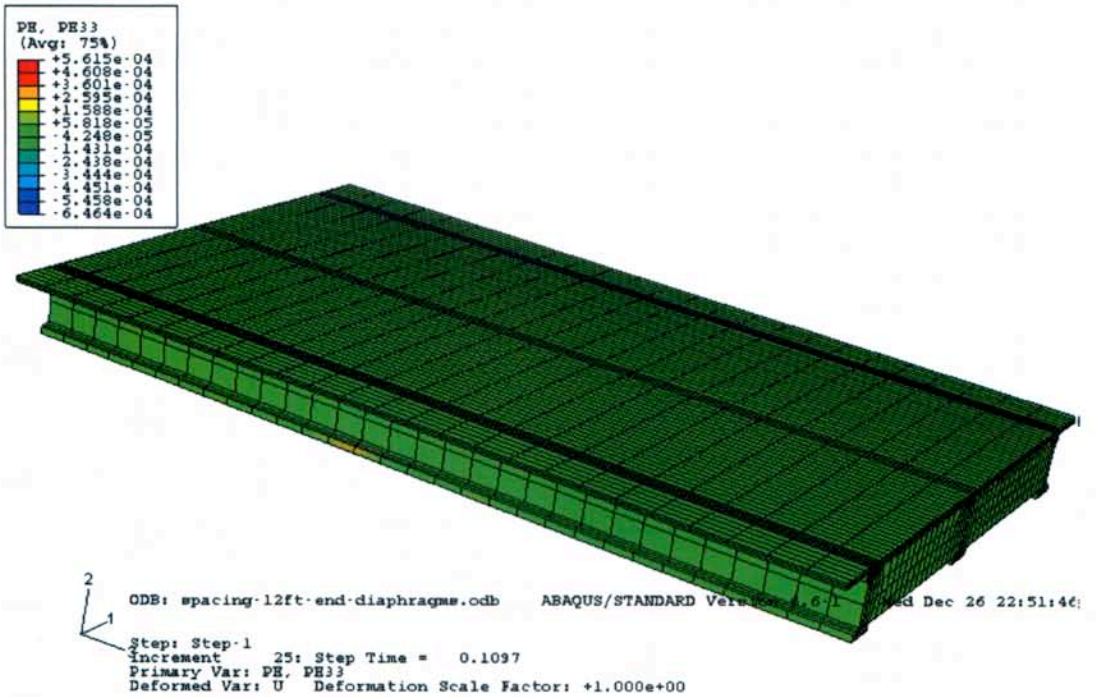

Figure I20. Longitudinal plastic strain distribution of the bridge of 12 ft girder spacing without end IDs